

Federal State Budgetary Educational Institution of Higher Education “Moscow State  
University of Technology “STANKIN”

As a manuscript

Kolesnichenko Ruslan Vladislavovich

Improving Accuracy of Technological Robots Based On The Usage Of Precision Dual-Motor Servo Drives

Specialty 05.02.05 - Robots, Mechatronics and Robotic Systems

Thesis for an academic degree  
Candidate of Technical Sciences (PhD)

Supervisor:  
Doctor of Technical Sciences, Professor  
Ilyukhin Yuriy Vladimirovich

Moscow – 2022

## Contents

<b>INTRODUCTION.....</b>	<b>5</b>
<b>CHAPTER 1. ANALYSIS OF KNOWN SOLUTIONS TO THE SCIENTIFIC PROBLEM OF IMPROVING ACCURACY OF MOVEMENTS AND EXPANDING FUNCTIONALITY OF ANALYTICALLY PROGRAMMABLE TECHNOLOGICAL ROBOTS.....</b> 12	
1.1 Areas of application of technological robots requiring increased accuracy of movements of end effector .....	12
1.1.1 Laser cutting.....	12
1.1.2 Laser welding .....	13
1.1.3 Robotic milling.....	14
1.2 Identification and analysis of factors affecting accuracy of movements of analytically programmable technological robots for processing objects with complex shapes of surfaces .....	15
1.3 Analysis of known solutions of construction of high-precision technological robots .....	18
1.4 Comparison of weight, size and cost indicators of technological robots built on geared dual-motor servo drives with technological robots built on gearless drives.....	24
1.4.1 Parameters of the manipulation mechanism.....	26
1.4.2 Selection of motors and gearboxes for dual-motor drives .....	28
1.4.3 Selection of gearless drive motors (direct drives).....	30
1.4.4 Comparative analysis of weight, size and cost indicators of industrial robots built on dual-motor and gearless servo drives.....	32
1.4.5 Main results and conclusions of the comparative analysis of the usage of dual-motor and gearless servo drives .....	34
1.5 Rationale for the choice of the purpose and objectives of the research .....	34
1.6 Conclusions on the first chapter .....	36
<b>CHAPTER 2. DESIGN FEATURES AND PROPERTIES OF PRECISION GEARED SERVO DRIVES FOR ANALYTICALLY PROGRAMMABLE TECHNOLOGICAL ROBOTS .....</b> 37	
2.1 Concept of precision geared servo drives for analytically programmable robots .....	37
2.2 Features of the mathematical model of a two-channel dual-motor geared servo drive .....	41
2.3 Structure of a computer simulation model of a two-channel dual-motor geared servo drive .....	53
2.4 Parameter adjustment method for two-channel precision dual-motor geared servo drive.....	55
2.5 Computer simulation and analysis of dynamic properties of a two-channel precision dual-motor geared servo drive .....	58
2.6 Conclusions on the second chapter .....	74

<b>CHAPTER 3. EXPERIMENTAL STUDY OF DYNAMIC PROPERTIES OF TWO-CHANNEL PRECISION DIGITAL SERVO DRIVES FOR HIGH-PRECISION TECHNOLOGICAL ROBOTS .....</b>	76
3.1 Purpose and objectives of the experimental study of precision dual-motor geared servo drive .....	76
3.2 Experimental stand for studying the dynamic properties of digital precision geared servo drives ..	76
3.3 Synthesis of a digital servo drive of experimental stand.....	83
3.4 Results of an experimental study of the properties of precision dual-motor servo drive.....	88
3.5 Experimental comparison of the dynamic properties of dual-motor geared servo drive with dynamic properties of traditional single-motor servo drive .....	88
3.6 Conclusions on the third chapter.....	93
<b>CHAPTER 4. DEVELOPMENT OF MATHEMATICAL AND COMPUTER SIMULATION MODEL OF TECHNOLOGICAL ROBOT WITH PRECISION SERVO DRIVES .....</b>	94
4.1 Description of mathematical model of technological robot.....	94
4.2 Method for adjustment of precision dual-motor drives of technological robot .....	102
4.3 Study of dynamic properties and accuracy of movements of technological robots with two-channel dual-motor drives of technological robots performing circular trajectory movements .....	104
4.3.1 Parameters of the manipulator, used in the research, constructed on conventional single-motor drives .....	104
4.3.2 Conditions for conducting a computational experiment to compare errors arising when manipulator with single-motor and two-channel dual-motor drives performs movements along circular trajectories ..	105
4.3.3 Development of a method for assessing dynamic accuracy of movements of precision technological robots built on drives with the developed structure performing robotic milling operation .....	106
4.3.4 Results of computer simulations .....	108
4.4 Conclusions on fourth chapter.....	117
<b>CHAPTER 5. RESERCH OF ACCURACY OF MOVEMENTS OF TECHNOLOGICAL ROBOTS WITH TWO-CHANNEL DUAL-MOTOR SERVO DRIVES WHEN PERFORMING ROBOTIC MILLING .....</b>	119
5.1 Features of milling by a technological robot.....	119
5.2 Mathematical model of the robotic milling process.....	122
5.3 Investigation of dynamic properties and accuracy of movements of technological robots with dual-motor drives performing robotic milling along a straight trajectory .....	125

5.3.1 Conditions for conducting a computational experiment to compare errors arising in robotic milling operation along straight trajectory performed by manipulator with single-motor and dual-motor drives..	125
5.3.2 Results of Computer Simulation of robotic milling along straight line .....	127
5.4 Study of dynamic properties and accuracy of movements of technological robots with dual-motor drives performing robotic milling along circular trajectory .....	129
5.4.1 Conditions for conducting a computational experiment to compare errors arising in robotic milling operation along a circular trajectory performed by manipulator with single-motor and dual-motor drives	130
5.4.2 Computer simulation results of milling along circular trajectory .....	131
5.4.3 Computer simulation results of milling along circular trajectory with adaptive load torque control	153
5.5 Conclusions on the fifth chapter.....	159
<b>CONCLUSION.....</b>	161
<b>REFERENCES .....</b>	163
<b>APPENDIX A. Stand control program code .....</b>	173
<b>APPENDIX B. Program code for obtaining symbolic model of a 4-link manipulator in MATLAB and SIMULINK.....</b>	184

## INTRODUCTION

**Relevance of the topic of the dissertation.** According to the forecasts published by the International Federation of Robotics (IFR) [1], in 2019, the number of functioning industrial robots in the world reached 2,722,077 units. According to this report, despite the economic crisis caused by COVID-19 pandemic, in the medium term, this crisis will cause an increase in digitalization of production, which will create growth prospects for the robotics industry worldwide. The outlook remains excellent. According to the results of the market analysis already published, in recent years, an increasing number of robots have been used in the automotive and electrical industries, where industrial robots are mainly used to perform basic technological operations such as welding and soldering, laser cutting and laser marking. In these operations, the robot tool is practically not affected by external forces associated with the machining process. In addition, more and more research is currently being carried out in the field of the usage of industrial robots in operations related to machining of parts. During such operations, significant forces act on the robot's tool. At the same time, the robot that carries the tool must obtain high static and dynamic accuracy of movements.

All of these operations can be performed by both machine tools and industrial robots. The cost of industrial robots is often significantly lower than the cost of machines designed for such operations. However, modern commercially produced universal industrial robots still cannot compete with machine tools in achieving high precision of movements, primarily due to their insufficient rigidity. This severely limits the usage of robots with open kinematic chain in such operations.

The possible usage of robots in such technological operations as milling, drilling, marking, assembly, measurement of products with large dimensions and complex shapes of surfaces, deburring, laser and plasma cutting is accompanied by high requirements to accuracy of movements of the robot's end effector, especially when it is exposed to external forces associated with machining, as noted in [81].

In order to expand the scope of application of technological robots, including realization of robotic milling, new solutions are needed in order to create precision industrial robots with increased dynamic accuracy of positioning and movement along the required trajectory.

Robots, designed to perform these and other technological operations, are called technological robots (TR). As Ilyukhin Y.V. wrote in his dissertation [2]: "their distinctive feature is the necessity to use contour motion control systems, considered in [3 - 14], for the implementation of fast and accurate movements of the end effector along the given trajectory, including force interaction of the end effector (EE) with the processed object". Such robots should have significant workspace and have an open

kinematic chain, as noted in [2]. Often the requirements to accuracy of robot movements are very strict. Permissible deviations of the actual position of the end effector from its desired position should not exceed several tens of micrometers. High accuracy of movements is especially important at analytical programming of technological robots, in which the coordinates of reference points are not corrected using the teaching method. Here we are talking about absolute accuracy of the robot's positioning, and not about repeatability of movements.

Analytical robot programming is an important tool for increasing productivity of the entire robot programming process. The labor intensity of this process can be significantly reduced as a result of the usage, for example, of CAM systems focused on robotics tasks. Such systems allow to generate robot motion programs by means of computer simulation, without actually starting the robot. This not only reduces the need to additionally use the robot to perform programming by teaching, where the points lying on the desired trajectory of the manipulation mechanism are pre-memorized. It also improves the efficiency of programming, because many data about the part and the robot itself are already known from the CAM system. In order to make analytical programming of robots more functional, it is necessary to have a precise manipulation mechanism that will perform movements with minimal deviation from the specified trajectory.

Currently existing technological robots are not distinguished by high accuracy of movements of end effectors under the influence of external forces associated with the process of technological operation. For example, commercially produced universal industrial robots are not yet capable of performing precision milling of parts. This is primarily due to insufficient dynamic rigidity of robots and imperfection of the mathematical models, used to build control algorithms. The errors of robot drives are significantly affected by the errors of transmissions (gearboxes), which have noticeable backlashes and high elastic compliance. As a rule, servo drives of robots have a structure in which transmissions are outside the position control loop of the control object. This solution ensures the operability of the drives, eliminating self-oscillations, but significantly reduces accuracy of the drive and the robot as a whole. Gearless drives (direct-torque drives), such as linear actuators, turn out to be unnecessarily massive and expensive. Therefore, the prospects for their usage in robotics are extremely limited.

That's why there is an urgent scientific task of improving accuracy and velocity of digital servo drives of technological robots. The solution to this problem presupposes:

- search for new technical means, structures and control algorithms for geared digital servo drives of technological robots, which allow, first of all, to eliminate influence of errors of transmissions on accuracy of manipulator movements and thus increase both accuracy and speed;

- development of a mathematical model of the manipulator used to implement robot control, taking into account the obtained structures and algorithms for controlling drives.

Improving accuracy and velocity of digital servo drives will significantly increase accuracy of the robot end effector during various process operations, such as laser and plasma processing.

The increase in dynamic rigidity and the associated increase in accuracy of the robot's end effector movements will increase the permissible contour speed and processing productivity. This, in turn, will contribute to the expansion of the scope and increase the efficiency of the usage of technological robots.

**The development of the research topic.** A lot of scientific research has been devoted to the issues of improving accuracy of technological robots. In the USSR and Russia, research in this direction was carried out by such scientists as Afonin V.L., Ilyukhin Yu.V., Klimchik A.S., Leskov A.G., Makarov I.M., Medvedev V.S., Poduraev Yu.V., Popov E.P., Timofeev A. V. [2 - 6, 13, 45, 52 - 54, 88]. In the world such studies have been carried out by Greenway B., Hoffmann Ch., Lange F., Mithran N., Şirinterlikçi A., Sörmmo O., Švaco M., Schneider U., Slamani M., Reinl C., Zhu Z. [10, 15, 20, 21, 24 - 28, 56, 58, 90, 91]. The results of experimental studies of factors that reduce accuracy of technological robots are presented in the papers of Bonev I. A., Hoffmann Ch., Schneider U., Şirinterlikçi A., Slamani M., Klimchik A. S. [13, 15, 26, 89, 91]. From these papers, it follows that the main factors reducing accuracy of robot positioning are elasticities and backlashes of mechanical transmissions of the manipulator drives. Therefore, in order to improve accuracy of technological robots, first of all, it is necessary to focus on increasing accuracy of servo drives of such robots as a result of reducing influence of elasticities and backlashes of their mechanical transmissions on accuracy of robot movements.

The features of servo drives, the problem of reducing influence of elasticities and backlashes of their mechanical transmissions on accuracy of movements are discussed in the papers of Baranov M.V., Ilyukhin Yu.V., Klubnikin P.F., Polksy V.A., Popov D.N., Popov E.P., Chemodanov B.K., Chernov E.I., Andreescu G.D., Mosadeghzad M., Rabinovici R., Schneider U., Slamani M. [2, 15, 26, 29, 60, 61, 73, 74]. Analyzing these papers, it has been established that one of the ways to improve accuracy of movements is the usage of dual-motor two-channel drives. For example, in [29, 74] it is proposed to use dual-motor drives with a two-channel structure. The peculiarity of two-channel drives is that one servo drive is a part of the coarse control channel and the second drive is a part of a fine control channel. In this case, the first channel is used to move the control object, while reproducing the control action with insufficient accuracy. The second channel eliminates the error of the first channel and thus ensures more accurate reproduction of the control action by the control object. But even in this case the gearboxes of the drives are outside the control loops. Therefore, their errors reduce accuracy of movements. In addition, it is difficult to integrate such two-channel drives into manipulator because of design issues.

Companies that produce electric motors, frequency converters and their control systems, such as Siemens AG, offer ready-made solutions applying dual-motor drives in order to reduce influence of backlash of the rack-and-pinion mechanical transmission on the positioning accuracy of the control object. The special feature of these solutions is the organization of the dual-motor drive structure according to the master / slave principle. Such drives are controlled by a numerical control system, where the required torque value between the master and slave motors is calculated. However, in such structure there is no separate position control between the master and slave drives, and the control is only based on velocity and not on position of the control object. Here, only position sensors mounted on the shafts of the master and slave motors are used.

The analysis of the known solutions presented in [29, 74] showed that a significant increase in accuracy of movements can be achieved when the drive is closed by control loop of the rotation angle of the control object and a backlash-eliminating device is mandatorily used together with a change in the structure of the control part of the drive. The idea of using an active backlash-eliminating device also leads to the expediency of building dual-motor servo drives.

In the papers of Ilyukhin Yu.V., Robertz S. G., Schiffer J. it is proposed to use dual-motor servo drives for the construction of industrial robots. In the papers of the authors Robertz S. G. and Schiffer J. [56, 58] the usage of such drives for the construction of technological robots with a closed kinematic circuit has been proposed. The peculiarity of the proposed solution lies in the usage of various control strategies for dual-motor drive with rack-pinion transmission as part of manipulator with parallel kinematic structure.

The idea of using high-precision dual-motor drives in robots with an open kinematic chain was proposed and considered in the dissertation by Y. V. Ilyukhin [2]. These drives are essentially two-channel drives, but the functions of the control channels differ from those of the two-channel drives considered in [29]. It should be noted that at present in the open scientific literature there are practically no results of experimental studies of the dynamic properties of dual-motor drives, which could provide new data confirming the effectiveness and feasibility of their usage for the construction of precision technological robots. Also, there are no papers in which a detailed analysis of accuracy of robot movements based on dual-motor drives, closed by the rotation angle of the control object, when performing, for example, robotic milling, has been carried out by means of computer modelling.

**The object of the study** is a technological robot with an open kinematic chain, built on precision dual-motor geared servo drives, closed by position control loop of the control objects (manipulator links).

**The subject of this research** are mathematical and computer models, control algorithms and dynamic properties of technological robots with precision dual-motor geared servo drives.

**Purpose and objectives of the study.** The purpose of the study is to increase accuracy of movements and expand functionality of analytically programmable technological robots as a result of their construction on dual-motor geared servo drives with controlled torque of their interaction.

To achieve the goal of the research, the following scientific **tasks** were solved:

- identification and analysis of factors affecting accuracy of movements of analytically programmable technological robots when processing objects with complex shape of surface;
- development of the structure and mathematical model of precision servo drives that provide high dynamic accuracy of technological robots without significant loss of speed;
- conducting an experimental study of the dynamic properties of dual-motor geared servo drives with the developed structure of the control system;
- development of a mathematical model of technological robot taking into account the identified factors;
- development of a method for assessing accuracy of movements of precision technological robots built on drives with the developed structure and robots with drives of the traditional structure, which makes it possible to establish qualitative and quantitative relationships between the deviation of the end effector from the desired trajectory and the parameters of the robotic milling operation;
- computer study of dynamic properties of precision technological robots built on drives with the developed structure in comparison with robots built on drives with traditional structure.

**The scientific novelty** is as follows:

- the structure of a two-channel digital geared servo drive, closed by position control loop of the control object, which is distinguished by the presence of a control channel of the torque drive-loader;
- mathematical model and structure of a technological robot with a complex of two-channel digital dual-motor servo drives, which reflect the effect of the force interaction of the tool with the processed object, and an algorithm for adaptive control of the loader torque;
- the results of the analysis of movements accuracy of two-channel digital servo drives and the justification of the expediency of their use for construction of analytically programmable technological robots;
- recommendations for the selection of characteristics of the motor shaft position sensor in the internal control loop of the main channel of the precision servo drive, which excludes self-oscillating processes;

- dependences of accuracy of the robot's end effector movement along typical desired trajectories on the nominal values of the machining process parameters.

**The theoretical significance of the paper** lies in the creation of mathematical models and computer control algorithms that form the theoretical basis for the construction of analytically programmable technological robots with precision dual-motor servo drives for performing high-precision technological operations, for example, dimensional robotic machining.

**Practically significant results of the paper** are the method of adjustment of dual-motor precision servo drives of industrial robots, as well as recommendations for the selection of equipment designed to significantly increase accuracy of robotic milling.

**Research methods.** In the course of the dissertation, the methods of the control theory, computational experiment, mathematical and physical modeling with the usage of computer technology, Matlab, SolidWorks software environments were used. Experimental studies were carried out using modern measuring equipment and computer technology. The results of experimental studies confirmed the adequacy of mathematical models and the reliability of the conclusions.

#### **The main provisions to be defended:**

- The proposed structural diagram and mathematical model of a precision technological robot built on dual-motor geared servo drives provide significant increase in dynamic rigidity and accuracy of movements.
- The results of theoretical and experimental research substantiate the expediency of using technological robots with dual-motor drives at their analytical programming and for the implementation of technological operations that require increased accuracy of movements.
- A developed method for assessing accuracy of movements of precision technological robots built on drives with a developed structure, and robots with drives of a traditional structure, makes it possible to establish qualitative and quantitative relationships between the deviation of the end effector from the desired trajectory and the parameters of the performed robotic milling operation.

**The reliability of the results of the study** is determined by the correct usage of the mathematical apparatus of robotics and control theory and is confirmed by modern research methods that correspond to the goals and objectives set in the research, the consistency of the results of computer modeling and

experimental research. Scientific provisions, conclusions and recommendations formulated in the thesis are supported by factual data presented in the figures and tables.

**Approbation of the paper.** The main results of the thesis were reported and discussed at scientific and technical conferences, including the International School of Young Scientists and Specialists within the framework of the International Exhibition "Metalworking - 2016" (Moscow, 2016), the 26th International Symposium on Robotics and Automation of Production DAAAM (Zadar, Croatia, 2016), the Scientific and Practical Conference "Design of Machines, Robots and Mechatronic Systems" (Orel, 2017), at the II International School-Conference of Young Scientists "Dynamics of Complex Networks and Their Application in Intelligent Robotics" (DCNAIR, Saratov, 2018), at scientific seminars of the Department of Robotics and Mechatronics of MSUT «STANKIN».

**Publishing.** 12 articles have been published on the topic of the dissertation. Of these, 5 articles have been published in publications recommended by the Higher Attestation Commission of the Russian Federation; 3 articles have been indexed in the Scopus database, 3 publications have been published in the form of abstracts of presentations.

**Implementation of research results.** The results of the study were introduced into the educational process of the Moscow State University of Technology «STANKIN».

**Compliance with the specialty passport.** The results of the thesis correspond to paragraphs 2, 3 and 7 of the passport of the specialty 05.02.05 "Robots, mechatronics and robotic systems".

**Structure and volume of paper.** The thesis consists of an introduction, 5 chapters and a list of references. It contains 187 typewritten pages, including 95 figures, 30 tables and a bibliography of 87 titles.

# **CHAPTER 1. ANALYSIS OF KNOWN SOLUTIONS TO THE SCIENTIFIC PROBLEM OF IMPROVING ACCURACY OF MOVEMENTS AND EXPANDING FUNCTIONALITY OF ANALYTICALLY PROGRAMMABLE TECHNOLOGICAL ROBOTS**

## **1.1 Areas of application of technological robots requiring increased accuracy of movements of end effector**

The analysis of information sources made it possible to identify the areas of application of robots that require increased accuracy of movements of their end effectors (EE). The paper [2] presents a classification of robotic technological operations (TO) from the point of view of the formation of requirements to the motion control system of the end effector, in which such operations are divided into 2 types. According to this classification, "the first type includes operations that are performed without force contact. The second type includes operations that are accompanied by a force interaction of the robot's end effector with the processed object", as noted in [2].

Among the operations of the first type are robotic laser and plasma cutting, laser welding, marking, precision assembly of miniature devices using robots, measuring coordinates of products with large dimensions and complex shapes of surfaces, as well as laser surgery operations. "As a rule, for this type of TO, the requirements to deviations from the nominal trajectory of the EE are more stringent than the requirements to deviations of the orientation angles of the end effector", as noted in [2].

Among the TO of the type 2 are almost all robotic machining operations, which require both increased accuracy of movements and increased rigidity of the manipulation mechanism.

Let's consider some of these technological operations and determine the requirements that they impose on the robotic systems used to perform them.

### **1.1.1 Laser cutting**

Laser cutting allows to cut materials with a focused laser beam, which provides high concentration of energy and allows cutting materials such as metal, plastic, wood, paper, glass, rubber, ceramics, etc. The thickness of the steel products to be cut can be varied from 0.2 mm to 20 mm and narrow cuts with a minimal heat affected zone can be carried out. The usage of technological robots makes it possible to carry out laser cutting along a complex path on both flat and three-dimensional parts.

According to the results of the study given in [2], when performing laser cutting, the maximum contour speed of the robot's EE can be 67 mm/s, the permissible error of the EE position is 0.05 mm, the minimum radius of the trajectory performed by the tool is 5 mm, the minimum value of the natural frequency of the mechanical subsystem is 231 rad/s. "Angular errors in laser cutting depend on the permissible inclination of the cutting edges and are equal to about 2...3 degrees", as noted in [2].

In general, laser cutting with a cutting width of about 0.2–0.3 mm makes it possible to obtain smooth and even edges of machined parts with a cutting surface irregularity height of no more than 20  $\mu\text{m}$  at a sufficiently high cutting speed. The value of the required contour velocity of the EE in laser cutting can vary over a wide range from values close to 0 to the maximum value presented above. However, it is worth noting that when the laser, as an intense concentrated heat source, is being moved at high speed, very little heat is transferred to the material of the part. This ensures a very low temperature deformation of the part and a high quality of the surface layer, as indicated in [7].

### **1.1.2 Laser welding**

Laser welding allows obtaining clean welds with minimal ingress of foreign substances into the weld. It is possible to achieve a narrow and deep weld, which minimizes the heat-affected area and produces an almost uniform metal structure at the joint, as noted in [8].

During the welding process, factors such as high material strength, insufficient thickness of the welded plate and thermal distortion can cause the laser to deviate from the joint line. Therefore, during the welding process, it is necessary to monitor the weld seam line with a sensor by detecting the error between the focus point of the laser beam and the joint line. Since the focal length is within 100  $\mu\text{m}$  during laser welding, a good result can only be obtained if the error between the focal length of the laser beam and the joint line is maintained within 200  $\mu\text{m}$ , as shown in [9].

There are already developed laser welding systems in which drives are able to track the weld at a speed of 42 m/min with a tracking error of 1 mm [10] or, for example, at a speed of 3 m/min to track the trajectory with an error of 0.1 mm [11]. In the system presented in [12] at a speed of 20 m/min, the average error value at the linear joint of the welded parts is 0.3 mm. For example, when implementing algorithms for compensating the error of welding seam tracking, it is possible to achieve an average error value of 0.1 mm, and a maximum error of 0.15 mm at a cutting speed of 4.8 m/min (80 mm/s) for a curved path and 6 m/min for a straight line, as presented in [11].

When performing a robotic welding operation, according to the results of the study given in [2], the generalized requirements to the actuator complex are as follows: the maximum contour velocity of

the EE reaches 11 mm/s, the permissible error of the EE position is 0.05 mm, the minimum radius of the trajectory performed by the effector is 5 mm, the minimum value of the natural oscillation frequency of the mechanical subsystem – 97 rad/s. As indicated in [2], "angular errors in laser cutting depend on the permissible inclination of the cutting edges and are approximately 5...10 degrees".

### **1.1.3 Robotic milling**

For milling operations in traditional mechanical engineering, CNC machines are usually used, which provide high repeatability (up to 2  $\mu\text{m}$ ) and high accuracy (up to 5  $\mu\text{m}$ ). They are typically used to process metal workpieces of the parallelepiped shape at high material removal rate.

Modern CNC machines have a wide workspace, which allows us to apply them on a wide range of operations. In addition, they are useful for the processing of composite materials, which are increasingly applied due to their high mass-to-force ratio. However, despite the many advantages, CNC machines remain quite expensive and their workspace is limited and cannot be further expanded, which is very important in the aerospace and shipbuilding industries.

For milling operations, robots have a number of advantages over machines, such as also a wide workspace, which can be further expanded with additional axes. They also have a competitive price, which makes them a cost-effective solution for milling of large parts. However, the main obstacle hindering the usage of robots in milling is their low accuracy (on average about 700  $\mu\text{m}$ ) and repeatability (about 200  $\mu\text{m}$ ) compared to CNC machines, as noted in [13].

Friction, backlash in mechanical transmissions and link compliance significantly affect the positioning accuracy of manipulators. This is mostly due to the presence of forces acting on the tool in the process of performing a technological operation. Thus, modern universal technological robots have only one to fiftieth (1/50) of the rigidity of conventional machines, as indicated in [14]. Unfortunately, these problems cannot be overcome with calibration alone, and errors still remain when performing movements along both straight and circular path.

This indicates the necessity and importance of conducting research on improving accuracy of robots performing machining operations. In one of the experimental studies [15], it was revealed that the errors even during the performance of a rough milling operation, such as deburring, are in the range of 100  $\mu\text{m}$ . A number of studies have also been carried out within the framework of the European projects HEPHESTOS and COMET to develop innovative systems for robotic milling. Analyzing the presented results of these studies [19-22], it is possible to formulate the desired values of the robot EE motion parameters for robotic milling. Thus, according to [2], "for robotic milling of aluminum alloy products at a contour speed of 10 mm/s – 20 mm/s, a cutting depth of 1 mm, the minimum value of the natural

oscillation frequency of the mechanical subsystem is 50 rad/s and angular deviations of the EE – 0.15 mrad, the deviations of the EE position from the desired position should not exceed  $100 \mu\text{m}$ ". Thus, the desired values of the robot EE motion parameters for operations requiring increased accuracy of movements of their tools, can be compiled into a Table 1.1.

Table 1.1 – Desired values of EE motion parameters

	Robotic cutting	Robotic welding	Robotic milling
Deviation of the EE position from the desired position, mm	0.05	0.1	0.1
EE contour velocity, mm/s	60-70	50	10-20
Minimum value of the natural oscillation frequency of the mechanical subsystem, rad/s	230	100	50

As a result, the following requirements can be formulated to technological robots designed for the considered TO. Since at robotic milling there are forces acting on the technological robot as a result of the interaction between the tool and the workpiece, the requirements imposed on robots when performing this TO will be considered primary. However, the requirement to deviation of the EE from the desired position, which should not exceed  $100 \mu\text{m}$ , is usually not achievable with traditional industrial robots, as shown in [19]. There, using a commercially produced technological manipulator with an open kinematic chain, the deviation of the EE from the trajectory in the process of robotic milling was 2.79 mm. The accuracy was improved by using a trajectory error compensation algorithm and a simulation model that took into account elastic deformations of the robot's links. In this case, the deviation of the EE from the trajectory was 0.51 mm.

Thus, it can be concluded that modern mass-produced universal industrial robots in the current form cannot be used to perform precision technological operations.

## **1.2 Identification and analysis of factors affecting accuracy of movements of analytically programmable technological robots for processing objects with complex shapes of surfaces**

Modern mass-produced industrial robots usually have high repeatability values. As stated in GOST R 60.3.3.1-2016/ISO 9283:1998 [23], "positioning accuracy characterizes the difference between a given position and the average of the actual positions recorded when the robot moves to a given position from the same direction". According to [15] typically the positioning accuracy of industrial manipulators is around  $\pm 1 \text{ mm}$ , but values of  $0.3 \text{ mm}$  can be achieved using compensation algorithms. At the same time, typical repeatability values of modern robots lie in the range of  $0.1 \dots 0.03 \text{ mm}$ . That's

why high repeatability alone is not sufficient for analytically programmable technological robots performing precision technological operations.

The robot accuracy can be influenced by a number of factors, which in [15] are classified as follows:

1. Factors caused by the external environment, such as temperature change resulting in changes in link lengths, dimensions of mechanical transmission elements, dry and viscous friction coefficients, parameters of electronic components, sensitivity of sensors to temperature changes, as well as humidity, electrical noise, etc.

2. Parametric factors. These include kinematic parameters, such as length of the robot links, changes in the parameters of drives and, in particular, mechanical transmissions. Parametric factors can also include errors of manufacturing and assembly of the manipulator in the form of deviations of dimensions of the manipulation links from the nominal values, leading to displacements and misalignments of the link axes.

Parametric factors also include dynamic parameters, such as elastic compliance determined by the geometric properties and material properties of the manipulator links and the base, as well as the limited dynamic capabilities of the servo drives of the manipulators, the changing moments of inertia of the links in various manipulator configurations, as well as various nonlinearities of the drives and mechanical transmissions, such as backlash, hysteresis, etc.

3. Measurement-related factors, e. g., resolution, nonlinearity of feedback signals of the sensors.

4. Computational factors, such as errors in calculating the robot's trajectory as a result of rounding, insufficient number of bits to represent the values, discreteness of digital control processes.

5. Factors depending on the operation performed by the robot, related to the kinematics of the desired movements and the forces acting on the EE as a result of the contact interaction of the tool with the workpiece. These include errors in installation of the robot base, errors in representation of the dimensions of the machined part due to their deviation from the nominal values and values embedded in the kinematic model, errors due to inaccurate "binding" of the coordinate system of the manipulator to the coordinate system of the processed product during calibration, as well as errors introduced by changes in the hardness of the part and wear of tools, robots, etc.

It should be noted that movement accuracy of the tool of technological manipulator significantly depends on the method of organization of its control system (CS). In most modern technological robots, kinematic control is used, where the inverse kinematics problem for the manipulator mechanism is solved and the corresponding angles in its joints are calculated on the basis of the manipulator kinematics model. Reference values, proportional to the calculated angles, are set to the inputs of the manipulator's servo drives. The more accurate the kinematic model is and the more fully action of external factors is

taken into account, the higher is the accuracy of tool movements. The inconsistency of such mathematical models used for kinematic control of robot motion with real manipulators is also one of the main factors affecting robot accuracy.

In addition, kinematic control does not incorporate the dynamic properties of the manipulator and, above all, of the drives, which can also lead to increase in deviation of the center point of the tool from its desired trajectory.

In the papers [16, 17] it is proposed to divide a number of factors that negatively affect accuracy of the manipulator, which may not be taken into account by its kinematic model, "into two groups: factors due to the features of the performed technological operation (these include factors of the 1st and 5th groups mentioned above), and factors related to the features of the technological robot" (factors of the 2nd – 4th groups mentioned above). Further in the course of the research, presented in this paper, we will focus on the factors associated with the features of the technological robot, since these factors have the greatest impact on accuracy of manipulators, as noted in [2]. At the same time, after overcoming influence of the most potent factors, it is advisable to move on to eliminating influence of other factors.

In industry, technological robots with an open kinematic chain are mainly in demand. Manipulators with a closed kinematic chain are also used to perform such technological operations as, for example, robotic milling. Although such manipulators have significantly higher accuracy, as presented in [18, 24], they have a limited workspace and cannot be effectively used for machining large parts.

However, robots with an open kinematic chain have relatively low stiffness. For example, stiffness of IRB6400 robot is about  $0.5 \text{ N}/\mu\text{m}$ , while stiffness of typical CNC milling machine tool is about  $30 \text{ N}/\mu\text{m}$ . Therefore, a force of 500 N acting on the robot tool results in tool position error of about 1 mm. The same force, if machine tool is used, will cause deviation less than 0.02 mm, as stated in [25].

The results of various theoretical and experimental studies [13, 15, 26] show that the main factors that reduce the positioning accuracy and stiffness of the robot, also during the robotic milling operation, are elasticities and backlashes of the mechanical transmissions of the manipulator drives. For example, "when using the most common in robotics planetary and wave gearboxes, which have errors of 3... 6 arc minutes, the error component of the position of the manipulator link with length of 1 meter can reach 1.75 mm. And at the action of external forces and moments of unbalance forces of manipulation mechanism of TR with open kinematic chain the elasticity of such transmissions can lead to an error of 5...10 mm", as noted in [81]. This factor significantly limits the usage of manipulators with such drives for operations that require increased accuracy of movements of end effector.

Therefore, traditional geared drives turn out to be of little use for the construction of precision technological robots. Hence the conclusion follows that in order to improve accuracy of technological

robots, it is necessary first of all to achieve increase in accuracy and rigidity of their servo drives, while not worsening their performance. Therefore, the further research is aimed at finding ways to improve accuracy of movements of technological robots as a result of improving their digital servo drives.

### **1.3 Analysis of known solutions of construction of high-precision technological robots**

To reduce influence of the factors, listed in the paragraph 1.2, on the manipulator accuracy, it is advisable to carry out a number of measures. Thus, in case of imperfect mathematical models and their deviation from the actual manipulators and in case of inaccurate “binding” of the manipulator coordinate system to the coordinate system of the workpiece, it is advisable to complicate the kinematic model used in robot programming by introducing data of manipulator calibration. The accuracy of robot calibration can be further improved, for example, by using additional equipment, such as laser tracker that monitors movement of the manipulator tool in workspace, as suggested in [27, 28]. It may also make sense to correct the parameters of the mathematical model as a result of identification of kinematic parameters of the manipulation mechanism. Dynamic identification of manipulator parameters and its control on the basis of these parameters require a very large volume of calculations, which is still not economically favourable for many tasks solved with the help of industrial robots.

When the dimensions of machined parts and assemblies deviate from their nominal values, it may also make sense to check the manufacturing quality of these parts and assemblies before they enter the manipulator's workspace.

If the error component of the manipulator link position sensors is significant, it is naturally advisable to increase accuracy of these sensors, to use precision sensors, for example, photoelectric sensors.

In case of insufficient rigidity of the manipulation mechanism links, it is advisable to increase the metal content of the mechanism, to use materials with the highest possible modulus of elasticity. However, this will lead to a significant increase in its cost. Therefore, it is important to maintain balance between rigidity of the links and cost of the manipulation mechanism.

The main factors listed above that reduce movements accuracy of technological robots and limit their application, as well as the ways to reduce the influence of these factors, are listed in Figure 1.1.

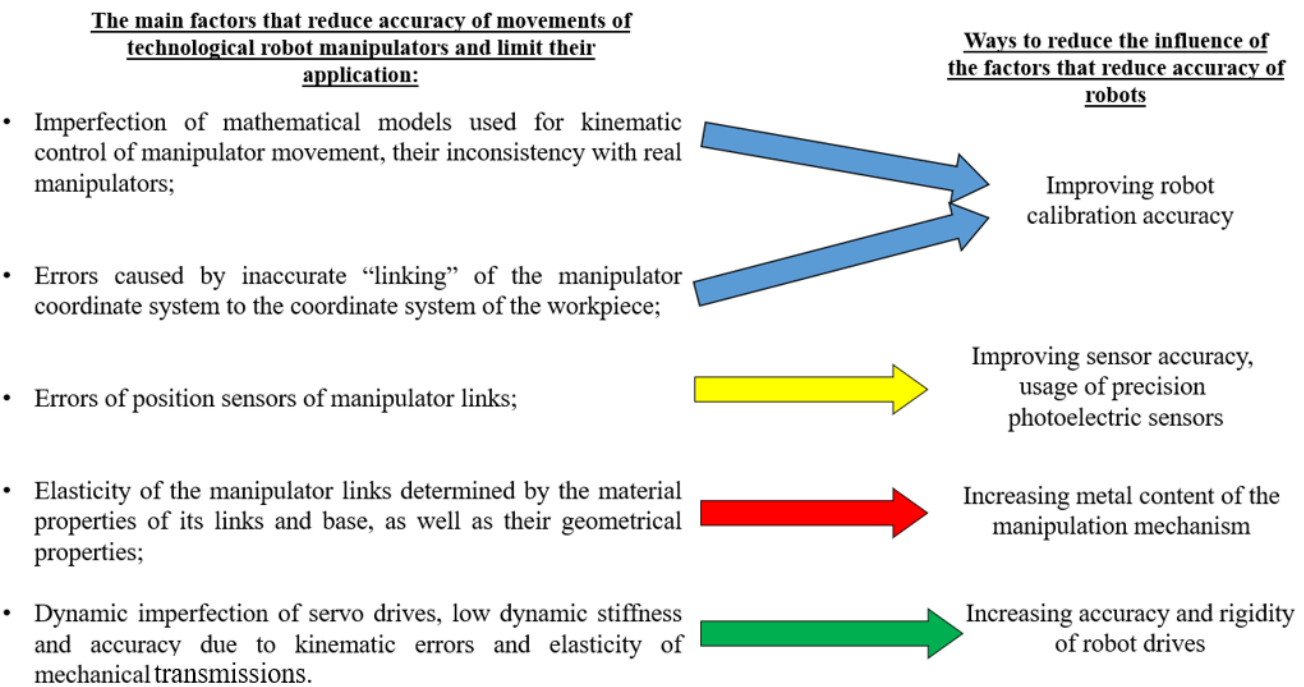


Figure 1.1. Main factors reducing accuracy of technological robots' movements and the ways to reduce influence of these factors

To reduce the influence of dynamic imperfections of servo drives on accuracy of technological manipulators, it is advisable to increase accuracy and stiffness of robot drives themselves. At present, considerable efforts of scientists are aimed at increasing accuracy of servo systems with elastic mechanical transmissions and improving their control methods, as demonstrated in [29-40]. Increase in accuracy and stiffness of robot drives can be achieved, for example, by using gearless drives. However, the usage of gearbox, as a rule, improves mass, energy and cost parameters of the drives and the robot as a whole. Therefore, in contrast to the machine tool industry, where gearless drives are widely used, as for example in [41], in robotics, mainly geared servo drives closed by position control loop of the motor shaft are used, as discussed in [29, 42]. In such drives, mechanical transmission is outside the closed position control loop, which, of course, simplifies the solution of the problem of ensuring stability of servo drives and technological robots in general. However, accuracy of tool movements can be significantly reduced due to influence of elastic deformations and backlashes in mechanical gears. Nevertheless, the question of feasibility of using gearless servo drives remains open and requires more thorough research.

It is also possible to reduce the influence of the dynamic imperfection of servo drives by introducing corrective and compensating links. For example, by introducing corrective feedback by the signal from an external sensor that determines position of the Tool Centre Point (TCP) of the manipulator. However, the introduction of such links is often ineffective in practice due to the influence of nonlinearities such as ‘dead zone’ caused by gear backlash.

Nowadays, mechanical backlash-eliminating devices are sometimes used, which allow us to eliminate the system's self-oscillations. But such devices are also characterized by the presence of an elastic element, which introduces even greater elastic deformations into the system, as noted in [2, 29]. At the same time, increase in the stiffness coefficient of such devices is possible only by increasing their mass-dimensional parameters, which is not favorable from the economic point of view. In order to bring the values of stiffness coefficients of the manipulator with such devices in the drives up to the values peculiar to machine tools, such devices should be incommensurably large in comparison to the manipulator. In this case, their mass increases significantly, which requires the usage of significantly more powerful motors. Therefore, their application in robotics turns out to be unjustified.

In machine-tool construction, for example, the influence of backlash is often compensated by correcting the reference input generated by CNC devices, as demonstrated in [34, 37, 38], but this approach has not been widely used in technological robotics. "It is not possible to significantly improve accuracy in this case, especially with frequent changes in the direction of motion of the control object", as noted in [55]. Some tasks requiring increased accuracy of manipulator movements, such as inserting studs into holes, can be solved through the usage of remote compliance devices (RCCs) and force and moment sensors. These devices work well for robot and workpiece inaccuracy, but they also have an elastic element, which introduces even more elastic deformation into the system. In addition, it is theoretically possible to create an adaptive control system with dynamic trajectory correction set by the robot controller taking into account the manipulator deviations [19 - 22, 24, 25, 43 - 48], or to apply artificial intelligence methods [49 - 54]. But in all the above cases, backlash of mechanical gears of the robot drives is still physically unselected, which is especially evident when external forces or forces caused by the unbalance of the manipulator mechanism act on the manipulator tool. Also, when using analytical programming of technological robots, it limits the trajectory of the robot's EE motion, forcing while programing to exclude from trajectory the areas with a sharp change of the direction of EE motion, since in this case backlashes of mechanical gears of the robot's drives still physically manifest themselves, which leads to a deviation of the EE from the desired position.

Thus, we can conclude that there is a problem in robotics, that the usage of modern serial technological manipulators in the operations listed in paragraph 1.2 is significantly limited due to their insufficient accuracy and stiffness of their drives, which include mechanical gears. Therefore, the task arises of searching for ways to reduce influence of elasticity and backlash of gearboxes of servo drives on accuracy of technological robots.

In this case, it is quite rational to use drives with two coordinated controlled motors. One of them is a part of the main servo drive closed by position control loop of the manipulator link, and the second one, called loader, plays the role of a torque generator counteracting the main motor. The peculiarities

of construction of such type of drives are considered in [2, 29, 55, 56]. Due to a significant increase in stiffness of dual-motor geared drives, the movement of the robot's EE along a given trajectory is carried out with high accuracy. However, the usage of dual-motor drives is accompanied by two serious problems. Firstly, the inclusion of an elastic gearbox with backlash in the control loop can lead to intensive self-oscillations, which must be excluded. Secondly, electromechanical drive subsystems are prone to the occurrence of relatively low-frequency weakly damped oscillations that need to be damped, as noted in [59].

Earlier works have already been published on dual-motor drives, but operating with a split load, as well as on two-channel tracking drives operating on the principle of coarse and fine control, e.g. [29]. The usage of these types of drives can eliminate backlash caused by mechanical transmissions and can eliminate self-oscillations. However, deflections introduced by deformations of the transmissions of the actuators when external forces act on them remain unselected.

In dual-motor drives the negative influence of elasticities and backlashes of transmissions is excluded due to force closure of elastic elements of the main servo drive and the loader. The structure of such a drive implies an installation of the main position feedback sensor on the rotation axis of the manipulator link, which is unconventional for robotics. However, as shown in [29], “a nonlinear element of the type “dead zone”, which is inside the position control loop, in combination with elasticity of the mechanical transmission, is capable of causing self-oscillations in the drive. The drives, in which significant amplitudes of self-oscillations are observed, do not provide the required accuracy of the EE position, they quickly wear out and therefore are unsuitable for creation of precision TR. Thus, when using drives of such a structure, there is a problem of exclusion of intensive self-oscillations.

In [29], servo drives with backlashes and elastic deformations of mechanical gears are analyzed, and conditions for the occurrence of self-oscillations are considered. The equations, obtained using transfer functions of such drives, which characterize conditions of occurrence of self-oscillations, are presented there. From these equations the conditions when these equations have no solution, which means when the existence of limit cycles is impossible, are obtained. As a result, it is proved there that the disruption and exclusion of self-oscillations in servo drive with backlash and elastic deformations is possible only in the presence of constant acting torque applied to the shaft of the control object.

Secondly, electromechanical subsystems of drives due to insufficient stability margins of their control system are prone to occurrence of relatively low-frequency weakly damped oscillations. Therefore, the problem of damping such oscillations also arises. But in the literature the solutions, simultaneously excluding limit cycles and realizing necessary damping of oscillations, are insufficiently considered. Most of the known solutions are aimed at increasing the malleability of robots [61-63], which contradicts the above-mentioned requirements.

Examples of application of dual-motor drives to compensate influence of mechanical gear backlash can be found in [29, 56 - 58]. In [57], the structure of a dual-motor drive organized on the master / slave principle is proposed, shown in Figure 1.2. Such a drive is controlled by a numerical control system, where the required torque value between the master and slave motors is calculated.

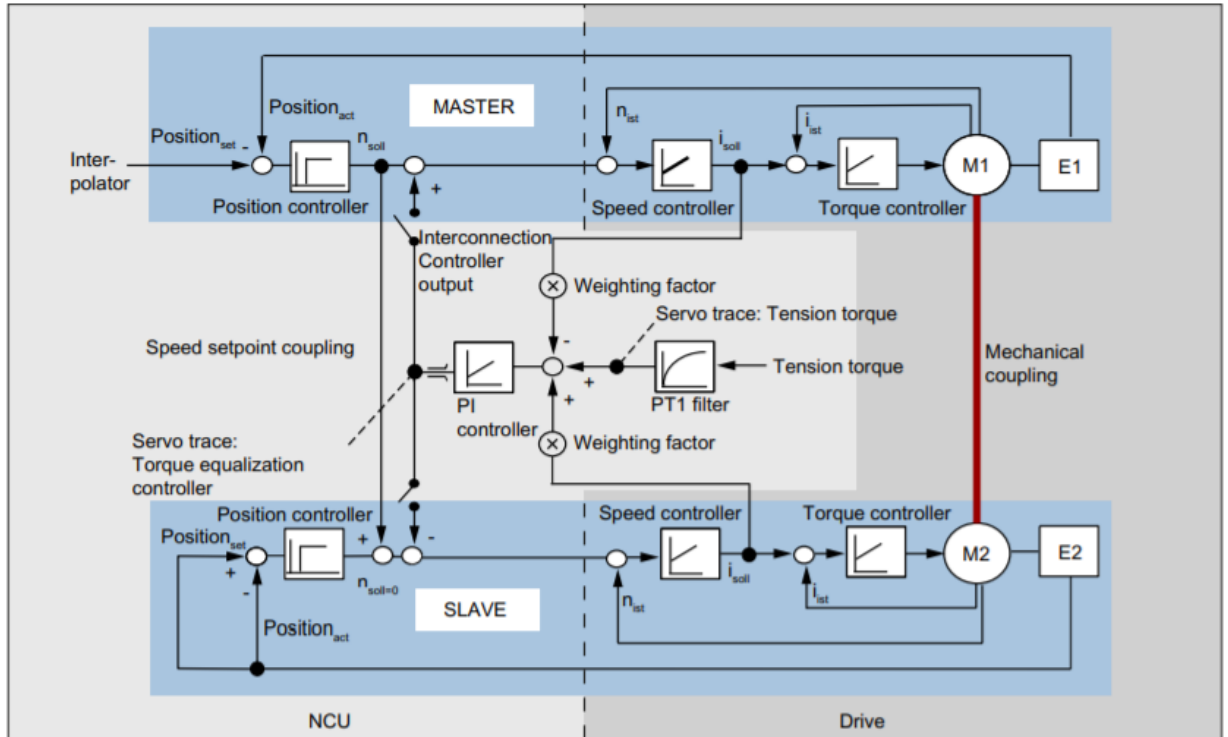


Figure 1.2. Structure of a dual-motor drive operating in master/slave mode

This structure is used to determine the speed setpoint for the master and slave drives. However, this drive is only speed-controlled, not position-controlled. There is no separate position control between the master and slave drives. Also, a significant disadvantage of this structure is that there is no position control of the control object. Here position sensors, that are mounted only on the shafts of the master and slave motors, are used.

In works [56, 58] application of dual-motor drives for construction of manipulator EU FP-6 project SMErobot with parallel kinematic structure is proposed. However, manipulators of anthropomorphic type with open kinematic chain have a larger workspace as a rule, they are able to move the tool to hard-to-reach places of the processed products. Figure 1.3 shows the structure of the dual-motor drive proposed in [56]. Here, as well as in Figure 1.2, there is no position sensor of the control object, and the Cart, acting as a control object, is outside the position control loop.

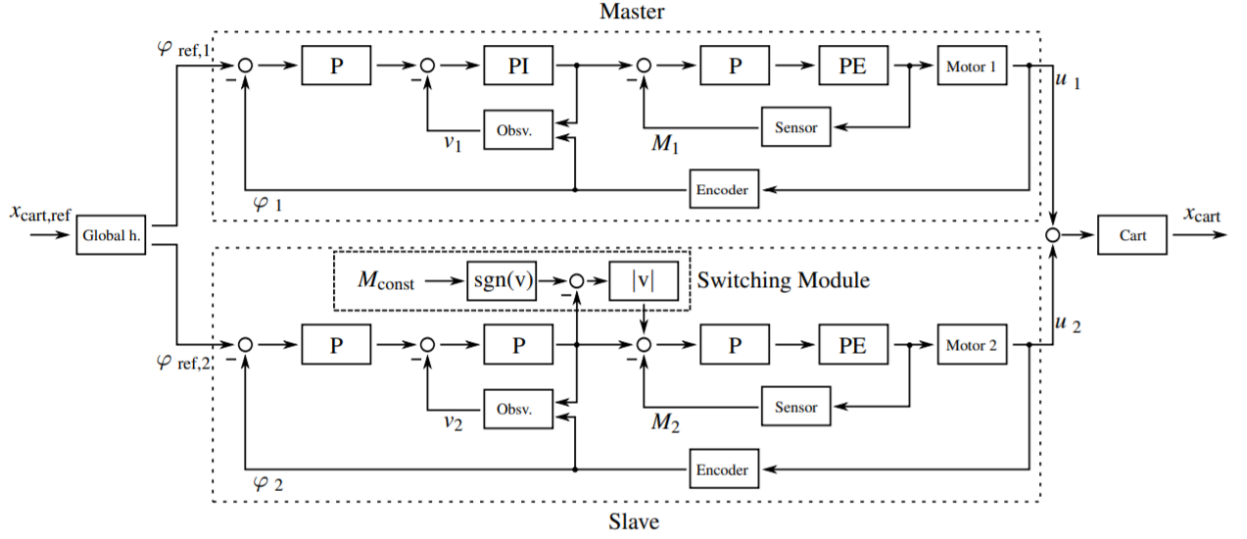


Figure 1.3. Structure of the dual-motor actuator proposed in [56].

In [58], different control strategies for a dual-motor drive with rack-and-pinion gears for the same manipulator with a parallel kinematic chain are investigated. The structure of such a drive is shown in Figure 1.4, where signals  $u_1$  and  $u_2$  correspond to the desired torque values applied to the first and second motor.

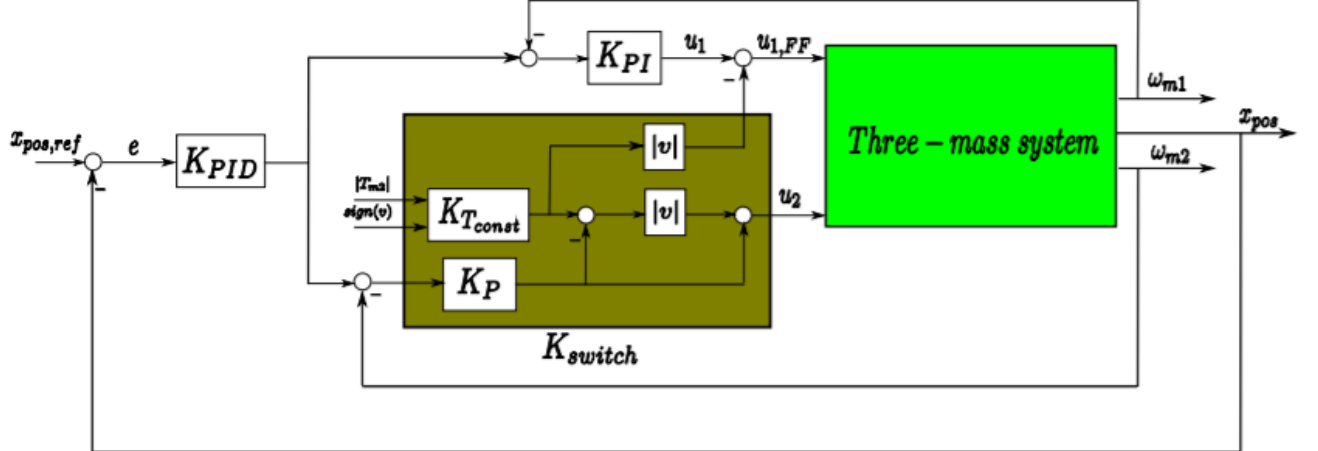


Figure 1.4. Structure of a dual-motor drive controlled by the position of the control object.

In this paper, the drive is firstly considered as a 2-mass nonlinear system consisting of a single motor and load. An experiment is then conducted to confirm that the effects of backlash and elasticity of the mechanical transmission on the position of the control object in such a 2-mass system can be eliminated. Then the actuator is considered as a 3-mass nonlinear system consisting of two motors and a load. In this structure, the actuator is already controlled by the position of the control object. At the same time, when conducting computational experiments with the help of computer simulation, the drive

formed by the first motor is not considered as a system of cascade control loops with current, velocity and position feedback loops of its shaft, but simplistically only velocity feedback loop. The loader here is also considered. However, in a drive of this structure, the current, velocity and position control loops of the first motor can have a significant effect on the dynamic properties of the entire dual-motor drive, so they must also be considered.

The thesis [2] presents the concept of a precision drive with a backlash-eliminating device acting as a loader. However, the issues of practical application of such drives for construction of technological manipulators are not sufficiently considered there. At the moment there are no experimental studies of dynamic properties of such drives, which could confirm the feasibility of their usage for constructing technological robots. There are also no works in which at least by means of computer simulation the analysis of accuracy of technological operations, for example, robotic milling, performed by a manipulator built on dual-motor drives has been carried out.

To summarize, we can state that from the known solutions physically backlash is excluded and also the elasticity of mechanical gears of drives is significantly reduced only when using gearless and dual-motor geared servo drives. As it is stated in [2], “at existence of several admissible technical solutions satisfying the presented requirements, the variant which is characterized by the minimum value of its complexity estimation as well as the best values of mass and dimensional indices should be chosen”. In [2] it is proposed to use its cost as the main criterion for assessing the complexity of the control system of a robotic system. Thus, it is important to compare the mass dimensions and cost of construction of robots on gearless and dual-motor geared servo drives.

#### **1.4 Comparison of weight, size and cost indicators of technological robots built on geared dual-motor servo drives with technological robots built on gearless drives**

As discussed in paragraph 1.3, gearless (direct) drives can be used to eliminate errors and elastic deformations in mechanical gears. Their main advantages are that there is no backlash caused by the transmissions, but such drives can be unnecessarily massive and expensive when installed on an industrial robot. The usage of dual-motor drives can also result in a significant increase in the mass and cost of a technological manipulator built on them.

Therefore, for the usage of drives with this structure in technological manipulators, the problem of economic justification of the usage of the second motor and gearbox arises. It is necessary to evaluate the feasibility of constructing a technological manipulator on drives of this type and to analyze their properties and their influence on the characteristics of the robot built on these drives in comparison with gearless drives.

To solve this problem, the selection of commercially available motors and gearboxes for dual-motor drives, as well as motors for gearless drives of manipulator links of medium load capacity is carried out. Power, mass-size and cost parameters of manipulators with both types of drives are determined and compared.

In the majority of technological manipulators of average load-carrying capacity, produced nowadays in series, the motors of drives of the fourth, fifth and sixth links are located on the third link, which provides the equilibrium of the whole mechanism, especially when a heavy tool or an object to be moved is installed on the manipulator flange. In such a case, the torque is transmitted to the manipulator links by means of long shafts and belt gears. At the same time, the motors of the first, second and third links are located directly on the axes of the links driven by them. In general, in manipulators with an open kinematic chain the major axes and the major links are being distinguished (column, shoulder, elbow links), which move the tool or workpiece in space, and minor links (fourth, fifth, sixth links), which control its orientation. We will call the links set on the major axes as carrying links and the links set on the minor axes as orienting links.

Orienting links, as a rule, have small lengths in comparison with the carrying links, therefore, when the output shafts of the drives of these links deviate from their desired values due to the presence of elasticity and backlash of mechanical gears, their contribution to the deviation of the manipulator tool from the set position is significantly less. Therefore, this study considers the manipulator design with installed dual-motor and gearless drives only on the carrying links. In general, such a design requires further research and development, however, the objective of this study is to prove the feasibility of this arrangement of dual-motor drives compared to direct and torque drives. It is accepted in this study that such a design is physically realizable.

In universal 6-axis industrial robots, the “shoulder” link is the first rotational kinematic pair, so all forces and moments developed by the actuators of this link are not balanced by the reaction forces and moments of the links they hold, as noted in [4]. The drive of the robot column rotation, in turn, has an error that is not compensated by the static moment of the other robot links. Thus, the drives of these links are of the greatest interest in the study, as being the most loaded and contributing the largest component of the positioning error of the robot.

### 1.4.1 Parameters of the manipulation mechanism

In this study, a manipulation mechanism with load capacity of 16 kg and six degrees of freedom is considered. The most frequently used in modern robotics AC synchronous motors with vector control are considered. The kinematic diagram of the manipulator is shown in Figure 1.5.

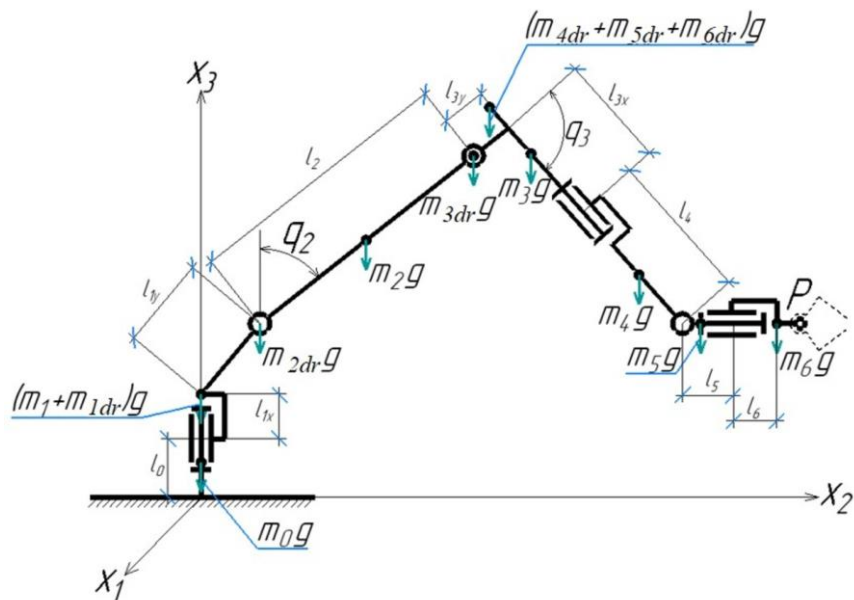


Figure 1.5. Kinematic diagram of the manipulator

Table 1.2 presents the values of kinematic parameters of the manipulation mechanism involved in the study. In the course of analyzing the manipulator parameters for motor selection, first of all, it is necessary to determine the required nominal angular velocities and torques developed by the drives. On their basis it is necessary to determine the permissible values of transmission ratios and moments of inertia of gearboxes. To determine the parameters of dual-motor drives, the parameters of single-motor geared drives are determined first, then based on these data the parameters of loader motors and gearboxes are determined. To ensure elimination of backlash in such a drive when changing the direction of motion of the control object, the same requirements are imposed on the power and rated torque of both of the motors.

Table 1.2 - Parameters of the manipulator

	base	links					
		column	shoulder	elbow	fourth	fifth	sixth
Mass, kg	53	39.7	24.3	22.2	5.6	4.5	0.2
Length, m	$l_0 = 0.39$	$l_{1x}=0.26$ $l_{1y}=0.285$	$l_2 = 0.715$	$l_{3x}=0.26$ $l_{3y}=0.035$	$l_4 = 0.18$	$l_5=0.15$	$l_6=0.01$

The maximum values of angular velocities of carrying manipulator links, which should be provided by its drives, are presented in Table 1.3. They are taken in accordance with such values of modern serially produced universal industrial robots.

Table 1.3 - Maximum angular velocities of carrying manipulator links

	<b>Manipulator column</b>	<b>Shoulder link</b>	<b>Elbow link</b>
maximum angular velocity, rad/s	2.72	2.72	2.72

The required torques to be developed by the drives of the manipulator's carrying links are calculated in accordance with the method of calculating energy parameters of drives, presented in [64], and the required motor power is estimated. The calculation assumes that the dynamic stiffness of the drives is infinitely high. In this case, the mutual influence of the manipulator mobility degrees does not manifest itself, and it can be considered that when one of the links moves, the others remain stationary. Therefore, when calculating the required torques developed by the drives, in addition to static moments, dynamic moments are taken into account, but depending only on the moment of inertia of the links of the manipulation mechanism. As a result, the requirements presented in Table 1.4 are obtained. As can be seen in the table, the column and shoulder link drives have the same power requirements. This is due to the fact that the maximum moment of inertia of the drives of these links is practically the same, and it is achieved when the manipulator is pulled when its TCP is maximally distant from its base.

Table 1.4 - Requirements to the drives of manipulator links

	<b>Manipulator column</b>	<b>Shoulder link</b>	<b>Elbow link</b>
<b>M, N*m</b>	964.5	964.5	438.2
<b>ω, rad/s</b>	26	26	26
<b>P, W</b>	2626	2626	1193

According to these requirements, motors and gearboxes, mass produced by the industry at present, were selected. According to the methodology presented in [64], firstly, the selection of motors was carried out according to the known values of the required power, presented in the Table 1.4. Then the necessary gear ratios were determined and the gearboxes were selected taking into account that their backlash should not exceed 1 arc minute. It was also necessary to ensure that the rated speed and torque values of the selected gearboxes are greater than the previously calculated required values. It was also important at this stage to pay attention to the moment of inertia. The total moment of inertia  $J_{dr}$  of the motor and gearbox corresponds to the maximum load. With the already known values of the load

moment of inertia on the gearbox output shaft  $J_{load}$  and the moment of inertia of the motor rotor  $J_{mot}$ , the range of possible gearbox ratios  $i_{red}$  can be selected using the formula:

$$J_{dr} = J_{mot} + J_{red} = \frac{J_{load}}{i_{red}^2}.$$

$$\frac{J_{dr}}{J_{red}} \leq 1 - \text{almost shock-free load};$$

$$\frac{J_{dr}}{J_{red}} \leq 3 - \text{moderate shock load};$$

$$\frac{J_{dr}}{J_{red}} > 3 - \text{impact shock load.}$$

In the industrial robot, a load with moderate shocks is adopted. Therefore, the following condition must be fulfilled:

$$1 < \frac{J_{load}}{J_{mot} * i_{red}^2} \leq 3$$

In addition, when selecting a motor-gearbox system, attention should also be paid to the following facts:

- 1) it is necessary that the gearbox fits the diameter of the motor output shaft and is easy to install;
- 2) for the TR drive, it is desirable that the gearbox has a flange instead of an output shaft;
- 3) if possible, the drive should have minimum mass;
- 4) it should also have a minimum cost.

#### **1.4.2 Selection of motors and gearboxes for dual-motor drives**

Taking into account the above-mentioned conditions, the motors and gearboxes of the manipulator's dual-motor drives have been selected. Due to the installation of the second motors and gearboxes on the manipulator, the mass of its links and total mass have increased, which has led to an increase in the required torques developed by its drives. Their newly calculated values are presented in Table 1.5. The parameters of the selected motors and gearboxes are presented in Table 1.6 for the drive of the manipulator elbow link and in Table 1.7 for the drive of the shoulder link and the column. The data on the cost of motors and gearboxes presented in the tables are obtained from different supplier companies in Moscow during the period February - March in 2018.

Table 1.5 - Requirements to the energy characteristics of dual-motor drives of carrying manipulator links

	<b>Manipulator column</b>	<b>Shoulder link</b>	<b>Elbow link</b>
<b>M, N*m</b>	1150	1150	438.2
<b>ω, rad/s</b>	26	26	26
<b>P, W</b>	3132	3132	1193

Table 1.6 - Results of motors and gearboxes selection for dual-motor drive of elbow link

Nº	U <sub>nom</sub> , V	A <sub>nom</sub> , A	n <sub>nom</sub> , rpm	M <sub>nom</sub> , N*m	W, W	J <sub>mot</sub> , kg*m <sup>2</sup>	m, kg	S <sub>l</sub> , mm	S <sub>w</sub> , mm	P, €
<b>Motors of the drive of elbow link</b>										
1	Siemens 1FK7060-5AF71-1EB5									
	600	3.7	3000	4.7	1476.5	7.7 · 10 <sup>-4</sup>	8.302	200	126	1793.8
2	KEB C4.SM.001-320F									
	230	7.1	3000	5	1476.5	5.4 · 10 <sup>-4</sup>	6.6	294	92	2220.8
3	Kollmorgen AKM43L-ANC22-004572									
	240	11.2	6000	4.73	1590	2.16 · 10 <sup>-4</sup>	4.98	210.3	100	1975.1
4	Bosch Rexroth MS2N05-C0BNN-CSLD1-NNANN-NN									
	600	3.55	3000	6.1	1916.4	4 · 10 <sup>-4</sup>	7	254	98	1096
5	Mitsubishi HG-JR153BWDC									
	200	11	3000	4.8	1508	4.3 · 10 <sup>-4</sup>	7.3	245	90	1949.4
<b>Gearboxes of the drive of elbow link</b>										
Nº	i <sub>gear</sub>	n <sub>nom</sub> , rpm	M <sub>nom</sub> , N*m	C <sub>gear</sub> , N*m/rad	J <sub>gear</sub> , kg*m <sup>2</sup>	m, kg	S <sub>l</sub> , mm	S <sub>w</sub> , mm	P, €	
1	Spinea TS170-125-E-P19-0589 A with flange for motor mounting									
	125	2000	495	378152	1.15 · 10 <sup>-4</sup>	10.8	93	190	3729	
2	Harmonic Drive HFUC-50-2UH 120 (oil lubrication) can be used with Siemens 1FK7060-5AF71-1EB5 motor according to the requirement to moment of inertia; a housing with bearings and mounting for the motor is required									
	120	3000	529	440000	12.6 · 10 <sup>-4</sup>	8.9	90	190	6209.2	
3	Wittenstein TP 050S-MA3-110-0G1 with mounting for motor									
	110	3500	675	44690	2.2 · 10 <sup>-4</sup>	13.4	206	179	3904	
4	Fyne Cyclo FC-A35G i=119 with adapter for motor mounting									
	119	2975	544	110000	4.58 · 10 <sup>-4</sup>	9.6	85	180	1710	
5	Nabtesco RV-60 i=121 a housing with bearings and mounting for the motor is required									
	121	6050	547	196000	0.328 · 10 <sup>-4</sup>	10	71.5	200	1719	

Table 1.7 - Results of motors and gearboxes selection of dual-motor drives for column and shoulder links

Nº	U <sub>nom</sub> , V	A <sub>nom</sub> , A	n <sub>nom</sub> , rpm	M <sub>nom</sub> , N*m	W, W	J <sub>mot</sub> , kg*m <sup>2</sup>	m, kg	S <sub>l</sub> , mm	S <sub>w</sub> , mm	P, €
<b>Motors of the drives of column and shoulder links</b>										
1	Siemens 1FK7083-2AF74-1EB1									
	600	7.4	3000	10.5	3298.7	$26 \cdot 10^{-4}$	15.9	266	130	1930.4
2	KEB D4.SM.001-420F									
	230	18.2	4000	12	3602.4	$12.7 \cdot 10^{-4}$	11.2	315	110	2848
3	Kollmorgen AKM52L-ANC22-00									
	240	11.6	3500	8.7	3177.7	$6.37 \cdot 10^{-4}$	6.9	203.5	130	1979.9
4	Bosch Rexroth MS2N06-D1BNN-CSUL2-NNANN-NN									
	600	4.9	3000	9	2827.4	$15.4 \cdot 10^{-4}$	10.5	254	261	1241
5	Mitsubishi HG-JR353BWDC									
	200	17	3000	10.5	3298.7	$13.2 \cdot 10^{-4}$	13	228	130	2534.9
<b>Gearboxes of the drives of column and shoulder links</b>										
Nº	i <sub>gear</sub>	n <sub>nom</sub> , rpm	M <sub>nom</sub> , N*m	C <sub>gear</sub> , N*m/rad	J <sub>gear</sub> , kg*m <sup>2</sup>	m, kg	S <sub>l</sub> , mm	S <sub>w</sub> , mm	P, €	
1	Spinea TS220-125-E-P28-0585 with flange for motor mounting									
	125	2000	1250	1065702	$4.8 \cdot 10^{-4}$	22.4	131.5	238		4327.4
2	Harmonic Drive HFUC-65-2UH 120 (oil lubrication) a housing with bearings and mounting for the motor is required									
	120	2400	951	980000	$46.8 \cdot 10^{-4}$	20.9	115	260		8244.9
3	Wittenstein TP 110S-MA3-110-0K1 with mounting for motor									
	110	3000	1750	4992000	$9.8 \cdot 10^{-4}$	35.4	258.4	247		5598
4	Fine Cyclo F2C(F)-T455 i=118,5 requires a mounting for the motor installation									
	118.5	2962	1090	732200	$1.92 \cdot 10^{-4}$	24	113	230		4265
5	Nabtesco RV-160 i=129 a housing with bearings and mounting for the motor is required									
	129	3225	1343	1348000	$1.1 \cdot 10^{-4}$	20	96	239.9		2370

#### 1.4.3 Selection of gearless drive motors (direct drives)

When gearless drives were installed on the manipulator, the mass of its links and its total mass increased, which also led to an increase in the required torques developed by the drives. Their newly calculated values are presented in the Table 1.8.

Table 1.8 - Requirements to the energy characteristics of gearless drives of carrying manipulator links

	Manipulator column	Shoulder link	Elbow link
M, N*m	1160	1160	438.2
o, rad/s	26	26	26
P, W	3159	3159	1193

A significant disadvantage of such drives is the need to provide a coolant supply to obtain the required energy performance. This is particularly difficult in robots with open kinematic chains, which severely limits the usage of such drives in robotics.

It is also worth adding that at present the choice of gearless drive motors is not so large. In the power range under consideration, the choice is very limited, as the industry mainly uses more dynamic drives with lower torque and higher speeds. This makes it necessary to select motors with higher power rates, which are able to provide high torque at low speeds.

Table 1.9 – Results of the selection of motors of direct drive for elbow link

Nº	U <sub>nom</sub> , V	A <sub>nom</sub> , A	n <sub>nom</sub> , rpm	M <sub>nom</sub> , N*m	W, W	J <sub>mot</sub> , kg*m <sup>2</sup>	m, kg	S <sub>l</sub> , mm	S <sub>w</sub> , mm	P, €
<b>Motors of the drive of elbow link</b>										
1	Siemens 1FW6160-0TB07-1JC2 coolant supply, US patent US5584621 for use in robot joints, bearings, encoder, brake are required									
	600	18	594	170	10574.6	0.258	48.3	130	440	9703.8
2	Etel TMB+0360-070 TF coolant supply, housing, bearings, encoder, brake are required									
	600	56.7	596	26	1622	0.152	39.9	130	365	don't ship to Russia
3	Kollmorgen KBMS-88H03-C housing, bearings, encoder, brake are required									
	400	45.2	545	425	24255.7	0.315	11	270.8	331.5	22625.9
4	Bosch Rexroth MST290E-0004-FH-NOPU-NNNN и MRT290E-3N-0200-NNNN coolant supply, housing, bearings, encoder, brake are required									
	540	12.5	575	40	2408.5	0.17	36.7	195	310	7584
5	Alxion 500STK2M 2C010HA coolant supply, housing, bearings, encoder, brake are required									
	400	14.8	588	50	3078.8	0.433	43	120.5	502	5260

Table 1.10 – Results of the selection of motors of direct drive for column and shoulder link

Nº	U <sub>nom</sub> , V	A <sub>nom</sub> , A	n <sub>nom</sub> , rpm	M <sub>nom</sub> , N*m	W, W	J <sub>mot</sub> , kg*m <sup>2</sup>	m, kg	S <sub>l</sub> , mm	S <sub>w</sub> , mm	P, €
<b>Motors of the drives of column and shoulder links</b>										
1	Siemens 1FW6190-0TB10-2JC2 10 bar coolant supply, US patent US5584621 for use in robot joints, bearings, encoder, brake are required									
	600	30	1290	70	9456	0.678	75.8	160	502	14065.2
2	Etel TMB0360-150 3UFN coolant supply, housing, bearings, encoder, brake are required									
	300	72.7	1240	26	3376.5	0.327	70.9	210	385	don't ship to Russia
3	Kollmorgen KBMS-163H02-A requires housing, bearings, encoder, brake									
	400	39.5	1090	200	22828.9	1.72	136	193.3	537.2	37420.3
4	Bosch Rexroth MST450E-0006-FH-NOKR-NNNN и MRT450E-3N-0350-NNNN coolant supply, housing, bearings, encoder, brake are required									
	540	32	1400	60	8796.5	1.01	81.9	210	480	9990
5	Alxion 500STK3M 3C010HA coolant supply, housing, bearings, encoder, brake are required									
	400	30.7	1180	50	6178.5	0.649	58	148	502	6900

#### 1.4.4 Comparative analysis of weight, size and cost indicators of industrial robots built on dual-motor and gearless servo drives

After selection of motors and gearboxes of dual-motor and gearless drives of the technological robot, it is possible to obtain the mass-size and cost parameters of the manipulator itself built on them. Table 1.11 shows the initial parameters of the manipulator with conventional single-motor drives. With both gearless and dual-motor drives, the mass of the manipulator increases. In order to quantify the change in mass of the manipulator with such drives, it is necessary to determine the value of the mass of the manipulator without the drives of the carrying links. With the mass of motors and gearboxes of the carrying links of 69 kg and the total mass of the manipulator with an average load capacity of 235 kg, the mass of the robot without the drives of the carrying links is 166 kg. The approximate volume of the drives of carrying links is determined by the formula

$$\begin{aligned}\sum V_{dr} &= 2 * (\sum V_{avg_{mot}} + \sum V_{avg_{red}}), \\ V_{avg_{mot}} &= S_{l_{mot}} * S_{w_{mot}}^2, \\ V_{avg_{red}} &= \pi * S_{l_{red}} * \left(\frac{S_{w_{red}}}{2}\right)^2,\end{aligned}$$

where  $S_{l_{mot}}$  and  $S_{w_{mot}}$  – length and width of the motors of the carrying links,  $S_{l_{red}}$  and  $S_{w_{red}}$  – length and width of the gearboxes of these links, respectively. This parameter compares the volume of space occupied by the drives. The volume of the motors is defined as the volume of a parallelepiped and the volume of the gearbox is defined as the volume of a cylinder. The volume of gearless drives is also defined as the volume of a cylinder.

Table 1.11 - Initial manipulator parameters required for the study

Parameter	Value
$\sum M$ , mass of the robot without drives of carrying links, kg	166
M, robot mass, kg	235
$\sum V_{dr}$ , volume of the drives of carrying links, mm <sup>3</sup>	30 420 700
P, cost of the robot without drives of carrying links, €	39 447.8
P, cost of the robot, €	57 486

In the course of the study, the weight and dimensions of the drives were also determined. Using the available length and width data for motors and gearboxes, the space volume of the motors and gearboxes was determined using the following formula:

$$V_{\Sigma} = 2 * \left( \frac{\sum_{i=1}^5 S_{l_{mot}}}{5} * \left( \frac{\sum_{i=1}^5 S_{w_{mot}}}{5} \right)^2 + \pi * \left( \frac{\sum_{i=1}^5 S_{w_{mot}}}{5} \right)^2 * \frac{\sum_{i=1}^5 S_{l_{red}}}{5} \right).$$

The results are presented in the Table 1.12.

Table 1.12 – Comparison of mass-size and cost indicators of dual-motor and gearless drives of carrying links of manipulator

Drive type	elbow link drive					column and shoulder link drives				
	m, kg	V <sub>mot</sub> , mm <sup>3</sup>	V <sub>red</sub> , mm <sup>3</sup>	V <sub>Σ</sub> , mm <sup>3</sup>	P, €	m, kg	V <sub>mot</sub> , mm <sup>3</sup>	V <sub>red</sub> , mm <sup>3</sup>	V <sub>Σ</sub> , mm <sup>3</sup>	P, €
Dual-motor	34.6	2 464 700	3 022 079	10 973 568	9 145	71.9	5 867 650	6 620 615	24 976 537	14 135.8
Gearless	35.8	-	-	20 188 545	11 293.4	84.5	-	-	3 351 539	17 093.9

According to the presented data, we can see that dual-motor drives have smaller mass-size and cost indicators than gearless drives. Table 1.13 presents mass, dimensions and cost indicators of the technological manipulator built on dual-motor drives and the manipulator built on gearless drives.

Table 1.13 – Comparison of mass-size and cost indicators of manipulators built on dual-motor and gearless drives of carrying links

	ΣM, robot mass, kg	ΣV <sub>dr</sub> , volume of the drives of carrying links, mm <sup>3</sup>	P, robot cost, €
Dual-motor drives	344.4	60 926 643	76 864.4
Gearless drives	370.8	87 219 342	84 929

The presented data also show that the usage of gearless drives in the carrying links of technological manipulators leads to a greater increase in the mass-size and cost indicators of such robots.

Equipping the carrying links of the manipulator with gearless drives led to an increase in its cost by 47.7 %, and with dual-motor drives - by 33.7 %. The manipulator weight's increase when using gearless drives was 57.8 %, and when using dual-motor drives - 46.6 %. At the same time, the usage of almost each motor of gearless drives requires the supply of coolant and installation of additional strapping (bearings for the rotor, encoder, brake). As a result, it is concluded that the usage of gearless drives to eliminate errors and elastic deformations of mechanical transmissions in manipulators of TR leads to higher costs than the usage of dual-motor drives. Materials on this research were published in [75, 81]. Thus, taking into account the weight, dimensions and cost of the drives, it is more appropriate to construct precision technological robots on dual-motor geared drives, which are studied in more detail in the following paragraphs of the thesis.

#### **1.4.5 Main results and conclusions of the comparative analysis of the usage of dual-motor and gearless servo drives**

On the basis of the conducted research the following conclusions are made:

- 1) the inclusion of mechanical gears in the control loop of the position of the CO of the drives in order to eliminate backlashes, deformations of transmissions and to exclude self-oscillations, is expedient through the usage of dual-motor actuators, in which one motor sets the speed or position of the control object, and the other is a loader that creates a resistive moment to the main motor;
- 2) the usage of gearless drives in robotics is limited;
- 3) the usage of gearless drives leads to a greater increase in energy, mass-size and cost indicators of manipulators built on such drives than the usage of dual-motor drives (without taking into account the harnessing, including couplings, shafts, bearings, as well as without taking into account the cost of maintenance of such drives, including coolant supply).

Thus, the results of this study substantiate the feasibility of using dual-motor geared servo drives for constructing high-precision analytically programmable technological robots.

#### **1.5 Rationale for the choice of the purpose and objectives of the research**

The main problem, identified as a result of the analysis of the state of the scientific research of improving accuracy of movements of technological robots with geared servo drives, is the limited application of modern commercially available technological robots for such operations as milling, drilling, marking, assembly, measurement of coordinates of products with large dimensions and complex shapes of surfaces, deburring, laser and plasma cutting. It is caused by the lack of accuracy and rigidity of such manipulators, which does not allow them to compete with machine tools in this area, as noted in [81]. Therefore, there is a need for research that aims to improve accuracy and stiffness of technological robots without loss of productivity and expand the scope of their application. This problem is supposed to be solved by increasing accuracy and stiffness of the geared servo drives of manipulators during their analytical programming, when the drives are subjected to forces caused by the performed TO, for example, mechanical processing, as well as in the case of the need of performing fast movements along a complex trajectory, for example, in laser cutting.

Providing the research, it makes purposeful to use the methodology proposed in [2]. It is stated there that the role of negatively acting factors in the formation of the error of the EE of the TR movement

is different, and there are dominant (the strongest) factors. The proposed methodology is based on the fact that at first a hierarchy of factors is established according to the degree of their influence on the accuracy of TR, which will make it possible to eliminate them step by step when conducting the study. “In this case, each stage is associated with overcoming the influence of the most potent factor and then proceeding to eliminate the influence of subsequent hierarchically arranged factors”, as stated in [2].

As shown in paragraph 1.2, the main factors that reduce the positioning accuracy and rigidity of the robot are elasticity and backlash of mechanical gears of manipulator drives. Therefore, in order to achieve the research goal, first of all, it is important to solve the task of searching for the ways to reduce the influence of elasticity and backlash of servo drive gearboxes on the accuracy of technological robots by increasing efficiency of robot contour control systems through targeted changes in their structures and their parameter values. The solution, developed in this case, must be justified and economically more efficient than other solutions. There may be several acceptable solutions that fulfil the requirements. In this case, the solution that is characterized by the minimum value of its complexity estimation should be chosen. In [2] it is proposed to use its cost as the main criterion for assessing the complexity of the control system of a robotic system.

The other task is to develop a mathematical model and a structural scheme, which by control means provide significantly higher static and dynamic accuracy and stiffness of the robot without loss of speed and without changing structural elasticity of gears of the technological robot. It should differ from the known solutions by purposeful increase in dynamic stiffness of the drives and damping of oscillations in a dual-motor servo drive with elastic gearboxes with backlash.

The most expedient way to solve the problem of increasing accuracy and rigidity of technological robots, according to the analysis in paragraph 1.4, is to use the concept of a precision drive with a controlled backlash-eliminating device proposed in [2]. The usage of classical gearless drives, which develop high torque but low rotational speed, to play the role of a loader (backlash- eliminating device), is not suitable for application in robotics, because it leads to a significant increase in the mass-dimensional parameters of the drive, as shown in paragraph 1.4. It seems to be quite feasible to use a velocity-controlled, torque-limited, geared drive as a loader. This would allow the usage of commercially available drive modules with current and velocity control loops as loaders without the necessity to design and manufacture such modules, which would significantly increase the cost of such a solution. Therefore, one of the objectives of the research is to conduct a computer study of the dynamic properties of a dual-motor drive with such a loader in order to determine the possibility of using such drives to build manipulators of TR.

At the same time, there arises the task of computer simulation and research of dynamic properties of precision technological robots built on the drives of the developed structure in comparison with the

robots built on the drives of the traditional structure. The task arises to develop recommendations for tuning the parameters of mathematical models of such drives. In addition, there is a task of creating a methodology for assessing accuracy of movements of technological robots with the proposed and traditional structures of control system, as well as the task of comparing these assessments. It is important to establish qualitative and quantitative relationships of deviation from the desired trajectories of the manipulator with the developed structure when performing movements along different typical trajectories at different motion parameters, especially during the execution of technological operations like robotic milling.

The materials presented in this chapter have been published by the author in [75, 81, 82, 85].

## **1.6 Conclusions on the first chapter**

In the first chapter, as a result of analyzing the requirements to the motion parameters of robots' EE at precision technological operations, it was concluded that modern mass-produced universal industrial robots as they are, cannot be used to perform precision technological operations.

In order to increase accuracy of robots, it is necessary to achieve, first of all, increase in accuracy and rigidity of their servo drives, including mechanical gears, without worsening their performance. Therefore, there arises a scientific problem of searching for ways to reduce the influence of elasticity and backlash of gears of servo drives on the accuracy of technological robots. From the known solutions presented in the first chapter, backlash is physically eliminated and the elasticity of the mechanical gears is significantly reduced only when using gearless and dual-motor geared servo drives. And as a result of the study presented in paragraph 1.4 comparing mass, dimensions, and cost indicators of constructing high-precision analytically programmable TR on geared dual-motor and gearless drives, the feasibility of using dual-motor drives is shown.

The chapter concludes with a justification of the choice of the aim and objectives of the research. It is noted that it is quite reasonable to use as a loader a geared servo drive, controlled by velocity in the torque limiting mode. Therefore, it is important to carry out a simulation study of the dynamic properties of a dual-motor drive with such a loader in order to determine the possibility of using such drives for the construction of manipulators of TR. At the same time, it is also important to carry out a simulation study of the dynamic properties of technological robots built on such drives in comparison with the robots built on the drives of the traditional structure.

## CHAPTER 2. DESIGN FEATURES AND PROPERTIES OF PRECISION GEARED SERVO DRIVES FOR ANALYTICALLY PROGRAMMABLE TECHNOLOGICAL ROBOTS

### 2.1 Concept of precision geared servo drives for analytically programmable robots

At present, commercially available anthropomorphic-type technological robots are built mainly on geared servo drives of traditional structure. Such a drive is shown schematically on Figure 2.1 and its structure - on Figure 2.2. In such a drive, the position sensor of the main feedback is mounted on the motor shaft, and the gearbox, which has backlash and elastic deformation, is outside the closed position control loop. This structure provides stability, but reduces the positioning accuracy of the manipulator link, which is unacceptable for the construction of precision technological robots.

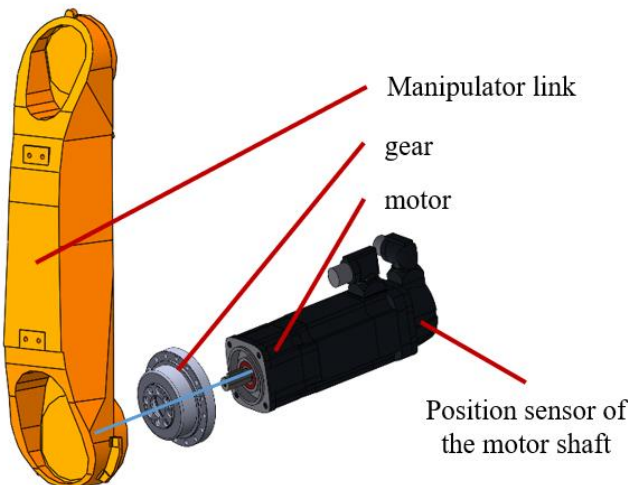


Figure 2.1. Conventional geared servo drive of a technological robot

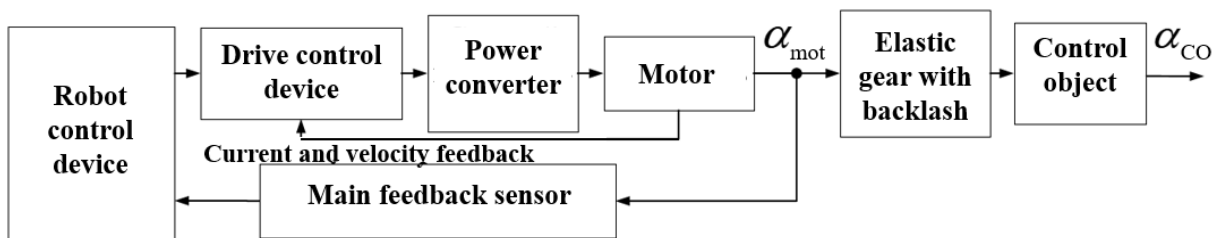


Figure 2.2. Structure of conventional geared servo drive of technological robot

In the first chapter, as a result of the analysis of the main factors that reduce accuracy of movements of technological robots and ways to reduce their influence, it is concluded from the known solutions that backlash is physically excluded and elasticity of mechanical drives is significantly reduced

only when using gearless and dual-motor geared servo drives. As a result of comparative analysis of the weight, size and cost indicators of industrial robots built on dual-motor and gearless servo drives, the expediency of using such drives for the construction of technological robots is substantiated.

First of all, the difference between the structure of such a drive and the structure presented in Figure 2.2 is the installation of the main feedback sensor of the drive's position on the shaft of the control object, that means on the rotation axis of the manipulator link, which is unconventional for servo drives of robots. The structure of such a drive is shown in Figure 2.3. In particular, such a solution is proposed in [2, 31].

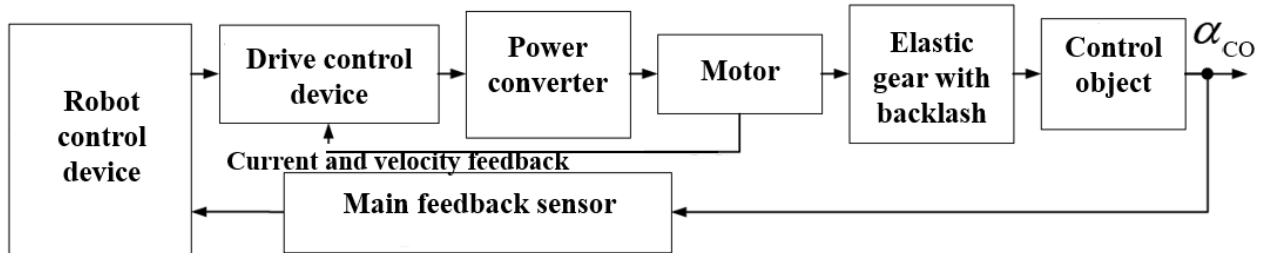


Figure 2.3. Structure of the geared servo drive of a technological robot when installing a position sensor on the shaft of the control object

"When using such a structure, the nonlinear element "dead zone", which characterizes backlash of the mechanical transmission, in combination with its elasticity, as shown in [29], is inside the position control loop of the drive. This element is capable of causing self-oscillations in the drive. It is also shown that the elimination of self-oscillations in such a drive is possible only by applying constant torque to the shaft of the control object. This torque is intended for eliminating backlash of the gear. To generate a torque counteracting the main motor, a second loader motor is used, which plays the role of an active controlled backlash eliminator. Schematically, such a drive is shown in Figure 2.4.



Figure 2.4. Dual-motor geared servo drive of technological robot

The basic concept of constructing a dual-motor geared servo drive of technological robot is presented in [2]. "A position sensor is installed on the shaft of the first motor of the drive, which allows us to form a drive closed by position control loop of the motor shaft. Such drive has a traditional cascade structure in the form of three nested control loops: an external position control loop of the motor shaft, an inner velocity control loop of the motor shaft, and an internal current control loop of the motor windings. This drive plays a subordinate role, is located inside the main position control loop of the manipulator link belonging to the main, precision drive, and therefore can be called an internal servo drive (ISD)."

Accuracy of precision servo drive depends significantly on the accuracy and resolution of the position sensor, mounted on the shaft of the drive-controlled manipulator link. Therefore, it is advisable to use a precision incremental encoder in combination with a quadrature counter as such a sensor. Thus, the dual-motor geared servo drive of the proposed structure uses two position sensors. One of them is installed on the motor shaft, and the other is on the axis of the manipulator link.

The dual-motor drive can be controlled directly by the control device of technological robot. This device generates a setpoint for the controller of the precision drive, and the latter forms control impacts fed to the controller of ISD. And the precision drive controller does not have to be a separate device. Its functions can be realized on the robot control device.

An important advantage of such a concept of building a dual-motor drive, proposed in [2], is that it can be built using frequency converters, motors and gearboxes that are currently mass-produced and widely used in industry. However, the principles of control, mathematical model and structure of the torque drive-loader are not considered in detail in the paper [2].

Thus, for the usage of such drives for the construction of technological robots, it is important to continuously control the torque developed by the loader in order to maintain the tension torque between the ISD and the drive-loader at a minimum level sufficient to exclude self-oscillations. Such control will allow us to perform technological operations with less consumed power, to reduce energy consumption, heating of motor windings, friction losses between the ISD and the loader. Therefore, it is proposed to add a control channel for the torque drive-loader. Such a torque drive control channel is needed to control the torque of the drive-loader both while performing technological operations of the first and second types, and during the performance of spatial movements by the robot during point-to-point movements. In analytical programming of a technological robot built on dual-motor drives, in some cases it is possible to estimate in advance the moment acting on the manipulator drives while performing a technological operation, and to set the required torque of the drive-loader.

Structure of the control system of a two-channel servo drive of a technological robot is shown in Figure 2.3, in which there is an implemented channel, controlling position of the controlled object by

signal  $\beta$ , and a channel of loader torque control by signal  $M_{load}$ . The loader in such a drive can be a torque drive closed by currents in the windings of its motor and controlled by the developed torque. However, most industrial drives are not torque drives. They do not have the ability to directly control the moment. Moreover, in industry, there are mainly tasks to implement velocity or position control. Thus, in order to solve the problem of controlling the developed torque, it is necessary to solve the problem of controlling the movement velocity.

However, in accordance with the concept proposed in [2] and developed in this work, in order to build the drive, which structure is presented in Figure 2.3, it is advisable to use frequency converters common in the industry, both for the ISD and for the loader. This structure has scientific novelty and is distinguished by the presence of a control channel for the torque drive-loader.

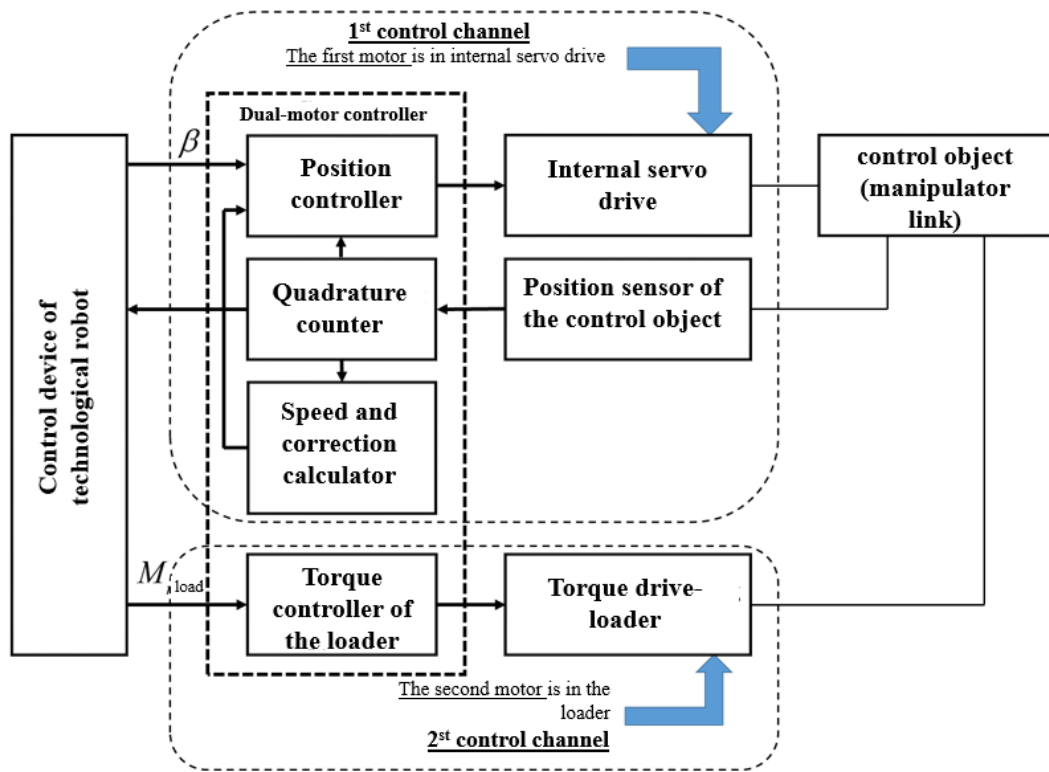


Figure 2.3. Proposed structure of two-channel dual-motor servo drive of technological robot

Thus, it was proposed to use a complete drive as a loader, closed by velocity control loop of its motor shaft and operating in the mode of controlled limitation of the developed torque.

As follows from Fig.2.3, the dual-motor servo drive of the robot is a two-channel device. The first control channel serves to control the position of the manipulator link and contains a servo drive closed by position control loop of the manipulator link using a position sensor on the link's shaft. The reference input  $\beta$  for this drive is generated by the control device of the technological robot. An integral position controller of this drive, as well as a speed calculator of the control object, are implemented in

the drive controller. Inside the control loop of the drive of the first control channel there is an internal servo drive, closed by the position control loop of one of the motors. The internal servo drive consists of three nested control loops: an external position control loop, a subordinate velocity control loop of the motor shaft and an internal torque control loop. The torque is regulated by controlling current in the armature winding of the DC motor or the currents in the phase windings of the AC motor. There are no fundamental differences in the design of the drive of the first channel from the way it is done in the work [2]. But in general, the structure of the precision drive has changed, and these changes are due to the peculiarities of the organization of the second control channel.

The second control channel serves to create the required force counteraction to the drive of the first channel and contains a drive-loader. From the control device of the technological robot, a second reference input  $M_{load}$  is fed to the input of the drive-loader. It determines the direction of rotation and, more importantly, the sign and the value of the electromagnetic moment being created. The loader drive must have a sufficiently high speed at that. In this case, the loader's torque quickly reaches the limit value corresponding to the desired limit level and is then maintained at this level with high precision.

The movement of the manipulator link is determined by the total torque, which consists of the torque of the motor of the first channel and the moment of resistance created by the loader. The correct operation of the control channels and the entire dual-motor servo drive is achieved by the coordinated generation of reference inputs in the control device of the technological robot.

The presence of a second control channel is a fundamentally important difference between the proposed structure of the precision drive and the well-known solutions considered, in particular, in [2, 31]. Thanks to this, it is possible to build an energy-efficient adaptive system in which the torque developed by the loader is regulated, and its desired value is calculated taking into account the features of the technological operation performed.

To study the dynamic properties of a robot with precision dual-motor servo drives, it is necessary to develop a mathematical model of a drive-loader, which is a drive, closed by velocity control loop of its motor shaft, with a controllable level of electromagnetic torque limitation.

## **2.2 Features of the mathematical model of a two-channel dual-motor geared servo drive**

First of all, a mathematical model of the internal servo drive (ISD) was developed. We considered in the model the most commonly used in modern robotics AC synchronous motors with vector control [30, 55, 86].

The ISD is a servo drive with a traditional structure in the form of a cascade system of three nested control loops, as presented in [30, 42, 87]. The internal torque control loop of the motor (torque

control subsystem) includes a motor, a three-phase transistor power converter, current sensors in the two-phase windings of the motor, an ADC and a subsystem controller that performs Clark and Park's forward and inverse transformations, presented in [30, 86], and implements vector control using two current PI-controllers. The torque control subsystem is a component of the velocity control loop that encloses it. The operation of the resulting velocity control subsystem is organized by a controller that implements velocity PI-controller and calculates speed of the motor shaft based on the data from the motor shaft position sensor. The external loop for regulating position of the motor shaft contains a closed velocity control loop, a position P-controller and a sensor (resolver) installed on the motor shaft.

When forming a mathematical model of the ISD, it is advisable to take into account that, as shown in [30], the dynamic properties of the torque control subsystem based on a vector-controlled AC synchronous motor are similar to the dynamic properties of a closed current control subsystem based on a separately excited DC commutator motor. Therefore, later, instead of simulating the torque control subsystem, its analogue is considered in the form of a mathematical model of the current control subsystem based on a DC commutator motor. The condition for the equivalence of the replacement of the mathematical description of the torque control subsystem of a vector controlled synchronous AC motor with a separately excited DC commutator motor is the equality of the values of the same parameters of their windings, power converters and PI-controllers [30].

In accordance with [30], the structure of the torque control subsystem, called the mechatronic power unit (MPU), is as shown in Figure 2.4.

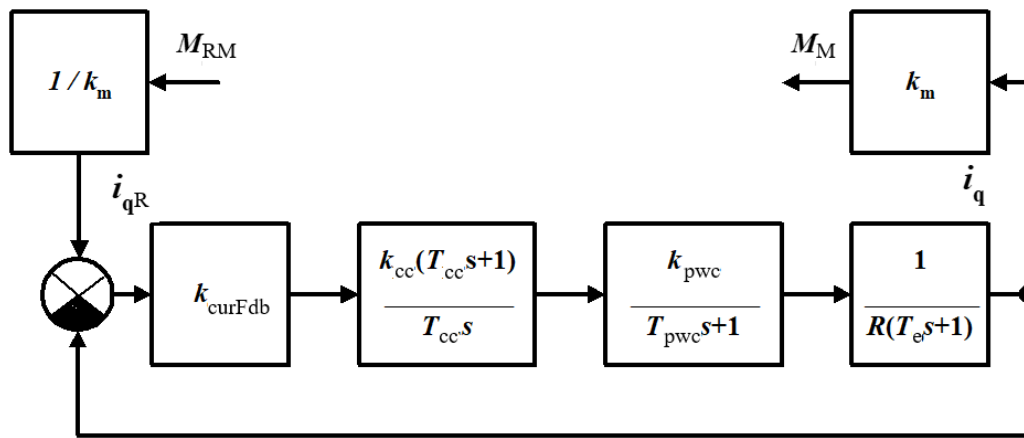


Figure 2.4. Structural diagram of the mathematical model of the torque control subsystem (mechatronic power unit)

In Figure 2.4, the following notations are used:  $M_{RM}$  and  $M_M$  - reference and actual motor torque, respectively;  $i_{qR}$  and  $i_q$  - the reference and actual torque-generating current in the virtual winding of the motor, which magnetic axis is perpendicular to the direction of action of the magnetic flux of the

rotor;  $k_{cc}$  and  $T_{cc} = \frac{1}{k_{ic}}$  – gain and time constants of current PI-controllers, respectively;  $k_{ic}$  – gain coefficient of integral control component;  $k_{pwc}$  and  $T_{pwc}$  – gain and time constant of each channel of a three-phase power converter, respectively;  $R$  is the active resistance of the phase winding;  $T_e = \frac{L}{R}$  – electromagnetic time constant;  $L$  is the inductance of the phase winding;  $k_{curFdb}$  - current feedback coefficient;  $k_m$  - motor torque coefficient, which is determined by the formula

$$k_m = p_p |\Phi| w,$$

where  $p_p$  – a number of pairs of motor poles;  $\Phi$  is the magnetic flux of the rotor;  $w$  – equivalent number of the turns of the phase winding.

In [30] it is shown that the rules for tuning two identical PI-controllers of MPU with vector control do not differ from the rules of tuning PI-controller of the armature current control subsystem of a separately excited DC commutator motor to the technical optimum. In addition, the synthesis of the controllers of MPU with vector control can be carried out using a model of a current control subsystem based on a separately excited DC commutator motor. It is also important that the analysis of the dynamic properties of the torque control subsystem with vector-controlled synchronous AC motor can be carried out using computer simulation model of the current control subsystem of a separately excited DC commutator motor.

Therefore, in order to improve dynamic properties of the ISD, it is advisable to adjust the MPU to the technical optimum, as discussed in [30, 42, 87]. To do this, it is necessary to select the time constant and the gain coefficient of the PI-controllers in accordance with the equations

$$T_{cc} = T_e$$

$$k_{cc} = \frac{RT_e}{2T_{pwc}k_{curFdb}k_{pwc}}.$$

The design of mathematical models of the velocity control subsystem and the ISD position control loop does not differ from the known approaches typical for drives with DC commutator motors, presented in [30, 42, 87]. The peculiarity of the digital drive under consideration is the usage of a speed calculator based on the data received from the rotor position sensor. The speed estimate is obtained as a result of calculating the first inverse difference of the position of the motor shaft. To reduce overshooting, the time constant of the velocity PI-controller is chosen to be 4 times less than the cutoff frequency of the open velocity control loop, and the value of this cutoff frequency is chosen to be

approximately 3 times more than the cutoff frequency of the open-loop drive. It should be noted that adjusting the parameters of the controllers of a real servo drive is not an easy task. Paragraph 2.4 is devoted to this issue.

An ISD closed by position control loop does not have an integrating property, it is a static system. Therefore, an integral regulator is used in the external control loop of the first channel of a two-channel dual-motor servo drive. In addition, to improve the dynamic properties of such a drive, corrective feedback of velocity of the control object (manipulator link) is used.

One of the features of the precision dual-motor servo drive is that the control loop of the control object, which is the manipulator link, includes a nonlinear mechanical subsystem. It consists of a gearbox and a control object (a manipulator link), and the gearbox has elasticity and backlash. The presence of backlash can be reflected in a mathematical model of the drive using a link with a nonlinear characteristic of the type "dead zone", as proposed in [29]. This can lead to the occurrence of self-oscillations in the drive with the described structure. "One of the tasks associated with the creation of a high-quality servo drive is to determine the necessary torque created by the loader, and the values of the parameters of the control algorithms implemented by the controller of the precision drive, in which self-oscillations are excluded", as noted in [92].

According to [2, 59], "the main idea underlying the determination of the required loader torque and setting the parameters of the control means of a precision drive closed by the position of the control object is as follows. The usage of the harmonic linearization method makes it possible to replace a nonlinear link of the type "dead zone" with a coefficient  $q(A)$  of harmonic linearization." Taking into account this coefficient, it is possible to write the linearized equation of mechanical transmission

$$M_{dr} = q(A)_{MIN} \cdot \frac{C_{red} + \chi \cdot s}{C_{red}} \cdot \left( \frac{\alpha_{mot}}{i} - \alpha_{co} \right) \quad (2.1)$$

where  $M_{dr}$  – torque at the output shaft of the gearbox with gear ratio  $i$ ;  $\alpha_{mot}$  and  $\alpha_{co}$  – rotational angle of the motor shaft and the manipulator link, respectively;  $C_{red}$  - stiffness coefficient of the mechanical transmission;  $\chi$  is the coefficient of loss due to internal viscous friction in the mechanical transmission,  $q(A)_{MIN}$  - minimal value of the harmonic linearization coefficient  $q(A)$ .

Based on the stability margins of a harmonically linearized servo drive, the gain values of its controllers should be determined at a minimum value  $q(A)_{MIN}$  of harmonic linearization coefficient  $q(A)$ , because the stability margins in this case are less than with other values of  $q(A)$ . In the absence of a moment of external forces  $q(A)_{MIN}=0$ . Therefore, without a loader, no control structures and algorithms can guarantee the absence of self-oscillations in the servo drive of the type under

consideration, as shown in [29]. And if  $q(A)_{MIN} > 0$ , then it is possible to build a drive in which there are no self-oscillations. Consequently, when designing a drive of such a structure, the problem arises of determining the value of the loader torque, at which the changes in the coefficient  $q(A)$  are limited from below.

Moment of external forces  $M_{ext}$  acting on the control object includes the moment created by the loader. As shown in [2, 31], "the action of this moment leads to the fact that oscillations of the motor shaft and of the control object occur not around zero values, but relative to certain displacement angles due to the external moment  $M_{ext}$  and stiffness coefficient  $C_{red}$  of the mechanical transmission. At the same time, a constant component  $\theta_0$  of the torsional angle  $\theta$  of the equivalent elastic element characterizing the gearbox appears. Harmonic linearization of a nonlinear link of the type "dead zone" makes it possible to detect not only a variable, but also a constant component  $\varphi$  at its output when a constant moment of external forces acts on the control object" [92].

As shown in [2], "there is a relationship between the minimum value of  $q(A)_{MIN}$  of harmonic linearization coefficient  $q(A)$ , the values  $M_{ext}$ ,  $C_{red}$  and half the backlash of the mechanical transmission  $\sigma$ ":

$$q(A)_{MIN} = f \left\{ \frac{M_{ext}}{C_{red}\sigma} \right\},$$

while  $M_{ext}(C_{red}\sigma)^{-1} = \frac{\varphi}{\sigma}$ . The more  $M_{ext}$  and less  $\sigma$ , the narrower the range of possible values of the harmonic linearization coefficient  $q(A)$ . Its minimum value  $q(A)_{MIN}$  grows with increasing  $\frac{\varphi}{\sigma}$ , and the maximum value is 1, as in the case of no backlash. For example, as shown in [92], "when  $M_{ext} = 45$  Nm,  $C_{red} = 250000$  Nm/rad,  $\sigma = 1.4545 \cdot 10^{-4}$  rad we have  $q(A)_{MIN} \approx 0.65$ ". Thus, as shown in [2], the required tension torque between the loader and the ISD can be determined by the formula:

$$M_{tens} = q(A)_{MIN} \cdot \sigma \cdot C_{red}, \quad (2.2)$$

where  $q(A)_{MIN} \approx 0.2$ . This is the minimum torque value required to eliminate self-oscillations in a precision dual-motor drive.

However, as mentioned earlier, in order to reduce the consumed energy, for example, in the case when the direction of action of the load acting on the drive coincides with the direction of action of the loader during TO, the loader torque can be reduced. Therefore, it is advisable to introduce the 2<sup>nd</sup> control channel into the drive, controlling the loader torque. As substantiated in paragraph 2.1., in the developed new structure of the digital dual-motor geared servo drive, a complete drive is used as a loader, closed

by the rotational velocity of the motor shaft and operating in the mode of controlled limitation of the developed torque. Since a synchronous motor with the same parameters as the ISD motor is used in the construction of the loader, the model of a separately excited DC commutator motor is also used as its mathematical model. The loader also has a mechanical transmission on the motor shaft, through which it acts on the drive control object. Linearized equation of mechanical transmission is (2.1).

The mathematical model of the loader contains control loops of current and velocity of its shaft, forming a cascade system of nested control loops. The model contains a current PI- and a velocity P-controllers. The presence of an integral component of the velocity controller is not necessary here, since it is important to eliminate the static error in the current flowing in the motor windings, and in the torque control loop, not velocity. It is also important to reflect in the loader model the influence of time quantization of signals in the velocity control loop on the dynamic properties of the loader, which is taken into account using the delay link.

Therefore, the transfer function  $W_s(s)$  of the open velocity control loop has the form

$$W_s(s) \approx \frac{k_{sc}k_m k_{spdFdb}}{k_{curFdb}J_{mot}s((\omega_{cc}^{-1} + T_s)s + 1)} \quad (2.3)$$

where  $k_{sc}$  – gain of velocity P-controller;  $k_{spdFdb}$  – velocity feedback coefficient;  $s$  – Laplace operator;  $\omega_{cc}$  – cut-off frequency of the open current control loop;  $T_s$  – time constant in the velocity control loop.

The second control channel in a dual-motor drive is implemented by controlled limitation of the torque developed by the loader motor in the velocity control loop. With the second control channel, it becomes possible to regulate the loader torque in such a way that at each moment of time the smallest torque value is created, sufficient to eliminate the backlash and the danger of occurrence of self-oscillations. For example, in this case, the value of the moment  $M_{loader}$ , that the loader should develop can be determined by the formula (2.4).

$$M_{loader} = \begin{cases} 0, & \text{if } M_{load} \geq M_{tens}; \\ -M_{tens}, & \text{if } M_{load} < M_{tens}; \end{cases} \quad (2.4)$$

where  $M_{load}$  – the calculated value of the torque acting on the drive from the load. This value must be determined by the torque calculator and it depends on, for example, the TO performed by the drive as part of the technological robot. If the drive is used as part of a TR during an operation such as milling, to determine the value of the  $M_{load}$  it is necessary to take into account the moment, caused by the

imbalance of the manipulator links in the current configuration, and the predicted component of the torque depending on the cutting forces.

The calculated value of the desired torque of the loader  $M_{loader}$  (taking into account the gearbox ratio), the motor torque coefficient  $k_m$  and the current feedback coefficient  $k_{curFdb}$  are used to limit the torque developed by the loader according to the formula (2.5).

$$I_R = \begin{cases} f_1, & \text{if } V_P > f_1 \\ V_P, & \text{if } f_2 \leq V_P \leq f_1, \text{ where} \\ f_2, & \text{if } V_P < f_2 \end{cases}$$

$$f_1 = \begin{cases} \frac{M_{loader} k_{curFdb}}{k_m i}, & \text{if } sign(V_R) > 0 \\ +\infty, & \text{if } sign(V_R) \leq 0 \end{cases}, \quad (2.5)$$

$$f_2 = \begin{cases} -\infty, & \text{if } sign(V_R) > 0 \\ \frac{M_{loader} k_{curFdb}}{k_m i}, & \text{if } sign(V_R) \leq 0' \end{cases}$$

$V_p$  – signal at the output of the loader velocity P-controller (before its limitation),  $I_R$  – reference input signal of the current control loop of the loader. That means, it is a signal  $V_p$ , limited at the top or bottom by the moment  $M_{loader}$ .  $V_R$  – reference input signal of the velocity control loop of the loader, corresponding to the desired rotation velocity of its shaft. Since the loader is designed for torque control, it is enough to set a constant value, for example, 1000 rpm (314.16) rad/s, and change the maximum value of the torque developed by the loader.

Thus, a mathematical model has been developed containing a second channel for controlling the loader torque, at which it always develops the minimal required torque, taking into account the external load, sufficient to eliminate self-oscillations in a dual-motor geared servo drive. However, in a dual-motor drive with the described new structure, relatively low-frequency weakly damped oscillations may occur, which must be damped. This is revealed if we write a transfer function of the electromechanical subsystem of the first channel for controlling position of dual-motor servo drive, consisting of the ISD and the mechanical subsystem (without the loader).

In this case, the mechanical subsystem consists of elastic mechanical transmission with backlash and mechanical control object with moment of inertia  $J_0$ . Its mathematical model is described by the transfer function

$$W_0(s) = \frac{1+T_g s}{\omega_0^{-2} s^2 + 2\xi_0 \omega_0^{-1} s + 1}, \quad (2.6)$$

where  $\omega_0 = \sqrt{\frac{C_{red}}{J_0}}$  and  $\xi_0$  – the circular frequency of natural oscillations and the coefficient of relative

damping of the mechanical subsystem, respectively, and  $\xi_0 = 0,5 \cdot T_g \cdot \omega_0$ , but  $T_g = \chi/q(A)/C_{red}$  – the time constant of the elastic gear. E. g., when  $C_{red} = 250000$  Nm/rad and  $J_0 = 10$  kgm<sup>2</sup> circular frequency  $\omega_0 = 158.1$  rad/s. The value of the coefficient  $\xi_0$  is small, and usually lies in the range 0.05 ... 0.2.

The ISD, as well as the entire precision drive, is digital. At a sufficiently high quantization rate of signals in time, which is usually realized, the properties of such a drive practically coincide with the properties of its continuous analogue, as shown in [65]. The ISD and the mechanical subsystem are dynamically interconnected and form a single dynamic electromechanical subsystem of the precision drive. Despite the fact that the internal drive is a servo drive, its motor shaft is displaced under the action of the moment of reaction forces from the elastic gear. Therefore, the value of the resulting stiffness of the electromechanical subsystem decreases, and this leads to a decrease in the resonant frequency of the electromechanical subsystem.

According to [2], the dynamic properties of the dominant component of the electromechanical subsystem of the first channel of the dual-motor servo drive can be characterized by the transfer function in a simplified form, but with acceptable in practice accuracy. This function is the ratio of the Laplace transform of the rotation angle of the control object  $\alpha_{co}(s)$  to the Laplace transform of the reference input  $U(s)$ , fed to the ISD, obtained at zero initial conditions. This function is described as:

$$W_{em}(s) = \frac{1+T_g s}{i \cdot k_{ps2}(\omega_1^{-2}s^2 + 2\xi_1\omega_1^{-1}s + 1)(T_{sd2}s + 1)} \quad (2.7)$$

where  $s$  – Laplace operator;  $i$  – gear ratio;  $T_{sd2}$  – time constant of the aperiodic link, which reflects the effect of the internal drive closed by position of its motor shaft by means of a sensor with gain coefficient  $k_{ps2}$ ,  $\omega_1$  and  $\xi_1$  – circular frequency and damping coefficient, which characterize the manifestation of the resonance properties of the subsystem. The value of the coefficient  $k_{ps2}$  can be obtained from its linearized characteristic, as shown in [65]. It should be noted that  $\omega_1$  is significantly less than  $\omega_0$ , and the value of  $\xi_1$  is small. Therefore, weakly damped oscillations can occur in the electromechanical subsystem. For example, if a structural diagram of the electromechanical subsystem of the first channel of a dual-motor drive is drawn up from the transfer function (2.7), it will look like this in Figure 2.5, where  $C_{eqv}$  and  $\chi_{eqv}$  – the equivalent stiffness of the gear and the equivalent coefficient of losses due to internal viscous friction in the mechanical transmission, reduced to its output shaft.

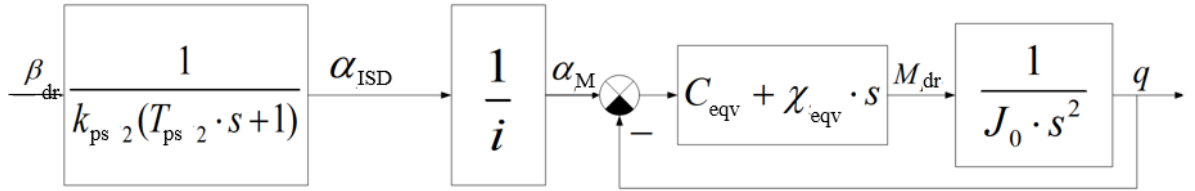


Figure 2.5. Structural diagram of the electromechanical subsystem of the first position control channel of the dual-motor servo drive

An example of Bode diagram (gain) of such subsystem is shown in Figure 2.6. It shows that at the frequency  $\omega_1 = \sqrt{\frac{C_{eqv}}{J_0}} = \sqrt{\frac{q(A)_{MIN} \cdot C_{red}}{J_0}} = \sqrt{\frac{0,2 \cdot 710000 N \cdot m}{10 kg \cdot m^2}} \approx 119.2 \frac{rad}{s}$  there is a resonant peak. This circumstance makes it much more difficult to ensure stability and expand the bandwidth of a precision drive. At the same time, the value of the damping coefficient is small:  $\xi_1 = \frac{\chi_{eqv}}{2} \sqrt{\frac{1}{C_{eqv} \cdot J_0}} = \frac{500}{2} \sqrt{\frac{1}{0,2 \cdot 710000 \cdot 10}} = 0.21$ .

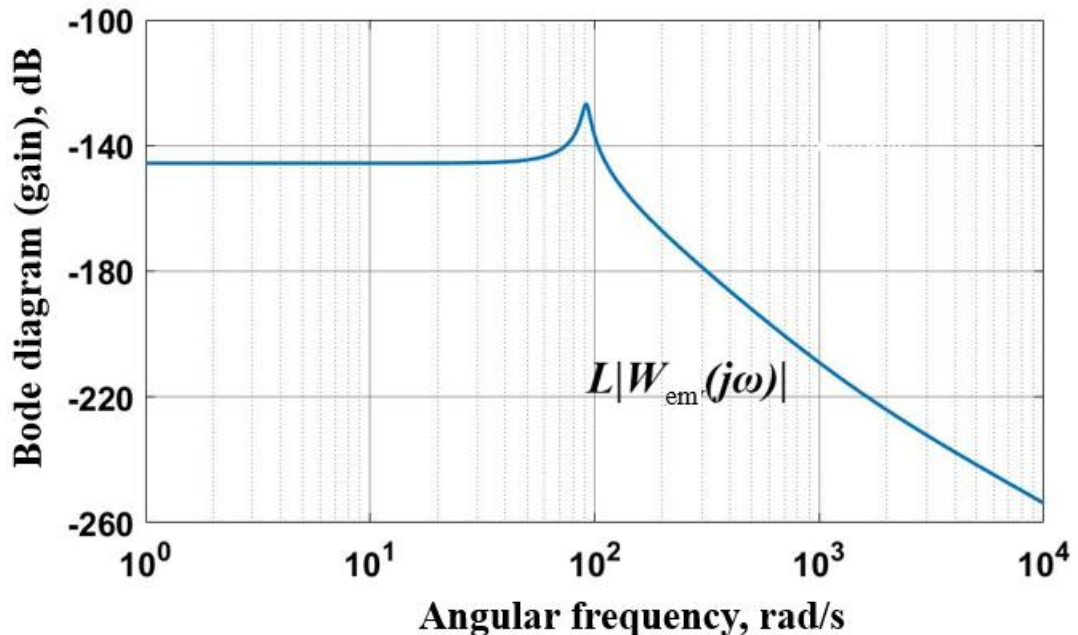


Figure 2.6. Electromechanical subsystem of a dual-motor servo drive

The position feedback of the drive control object contains the gain coefficient of the position sensor installed on the shaft of the control object. In the forward chain of the position control loop there is an integral controller with a transfer function

$$W_{IC}(s) = \frac{k_{IC}}{s}. \quad (2.8)$$

It is possible to implement a stable control system exactly with the integral controller, since with its usage the Bode diagram of the system has an inclination in the area of the cut-off frequency -20 dB/Dec. According to [2], in order to achieve stability and obtain acceptable transients of a precision servo drive, its cut-off frequency in the open state must satisfy the condition

$$\omega_d \leq \omega_1 \xi_1.$$

Given, that

$$\omega_d = k_{IP} \cdot \frac{k_{ps}}{i \cdot k_{ps2}},$$

where  $k_{ps}$  – main feedback gain coefficient of the position sensor of the control object, we get a requirement for determining the value of the controller gain

$$k_{IC} \leq \omega_1 \cdot \xi_1 \cdot i \cdot \frac{k_{ps2}}{k_{ps}}. \quad (2.9)$$

It is important to note that the presence of an oscillating link in the electromechanical subsystem, as can be seen from the expression (2.7), indicates the need to take measures to damp oscillations to increase speed and accuracy of movements of the servo drive.

The analysis of the obtained mathematical model of the electromechanical subsystem of the first control channel of the drive showed that in order to weaken the influence of its resonance properties on the dynamic properties of the dual-motor drive, it is advisable to introduce corrective links. They will contribute to an increase in the damping of oscillations of this subsystem, which will make it possible to increase the cutoff frequency  $\omega_d$  of the open-loop drive and, as a result, to increase speed and increase dynamic rigidity of the drive. According to [2], the increase in oscillation damping can be achieved by means of corrective feedback of the velocity of the manipulator links, introduced at the inputs of internal servo drives. It can be considered that “as a result of such correction the parameter  $\xi_1$  in  $W_{em}(s)$  is replaced by the parameter  $\xi_2$ , the desired values of which are in the range of 0.7...1”, as shown in [2].

Such corrective velocity feedback (VF) of the control object (CO), which is fed to the input of the ISD closed by the position of its motor shaft, contains a gain factor. A change in the value of this coefficient changes the gain Bode diagram shown in Figure 2.6 in such a way that the resonant peak is cut off, as shown in Figure 2.7. It shows the gain Bode diagram of the transfer function  $W_{VF}^{-1}(s)$  of VF. This can be explained as follows. If we consider a system with transfer function  $W_{em}(s)$ , closed by feedback  $W_{VF}(s)$ , the resulting closed-loop transfer function will be determined as follows:

$$\Phi(s) = \frac{W_{em}(s)}{1 + W_{em}(s)W_{VF}(s)}.$$

If  $W_{em}(s) \ll W_{VF}^{-1}(s)$ , then  $\Phi(j\omega) = |W_{em}(j\omega)|$ , but if  $W_{em}(s) \gg W_{VF}^{-1}(s)$ , then  $\Phi(j\omega) = |W_{VF}(j\omega)|$ . Accordingly, gain of  $\Phi(j\omega)$  on the first frequency band, where  $W_{em}(s) \ll W_{VF}^{-1}(s)$ , will be close to the gain of  $|W_{em}(j\omega)|$ , and on the second band – to the gain of  $|W_{VF}(j\omega)|$ . With the correct setting of the feedback gain coefficient, it is possible to achieve the situation when there is practically no resonant peak on the resulting Bode diagram. Thus, damping of oscillations arising in the drive of such structure is realized.

The value of the gain coefficient  $k_{velFdbCO}$  in the velocity feedback of the control object of dual-motor servo drive, according to the method presented in [2], should be determined taking into account the current value of the circular frequency of natural oscillations of the electromechanical subsystem  $\omega_1$  according to the formula

$$K_{velFdbCO} = \frac{k_{ps2}i}{\omega_1}. \quad (2.10)$$

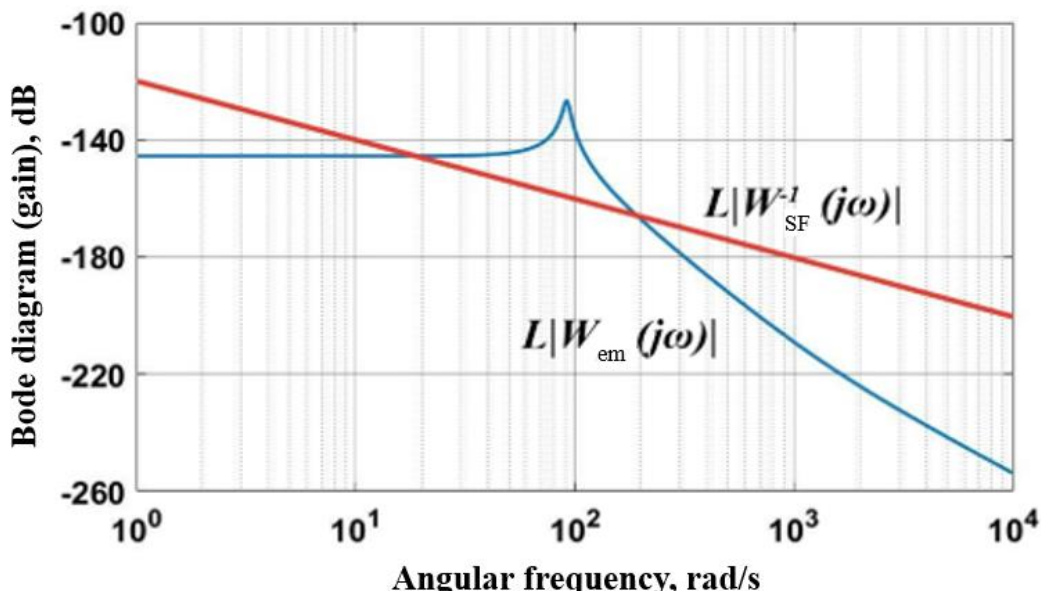


Figure 2.7. Bode diagram (gain) of the electromechanical subsystem  $W_{em}(j\omega)$  and corrective velocity feedback  $W_{VF}^{-1}(j\omega)$  of the dual-motor servo drive

When the drive control object is a manipulator link, the frequency  $\omega_1$  can change depending on the configuration that the manipulator adopts in the process of performing technological operations. This is due to the variation in the moment of inertia  $J_0$  of moving parts of the manipulator moved by the considered drive. The results of the study [2] show that it is advisable to adjust the controllers of the

internal drive in such a way that its open loop cut-off frequency  $\omega_{d2}$  is close to the minimal value  $\omega_{0,MIN}$  of natural oscillation frequencies of the mechanical subsystem. The frequency  $\omega_{0,MIN}$ , relevant to the most unfavorable situation, is calculated by the formula

$$\omega_{0,MIN} = \sqrt{\frac{C_{eqv}}{J_{0,MAX}}}, \quad (2.11)$$

where  $J_{0,MAX}$  – is the maximum value of the moment of inertia of the moving part of the manipulator moved by the considered drive. With a decrease in the moment of inertia  $J_0$  the frequency  $\omega_0$  increases, and the damping coefficient increases. Thus, the quality of the electromechanical subsystem is improved. In addition, the internal drive begins exerting an increasingly strong damping effect.

The cut-off frequency of an open-loop precision drive is determined by the formula

$$\omega_d \leq \omega_1 \cdot \xi_2,$$

from which it follows that it is higher than it was before without damping with corrective velocity feedback of the control object. It is also worth adding that in order to increase the dynamic rigidity and accuracy of the drive responding to time-varying input signals, it is advisable to increase the frequency values  $\omega_0$  and  $\omega_d$ . An increase in the stiffness coefficient, gear ratio and feedback gain coefficient  $k_{ps2}$  of the position sensor of the motor shaft also has a positive effect on accuracy.

It can be concluded that the introduction of an external torque impact in the drive leads to the fact that the properties of mechanical transmission with backlash are close to the properties of backlash-free transmission. As a result, the servo drive can be closed by position control loop of the manipulator link, and therefore it does not have a static error due to “elasticity and backlash of the mechanical transmission, and it is able to ensure high accuracy of movements of the control object. This can be interpreted as an infinitely large static stiffness of the servo drive”, as presented in [92]. Positioning errors in this case are only due to the limited accuracy of the position sensor of the control object. The dynamic rigidity of the servo drive, which manifests itself when a changing moment of external forces is applied to the control object, can also be significantly increased as a result of a rational choice of the structure and parameter values of its controllers.

As a result, a mathematical model of a digital dual-motor geared servo drive was developed. Its peculiarity is the presence of a second control channel, which makes it possible to control the torque developed by the loader. The loader itself is a drive, closed by velocity control loop, with a controlled torque limitation. Such a mathematical model makes it possible to study the influence of the

dynamic properties of a digital drive (torque loader) with two nested control loops on the properties of a precision dual-motor drive. This model also makes it possible to conduct a simulation study of a robot with dual-motor drives, taking into account algorithms for adaptive torque control created by loaders.

### 2.3 Structure of a computer simulation model of a two-channel dual-motor geared servo drive

Based on the concept of designing a precision dual-motor geared servo drive described in paragraph 2.1 and taking into account the features of its mathematical model presented in paragraph 2.2, a computer simulation model of such a drive was developed. The structure of the drive presented in Figure 2.3 is taken as a basis. Development of simulation model is necessary to determine the drive response to various typical reference input and perturbation impacts. Later, this model made it possible to create a computer simulation model of the manipulator built on the considered drives, and to analyze its dynamic properties.

The structure contains 2 control channels (position control channel of the control object and the loader torque control channel), 5 nested control loops in the first control channel (3 control loops of current, velocity and position of the internal servo drive and 2 control loops of the general dual-motor drive, namely, velocity and position control loops of the manipulator link), as well as 2 control loops in the 2<sup>nd</sup> control channel (current and velocity control loops of the loader).

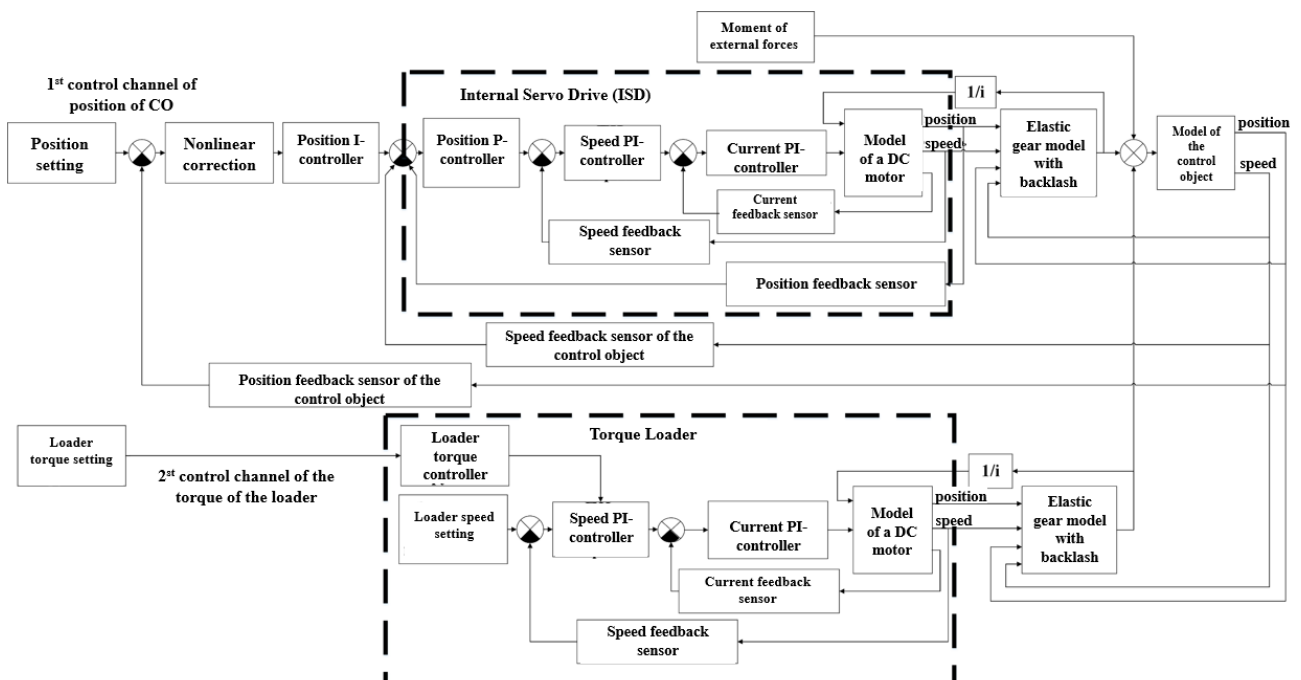


Figure 2.8. Structure of the computer simulation model of the drive

When designing a computer simulation model of the internal servo drive, transfer functions (2.6) - (2.7) were used. As presented in paragraph 2.2, the model is a classic cascaded system of nested control loops based on the DC motor model. The structural diagram of the simulation model of mechanical transmission is compiled according to the transfer function (2.1) and is presented in Figure 2.9. Backlash in this model is taken into account using a nonlinear link with saturation, and elasticity is taken into account using the  $C_{gear}$  stiffness coefficient and the  $K_{sita}$  viscous friction coefficient.

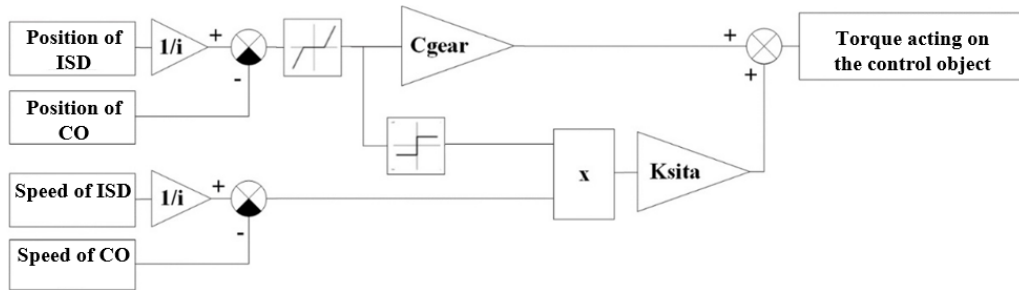


Figure 2.9. Computer simulation model of mechanical transmission

A computer simulation model of the loader and its mechanical transmission was developed in the same way. The second control channel of the drive is used to feed to the input of the loader a signal corresponding to the desired tension torque between the internal servo drive and the loader, which either comes from the upper level control device or is calculated in the torque controller according to the formula (2.4). The signal from the controller output must be divided by the motor torque coefficient of the loader to determine the value of the current control signal, and this signal is fed to the current control loop. At the output of the simulation model of the loader there is a signal equal to the actual torque of the loader, taking into account the moment of reaction forces from the gear.

Both control loops of the entire dual-motor drive are implemented with the usage of a signal from the position sensor of the control object. A precision photopulse angular position sensor with a discreteness of at least 250000 pulses per revolution is used, which is also reflected in the model.

In the forward chain of the drive position control loop, an integral controller with a transfer function (2.8) is used, since exactly this type of controller enables us to implement a stable control system. Also, as presented in paragraph 2.2, the drive uses corrective velocity feedback of the CO, which is required to damp low-frequency oscillations. It is implemented by a signal received from the output of the quadrature counter of the position sensor of the CO.

In addition, in the position control loop of a dual-motor drive there is a block of nonlinear correction of the control action fed to the position I-controller. The reason for this correction I that at high values of input signals, intense low-frequency weakly damped oscillations may occur as a result of manifestation of nonlinear properties of digital servo systems. At the same time, there are no such

oscillations with small values of input signals. Therefore, in order to exclude oscillations in the position control loop, it is advisable to use nonlinear correction. In [65] a variant of such correction is presented. When the error values fed to the input of the position P-controller do not exceed a predetermined value modulo, the nonlinear correction does not actually manifest itself in any way. However, at large deviations, nonlinear correction provides a significant reduction in the gain in the position control loop, which is required to eliminate intense oscillations.

## **2.4 Parameter adjustment method for two-channel precision dual-motor geared servo drive**

To determine the parameters of the control system of a dual-motor drive, first of all, it is necessary to determine parameters of motors and gears of the internal servo drive and loader. As mentioned earlier, the idea is to use commercially available motors and gears. In order to ensure the elimination of backlash in such a drive when changing the direction of movement of the control object, the same requirements are imposed on the power and rated torque of the motors of the internal servo drive and the loader. Therefore, in order for the dual-motor drive to provide torque equal to half the value of the rated torque of the motor (taking into account the gearbox ratio), it is advisable that the models and parameters of the motors and gearboxes of the loader and the internal servo drive coincide. In this case, the conditions listed in paragraph 1.4.1 must be followed at the selection process.

After the motors and gearboxes are determined, the coefficients of the current and velocity PI-controllers and the position P-controller of the ISD are adjusted as a system of nested control loops according to the method presented in [65]. In the first case, when the parameters of the mathematical model of the drive are known, for example, the bit depth of the DAC and ADC in the current loop, it is possible to adjust the coefficients of the controllers analytically. In the second case, when not all the parameters of the mathematical model are known, the synthesis of the drive control system can be carried out empirically by adjusting the coefficients of the controllers of this drive, and the parameters of transient processes can be determined experimentally.

Let's first consider the analytical method of adjusting coefficients of the drive controllers. First, the approximate values of the cutoff frequency in the position, velocity and current control loops of the ISD are determined. At the same time, the current loop is adjusted to the technical optimum, when the overshooting does not exceed 5% of the reference value with the minimum transient time. The velocity loop is adjusted to a symmetrical optimum when the overshooting does not exceed 50%.

Since the models of the internal servo drive and loader motors are the same, the values of the controllers' coefficients of the current and velocity control loops are the same, so the values of the current and velocity PI-controller of the loader can be determined immediately.

After that, the natural frequency of oscillations of the electromechanical subsystem, consisting of an internal servo drive and a gearbox, is determined. It can be determined by computer simulation, applying a single step impact to the input of the internal servo drive model, and determining the frequency of natural oscillations of the system at the output of the gearbox model. In this case, the forced oscillations of the system will attenuate quickly, but natural oscillations will attenuate slowly, which makes it possible to determine their frequency according to the graph of changes of the position of the output shaft of the gear. Analytically, the value of the natural frequency of oscillations of the electromechanical subsystem can be determined by the formula (2.11).

Then the obtained value of the natural frequency is used to determine the value of the gain coefficient of the velocity feedback of the control object and the gain coefficient of the position I-controller of the dual-motor drive according to formulas (2.8) and (2.9) given in paragraph 2.2. First, it is necessary to determine the value of the gain of velocity feedback of the control object and make sure that at this value low-frequency oscillations are damped. This can be done both by the Bode diagram of the electromechanical subsystem of the drive with velocity feedback control loop of the CO, as shown in Figure 2.7, and by mathematical model at computer simulation. At the same time, when such a subsystem responds to a step input, a slight overshooting is allowed, no more than 20%. Then the value of the gain of the position I-controller of the dual-motor drive is determined. It is also possible to provide computer simulations to ensure that the transient time at a certain value of the coefficient is minimal, the oscillations are fully damped and there is no overshooting.

To exclude oscillations in the position control loop of the dual-motor drive at high input values, as mentioned in paragraph 2.2, it is advisable to use a nonlinear correction algorithm. The correct operation of the algorithm can also be verified with the help of computer simulation.

Thus, the algorithm for analytical adjustment of the parameters of the control system of a dual-motor drive is as follows:

- 1) Selection of the motor according to the conditions given in paragraph 1.4.1.
- 2) Selection of the gearbox, also according to conditions presented in paragraph 1.4.1.
- 3) Adjustment of the coefficients of current, velocity and position controllers of the internal servo drive and loader as a system of nested control loops by the method presented in [65].
- 4) Determination of the natural frequency of oscillations of an electromechanical subsystem consisting of an internal servo drive and a gearbox, by formula (2.11).
- 5) Determination of velocity feedback gain of the control object by formula (2.10).
- 6) Determination of the gain of position I-controller of the dual-motor drive by formula (2.9).
- 7) Setting up an algorithm for nonlinear correction of error fed to the input of the position controller of the dual-motor drive.

Now let's consider an empirical way to adjust the coefficients of drive controllers. First, the current PI-controller of the ISD is adjusted when the loader is not connected. In this case, gain of the integral component is set to 0, step input impacts are applied to the current loop and the current sensor signal is monitored, increasing the value of the gain of the proportional component until the steady-state error is equal to 0. At the same time, the transient time should be close to the minimum. Then, after determining the value of the coefficient in proportional component, the coefficient of the integral component is increased until the overshooting is equal to 5%. After that, the gain coefficients of the velocity PI-controllers are adjusted using the same method. And in the velocity control loop the overshooting of up to 50% is allowed.

After that, it is possible to immediately set the same values of the gain coefficients of the current and speed controllers of the loader, to determine the minimal value of the tension torque between the ISD and the loader using the formula (2.8), which is required to exclude self-oscillations in the entire drive, and to connect the loader. Since the loader has been connected, and additional load was added to the ISD motor and the moment of inertia of the load of the ISD has changed. This requires adjusting the gain value of the proportional component of the speed controller. After such adjustment, it is possible to proceed to adjustment of the position control loop of the ISD.

At adjustment of the gain coefficient of the position P-controller of the ISD the damping properties of the corrective velocity feedback of the CO are manifested when there are no more than 3-4 oscillations in the response of the electromechanical subsystem shown in Figure 2.5 to a step input.

Accordingly, the initial value of the gain coefficient of the position controller can be determined according to the method presented in [65] as a coefficient of a position P-controller of a classical system of nested control loops, so that during the response of the ISD to a step input there is no overshooting and the duration of the transient process is close to the minimum. Then, after the introduction of corrective velocity feedback, the value of this gain of the position controller can be increased until there are 3 to 4 oscillations in the transient process of position of the CO, as shown in figure 2.10.

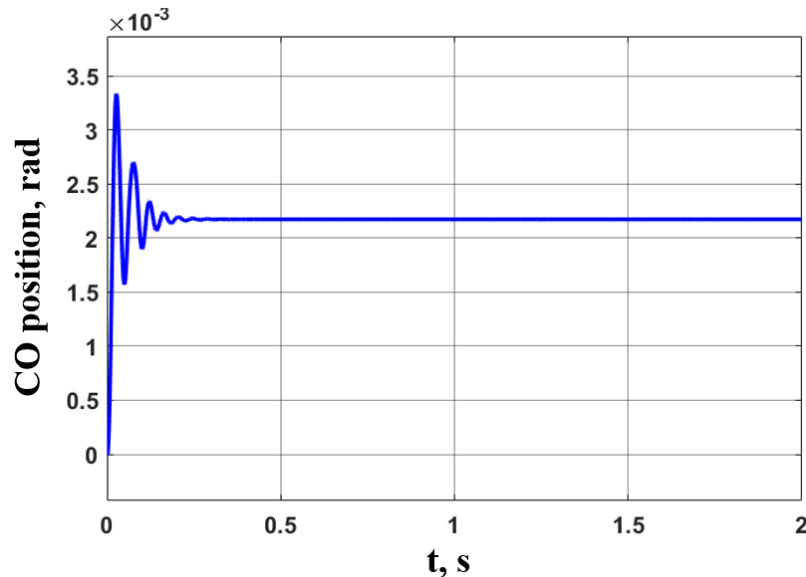


Figure 2.10. Transitional process of position of the CO

The amplification of the corrective velocity feedback of the CO is adjusted in such a way that the oscillations shown in Figure 2.10 are damped, and overshooting does not exceed 20–30% when the drive is responding to a step position input. And finally, it remains to introduce a position integral controller of the CO of the drive and adjust its coefficient so that the steady-state error is equal to 0, and there is either no overshooting, or it does not exceed 5%, depending on the requirements to the precision drive.

## **2.5 Computer simulation and analysis of dynamic properties of a two-channel precision dual-motor geared servo drive**

To analyze the dynamic properties of the proposed design of a dual-motor servo drive, it is advisable to conduct computer simulation of the drive of such a structure. For example, we can consider the drive of the manipulator with open kinematic chain of the type PUMA. We consider the drive, which rotates the manipulator around its vertical axis. In this case, there is no static moment in the drive. It is important to make sure that the proposed solution will provide high quality of control in the absence of intense self-oscillations in a system that includes elastic gear with backlash in the position control loop of a massive control object.

The mathematical and computer simulation model reflect the properties of the KEB B3 actuator motor and the Harmonic Drive HFUC-2A precision wave gearbox of size 50. The parameters values of such motor can be found in [66]. The motor has rated rotational frequency 4000 rpm, nominal torque 2

Nm, moment of inertia of the rotor  $5.7 \cdot 10^{-5}$  kgm<sup>2</sup>, motor EMF coefficient 0.577 Vs, electromagnetic time constant 3.2 ms and winding resistance 9.2 Ohm.

The gearbox has gear ratio 100, backlash of 1 arc minute and its hardness factor is 250000 Nm/rad. Parameter  $\chi$  is assumed to be equal to 500 Nms/rad. The loader creates a constant torque of 45 Nm. To identify the potential accuracy of the drive, a precision position sensor of the main feedback of the CO was taken. "A change of one unit of the decimal number corresponding to the code at the output of the quadrature counter occurs when the manipulator is rotated by an angle  $1.75 \cdot 10^{-6}$  rad. It is assumed that the PWM frequency in the drive power converter is 20 kHz", as shown in [92]. The parameter values of the internal servo drive controllers are selected in accordance with the rules for adjusting the system of nested control loops. Such rules are given, for example, in [65]. The motor shaft position feedback sensor has a resolution of 5000 discretes per revolution. The cutoff frequency of the open-loop internal servo drive is 105 rad/s.

Computer simulation of such control object, which has a moment of inertia of 10 kgm<sup>2</sup> and is driven only by an internal drive closed by the position control loop of the motor shaft, without a corrective velocity feedback of the CO, revealed its significant oscillations (Figure 2.11). It can be seen that when it is responding to a step input of 0.01 rad oscillations of the rotation angle  $\alpha$  of the control object are weakly damped and last more than 1 s. It has been established that the resonant frequency of the electromechanical subsystem is approximately equal to 35 rad/s.

This simulation result indicates that a weakly damped electromechanical subsystem will not significantly increase accuracy of the servo drive, since it forces us to limit its cutoff frequency.

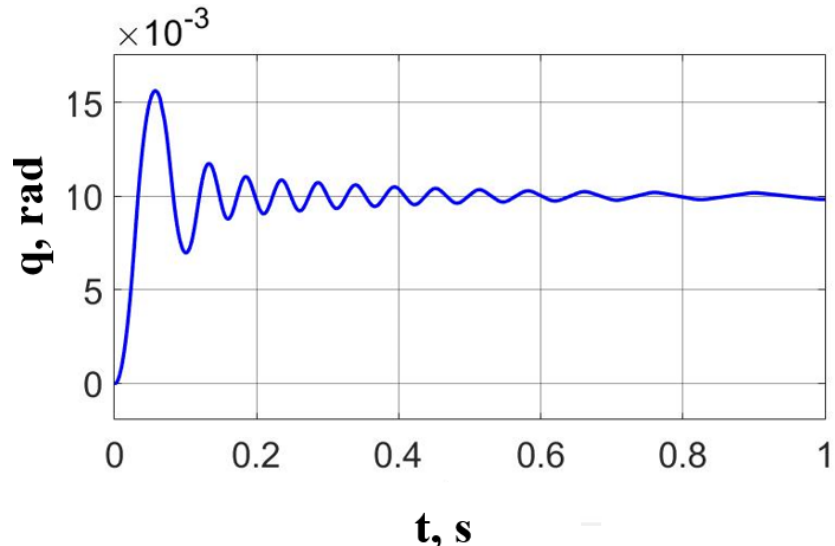


Figure 2.11. Transient process of position control of the CO by **internal servo drive without corrective velocity feedback**

A closed-loop precision servo drive also reveals significant and slow-damped rotation oscillations  $\alpha$  of the control object while responding to an input impact  $\beta = 0.25$  rad (Figure 2.12). This simulation result was also obtained in the absence of corrective velocity feedback of the control object. It confirmed the conclusion that, despite the high potential accuracy of the considered drive, its usage for the construction of technological robots is impossible without the introduction of correction.

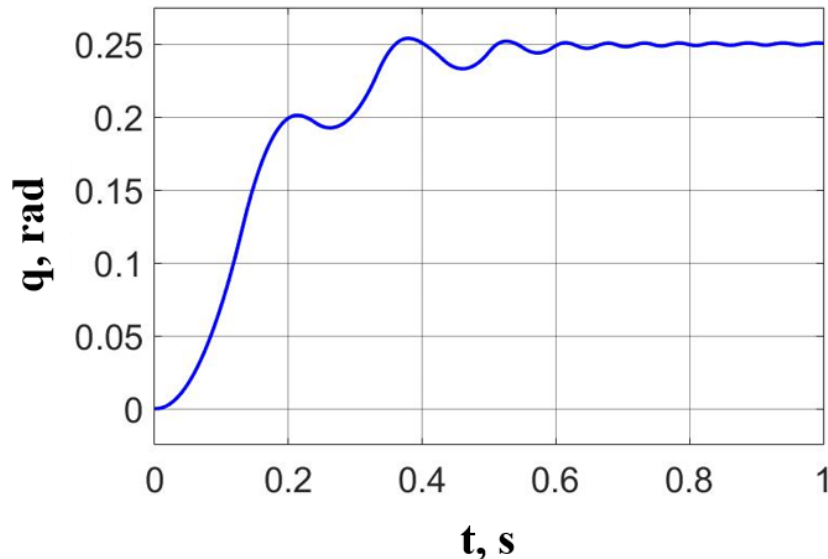


Figure 2.12. Transient process of position control of the CO by **precision drive without corrective velocity feedback**

The introduction of corrective velocity feedback of the control object has the necessary damping effect and fundamentally changes the nature of the object's movement. With the value of the feedback gain coefficient  $K_{occ} = 9000$  s the transient process takes the form shown in Figure 2.13. It can be seen that oscillations caused by elasticity of the gear are completely damped. Tuning the controllers provides cut-off frequencies of the open-loop precision drive  $\omega_d$  and open-loop internal drive  $\omega_{d2}$ ,  $8.976\text{ s}^{-1}$  and  $127\text{ s}^{-1}$  respectively.

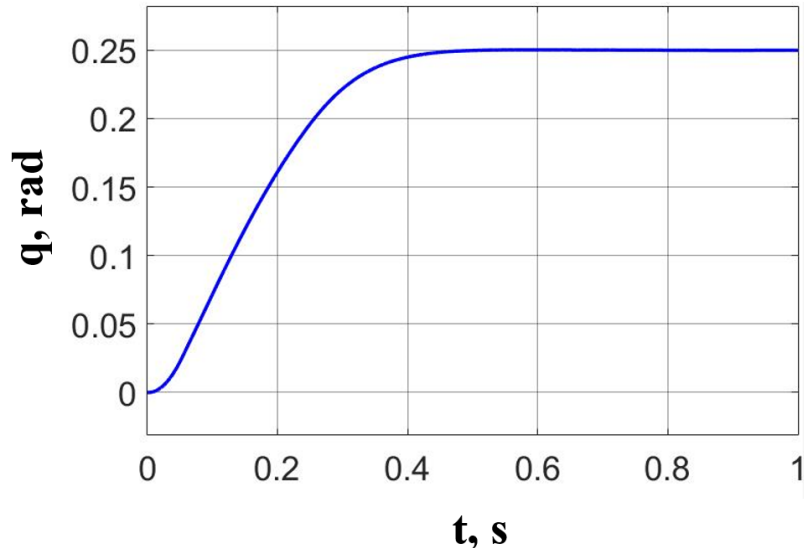


Figure 2.13. Transient process of position control of the CO by **precision drive with corrective velocity feedback**

Computer simulation studies have confirmed the high accuracy of the considered dual-motor servo drive. When responding to constant input impacts the drive error tends to almost zero. After the onset of the steady-state mode, the drive error  $\delta = \beta - \alpha$  makes slight fluctuations. At a loader torque of 35 Nm, the amplitude of such oscillations is approximately equal to  $1 \cdot 10^{-7}$  rad. The offset of the constant component of the error relative to 0 is  $-3.9 \cdot 10^{-8}$  rad. At the same time, "elastic elements of the gear constantly remain pressed against each other, which ensures high accuracy of the considered geared servo drive. These fluctuations do not significantly affect positioning accuracy of the CO, and therefore their impact on the quality of the technological process can be neglected", as presented in [59, 92].

When responding to small initial input values, for example, when  $\beta = 0.1$  rad, at which the drive operates in the zone of linearity of its characteristics, the duration of the transient process is 0.25 s. This indicates a sufficiently high performance of the drive.

Variable input signal  $\beta$  is reproduced with great accuracy when using combined control. The results of the simulation confirmed the theoretical conclusion that it is necessary to incorporate a link of the rate of change of the input signal with gain coefficient  $k_{comb} = \omega_d^{-1} = 0.1114$  s. With such control, the amplitude of the drive error does not exceed  $3.9 \cdot 10^{-4}$  rad when responding to an input impact, varying with an amplitude of 0.1 rad and a circular frequency of 1 rad/s, as shown in Figures 2.14 and 2.15. With program control, the rate of change of the input signal can be calculated from analytical dependencies, in particular, as proposed in [67].

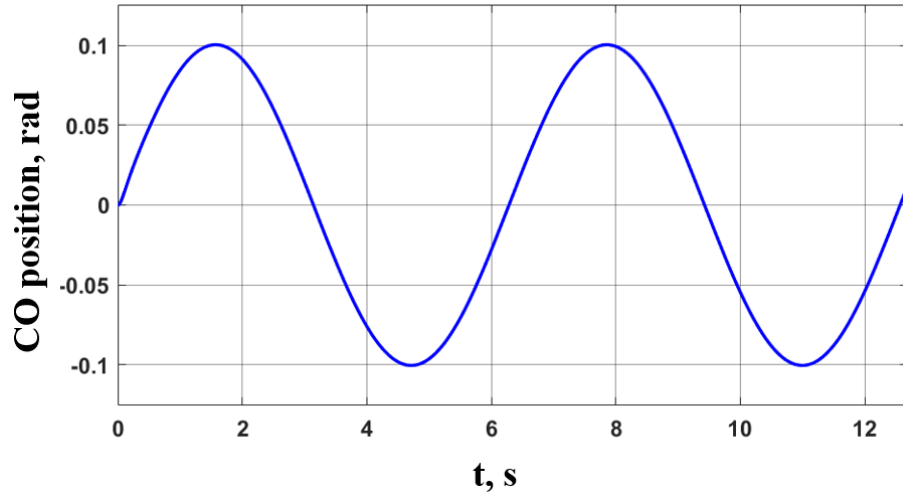


Figure 2.14. Precision drive response on sinusoidal position reference signal

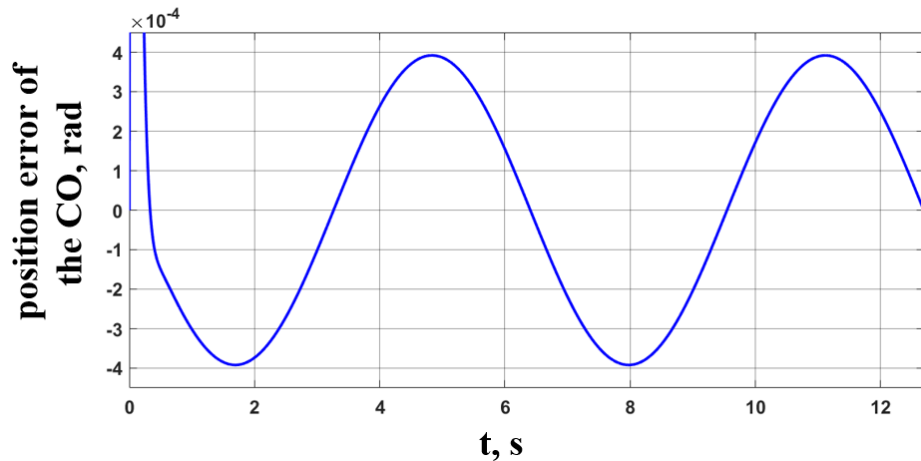


Figure 2.15. Position error of the CO when responding on sinusoidal position reference signal

During the simulation it was also found that with a significant initial reference input, the behavior of the drive is significantly affected by the inherent limitations of the drive elements. For example, when responding on a step input  $\beta = 5$  rad, most of the drive's transient time is taken up by operation at the maximum speed of 2 rad/s (Figure 2.16). Therefore, in case of large initial reference inputs, in order to ensure stability of the control processes and eliminate significant overshooting, it is advisable to use nonlinear correction of signal at the input of the position controller of the precision drive, e.g., described in [65].

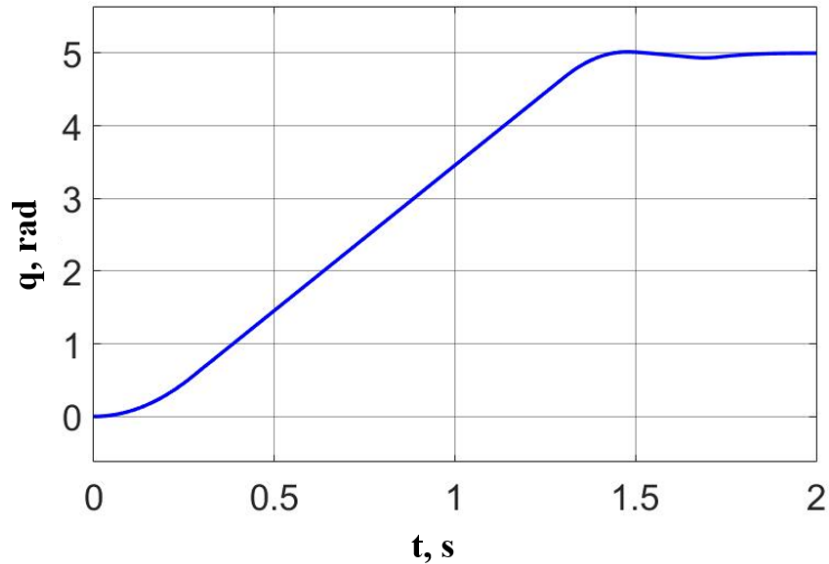


Figure 2.16. The precision drive response on the large reference input when the corrective velocity feedback of the control object and nonlinear correction of the input of the position controller are used

The results of computer simulations also indicate high stability of the servo drive properties. They showed that when the moment of inertia of the control object is reduced from 10 to 1  $\text{kgm}^2$ , the high quality of the transient process is maintained at the same value of  $k_{spdFdb}$ . With a more significant decrease in the moment of inertia, it is advisable to carry out adaptive adjustment of the value  $k_{spdFdb}$  to maintain the stability margins of the corrective contour.

A computer study of the drive's response to external disturbance has shown that in the steady state the constant external force is fully compensated, and the drive error  $\delta$  becomes zero. With a harmonic change in the angular moment of external forces, the resulting error of the drive in the steady-state mode also changes according to the harmonic law. At the amplitude of external torque  $M_{VAR} = 1 \text{ Nm}$  at the frequency  $\omega_{ext} = 20 \text{ rad/s}$ , the maximum recorded amplitude of error is equal to  $4 \cdot 10^{-6} \text{ rad}$  (Figure 2.17).

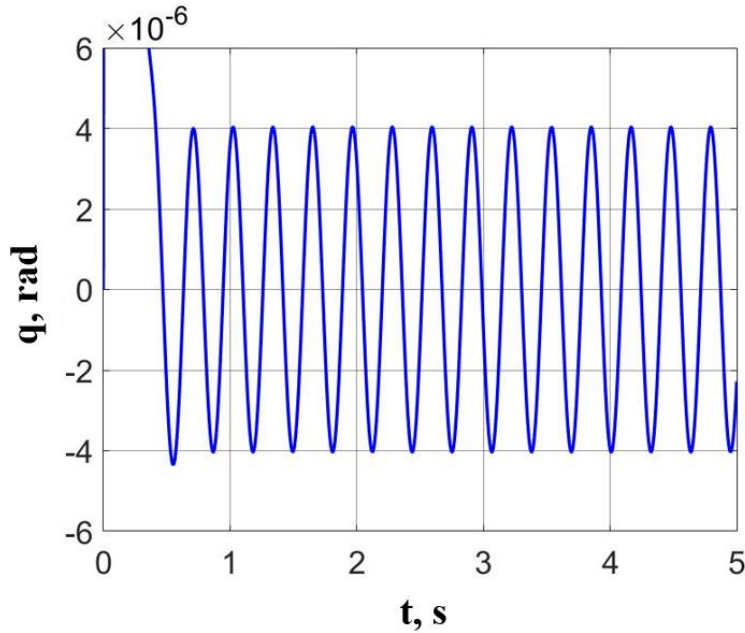


Figure 2.17. S Variation of the servo drive error under harmonic external torque with amplitude 1 Nm and frequency 20 rad/s.

Simulation shows that the position error of the control object increases in direct proportion to the amplitude of oscillations in the external force's momentum  $M_{VAR}$ . At  $\omega_{ext}$  less than 20 rad/s, its value is lower, the lower  $\omega_{ext}$  is. In particular, with the amplitude  $M_{VAR} = 1$  Nm and  $\omega_{ext} = 1$  rad/s the amplitude of the error  $\delta$  is equal to  $4.4 \times 10^{-7}$  rad. At circular frequency  $\omega_{ext}$  more than 20 rad/s  $\delta$  also decreases, which is due, among other things, to the damping action of a massive control object. In particular, when  $\omega_{ext} = 500$  rad/s the amplitude of  $\delta$  does not exceed  $5 \times 10^{-7}$  rad. When the tool is located 1 m away from the rotational axis of the drive output shaft, in the worst case, when  $\omega_{ext} = 20$  rad/s, the position error of the tool due to the dynamic stiffness of the drive does not exceed 4  $\mu\text{m}$ . Such an error can be neglected in most cases typical for technological robotics. Thus, the results of the study convince that such a drive has both high rigidity and sufficient damping.

Also, the simulation experiments were carried out when the drive operated in displacement mode responding to position reference input signal with abrupt changes of motion direction. In this case, the signal shown in Figure 2.18 was sent to the drive input.

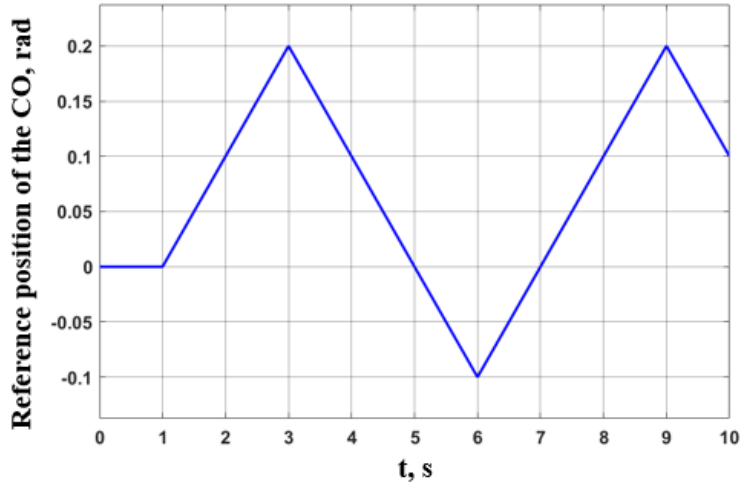


Figure 2.18. Position reference input of the CO with changes of motion direction

In this case, the combined input control described in [65] was used. The position controller of the precision drive received an input signal  $\beta(s)$  and a combined control signal passing through the system with a transfer function  $W_{comb}(s)$ :

$$W_{comb}(s) = \frac{10000s}{s + 10000} \cdot \frac{k_{ps2}}{\omega_d} \cdot \beta(s), \quad (2.12)$$

where  $k_{ps2}$  – gain coefficient of the precision position sensor of the CO shaft,  $\omega_d$  – cut-off frequency of the open-loop precision position drive, equal to  $8.976 \text{ s}^{-1}$ . Combined control in this case made it possible to increase the astatism order of the system and to eliminate velocity error at a linear rising input signal, as can be seen in the graph of the position error of the CO, shown in Figure 2.19.

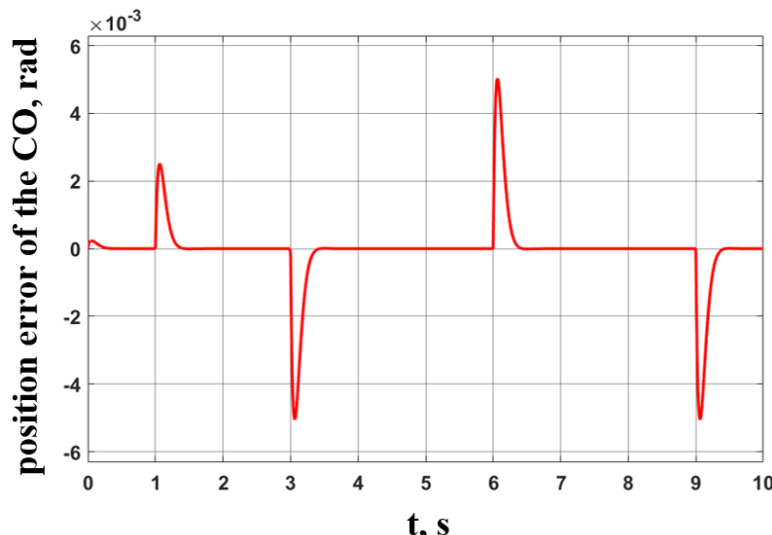


Figure 2.19. Position error of the CO while responding on the reference input with changes of motion direction

As mentioned earlier, the introduction of adaptive torque control of the loader into the drive allows us to have the smallest torque value at each time, sufficient to remove the backlash and eliminate the danger of self-oscillations. As a result of this introduction, efficiency should increase, current and energy consumption should decrease, and the heating of the motor of the drive-loader should decrease. In order to estimate this effect, energy  $P_{\Sigma}$ , consumed by the drive during operation, can be calculated using computer simulations, according to the following formula

$$P_{\Sigma} = \frac{1}{t_{sim}} \int_0^{t_{sim}} |I(t) \cdot U \cdot \eta| dt, \quad (2.13)$$

where  $I(t)$  - the current flowing in the motor windings,  $U$  – the voltage supplied to the motor windings equal to 230 V,  $\eta$  – the motor efficiency equal to 0.74,  $t_{sim}$  – the simulation time of the process of performing movements by the motor. To carry out such a study, an external moment was also applied to the drive, which simulated the process of performing technological operation with only one drive, shown in Figure 2.20. When moving in one direction, the moment with a positive sign acted on the drive, when moving in the other direction, the moment with the opposite sign acted on the drive. Thus, when acting, the drive was always counteracted by the load torque.

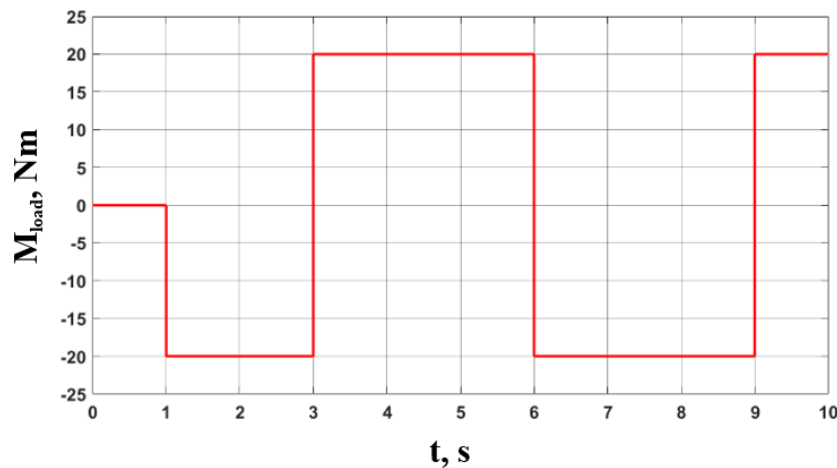


Figure 2.20. Change in the load torque applied to the drive by the performed technological operation

As a result, without adaptive control of the loader torque, the power consumption of the ISD motor was 241.4 W, the loader - 132.7 W, which in total was 374.1 W. The graph of current variation in motor windings of the loader and the ISD are presented in Figure 2.21.

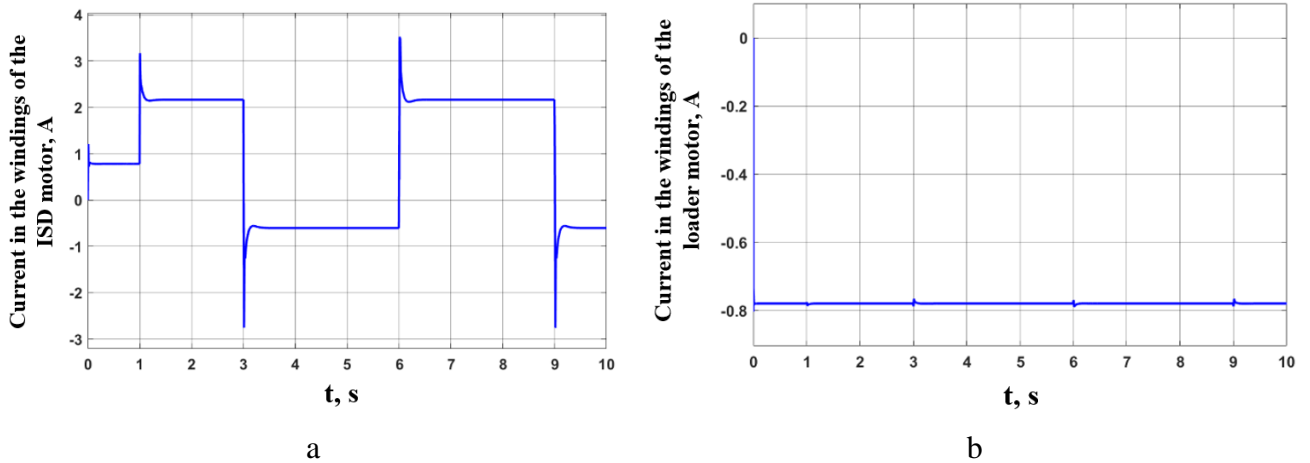


Figure 2.21. Current in the windings of the ISD (a) and loader (b) motors while responding on the reference input, with abrupt changes of motion direction

After switching on the adaptive torque control of the loader, the power consumption of the ISD motor was 175 W, the loader - 66.3 W, which in total was 241.3 W. This is less than without the usage of adaptive system. The graphs of currents in the windings of the loader and ISD motors in this case are presented in Figure 2.22. As can be seen in the figure, less current flows in the windings of the ISD motor, and therefore, the motor's torque is less at 1-3 s and 6-9 s, when there is a one directional movement. At the same time, the loader does not generate torque, the current in its windings is 0, since the load acting on the drive ensures the elimination of self-oscillations, since it is greater than the minimum required value  $M_{tens}$ . The graph of position error of the CO in this case is shown in Figure 2.23.

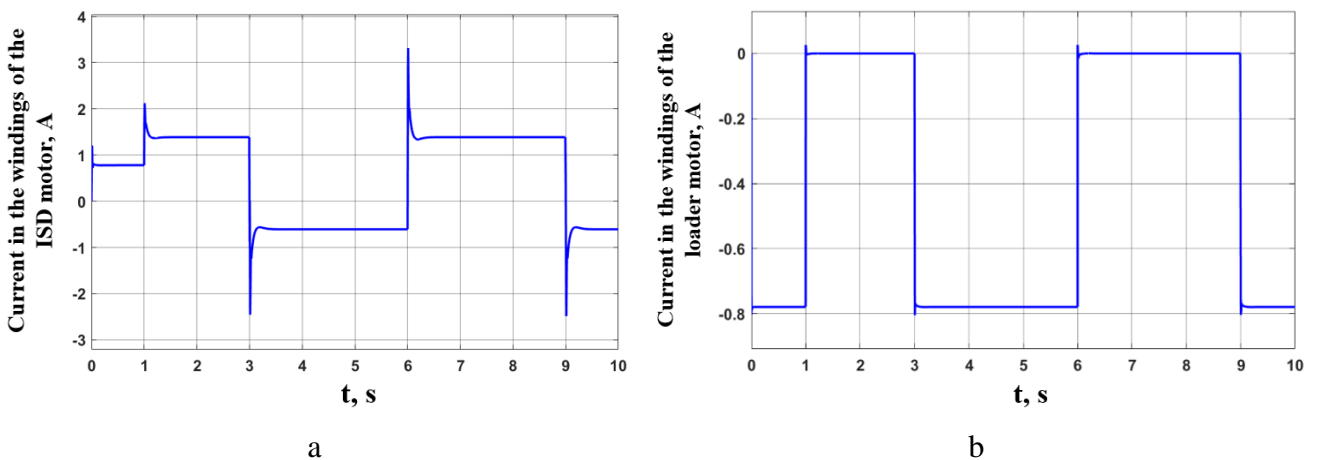


Figure 2.22. Current in the windings of the ISD (a) and loader (b) motors while responding on the reference input with abrupt changes of motion direction, **with adaptive control** of the loader torque

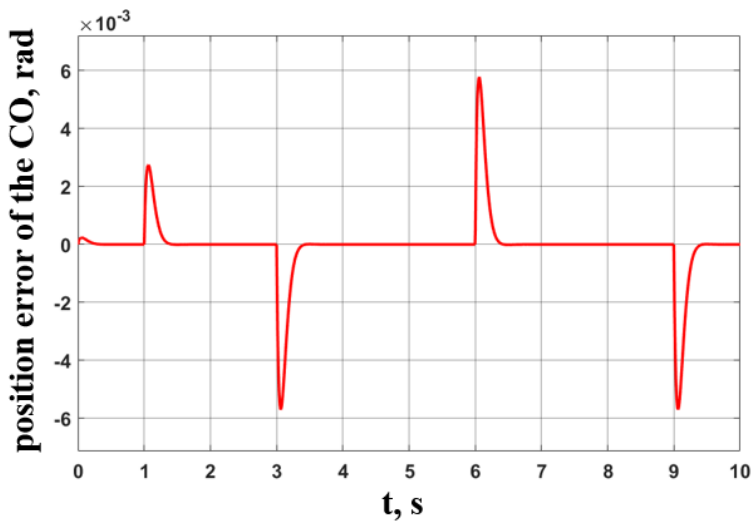


Figure 2.23. Position error of the CO while responding on the reference input with abrupt changes of motion direction, **with adaptive control** of the loader torque

Thus, the results of the computer simulation confirmed the expediency of using combined control and adaptive control loops of the loader torque, as well as the expediency of introducing a second control channel of the loader torque.

In order to further reduce energy consumption of the dual-motor drive and to make better use of its capabilities while responding on the position reference input with abrupt changes of motion direction, it is proposed to use a switching technique of the structure of the drive control system. The main idea is to use two identical drives, each of which can alternately play the role of the ISD and the loader. In case of using the drives to build analytically programmable robots, the external load can be predicted. Depending on the direction of action of this load, the internal servo drive that controls position of the CO can be realized either by the first motor or by the second. At the same time, if the load torque exceeds the minimum required tension torque between the drives, the loader can be switched off.

While providing computer simulations at the usage of adaptive control loop of the loader torque, when the direction of action of the load and the loader coincided, the loader was switched off as shown in Figure 2.22 (b), but such an event occurred only at the intervals of 1-3 s and 6-9 s, when the drive was rotating only in one direction. The usage of a structure-switching control system, where the loader and the ISD can change the roles with each other, will allow us to turn off the loader when rotating in both directions, if the load reaches a value, sufficient to eliminate self-oscillations in the drive.

To implement this idea, it is necessary to build an automatically controlled structure-switching block that operates depending on the currently implemented operation mode of the drive or the robot with such drive. In this case, the loader torque can be determined by the formula:

$$\begin{aligned}
 M_{loader_1} &= \begin{cases} 0, & \text{if } M_{load} \geq M_{tens}; \\ M_{tens}, & \text{if } M_{load} < M_{tens}; \end{cases} \\
 M_{loader_2} &= \begin{cases} 0, & \text{if } M_{load} \leq -M_{tens}; \\ -M_{tens}, & \text{if } M_{load} > -M_{tens}; \end{cases} \\
 M_{loader} &= \begin{cases} M_{loader_1}, & \text{if } \operatorname{sign}\left(\frac{d\beta(t)}{dt}\right) \geq 0; \\ M_{loader_2}, & \text{if } \operatorname{sign}\left(\frac{d\beta(t)}{dt}\right) < 0; \end{cases}
 \end{aligned} \tag{2.14}$$

Formula (2.14) defines the value of the function  $\operatorname{sign}\left(\frac{d\beta(t)}{dt}\right)$  depending on the direction of movement of the CO. In case of movement in one direction, the first derivative of the position control signal of the CO is positive, respectively, the output of this function will be equal to 1. When moving in the other direction, the first derivative is negative, the output of the function will be -1. Based on this value, it is possible to switch the roles of the loader and the ISD between both drives.

Figure 2.24 shows a structural diagram of a mathematical model of the drive with structure-switching control system and adaptive control loop of the loader torque. The combined position control is implemented by the corrective action calculator block with transfer function (2.12). In the motor mode selector block the value of the function  $\operatorname{sign}\left(\frac{d\beta(t)}{dt}\right)$  is determined. In the loader torque calculator block, the desired value of the loader torque is determined according to the formula (2.14), taking into account the value of the function  $\operatorname{sign}\left(\frac{d\beta(t)}{dt}\right)$  and the predicted load torque acting on the drive.

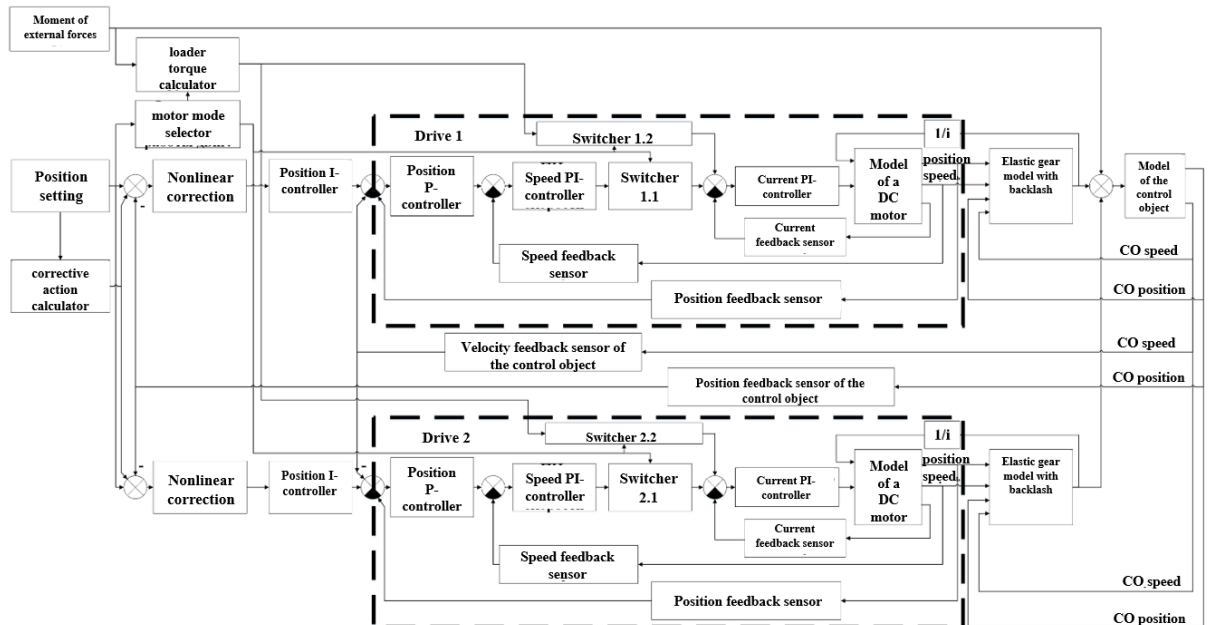


Figure 2.24. Structural diagram of the mathematical model of the drive with **structure-switching** control system and **adaptive control loop** of the loader torque

The signal on the output of the switcher blocks 1.1 and 2.1 is equal either to 0 for the ISD or to the reference torque value for the loader, based on the calculated value of the loader torque calculator, taking into account the gear ratio and the torque coefficient of the loader motor. From these switches the signal is fed to the input of the current control loop, where it is summed up with the signal coming from the output of the velocity PI-controller. The signal on the output of the switcher blocks 1.2 and 2.2 is equal to the output signal of the velocity PI-controller for the ISD or to 0 for the loader.

As a result of computer simulation of the drive, responding to the position reference input of the CO, shown in Figure 2.18 and with the applied load torque shown in Figure 2.20, it was found that the power consumption of the motor of the first drive was 125.7 W, the second – 102.5 W, which in total was 228.2 W. This is less than when using only the adaptive control loop of the loader torque. The graphs of the currents in the windings of the motors of both drives are shown in Figure 2.25. Table 2.1 shows the power consumption of a dual-motor drive with the structure shown in Figure 2.8 (without combined control, **without** adaptive load torque control loop and without structure-switching control system) and in Figure 2.24 **with** combined control, adaptive load torque control loop and structure-switching control system. In this case, the graph of the position error of the CO is shown in Figure 2.26.

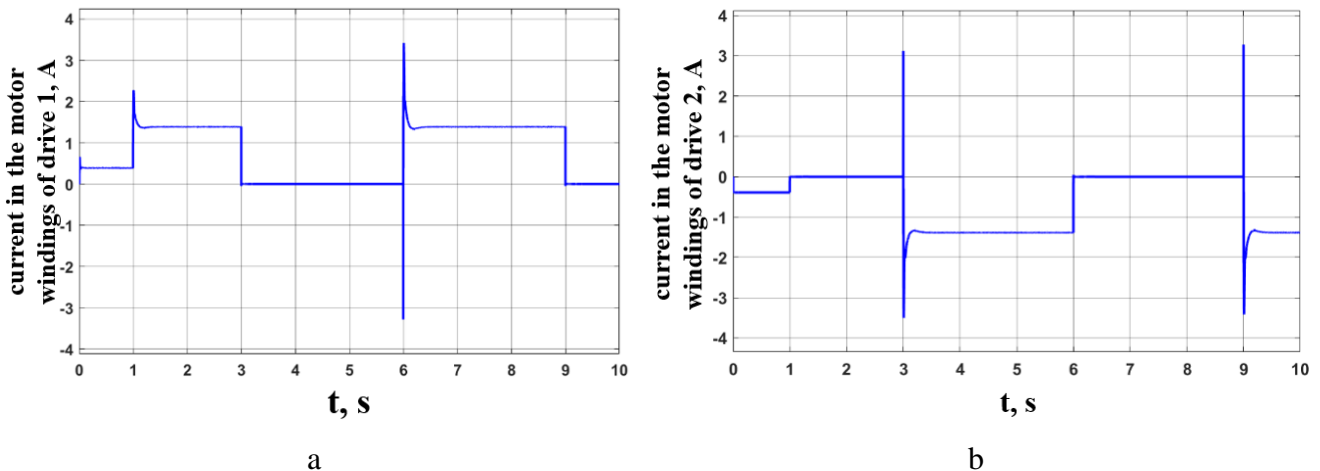


Figure 2.25. Current flowing in the windings of the motors of the first drive (a) and the second (b) while responding on the reference input with abrupt changes of motion direction **using adaptive system for controlling the loader torque and structure-switching control system**

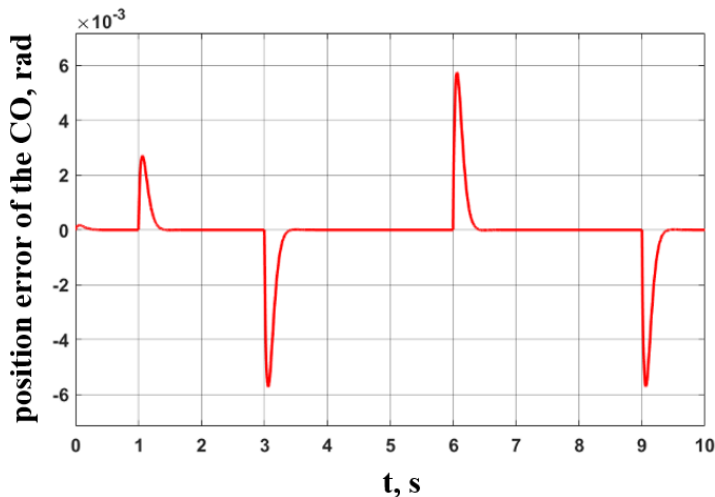


Figure 2.26. Position error of the CO while responding on the reference input with abrupt changes of motion direction when **using an adaptive system for controlling the loader torque and structure-switching control system**

Table 2.1 – Comparison of the power consumption P of dual-motor drive with the structures shown in Figure 2.8 and Figure 2.24.

	P of dual-motor drive	P of dual-motor drive with - Combined control; - Adaptive torque control.	P of dual-motor drive with - Combined control; - Adaptive torque control; - structure-switching control.
First drive	241.4	175	125.7
Second drive	132.7	66.3	102.5
$\Sigma$	374.1	241.3	228.2

Comparing Figure 2.26 to the Figure 2.23, the usage of the new structure of the drive control system did not affect the quality of transient processes of the drive responding on the reference input with abrupt changes of motion direction. And according to Table 2.1, it allowed us to reduce the power consumption of the drive by 39%.

As a result of the computer simulation, influence of the position sensor resolution of the ISD on the position control of the CO is revealed. It is established that at insufficient resolution of the position sensor, for example, of a resolver installed on the shaft of the ISD motor, self-oscillations may occur in the precision drive. Such oscillations are caused by the nonlinear static characteristic of the encoder, which is inside the position control loop of the ISD. And the position control loop of the ISD, possessing nonlinear properties, is inside the position control loop of the precision drive. This phenomenon is fundamentally important for the construction of precision technological robots. Apparently, for this reason, it is impossible to completely exclude self-oscillations. But it is quite possible to make them weak enough and not significantly affecting the accuracy of the precision drive.

For example, if this sensor is an encoder, operating in conjunction with a quadrature counter and producing 1024 pulses per revolution, then in the steady-state mode, the CO oscillates relative to the desired position with maximum amplitude  $1.476 \cdot 10^{-6}$  rad and frequency approximately 6.5 Hz. It should be noted that with one rotation of the sensor shaft, the number in the quadrature counter register changes to  $1024 * 4 = 4096$ . The same number corresponds to one revolution of the resolver, which is often installed on the shaft of the synchronous AC motors by manufacturers. The results of the study show that this is not enough to build a precision servo drive.

When using an encoder that creates 2048 pulses per revolution, which corresponds to the increment of the number in the quadrature counter register equal to 8192, the situation changes. In the steady-state mode, the CO makes much weaker oscillations relative to the desired position. Its maximum amplitude is  $3.2112 \cdot 10^{-8}$  rad at frequency of 450 Hz. Both of these cases are presented in Figures 2.27 and 2.28.

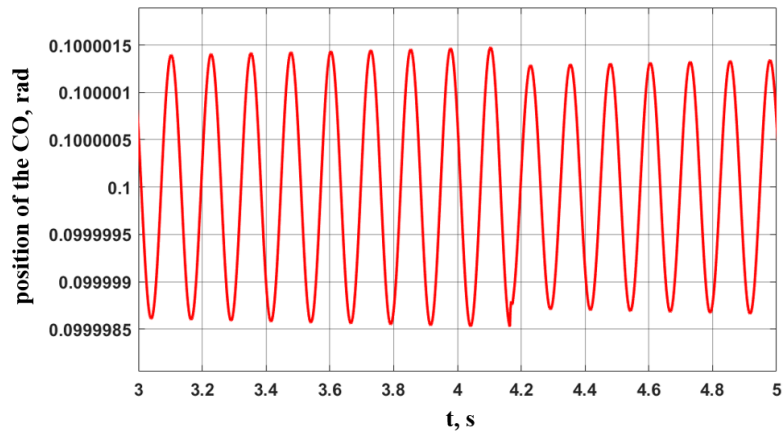


Figure 2.27. CO position in steady-state at the ISD position sensor resolution 1024 imp/rev

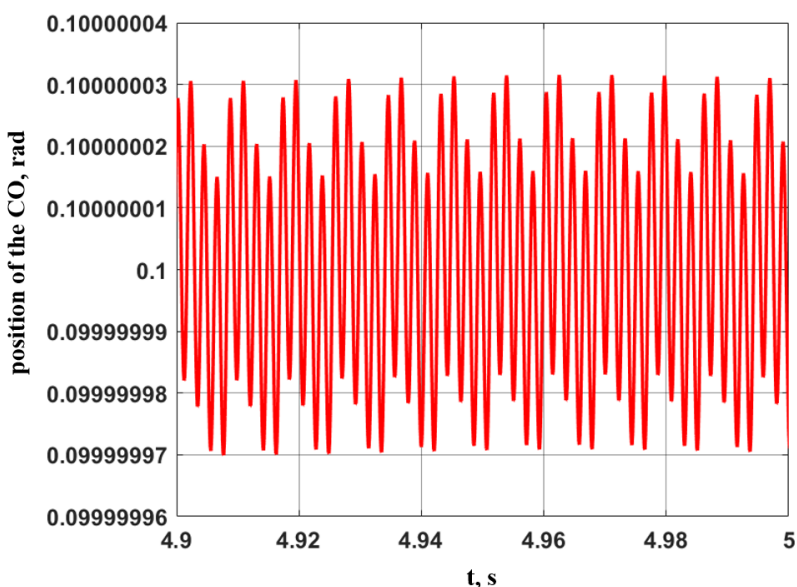


Figure 2.28. CO position in steady-state at the ISD position sensor resolution 2048 imp/rev

In order to determine the optimal value of the resolution of the ISD position sensor, a number of computational simulation experiments were carried out. During these experiments the resolution of the ISD position sensor was changed, a position control signal was fed to the drive simulation model, and after the onset of the steady state the amplitude of the resulting oscillations was determined by the signal from the high-precision position sensor of the CO. As a result, the dependence presented in Figure 2.29 was established.

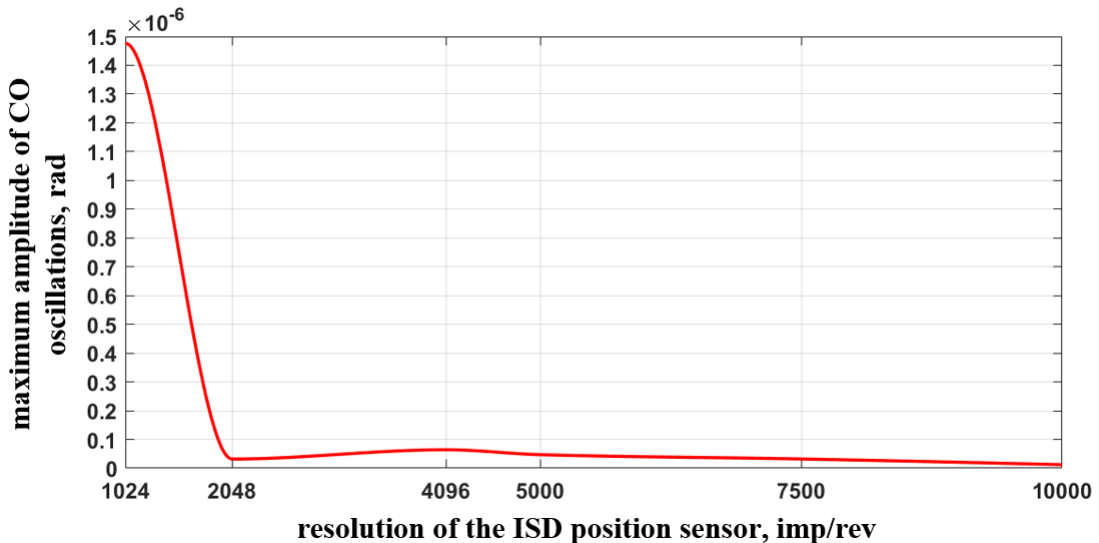


Figure 2.29. Dependence of the maximum amplitude of the CO oscillations on the resolution of the ISD position sensor

As can be seen in the figure, when the resolution of the ISD position sensor is increased up to the value of 2048 pulses per revolution, the amplitude of the resulting oscillations decreases, and after that its values do not exceed  $6.4329 \cdot 10^{-8}$  rad. And for example, with the value of 1028 pulses per revolution it is  $8.3 \cdot 10^{-5}$  rad, which in many cases is unacceptable for precision technological robots. With a resolution of 10000 pulses per revolution, the maximum amplitude of the CO oscillations equals to  $1.2398 \cdot 10^{-8}$  rad, i.e. more than 100 times less than with resolution of 1024 pulses per revolution.

This leads to the following recommendation for choosing the ISD position sensor. It is advisable to carry out computer simulation of precision drive with the recommended structure, with various characteristics of the position sensors of the ISD motor shaft. As a result of comparing the simulation results, the sensor is selected in which a compromise is achieved between positioning accuracy of the CO and cost of the sensor, which increases as its resolution increases. In particular, the results of the study showed that with the selected values of the drive parameters, such a compromise corresponds to a sensor with 2048 pulses per revolution of its shaft.

The materials presented in this chapter were published by the author in [17, 59, 82].

## 2.6 Conclusions on the second chapter

1 The conducted research shows the feasibility of using the proposed new structure of the precision dual-motor servo drive, which has the form of a two-channel drive, one of which is designed to control the torque developed by the torque loader drive. This structure makes it possible to significantly increase the dynamic stiffness and dynamic accuracy of the drive and expands its functionality due to the introduction of active oscillations damping, adaptive control of the torque loader and structure-switching control system of the drive.

2 A mathematical model of a precision two-channel dual-motor geared servo drive has been developed. Its peculiarity is that it makes it possible to control the torque developed by the loader, which is a drive, closed by its velocity control loop, with a controlled torque limitation. This model makes it possible to conduct a computer simulation research of a robot with dual-motor drives, taking into account algorithms for adaptive torque control created by the loader.

3 To investigate the dynamic properties of the proposed dual-motor drive, it is recommended to use the developed computer simulation model in Matlab/Simulink, based on the proposed mathematical model of the drive.

4 Practically important is the proposed method of adjusting parameters of the servo drive for precision technological robot. The method is characterized by a number of actions aimed at increasing dynamic stiffness and oscillations damping in the servo drives with newly developed structure.

5 Computer simulation results confirmed feasibility of the proposed modifications to the structure of the precision dual-motor drive. This concerns the introduction of the second control channel, which contains the torque-controlled loader drive, closed by velocity control loop, with adjustable limitation of the developed torque. The results confirm the usefulness of introducing adaptive control loop of the loader torque, which depends on the loading conditions by external forces arising during technological operations and the current configuration of the robot arm.

6 The energy efficiency of the drive is increased by using the proposed structure-switching method of the drive control system. If the roles of the motors of the drive can change as a result of switching the structure between the ISD and the loader, then it is possible to significantly reduce the power consumption of the drive. The results of computer simulations showed that this reduction is 39%, and the drive operates without deterioration of the quality of transient processes, also in displacement mode while responding on the reference input with abrupt changes of motion direction.

7 It is important to take into account the discovered effect of discreteness of the position sensor of the ISD motor shaft on intensity of self-oscillations of the control object when creating precision drives of technological robots. It is not sufficient to have high-precision position sensor of the control object.

It is also necessary to find position sensor of the ISD motor shaft, which properties allow us to achieve a compromise between cost of this sensor and its resolution, at which the amplitude of self-oscillations is sufficiently small and the positioning accuracy of the precision drive meets the requirements.

8 The results of theoretical analysis and computer simulation gave answers to the main questions of the study concerning the construction of dual-motor geared servo drives. They indicate that the recommended structure of the servo drive made it possible to achieve a significant increase in dynamic stiffness and controlled oscillations damping of the control object. It can be considered that at constant external torque the drive stiffness tends to infinity, and when the moment of external forces changes, it is large enough to solve many practically important problems of technological robotics. Thus, the considered dual-motor geared drive can be attributed to the class of high-precision servo drives and recommended for the construction of technological robots.

## **CHAPTER 3. EXPERIMENTAL STUDY OF DYNAMIC PROPERTIES OF TWO-CHANNEL PRECISION DIGITAL SERVO DRIVES FOR HIGH-PRECISION TECHNOLOGICAL ROBOTS**

### **3.1 Purpose and objectives of the experimental study of precision dual-motor geared servo drive**

The conclusions presented in Chapter 2, which allow us to recommend the considered dual-motor servo drive for the construction of technological robots, are made only on the basis of theoretical studies and computer simulation. Therefore, there is a need for an experimental study that could clarify the properties and capabilities of the proposed drives.

The aim of this stage of study is to determine the dynamic properties of two-channel dual-motor geared servo drives, to compare them with the properties of traditional servo drives, and to compare the results of the presented theoretical studies to the results of the experimental study. At the same time, it is important to verify in practice that the proposed solution provides high quality control.

To achieve this goal, it is necessary to create an experimental stand, which allows us to study the dynamic properties of such a drive, adjust its parameters and determine its dynamic properties. Also, since the purpose of the study is to compare the dynamic properties of the dual-motor drive with traditional drives, it is necessary to adjust the parameters also of the control system of the single-motor drive and to compare their dynamic properties.

### **3.2 Experimental stand for studying the dynamic properties of digital precision geared servo drives**

When developing the stand design, it was taken into account that the energy parameters of the drive should correspond to the parameters of the drive of the manipulator column, as this drive of the anthropomorphic type robot is one of the most loaded. It is exposed to large dynamic torque, caused by the moment of inertia of the other links of the manipulator. And at the same time this drive is not loaded with a static torque, which eliminates the influence of backlash, unlike the drive of the shoulder link. The arising position errors in this drive lead to larger deviations of the manipulator tool from the desired position as in the drives of other manipulator links.

Figure 3.1 shows the schematic diagram of the experimental stand (top view) of the study. Two motors are installed on the vertical platform: the motor of the internal servo drive (ISD) and of the torque loader. A resolver, which signal is used to determine speed and position of the internal drive, is installed

on the shaft of the first motor. A resolver is also mounted on the shaft of the loader motor. By means of rigid couplings, the shafts of these motors are fitted with pinions which mesh with the main gear wheel. These gears are mechanical transmissions that reduce rotational frequency of the output shaft of the drive and increase its torque. A precision position sensor (encoder) is also mounted on this shaft. Its signals are converted into digital code by a quadrature counter, which is used to close the main position feedback of the dual-motor drive.

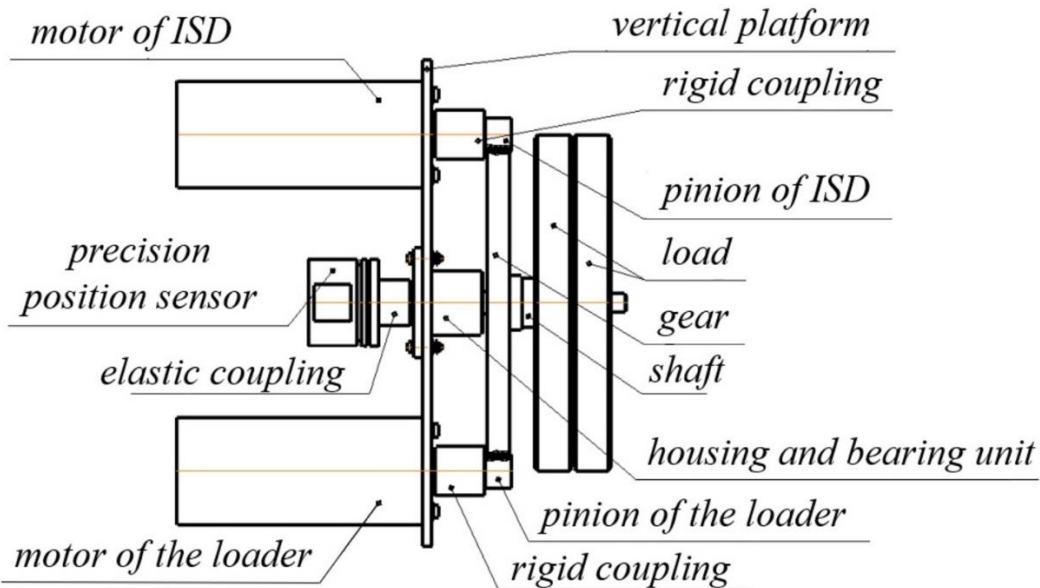


Figure 3.1 – Schematic diagram of dual-motor drive experimental stand (top view)

As the configuration of the manipulator's links changes while it's performing technological operation, the moment of inertia of the moving parts of the drives, including the shoulder link drive, also changes. According to [73], the moment of inertia of the moving parts of the drive in this case can change significantly, in some cases up to 10 times. In order to conduct experiments at different values of the moment of inertia on the stand, inertia of the manipulator link is simulated using removable plates. Their mass-dimensional parameters are selected in such a way that the resulting moment of inertia applied to the ISD motor shaft can be changed from 1 to 4 times when adding or removing this load.

Based on the diagram in Figure 3.1, an experimental stand was made, shown in Figure 3.2.



Figure 3.2 – Experimental stand of the dual-motor drive

To ensure elimination of backlash in such a drive when the control object (CO) is rotated both clockwise and anti-clockwise, the same requirements are imposed on the power and rated torque of the ISD motor and the loader motor. In this case, the dual-motor drive is able to provide torque relevant to half of the motor rated torque value (taking into account gear ratio of the gearboxes), and the parameters of the loader and ISD motors and gearboxes are the same. Therefore, the same PMSM motors B2.SM.000-6200 by KEB are used in the stand for both the ISD and the loader. Parameter values of such motors can be found in [66]. The motors nominal rotational frequency is 6200 rpm, nominal torque - 1 Nm, rotor moment of inertia -  $5.7 \times 10^{-5}$  kgm<sup>2</sup>, motor EMF coefficient - 0.577 Vs/rad, electromagnetic time constant - 3.2 ms and winding active resistance - 9.2 Ohm. The usage of such motors together with KEB Combivert 05.S4.D30-1270 V1.4 frequency converters, realizing vector control, made it possible to set a PWM frequency value of 16 kHz in the drive power converter.

Cylindrical gears with a gear ratio of 10, stiffness coefficient of 1294000 N\*m/rad and backlash of 6 angular minutes are used as gearboxes. Gear wheel and pinions are customized specifically for the stand, they are made of steel 45 with accuracy class 8-D according to GOST 1643-81. Their seating dimensions are made to 7 qualification, and the end runout of teeth is 20 microns for the pinions and 30 microns for the gear wheel. The gear wheel is made with a module 1 with 200 teeth with a dividing diameter of 200 mm. The pinions have 20 teeth and their dividing diameter is 20 mm.

The loader during operation creates a constant torque of 5 Nm on the gear. The loader motor is part of the drive, closed by velocity control loop of its shaft, and it responds to the input reference value of 150 rpm. It is important that such a drive operates in the mode of limiting the developed torque at the level of 0.5 N\*m.

To reveal potential accuracy of the dual-motor drive, a LIR-158A precision main position feedback sensor is selected. The sensor has such a resolution that the decimal number corresponding to the code at the output of its quadrature counter, changes by one unit when the CO is rotated by an angle of  $6.28 \times 10^{-6}$  rad. Position feedback sensors of the ISD motor shaft and loader motor shaft (resolvers) are

12-bit and generate a number of 4096 in the output register for one revolution. The drive controllers have internal converters of encoder signals. At the outputs of these converters, signals corresponding to those of equivalent encoders are generated, which are then processed by an external quadrature counter, which is one for the whole drive and is installed in the drive control device.

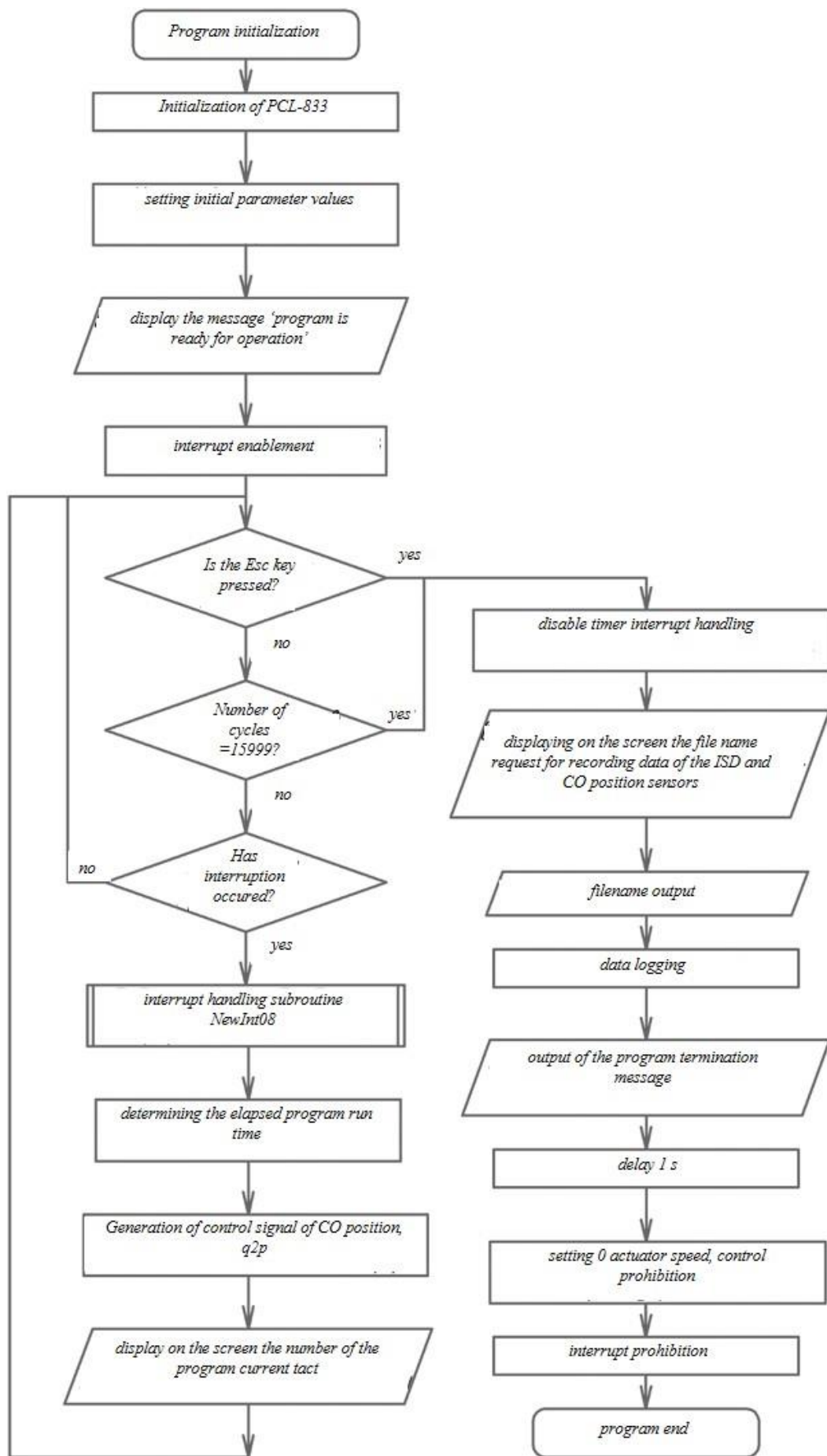
An industrial computer IPC Advantech 610 with ISA bus and running under DOS operating system is used as the drive control device. A 2-channel PCL-833 quadrature counter board is connected to ISA bus, which processes signals from LIR-158A sensor and encoder signals derived from the resolver signals on the ISD motor shaft.

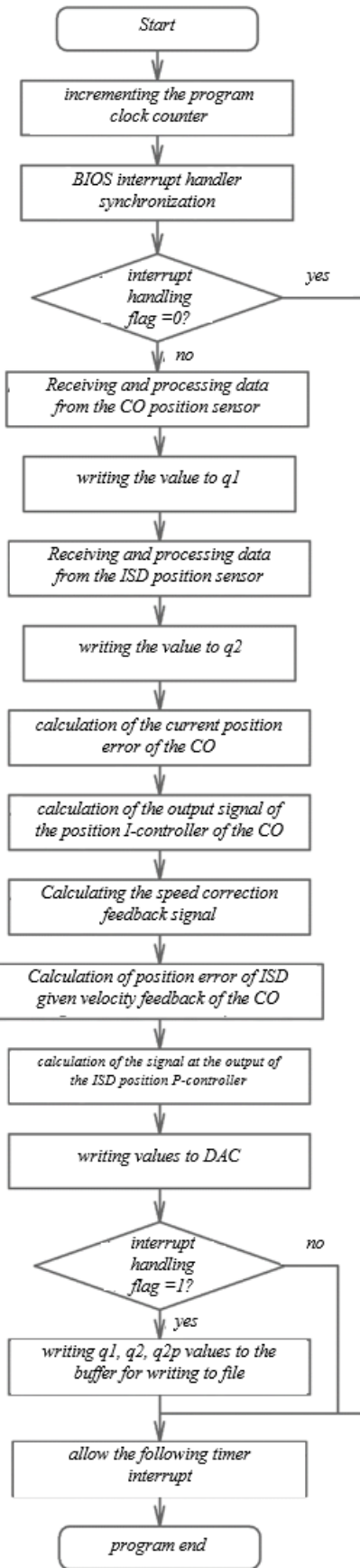
Digital data obtained as a result of processing signals from these sensors are used in the computer to calculate the reference input value, which is then converted by the DAC into voltage in the range of  $\pm 10$  V. This voltage is proportional to the reference value of the ISD motor rotational frequency, where 10 V corresponds to the value of 3000 rpm.

The calculation is performed by interrupts from the timer at frequency of 291 Hz, which is due to the period of the system 12-bit timer, running at 1193181 Hz ( $\sim 1.19$  MHz). With each interrupt a procedure written in C++ is called, in which the reference input value is calculated taking into account the current sensor values. Then the calculated value is fed as a digital code to the DAC ACL-6126, also connected to the ISA bus, and then the analog value is fed to the frequency converter of the first motor.

Thus, current and velocity control loops of the first motor are realized in the frequency converter KEB, and its position control loop is implemented in industrial computer, as well as speed and position control loops of the control object.

For the operation of the stand, a control program is executed on the industrial computer. The flowchart of the program's algorithm is presented in Figure 3.3. The source code of the control program, written in C++, is provided in Appendix A of the dissertation. In this program initialization of industrial computer is carried out first, checking the connection with devices connected to the ISA bus for real-time operation. These devices include a quadrature counter that processes the signal from the precision position sensor of the drive's CO, and also DAC that converts the reference input signal for the ISD velocity control loop. This signal is fed from the computer to the drive's frequency converter in analogue form. Also, at the beginning of the program the initial values of the variables are set. All counters used in the program are reset and a timer is set, which is used to trigger interrupts. The timer is set in such a way that the timer counter counts up to the value of 4096 and the frequency of interrupts is 291 Hz. After that, the interruption enable command is called in the main program, and the program goes into the waiting mode, until interruptions occur, or until the Esc key is pressed, or until the number of program cycles reaches 15999. In the last 2 cases, the program will go straight to termination.





b

Figure 3.3 – Block diagram of the algorithm of the main function (a) and interrupt handling function NewInt08 (b) of the stand control program

When calling the interrupt processing subroutine, which algorithm is shown in Figure 3.3 (b), firstly, the interrupt counter is incremented. Its value is used to synchronize the BIOS interrupt handler to maintain the necessary frequency value of 291 Hz, with which interrupts occur. Then, the signals from the position sensors of the ISD and loader are received. Based on these signals the outputs of the position controllers of the ISD and the loader are calculated. The calculated value for ISD is sent to the DAC to set the desired speed. If interrupts are enabled and are handled at that moment, the position sensor signals of the CO and ISD, along with the position reference input signal of the CO, are recorded into a buffer for subsequent writing to a file. At the end of the subroutine, permission for the next timer interruptions is enabled.

After the interrupt handling subroutine completes, the position reference input of the CO is generated, and the current cycle number of the control program is displayed on the screen. The program then proceeds to the final stage. Interrupt handling is disabled, and the filename for saving the position sensor signals of the ISD and CO, as well as the reference CO position values, is requested. A message indicating the completion of the program is then displayed, zero speed values are set for the drives, control is disabled, interrupts are disabled, and the program terminates.

Figure 3.4 shows the functional diagram of the stand. It illustrates that the industrial computer used in the stand, IPC Advantech 610, is connected via a high-speed industrial ISA bus to a quadrature counter PCL-833, which processes signals from the CO position sensor (LIR-158A) and the ISD position sensor, coming from the ISD frequency converter. Additionally, an ACL-6126 ADC is connected, which feeds the velocity reference signal to the motor frequency converter of the ISD.

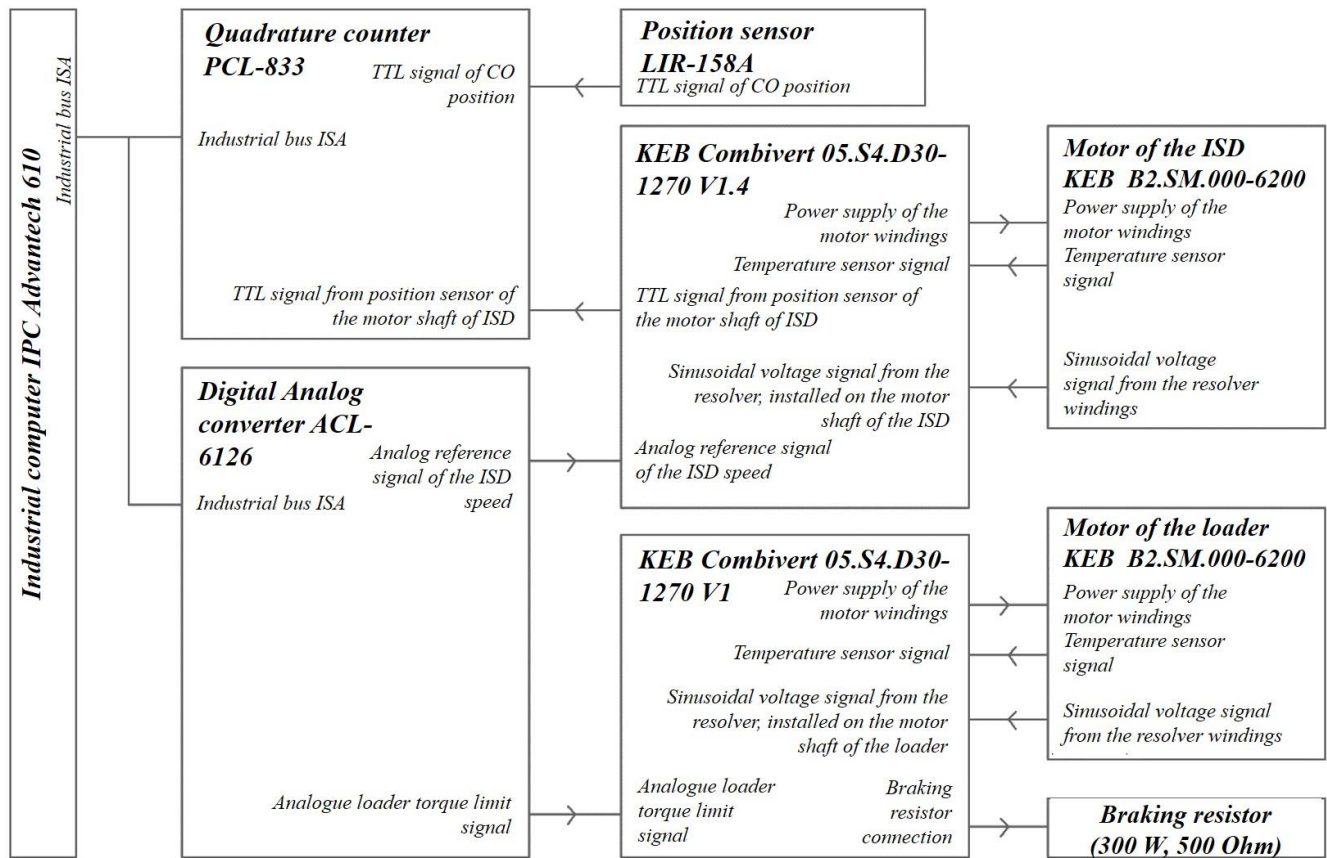


Figure 3.4 – Functional diagram of the stand

As can also be seen in the diagram, a braking resistor is connected to the loader, which dissipates the electricity generated by the loader into heat.

### 3.3 Synthesis of a digital servo drive of experimental stand

To prepare the stand for experiments, the synthesis of its control system as a cascade control system (with several inner control loops) was carried out. The methodology for tuning such a system is given in [65]. According to this technique, first of all, gain coefficients of the PI-controllers of the current and velocity control loops and P-controller of the ISD position control loop are adjusted. While tuning ISD, all the additional load with the inertia moment  $0.04 \text{ kg} \cdot \text{m}^2$  is installed on the output shaft of the control object, the loader drive is disconnected from the control system. It is present only to increase the moment of inertia of the CO in the form of a passive motor shaft with a reducer. Feedback signals are fed to the control system only from the resolver, installed on the ISD motor shaft. A precision position sensor is used to register the position of the CO without participating in the control process.

When setting the coefficients of the current, velocity and position controllers of the ISD, an important setting criterion is the duration of transients, which must be minimized. Also, an important

criterion is overshoot. Thus, in the ISD current control loop the value of the coefficient of the P-component of the controller is chosen to be 700, the value of the I-component - 100. At the same time, the overshooting in the loop should not exceed 5 % while responding to the step reference input. In the velocity control loop of the ISD, the value of the P-component gain of the velocity controller is 640, and the value of the I-component is 280. The overshooting in the velocity control loop does not exceed 50%. In the position control loop, the value of the P-component gain of the ISD is 0.5. The overshooting in this loop also does not exceed 5 %. These coefficient values were selected and used further in the stand.

After adjusting the controllers, the ISD responds to the input setpoint of the angular position of the CO equal to 0.1 rad, with a transient duration of 0.12 s, as shown in Figure 3.5. The transient process (a) and error (b) are shown here. Line 1 corresponds to the signal of the resolver, installed on the shaft of the ISD motor, taking into account the mechanical gear ratio (i.e. the value applied to the output shaft of the CO), and line 2 corresponds to the signal of the precision position sensor of the CO.

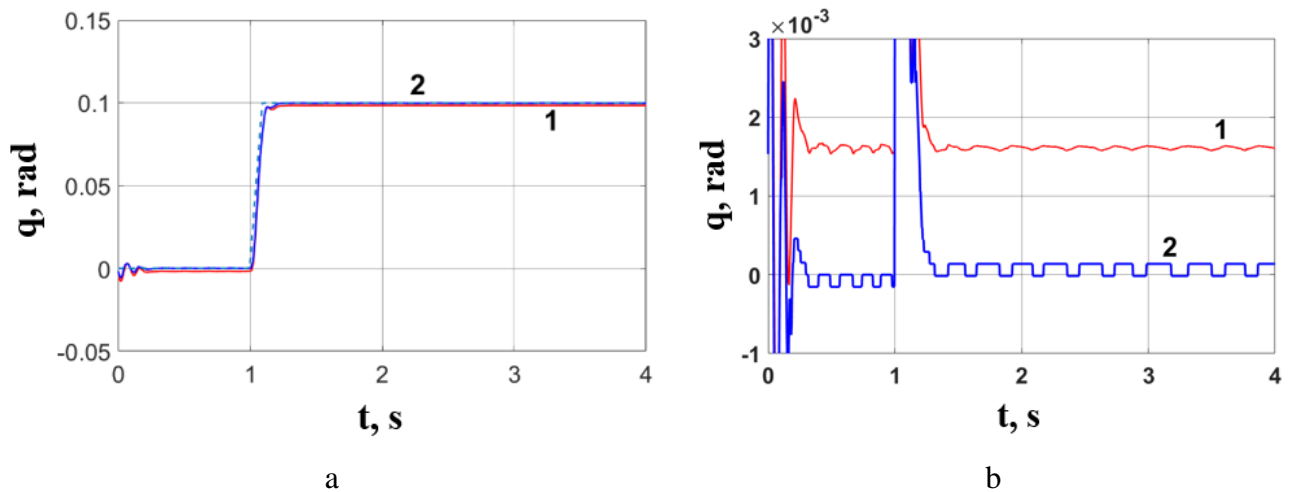


Figure 3.5 – Transient process (a) and error (b) at the **ISD** position control when the reference input is 0.1 rad after 1 s (1 - signal of the precision position sensor of the control object, 2 - resolver signal taking into account the mechanical transmission ratio)

Due to the fact that the mechanical transmission of the drive is outside the position control loop, there is a noticeable actual error between the desired and the actual positions of the CO in the figure. For example, the arithmetic mean of the error from the precision encoder signal of the CO position sensor is 1.6 % of the setpoint. If such a drive is used to control position of the shoulder link of a manipulator with a length of 1 m, such an error will lead to deviation of the axis on which the elbow link is mounted by about 1.6 mm, which in many practical applications is unacceptable for a technological robot.

Since the motors and gearboxes of the ISD and the loader are identical, the values of their controller gains after adjustment are also identical, which allows the loader control system to be set up

immediately. It is controlled in speed setting mode with a desired value of 150 rpm and a torque limit of 0.5 N\*m (half of the motor torque nominal value).

After connecting the loader, the drive consisting only of the ISD and the loader is able to respond to the input setpoints of 0.1 rad with a transient duration of 0.12 s, as shown in Figure 3.6, where line 1 corresponds to the resolver signal on the ISD motor shaft (taking into account the mechanical transmission ratio), and line 2 corresponds to the signal of the precision position sensor of the control object.

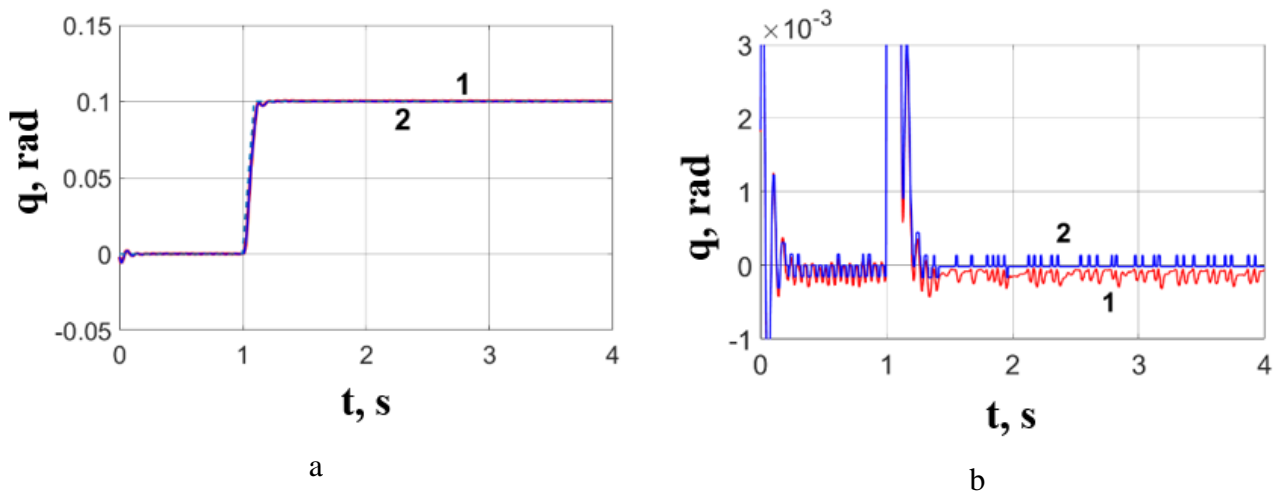


Figure 3.6 – Transient process (a) and error (b) during position control of the **ISD with the connected loader** responding to the input setpoint of 0.1 rad after 1 s (1 - signal of the precision position sensor of the control object, 2 - signal of the resolver taking into account the mechanical transmission)

Connection of the loader in this case, even without position feedback of the control object, reduced the arithmetic mean value of the CO position error to 0.15 % of the reference value. As can be seen in the Figure 3.6, the red line almost coincides with the blue line, which indicates a significant reduction in the error between the set and actual positions of the control object due to reducing the influence of backlash and elasticity of mechanical gears.

In Chapter 2 it was demonstrated using computer simulation that in such a drive, weakly damped oscillations can occur in the mechanical subsystem consisting of mechanical gear and a shaft with additional load, especially when using wave gearbox common in robotics with much lower value of the stiffness coefficient, for example,  $3.2 \times 10^4$  N\*m/rad. In this case in the stand, the stiffness coefficient of the mechanical transmission is large enough, so such oscillations are not noticeable in Figure 3.6. However, according to the conclusions of Chapter 2, the introduction of velocity feedback loop of the control object makes it possible to significantly increase gain of the position P-controller of the ISD and

to eliminate the possibility of such oscillations. Figure 3.7 shows the graphs of position error both **with** and **without velocity feedback control loop of the control object** at the increased value of the position P-controller gain of the ISD from the value 0.5 to the value 0.9.

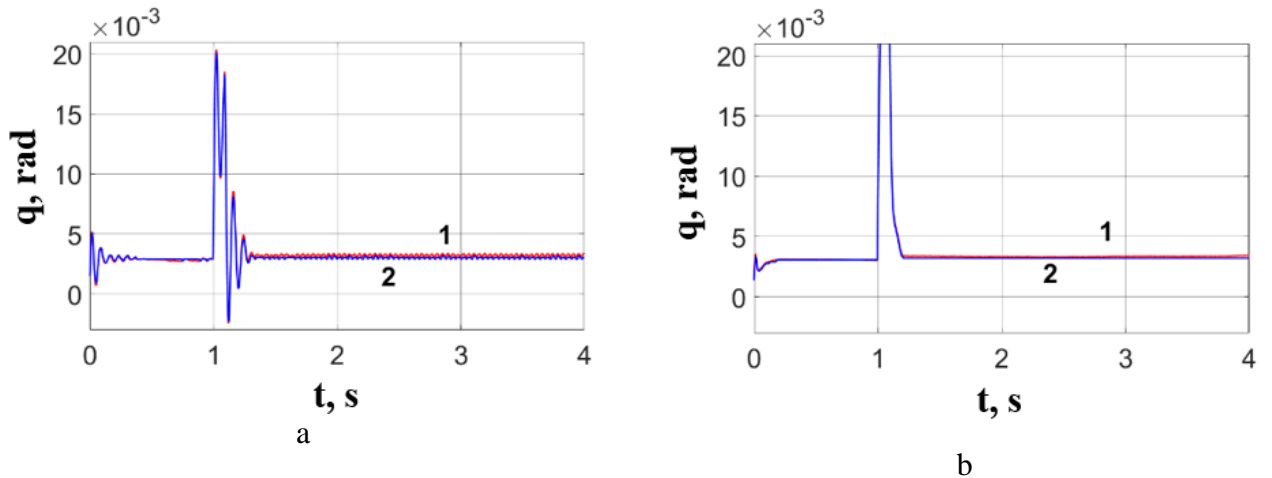


Figure 3.7 – Error of the ISD position **with the connected loader without velocity feedback control loop of the control object** (a) and **with it** (b) at responding to input setpoint 0.1 rad after 1 s (1 - signal of the precision position sensor of the control object, 2 - signal of the resolver taking into account the mechanical transmission)

As a result of increasing gain of the position P-controller of the ISD, low-frequency oscillations appeared, as shown in Figure 3.7(a). As can be seen in Figure 3.7(b), the velocity feedback control loop can damp such oscillations. However, the arithmetic mean value of the position error of the control object (according to precision position sensor) increased and amounted to 3.4 % of the reference value.

In [2] it is shown that to eliminate such an error it is necessary to close the main position feedback control loop of the control object of precision drive, and in the direct control loop to use an integral controller. At the value of the gain of drive position I-controller equal to 1.1, the overshooting is minimized and becomes less than 5% of the reference value, and the transients are as shown in Figure 3.8.

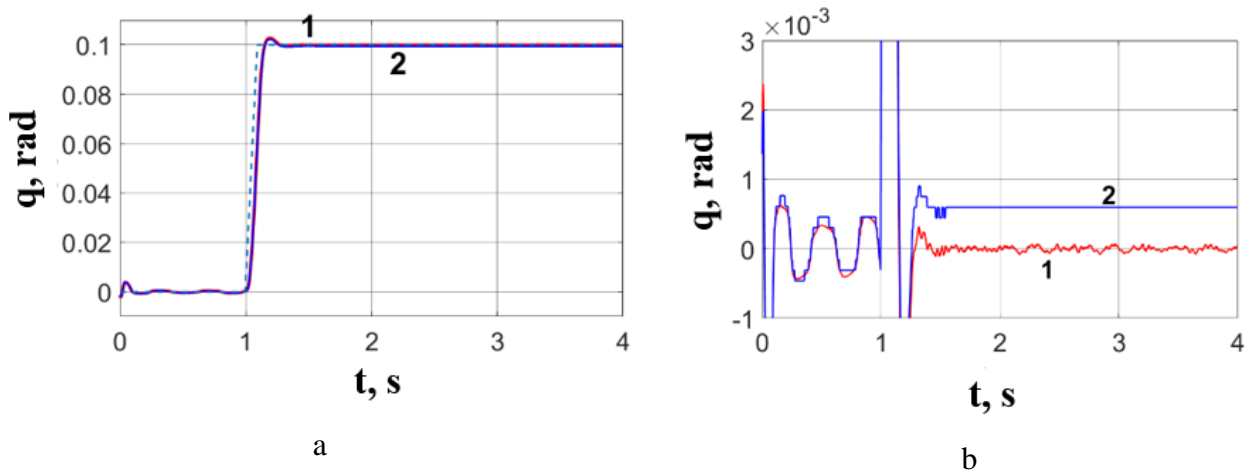


Figure 3.8 – Transient process (a) and error (b) during position control of a **dual-motor drive** responding to the input reference 0.1 rad after 1 s (1 - signal of the precision position sensor of the control object, 2 - signal of the resolver taking into account the ratio of the mechanical transmission)

If we do not introduce the corrective velocity feedback of the CO, and immediately close the main feedback loop of the precision drive, then with the same values of the drive controller gains, self-oscillations may occur during the transient process when responding to a reference input of 0.1 rad, as shown in Figure 3.9. Reducing the gain coefficients of the ISD position controllers and the entire drive would lead to a reduction in the cut-off frequency of the drive, which is already quite limited.

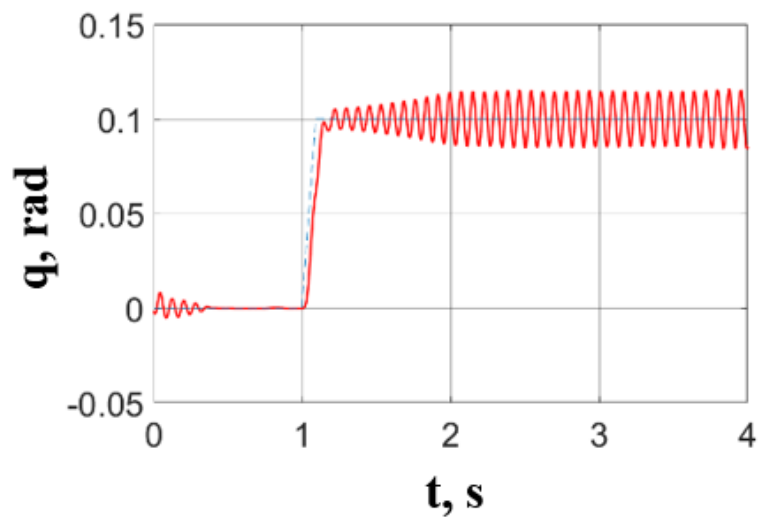


Figure 3.9 – Transient process during position control of a **dual-motor drive** without feedback loop of CO velocity when the setpoint is 0.1 rad after 1 s (calculated from the signal of a precision position sensor of the CO)

As a result of synthesis of the control system of the dual-motor drive, the estimate of the cut-off frequency of its open position loop was 27 rad/s. Thus, introducing corrective feedback of the CO velocity makes it possible to simultaneously increase the cut-off frequency of the drive and prevent the occurrence of self-oscillations.

### **3.4 Results of an experimental study of the properties of precision dual-motor servo drive**

The adjusted drive is capable of responding on a reference input of 0.1 rad with a transient time of 0.135 s. The arithmetic mean value of the error is close to 0 ( $3.7 \times 10^{-8}$  rad), and the maximum error in the steady-state mode is 0.0001 rad, which, when using such a drive to control the position of the shoulder link of a 1 m long manipulator, would lead to a deviation of the axis of the elbow link by about 100  $\mu$ m. Such a value is considerably smaller than that presented in Figure 3.5(a), but for technological operations such as robotic milling it is still quite large. Figure 3.8(b) shows oscillations occurring in steady state with an amplitude of approximately 0.00005 rad and frequency of  $4.4 \text{ s}^{-1}$ .

During computer simulation of the dual-motor drive it was found that such oscillations occur due to insufficient resolution of the position sensor installed on the shaft of the ISD motor. Thus, a sensor (equivalent encoder) with resolution of 1024 discrete per revolution is used in the stand. According to the computer simulation results presented in Section 2.5, increasing the sensor resolution to 2048 pulses per revolution reduces the maximum amplitude of such oscillations by nearly 46 times. Consequently, when using such a drive to control the position of the manipulator's shoulder link with length of 1 m, the deviation of the tool center point would be approximately 2.2  $\mu$ m. This leads to the conclusion that when designing a dual-motor drive, the position sensor for the ISD motor must have sufficiently high resolution. In this case, it is advisable to use an encoder generating at least 2048 counts per revolution.

Additionally, Figure 3.8(b) shows that in steady-state mode, the error value of the resolver signal, referred to the output shaft of the control object, is 0.0006 rad. Such a large error proves that accuracy of the drive without a main closed position feedback loop of the CO would be at least 6 times lower than the accuracy of the dual-motor drive with loader and such position feedback control loop.

### **3.5 Experimental comparison of the dynamic properties of dual-motor geared servo drive with dynamic properties of traditional single-motor servo drive**

Since the purpose of this study was to compare the dynamic properties of a dual-motor drive with conventional drives, the control system of a single-motor drive was also synthesized. For this case the

synthesized ISD with connected additional load was taken as a basis. The position of the control object was monitored using a LIR-158A precision encoder, but the main position control loop was closed by the ISD resolver signal. The gain coefficient of the position P-controller was adjusted to the value of 0.5 and the transient process was obtained, as shown in Figure 3.10, where the solid blue line is the signal corresponding to the position of the motor shaft taking into account the gear ratio, the solid red line is the signal corresponding to the position of the control object.

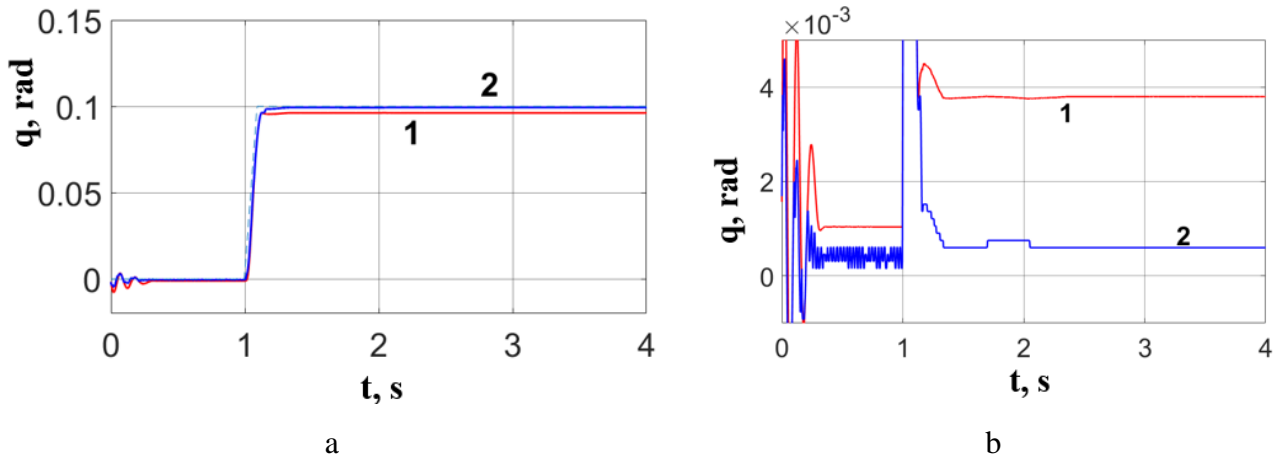


Figure 3.10 – Transient process (a) and error (b) at position control of **single-motor drive** responding to the input setpoint 0.1 rad after 1 s (1 - signal of the precision sensor of the position of the control object, 2 - signal of the resolver taking into account the ratio of the mechanical transmission)

As a result of this tuning, the cut-off frequency estimate of the open-loop single-motor drive was 46 rad/s, which is higher than the cut-off frequency estimate of the dual-motor drive. The drive is capable of responding on a reference input of 0.1 rad with a transient time of 0.12 s. In this case, the average value of the deviation of the CO from the reference position in steady state is 0.004 rad, although the resolver signal shows a deviation of 0.0006 rad. When using such a drive for position control of the shoulder link of the manipulator with a length of 1 m, it would lead to a deviation of the tool center point by about 4 mm, which is absolutely unacceptable for such technological operations as robotic milling.

In general, the obtained results, as, for example, in Figures 3.5 and 3.8, testify to the high accuracy of the dual-motor drive. Thus, when using a position sensor of the control object that generates 5000 pulses per revolution (excluding interpolation factor and quadrature pulse-counting mode), it has been established that while the drive was responding to a reference input of 0.1 rad, self-oscillations virtually disappeared, and the drive responded 40 times more accurately (taking into account the average and maximum values of the error).

In order to compare the dynamic properties of the dual-motor servo drive to the traditional single-motor one, a number of experiments were also carried out in which a sinusoidal input signal  $\beta(t) = \sin(\omega t)$  with amplitude 0.1 rad and frequency  $\omega$  equal to 0.1, 0.5 and 1 rad/s was set as the reference position value of the drive. Figure 3.11 shows the transient process (a) and the error (b) when a dual-motor drive is driven by a harmonic input signal with an amplitude 0.1 rad and frequency 0.5 rad/s.

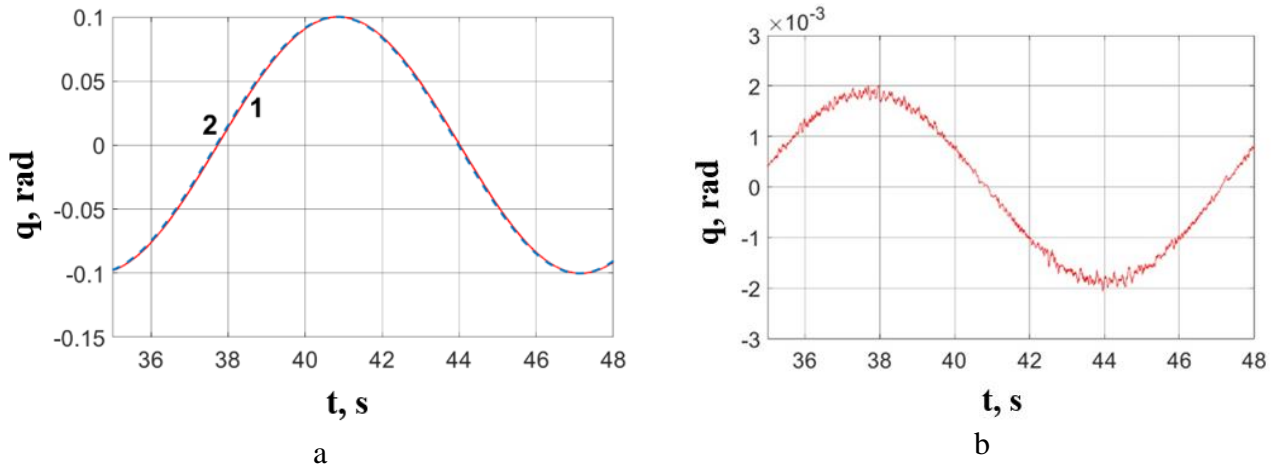


Figure 3.11 – Transient process (a) and error (b) when a **dual-motor drive** with auxiliary load responds to harmonic input signal with amplitude 0.1 rad and frequency 0.5 rad/s (1 - signal of the precision position sensor of the control unit, 2 - desired position of the CO)

As can be seen in Figure 3.11(a), the drive has velocity error, to eliminate which, both in the dual-motor and conventional drives, it is possible to use combined control loop with an additional component, proportional to the rate of change of the reference input. In addition to the input signal  $\beta(t)$ , the input signal  $Q(t)$ , determined by formula (3.1), is fed to the input of the position controller of both single- and dual-motor drives.

$$Q(t) = \frac{d\beta(t)}{dt} \frac{1}{\omega_{dp}}, \quad (3.1)$$

where  $\omega_{dp}$  – an estimate of the open loop cut-off frequency of the drive position. Thus  $\frac{d\beta(t)}{dt} = \omega \cdot \cos(\omega t)$  – is the rate of change of the input setpoint  $\beta(t)$ , which allows us not to use a differentiating device. As a result of application of the combined control, the graphs presented in Figures 3.12 and 3.13 are obtained.

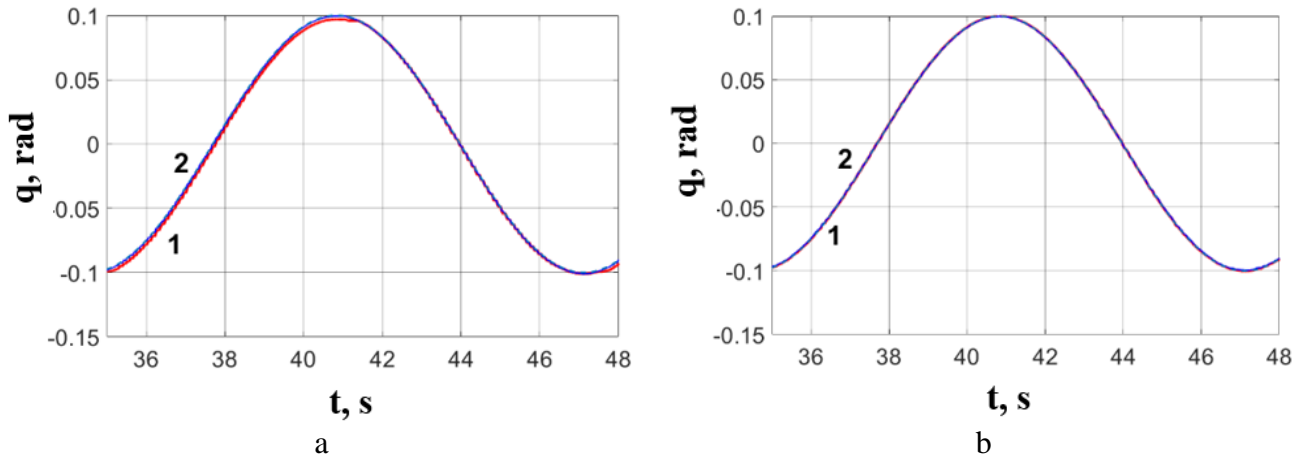


Figure 3.12 – Response on harmonic input signal with amplitude 0.1 rad and frequency 0.5 rad/s of a **single-motor** (a) and **dual-motor** (b) drive with additional load (solid blue line - resolver signal (taking into account the mechanical transmission ratio), solid red line - the signal of a precision position sensor of the CO)

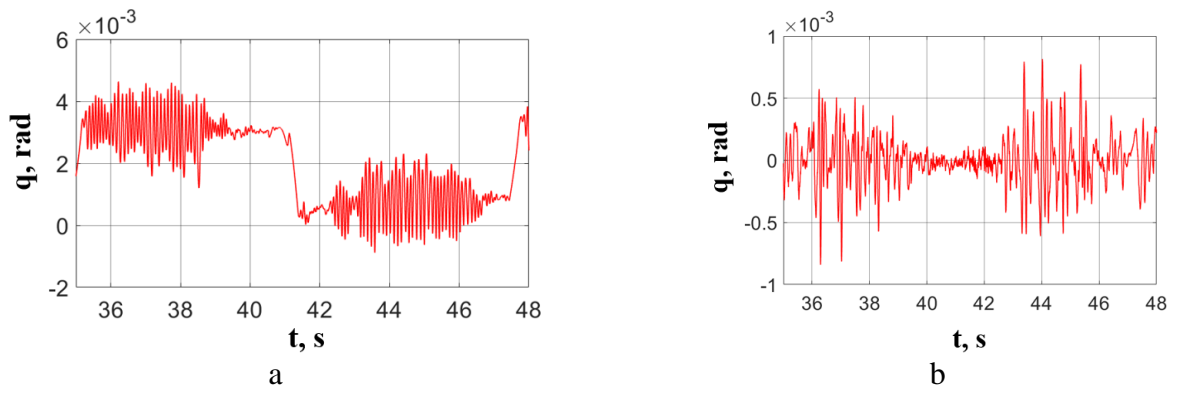


Figure 3.13 – Error of **single-motor** (a) and **dual-motor** (b) drive with additional load responding to harmonic input signal with amplitude of 0.1 rad and frequency of 0.5 rad/s (signal of precision position sensor)

When combined control is used for a single-motor drive, the value of  $\omega_{dp}$  is assumed to be 46 rad/s, for a dual-motor drive it is 27 rad/s. When increasing or decreasing the values of the cut-off frequency, the arithmetic mean and maximum values of the error are increasing, which confirms the correctness of estimation of cut-off frequencies. It is reasonable to consider the average values of the absolute value of the drive error  $|\delta_T|_{avg}$  and the maximum values of the error  $\Delta|\delta_T|_{max}$  deviation from  $|\delta_T|_{avg}$ , determined by formulas (3.2) и (3.3), as indicators of drive's accuracy.

$$|\delta_T|_{avg} = \frac{1}{T} \int_0^T |\delta_T(t)| dt, \quad (3.2)$$

$$\Delta|\delta_T|_{max} = \max(|\delta_T(t)| - |\delta_T|_{avg}). \quad (3.3)$$

Table 3.1 – Error values determined during the experiment.

	average value of the absolute value of the error, $ \delta_T _{avg}$ , rad				maximum deviation of the error from the average absolute value of the error, $\Delta \delta_T _{max}$ , rad			
	with additional load		without additional load		with additional load		without additional load	
input signal freq., rad/s	1-motor drive	2-motor drive	1-motor drive	2-motor drive	1-motor drive	2-motor drive	1-motor drive	2-motor drive
0.1	$15*10^{-4}$	$0.605*10^{-4}$	$12*10^{-4}$	$0.453*10^{-4}$	$6.8*10^{-3}$	$4*10^{-3}$	$5.1*10^{-3}$	$3*10^{-3}$
0.5	$20*10^{-4}$	$1.406*10^{-4}$	$16*10^{-4}$	$0.608*10^{-4}$	$6.4*10^{-3}$	$3.4*10^{-3}$	$4.5*10^{-3}$	$3.1*10^{-3}$
1	$23*10^{-4}$	$1.211*10^{-4}$	$21*10^{-4}$	$0.933*10^{-4}$	$7.1*10^{-3}$	$4.1*10^{-3}$	$5.1*10^{-3}$	$3*10^{-3}$

As a result of the experiment, the error values for single- and dual-motor drive are obtained and presented in Table 3.1. Figure 3.13 shows the response to a sinusoidal input signal with an amplitude 0.1 rad and frequency 0.5 rad/s by a conventional single-motor and dual-motor servo drive with an installed additional load. The backlash of the mechanical transmission of the single-motor drive is especially noticeable when the direction of rotation of the motor shaft is changed. The average value of the absolute value of the error in this case was  $20*10^{-4}$  rad. In the dual-motor drive the backlash of the mechanical transmission is eliminated, that's why the average value of the absolute value of the error in this case was  $1.406*10^{-4}$  rad.

At all the presented frequencies, both without and with additional load, the average value of absolute value of the error of the dual-motor drive is 14-26 times less than that of the single-motor drive. The maximum deviation of the error from the mean value of the absolute error is 1.7 to 1.8 times smaller for a dual-motor drive than for a single-motor drive. A more important indicator of drive's accuracy may be the maximum error value, shown in Figure 3.13. For the single-motor drive it is  $4.6*10^{-3}$  rad and for the dual-motor drive it is  $0.84*10^{-3}$  rad, indicating that the dual-motor drive is 5.5 times more accurate. By using a more accurate position sensor on the motor shaft of the internal servo drive, as mentioned earlier, the maximum error value can be further reduced.

Also, at reduction of the moment of inertia of the CO the average value of the absolute error of a dual-motor drive is 22-26 times less than that of a single-motor drive. As a result, in all considered cases the error of the dual-motor drive is noticeably smaller than that of the single-motor drive. This confirms the conclusions drawn in Chapter 2 of the dissertation, which state that the two-channel, dual-motor digital servo drives under consideration are highly precise and demonstrate their suitability for constructing analytically programmable industrial robots.

The materials presented in this chapter have been published in the author's work [76].

### 3.6 Conclusions on the third chapter

1. The results of the experimental study confirmed high accuracy of the dual-motor servo drive. The drive used in the experiments has the following dynamic properties. The duration of the transient process when responding to a step reference input 0.1 rad is 0.135 s; the average value of the error in the steady state does not exceed  $3.7 \times 10^{-8}$  rad, and the maximum error in the steady state is equal to  $1 \times 10^{-4}$  rad. This shows that the considered dual-motor servo drive with a position sensor generating 5000 pulses per revolution (excluding interpolation factor and quadrature pulse-counting mode) is 40 times more precise than a single-motor servo drive of the traditional structure, closed by the position control loop of the motor shaft. The experimental study also showed that the dual-motor servo drive responds on a harmonic reference input with amplitude 0.1 rad and frequency 0.5 rad/s with maximum error of  $8.4 \times 10^{-4}$  rad, which is 5.5 times more accurate than the single-motor servo drive.
2. It was also found that the relatively low resolution of the encoder on the motor shaft is an obstacle to further improve the dynamic properties of the dual-motor drive. The results of the computer simulation show that it is reasonable to use position sensor on the motor shaft of the internal servo drive with higher resolution. In particular, it has been demonstrated that using an encoder generating 2048 pulses per revolution achieves an optimal cost-accuracy compromise for the drive while eliminating self-oscillations.
3. When the moment of inertia of the control object is increased by 4 times, the presented accuracy improvement with a dual-motor drive is also maintained. However, when the moment of inertia changes more significantly, it is advisable to adaptively adjust the value of the ISD velocity controller gain and the velocity feedback coefficient of the control object in order to maintain high dynamic properties of the drive.
4. Thus, the experimental results confirm the findings of the theoretical research and justify the recommendation of two-channel, dual-motor digital servo drives for constructing technological robots with manipulation mechanisms with an open kinematic chain, when they are analytically programmed, and intended for technological operations requiring increased accuracy of movements, for example, for robotic milling or laser marking.

## CHAPTER 4. DEVELOPMENT OF MATHEMATICAL AND COMPUTER SIMULATION MODEL OF TECHNOLOGICAL ROBOT WITH PRECISION SERVO DRIVES

Following the conclusions drawn in chapters 1, 2, and 3 of the dissertation, it is advisable to conduct an analysis of the dynamic properties of a technological robot built on two-channel dual-motor geared servo drives and compare it with a robot built on traditional single-motor geared servo drives.

### 4.1 Description of mathematical model of technological robot

To conduct this study, a mathematical model of the robot is used, which incorporates the dynamic properties of the manipulator mechanism and drives, as well as the kinematic model of the technological robot's manipulator. The kinematic model describes four degrees of mobility that most strongly affect the accuracy of the robot's tool movements (Figure 4.1). Three of these degrees of freedom belong to the three-link planar angular mechanism, while the fourth is implemented via rotation of the column around the vertical axis  $Z_0$ . The manipulator's links are assumed to be absolutely rigid.

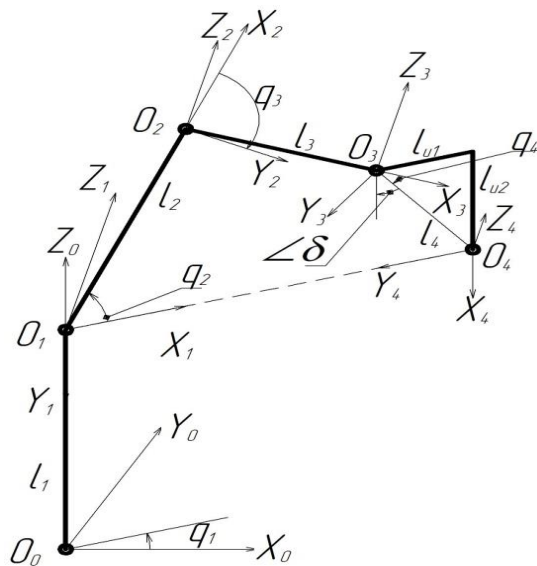


Figure 4.1. Kinematic diagram of the manipulator

The coordinate system used in the kinematic modelling of the studied robot manipulator is defined using the Denavit-Hartenberg method [4, 68, 69]. In Figure 4.1 the following notations are used:  $O_0X_0Y_0Z_0, O_1X_1Y_1Z_1, O_2X_2Y_2Z_2, O_3X_3Y_3Z_3, O_4X_4Y_4Z_4$  - the coordinate systems of the base, column, shoulder, elbow and wrist links of the manipulator, respectively;  $q_1, q_2, q_3, q_4$  - generalized coordinates of the manipulation mechanism;  $l_1, l_2, l_3, l_{u1}, l_{u2}$  - lengths of the manipulator links.

The wrist link refers to the tool mounted on the robot flange, designed for the tasks such as mechanical machining. The point  $O_4$  is the tool center point (TCP) of the manipulator. The relative positioning of the elements with lengths  $l_{u1}, l_{u2}$  does not change.

The value  $\beta$  represents the angle formed by the vertical axis and the manipulator's wrist link. During the technological operation performed by the manipulator, this angle must remain constant to ensure the tool maintains correct orientation relative to the workpiece at all trajectory points. The angle's value is calculated using the formula:

$$\beta = \frac{\pi}{2} - \text{atan} 2 \left( \frac{l_{u2}}{l_{u1}} \right).$$

The kinematic scheme of the robot manipulator under consideration corresponds to the homogeneous transformation matrix  $T_4$ , which determines the position and orientation of the tool at point  $O_4$  and is calculated by the formula:

$$T_4 = A_1 A_2 A_3 A_4,$$

where its constituent matrices  $A_1, A_2, A_3, A_4$  take the form

$$A_1 = \begin{bmatrix} \cos q_1 & 0 & -\sin q_1 & 0 \\ \sin q_1 & 0 & \cos q_1 & 0 \\ 0 & -1 & 0 & l_1 \\ 0 & 0 & 0 & 1 \end{bmatrix};$$

$$A_2 = \begin{bmatrix} \cos q_2 & \sin q_2 & 0 & l_2 \cos q_2 \\ -\sin q_2 & \cos q_2 & 0 & -l_2 \sin q_2 \\ 0 & 0 & 1 & 0 \\ 0 & 0 & 0 & 1 \end{bmatrix};$$

$$A_3 = \begin{bmatrix} \cos q_3 & -\sin q_3 & 0 & l_3 \cos q_3 \\ \sin q_3 & \cos q_3 & 0 & l_3 \sin q_3 \\ 0 & 0 & 1 & 0 \\ 0 & 0 & 0 & 1 \end{bmatrix};$$

$$A_4 = \begin{bmatrix} \cos(\beta + q_4) & -\sin(\beta + q_4) & 0 & l_4 \cos q_4 \\ \sin(\beta + q_4) & \cos(\beta + q_4) & 0 & l_4 \sin q_4 \\ 0 & 0 & 1 & 0 \\ 0 & 0 & 0 & 1 \end{bmatrix}.$$

From the last column of matrix  $T_4$  we extract the vector  $\vec{p}$ :

$$\vec{p} = \begin{bmatrix} \cos q_1 (l_3 \cos(q_2 - q_3) + l_2 \cos q_2 + l_4 \cos(q_2 - q_3 - q_4)) \\ \sin q_1 (l_3 \cos(q_2 - q_3) + l_2 \cos q_2 + l_4 \cos(q_2 - q_3 - q_4)) \\ l_1 + l_3 \sin(q_2 - q_3) + l_2 \sin q_2 + l_4 \sin(q_2 - q_3 - q_4) \end{bmatrix} = \begin{pmatrix} p_x \\ p_y \\ p_z \end{pmatrix},$$

which components are the solution to the direct kinematics problem (DKP) for the manipulator mechanism.

The components of the tool's velocity vector are determined by the formula

$$\begin{pmatrix} V_x \\ V_y \\ V_z \end{pmatrix} = J(q) \begin{pmatrix} \frac{dq_1}{dt} \\ \frac{dq_2}{dt} \\ \frac{dq_3}{dt} \\ \frac{dq_4}{dt} \end{pmatrix}, \quad (4.1)$$

where  $J(q)$  – the Jacobian matrix for the manipulator under consideration. It has the following form:

$$J(q) = \frac{d\vec{p}}{dt} = \begin{bmatrix} \frac{dp_x}{dq_1} & \frac{dp_x}{dq_2} & \frac{dp_x}{dq_3} & \frac{dp_x}{dq_4} \\ \frac{dp_y}{dq_1} & \frac{dp_y}{dq_2} & \frac{dp_y}{dq_3} & \frac{dp_y}{dq_4} \\ \frac{dp_z}{dq_1} & \frac{dp_z}{dq_2} & \frac{dp_z}{dq_3} & \frac{dp_z}{dq_4} \end{bmatrix}.$$

We note that the vector of moments  $M$  in the manipulator's joints is determined by the formula

$$M = J^T(q)F, \quad (4.2)$$

where  $F$  – vector of forces and moments acting on the end effector. Table 4.1 shows the parameter values of the manipulator mechanism used in the study.

Table 4.1 - Parameter values of the manipulator mechanism used in the study.

Parameter	Value
Column weight, $m_1$ , kg	55
Column length, $l_1$ , m	0.68
Weight of the shoulder link, $m_2$ , kg	38
Length of the shoulder link, $l_2$ , m	0.68
Weight of the elbow link, $m_3$ , kg	35
Length of the elbow link, $l_3$ , m	0.68
Weight of the wrist link, $m_4$ , kg	16
Length of the wrist link, $l_4$ , m	0.381
Length of the wrist link along the OY axis, $l_{u1}$ , m	0.68
Length of the wrist link along the OZ axis, $l_{u2}$ , m	0.68

The mathematical model of the dual-motor drive is described in Chapters 2 and 3. The distinctive feature of the drive model used here is that its output variable is the torque generated by the drive and applied to the corresponding manipulator link. The model receives feedback signals (the link's rotational speed and angle) from the manipulator mechanism model.

To develop a mathematical model of the robot, which takes into account the dynamic properties of the 4-link manipulator mechanism presented in Figure 4.1, the Matlab software package with the Symbolic Math Toolbox was used. A program (provided in Appendix B) was written using this toolkit to derive the manipulator's mathematical model in symbolic form. According to the methodology presented in [4], the manipulator's motion model is formulated using Lagrange's equations of the second kind. According to [4], the application of this methodology enables the derivation of numerical algorithms for simulating complex mechanisms, optimized for computational efficiency. The attached program first defines transition and homogeneous coordinate transformation matrices in symbolic form. It then solves the direct kinematics problem to determine the TCP position and the direct dynamics problem to compute TCP velocity projections onto Cartesian axes. Subsequently, using the Jacobian matrix (also in symbolic form), the program determines moments acting on the manipulator's actuators due to external forces and external torques applied to its tool during various technological operations. Next, it derives the link inertia matrices, components of the manipulator's inertial characteristics matrix, and components of the vector accounting for external forces and moments acting on the mechanism. By inverting the inertial characteristics matrix, the general equation of motion for the manipulator is obtained in symbolic form, enabling the generation of Simulink blocks implementing these equations for the computer simulation model of the manipulator's dynamics.

As a result of executing this program, the following equations of motion of the manipulator mechanism are obtained:

$$\begin{aligned}
\ddot{q}_1 = & 4\tau_1 + \dot{q}_1 \dot{q}_2 l_4^2 m_4 \sin(\pi - 2q_2 + 2q_3 + 2q_4) - \dot{q}_1 \dot{q}_2 l_4^2 m_4 \sin(\pi + 2q_2 - 2q_3 - 2q_4) - \dot{q}_1 \dot{q}_3 l_4^2 m_4 \sin(\pi - 2q_2 + 2q_3 + 2q_4) \\
& + \dot{q}_1 \dot{q}_3 l_4^2 m_4 \sin(\pi + 2q_2 - 2q_3 - 2q_4) - \dot{q}_1 \dot{q}_4 l_4^2 m_4 \sin(\pi - 2q_2 + 2q_3 + 2q_4) + \dot{q}_1 \dot{q}_4 l_4^2 m_4 \sin(\pi + 2q_2 - 2q_3 - 2q_4) \\
& + (\dot{q}_1 \dot{q}_2 l_4^2 m_4 \sin(2\beta - \pi - 2q_2 + 2q_3 + q_4))/3 - (\dot{q}_1 \dot{q}_3 l_4^2 m_4 \sin(2\beta - \pi - 2q_2 + 2q_3 + 2q_4))/3 - \\
& (\dot{q}_1 \dot{q}_4 l_4^2 m_4 \sin(2\beta - \pi - 2q_2 + 2q_3 + 2q_4))/3 - \dot{q}_3^2 l_2 l_4 m_4 \sin(\beta - \pi/2 + q_3 + q_4) - \dot{q}_3^2 l_2 l_4 m_4 \sin(\beta + \pi/2 + q_3 + q_4) \\
& + (\dot{q}_1 \dot{q}_2 l_3^2 m_3 \sin(\pi - 2q_2 + 2q_3))/3 - (\dot{q}_1 \dot{q}_2 l_3^2 m_3 \sin(\pi + 2q_2 - 2q_3))/3 + \dot{q}_1 \dot{q}_2 l_3^2 m_4 \sin(\pi - 2q_2 + 2q_3) - \\
& \dot{q}_1 \dot{q}_3 l_3^2 m_4 \sin(\pi + 2q_2 - 2q_3) - (\dot{q}_1 \dot{q}_3 l_3^2 m_3 \sin(\pi - 2q_2 + 2q_3))/3 + (\dot{q}_1 \dot{q}_3 l_3^2 m_3 \sin(\pi + 2q_2 - 2q_3))/3 - \\
& (\dot{q}_1 \dot{q}_3 l_3^2 m_4 \sin(\pi - 2q_2 + 2q_3) + \dot{q}_1 \dot{q}_3 l_3^2 m_4 \sin(\pi + 2q_2 - 2q_3) - (2\dot{q}_1 \dot{q}_2 l_4^2 m_4 \sin(2\beta - 2q_2 + 2q_3 + 2q_4))/3 + \\
& (2\dot{q}_1 \dot{q}_3 l_4^2 m_4 \sin(2\beta - 2q_2 + 2q_3 + 2q_4))/3 + (2\dot{q}_1 \dot{q}_4 l_4^2 m_4 \sin(2\beta - 2q_2 + 2q_3 + 2q_4))/3 - \\
& \dot{q}_1 \dot{q}_2 l_4^2 m_4 \sin(\beta + \pi - 2q_2 + 2q_3 + 2q_4) + \dot{q}_1 \dot{q}_3 l_4^2 m_4 \sin(\beta + \pi - 2q_2 + 2q_3 + 2q_4) + \dot{q}_1 \dot{q}_4 l_4^2 m_4 \sin(\beta + \pi - 2q_2 + 2q_3 + 2q_4) \\
& + (\dot{q}_1 \dot{q}_2 l_2^2 m_2 \sin(\pi - 2q_2))/3 - (\dot{q}_1 \dot{q}_2 l_2^2 m_2 \sin(\pi + 2q_2))/3 + \dot{q}_1 \dot{q}_2 l_2^2 m_3 \sin(\pi - 2q_2) - \\
& \dot{q}_1 \dot{q}_2 l_2^2 m_3 \sin(\pi + 2q_2) + \dot{q}_1 \dot{q}_2 l_2^2 m_4 \sin(\pi - 2q_2) - \dot{q}_1 \dot{q}_2 l_2^2 m_4 \sin(\pi + 2q_2) + \dot{q}_3^2 l_2 l_3 m_3 \sin(\pi/2 + q_3) + \\
& 2\dot{q}_3^2 l_2 l_3 m_4 \sin(\pi/2 + q_3) + (2\dot{q}_1 \dot{q}_2 l_2^2 m_2 \sin(2q_2))/3 + 2\dot{q}_1 \dot{q}_2 l_2^2 m_3 \sin(2q_2) + 2\dot{q}_1 \dot{q}_2 l_2^2 m_4 \sin(2q_2) - \\
& 2\dot{q}_1 \dot{q}_2 l_4^2 m_4 \sin(2q_3 - 2q_2 + 2q_4) + 2\dot{q}_1 \dot{q}_3 l_4^2 m_4 \sin(2q_3 - 2q_2 + 2q_4) + 2\dot{q}_1 \dot{q}_4 l_4^2 m_4 \sin(2q_3 - 2q_2 + 2q_4) - \\
& \dot{q}_1 \dot{q}_2 l_4^2 m_4 \sin(\beta - \pi - 2q_2 + 2q_3 + 2q_4) + (\dot{q}_1 \dot{q}_2 l_4^2 m_4 \sin(2\beta + \pi - 2q_2 + 2q_3 + 2q_4))/3 + \dot{q}_1 \dot{q}_3 l_4^2 m_4 \sin(\beta - \pi - 2q_2 + 2q_3 + 2q_4) - \\
& (\dot{q}_1 \dot{q}_4 l_4^2 m_4 \sin(2\beta + \pi - 2q_2 + 2q_3 + 2q_4))/3 - 2\dot{q}_4^2 l_4 m_4 \cos(\pi/2) * (l_3 \sin(\beta + q_4) - 2l_2 \sin(q_3 + q_4) - \\
& 2l_3 \sin(q_4) + l_2 \sin(\beta + q_3 + q_4)) + (2\dot{q}_1 \dot{q}_2 l_3^2 m_3 \sin(2q_2 - 2q_3))/3 + 2\dot{q}_1 \dot{q}_2 l_3^2 m_4 \sin(2q_2 - 2q_3) - \\
& (2\dot{q}_1 \dot{q}_3 l_3^2 m_3 \sin(2q_2 - 2q_3))/3 - 2\dot{q}_1 \dot{q}_3 l_3^2 m_4 \sin(2q_2 - 2q_3) - \dot{q}_3^2 l_2 l_3 m_3 \sin(\pi/2 - q_3) - 2\dot{q}_3^2 l_2 l_3 m_4 \sin(\pi/2 - q_3) + \\
& 2\dot{q}_1 \dot{q}_2 l_4^2 m_4 \sin(\beta - 2q_2 + 2q_3 + 2q_4) - 2\dot{q}_1 \dot{q}_3 l_4^2 m_4 \sin(\beta - 2q_2 + 2q_3 + 2q_4) - 2\dot{q}_1 \dot{q}_4 l_4^2 m_4 \sin(\beta - 2q_2 + 2q_3 + 2q_4) \\
& + 2\dot{q}_3^2 l_2 l_4 m_4 \sin(\pi/2 + q_3 + q_4) - \dot{q}_1 \dot{q}_2 l_2 l_4 m_4 \sin(\beta - \pi - 2q_2 + q_3 + q_4) + (\dot{q}_1 \dot{q}_3 l_2 l_4 m_4 \sin(\beta - \pi - 2q_2 + q_3 + q_4)/2 + \\
& \dot{q}_1 \dot{q}_3 l_3 l_4 m_4 \sin(\beta + \pi - 2q_2 + 2q_3 + q_4) + (\dot{q}_1 \dot{q}_4 l_3 l_4 m_4 \sin(\beta + \pi - 2q_2 + 2q_3 + q_4))/2 + (\dot{q}_1 \dot{q}_3 l_2 l_3 m_3 \sin(\pi + \\
& q_3))/2 + \dot{q}_1 \dot{q}_3 l_2 l_3 m_4 \sin(\pi + q_3) + \dot{q}_1 \dot{q}_4 l_3 l_4 m_4 \sin(\pi + q_4) - 2\dot{q}_1 \dot{q}_2 l_2 l_4 m_4 \sin(\pi + 2q_2 - q_3 - q_4) + \\
& \dot{q}_1 \dot{q}_3 l_2 l_4 m_4 \sin(\pi + 2q_2 - q_3 - q_4) - 2\dot{q}_1 \dot{q}_2 l_3 l_4 m_4 \sin(\pi + 2q_2 - 2q_3 - q_4) + \dot{q}_1 \dot{q}_4 l_2 l_4 m_4 \sin(\pi + 2q_2 - q_3 - q_4) + \\
& 2\dot{q}_1 \dot{q}_3 l_3 l_4 m_4 \sin(\pi + 2q_2 - 2q_3 - q_4) + \dot{q}_1 \dot{q}_4 l_3 l_4 m_4 \sin(\pi + 2q_2 - 2q_3 - q_4) + 6\dot{q}_1 \dot{q}_3 l_2 l_4 m_4 \sin(q_3 + q_4) + \\
& 6\dot{q}_1 \dot{q}_4 l_2 l_4 m_4 \sin(q_3 + q_4) - (\dot{q}_1 \dot{q}_3 l_2 l_4 m_4 \sin(\beta - \pi + q_3 + q_4))/2 - (\dot{q}_1 \dot{q}_4 l_2 l_4 m_4 \sin(\beta - \pi + q_3 + q_4))/2 + \\
& 2\dot{q}_2 \dot{q}_3 l_2 l_4 m_4 \sin(\beta - \pi/2 + q_3 + q_4) + 2\dot{q}_2 \dot{q}_3 l_2 l_4 m_4 \sin(\beta + \pi/2 + q_3 + q_4) + 2\dot{q}_2 \dot{q}_4 l_2 l_4 m_4 \sin(\beta - \pi/2 + q_3 + q_4) \\
& + 2\dot{q}_2 \dot{q}_4 l_2 l_4 m_4 \sin(\beta + \pi/2 + q_3 + q_4) - 2\dot{q}_3 \dot{q}_4 l_2 l_4 m_4 \sin(\beta - \pi/2 + q_3 + q_4) - 2\dot{q}_3 \dot{q}_4 l_2 l_4 m_4 \sin(\beta + \pi/2 + \\
& q_3 + q_4) + 2\dot{q}_1 \dot{q}_2 l_2 l_4 m_4 \sin(\beta - 2q_2 + q_3 + q_4) - \dot{q}_1 \dot{q}_3 l_2 l_4 m_4 \sin(\beta - 2q_2 + q_3 + q_4) - \dot{q}_1 \dot{q}_4 l_2 l_4 m_4 \sin(\beta - 2q_2 + \\
& q_3 + q_4) - \dot{q}_1 \dot{q}_2 l_2 l_3 m_3 \sin(\pi + 2q_2 - q_3) - 2\dot{q}_1 \dot{q}_2 l_2 l_3 m_4 \sin(\pi + 2q_2 - q_3) + (\dot{q}_1 \dot{q}_3 l_2 l_3 m_3 \sin(\pi + 2q_2 - q_3))/2 + \\
& \dot{q}_1 \dot{q}_3 l_2 l_3 m_4 \sin(\pi + 2q_2 - q_3) + 3\dot{q}_1 \dot{q}_3 l_2 l_3 m_3 \sin(q_3) + 6\dot{q}_1 \dot{q}_3 l_2 l_3 m_4 \sin(q_3) + 6\dot{q}_1 \dot{q}_4 l_3 l_4 m_4 \sin(q_4) - \\
& 4\dot{q}_1 \dot{q}_2 l_3 l_4 m_4 \sin(2q_3 - 2q_2 + q_4) + 4\dot{q}_1 \dot{q}_3 l_3 l_4 m_4 \sin(2q_3 - 2q_2 + q_4) + 2\dot{q}_1 \dot{q}_4 l_3 l_4 m_4 \sin(2q_3 - 2q_2 + q_4) + \\
& 2\dot{q}_1 \dot{q}_2 l_2 l_4 m_4 \sin(\pi - 2q_2 + q_3 + q_4) - \dot{q}_1 \dot{q}_3 l_2 l_4 m_4 \sin(\pi - 2q_2 + q_3 + q_4) - \dot{q}_1 \dot{q}_4 l_2 l_4 m_4 \sin(\pi - 2q_2 + q_3 + q_4) - \\
& (\dot{q}_1 \dot{q}_4 l_3 l_4 m_4 \sin(\beta + \pi + q_4))/2 - \dot{q}_1 \dot{q}_2 l_3 l_4 m_4 \sin(\beta - \pi - 2q_2 + 2q_3 + q_4) + \dot{q}_1 \dot{q}_3 l_3 l_4 m_4 \sin(\beta - \pi - 2q_2 + 2q_3 + \\
& q_4) + (\dot{q}_1 \dot{q}_4 l_3 l_4 m_4 \sin(\beta - \pi - 2q_2 + 2q_3 + q_4))/2 - 3\dot{q}_1 \dot{q}_3 l_2 l_4 m_4 \sin(\beta + q_3 + q_4) - 3\dot{q}_1 \dot{q}_4 l_2 l_4 m_4 \sin(\beta + q_3 + q_4) - \\
& (\dot{q}_1 \dot{q}_3 l_2 l_3 m_3 \sin(\pi - q_3))/2 - \dot{q}_1 \dot{q}_3 l_2 l_3 m_4 \sin(\pi - q_3) - 2\dot{q}_2 \dot{q}_3 l_2 l_3 m_3 \sin(\pi/2 + q_3) - 4\dot{q}_2 \dot{q}_3 l_2 l_3 m_4 \sin(\pi/2 + q_3) - \\
& \dot{q}_1 \dot{q}_4 l_3 l_4 m_4 \sin(\pi - q_4) - 4\dot{q}_2 \dot{q}_4 l_3 l_4 m_4 \sin(\pi/2 + q_4) + 4\dot{q}_3 \dot{q}_4 l_3 l_4 m_4 \sin(\pi/2 + q_4) + \dot{q}_1 \dot{q}_3 l_2 l_4 m_4 \sin(\pi + q_3 + q_4) + \\
& \dot{q}_1 \dot{q}_4 l_2 l_4 m_4 \sin(\pi + q_3 + q_4) + 2\dot{q}_1 \dot{q}_2 l_3 l_4 m_4 \sin(\beta - 2q_2 + 2q_3 + q_4) - 2\dot{q}_1 \dot{q}_3 l_3 l_4 m_4 \sin(\beta - 2q_2 + 2q_3 + q_4) - \\
& \dot{q}_1 \dot{q}_4 l_3 l_4 m_4 \sin(\beta - 2q_2 + 2q_3 + q_4) - \dot{q}_1 \dot{q}_2 l_2 l_4 m_4 \sin(\beta + \pi - 2q_2 + q_3 + q_4) + (\dot{q}_1 \dot{q}_3 l_2 l_4 m_4 \sin(\beta + \pi - 2q_2 + q_3 + q_4)/2 + \\
& (\dot{q}_1 \dot{q}_4 l_2 l_4 m_4 \sin(\beta + \pi - 2q_2 + q_3 + q_4))/2 + 2\dot{q}_1 \dot{q}_2 l_3 l_4 m_4 \sin(\pi - 2q_2 + 2q_3 + q_4) - 2\dot{q}_1 \dot{q}_3 l_3 l_4 m_4 \sin(\pi -
\end{aligned}$$

$$\begin{aligned}
& 2q_2 + 2q_3 + q_4) - \dot{q}_1 \dot{q}_4 l_3 l_4 m_4 \sin(\pi - 2q_2 + 2q_3 + q_4) - (\dot{q}_1 \dot{q}_4 l_3 l_4 m_4 \sin(\beta - \pi + q_4))/2 + 2\dot{q}_2 \dot{q}_4 l_3 l_4 m_4 \sin(\beta - \pi \\
& 2 + q_4) + 2\dot{q}_2 \dot{q}_4 l_3 l_4 m_4 \sin(\beta + \pi/2 + q_4) - 2\dot{q}_3 \dot{q}_4 l_3 l_4 m_4 \sin(\beta - \pi/2 + q_4) - 2\dot{q}_3 \dot{q}_4 l_3 l_4 m_4 \sin(\beta + \pi/2 + q_4) - \\
& (\dot{q}_1 \dot{q}_3 l_2 l_4 m_4 \sin(\beta + \pi + q_3 + q_4))/2 - (\dot{q}_1 \dot{q}_4 l_2 l_4 m_4 \sin(\beta\pi + q_3 + q_4))/2 + 2\dot{q}_2 \dot{q}_3 l_2 l_3 m_3 \sin(\pi/2 - q_3) + \\
& 4\dot{q}_2 \dot{q}_3 l_2 l_3 m_4 \sin(\pi/2 - q_3) + 4\dot{q}_2 \dot{q}_4 l_3 l_4 m_4 \sin(\pi/2 - q_4) - 4\dot{q}_3 \dot{q}_4 l_3 l_4 m_4 \sin(\pi/2 - q_4) + 2\dot{q}_1 \dot{q}_2 l_2 l_3 m_3 \sin(2q_2 - \\
& q_3) + 4\dot{q}_1 \dot{q}_2 l_2 l_3 m_4 \sin(2q_2 - q_3) - \dot{q}_1 \dot{q}_3 l_2 l_3 m_3 \sin(2q_2 - q_3) - 2\dot{q}_1 \dot{q}_3 l_2 l_3 m_4 \sin(2q_2 - q_3) + \dot{q}_1 \dot{q}_2 l_2 l_3 m_3 \sin(\pi - \\
& 2q_2 + q_3) + 2\dot{q}_1 \dot{q}_2 l_2 l_3 m_4 \sin(\pi - 2q_2 + q_3) - (\dot{q}_1 \dot{q}_3 l_2 l_3 m_3 \sin(\pi - 2q_2 + q_3))/2 - \dot{q}_1 \dot{q}_3 l_2 l_3 m_4 \sin(\pi - 2q_2 + q_3) + \\
& \dot{q}_1 \dot{q}_3 l_2 l_4 m_4 \sin(q_3 - \pi + q_4) + \dot{q}_1 \dot{q}_4 l_2 l_4 m_4 \sin(q_3 - \pi + q_4) - 4\dot{q}_2 \dot{q}_3 l_2 l_4 m_4 \sin(q_3 - \pi/2 + q_4) - 4\dot{q}_2 \dot{q}_3 l_2 l_4 m_4 \sin(\pi/ \\
& 2 + q_3 + q_4) - 4\dot{q}_2 \dot{q}_4 l_2 l_4 m_4 \sin(q_3 - \pi/2 + q_4) - 4\dot{q}_2 \dot{q}_4 l_2 l_4 m_4 \sin(\pi/2 + q_3 + q_4) + 4\dot{q}_3 \dot{q}_4 l_2 l_4 m_4 \sin(q_3 - \pi/2 + \\
& q_4) + 4\dot{q}_3 \dot{q}_4 l_2 l_4 m_4 \sin(\pi/2 + q_3 + q_4) - 4\dot{q}_1 \dot{q}_2 l_2 l_4 m_4 \sin(q_3 - 2q_2 + q_4) + 2\dot{q}_1 \dot{q}_3 l_2 l_4 m_4 \sin(q_3 - 2q_2 + q_4) + \\
& 2\dot{q}_1 \dot{q}_4 l_2 l_4 m_4 \sin(q_3 - 2q_2 + q_4) - 3\dot{q}_1 \dot{q}_4 l_3 l_4 m_4 \sin(\beta + q_4)
\end{aligned}$$

$$\begin{aligned}
\ddot{q}_2 = & 4\tau_2 - (\dot{q}_1^2 l_4^2 m_4 \sin(\pi - 2q_2 + 2q_3 + 2q_4))/2 + (\dot{q}_1^2 l_4^2 m_4 \sin(\pi + 2q_2 - 2q_3 - q_4))/2 - (\dot{q}_1^2 l_4^2 m_4 \sin(2\beta - \pi - \\
& 2q_2 + 2q_3 + 2q_4))/6 - (\dot{q}_1^2 l_3^2 m_3 \sin(\pi - 2q_2 + 2q_3))/6 + (\dot{q}_1^2 l_3^2 m_3 \sin(\pi + 2q_2 - 2q_3))/6 - (\dot{q}_1^2 l_3^2 m_4 \sin(\pi - 2q_2 + \\
& 2q_3))/2 + (\dot{q}_1^2 l_3^2 m_4 \sin(\pi + 2q_2 - 2q_3))/2 + (\dot{q}_1^2 l_4^2 m_4 \sin(2\beta - 2q_2 + 2q_3 + 2q_4))/3 + (\dot{q}_1^2 l_4^2 m_4 \sin(\beta + \pi - 2q_2 + \\
& 2q_3 + 2q_4))/2 - (\dot{q}_1^2 l_2^2 m_2 \sin(\pi - 2q_2))/6 + (\dot{q}_1^2 l_2^2 m_2 \sin(\pi + 2q_2))/6 - (\dot{q}_1^2 l_2^2 m_3 \sin(\pi - 2q_2))/2 + \\
& (\dot{q}_1^2 l_2^2 m_3 \sin(\pi + 2q_2))/2 - (\dot{q}_1^2 l_2^2 m_4 \sin(\pi - 2q_2))/2 + (\dot{q}_1^2 l_2^2 m_4 \sin(\pi + 2q_2))/2 - (\dot{q}_1^2 l_2^2 m_2 \sin(2q_2))/3 - \\
& \dot{q}_1^2 l_2^2 m_3 \sin(2q_2) - \dot{q}_1^2 l_2^2 m_4 \sin(2q_2) + \dot{q}_1^2 l_4^2 m_4 \sin(2q_3 - 2q_2 + 2q_4) + (\dot{q}_1^2 l_4^2 m_4 \sin(\beta - \pi - 2q_2 + 2q_3 + q_4))/2 - \\
& (\dot{q}_1^2 l_4^2 m_4 \sin(2\beta + \pi - 2q_2 + 2q_3 + 2q_4))/6 - (\dot{q}_1^2 l_3^2 m_3 \sin(2q_2 - 2q_3))/3 - \dot{q}_1^2 l_3^2 m_4 \sin(2q_2 - 2q_3) - \dot{q}_1^2 l_4^2 m_4 \sin(\beta - \\
& \pi - 2q_2 + 2q_3 + 2q_4) + -\dot{q}_1^2 l_2 l_4 m_4 \sin(\pi + 2q_2 - q_3 - q_4) + \dot{q}_1^2 l_3 l_4 m_4 \sin(\pi + 2q_2 - 2q_3 - q_4) - 4\dot{q}_3^2 l_2 l_4 m_4 \sin(q_3 + \\
& q_4) - 4\dot{q}_4^2 l_2 l_4 m_4 \sin(q_3 + q_4) - \dot{q}_1^2 l_2 l_4 m_4 \sin(\beta - 2q_2 + q_3 + q_4) + (\dot{q}_1^2 l_2 l_3 m_3 \sin(\pi + 2q_2 - 2q_3))/2 + \\
& \dot{q}_1^2 l_2 l_3 m_4 \sin(\pi + 2q_2 - q_3) - 2\dot{q}_2^2 l_2 l_3 m_3 \sin(q_3) - 4\dot{q}_2^2 l_2 l_3 m_4 \sin(q_3) - 4\dot{q}_4^2 l_3 l_4 m_4 \sin(q_4) + 2\dot{q}_1^2 l_3 l_4 m_4 \sin(2q_3 - \\
& 2q_2 + q_4) - 4g l_4 m_4 \sin(\pi/2) \cos(q_3 - q_2 + q_4) - \dot{q}_1^2 l_2 l_4 m_4 \sin(\pi - 2q_2 + 2q_3 + q_4) + (\dot{q}_1^2 l_3 l_4 m_4 \sin(\beta - \pi - 2q_2 + \\
& 2q_3 + q_4))/2 + 2\dot{q}_3^2 l_2 l_4 m_4 \sin(\beta + q_3 + q_4) + 2\dot{q}_4^2 l_2 l_4 m_4 \sin(\beta + q_3 + q_4) - \dot{q}_1^2 l_3 l_4 m_4 \sin(\beta - 2q_2 + 2q_3 + q_4) + \\
& 2g l_4 m_4 \sin(\pi/2) \cos(\beta - q_2 + q_3 + q_4) + (\dot{q}_1^2 l_2 l_4 m_4 \sin(\beta + \pi - 2q_2 + 2q_3 + q_4))/2 - 2g l_2 m_2 \sin(\pi/2) \cos(q_2) - \\
& 4g l_2 m_3 \sin(\pi/2) \cos(q_2) - 4g l_2 m_4 \sin(\pi/2) \cos(q_2) - \dot{q}_1^2 l_3 l_4 m_4 \sin(\pi - 2q_2 + 2q_3 + q_4) - \dot{q}_1^2 l_2 l_3 m_3 \sin(2q_2 - q_3) - \\
& 2\dot{q}_1^2 l_2 l_3 m_4 \sin(2q_2 - q_3) - 2g l_3 m_3 \cos(q_2 - q_3) \sin(\pi/2) - 4g l_3 m_4 \cos(q_2 - q_3) \sin(\pi/2) - (\dot{q}_1^2 l_2 l_3 m_3 \sin(\pi - 2q_2 + \\
& q_3))/2 - \dot{q}_1^2 l_2 l_3 m_4 \sin(\pi - 2q_2 + q_3) + 2\dot{q}_1^2 l_2 l_4 m_4 \sin(q_3 - 2q_2 + q_4) + 2\dot{q}_4^2 l_3 l_4 m_4 \sin(\beta + q_4) + (\dot{q}_1^2 l_2 l_4 m_4 \sin(\beta - \\
& \pi - 2q_2 + q_3 + q_4))/2 + (\dot{q}_1^2 l_3 l_4 m_4 \sin(\beta + \pi - 2q_2 + 2q_3 + q_4))/2 + 8\dot{q}_2 \dot{q}_3 l_2 l_4 m_4 \sin(q_3 + q_4) + \\
& 8\dot{q}_2 \dot{q}_4 l_2 l_4 m_4 \sin(q_3 + q_4) - 8\dot{q}_3 \dot{q}_4 l_2 l_4 m_4 \sin(q_3 + q_4) + 4\dot{q}_2 \dot{q}_3 l_2 l_3 m_3 \sin(q_3) + 8\dot{q}_2 \dot{q}_3 l_2 l_3 m_4 \sin(q_3) + \\
& 8\dot{q}_2 \dot{q}_4 l_3 l_4 m_4 \sin(q_4) - 8\dot{q}_3 \dot{q}_4 l_3 l_4 m_4 \sin(q_4) - 4\dot{q}_2 \dot{q}_3 l_2 l_4 m_4 \sin(\beta + q_3 + q_4) - 4\dot{q}_2 \dot{q}_4 l_2 l_4 m_4 \sin(\beta + q_3 + q_4) + \\
& 4\dot{q}_3 \dot{q}_4 l_2 l_4 m_4 \sin(\beta + q_3 + q_4) - 4\dot{q}_2 \dot{q}_4 l_3 l_4 m_4 \sin(\beta + q_4) + 4\dot{q}_3 \dot{q}_4 l_3 l_4 m_4 \sin(\beta + q_4) + 4\dot{q}_1 \dot{q}_4 l_3 l_4 m_4 \cos(\pi/2) \sin(\beta + \\
& q_4) - 8\dot{q}_1 \dot{q}_3 l_2 l_4 m_4 \cos(\pi/2) \sin(q_3 + q_4) - 8\dot{q}_1 \dot{q}_4 l_2 l_4 m_4 \cos(\pi/2) \sin(q_3 + q_4) - 4\dot{q}_1 \dot{q}_3 l_2 l_3 m_3 \cos(\pi/2) \sin(q_3) - \\
& 8\dot{q}_1 \dot{q}_3 l_2 l_3 m_4 \cos(\pi/2) \sin(q_3) - 8\dot{q}_1 \dot{q}_4 l_3 l_4 m_4 \cos(\pi/2) \sin(q_4) + 4\dot{q}_1 \dot{q}_3 l_2 l_4 m_4 \cos(\pi/2) \sin(\beta + q_3 + q_4) + \\
& 4\dot{q}_1 \dot{q}_4 l_2 l_4 m_4 \cos(\pi/2) \sin(\beta + q_3 + q_4)
\end{aligned}$$

$$\begin{aligned}
\ddot{q}_3 = & 4\tau_3 + (\dot{q}_1^2 l_4^2 m_4 \sin(\pi - 2q_2 + 2q_3 + 2q_4))/2 - (\dot{q}_1^2 l_4^2 m_4 \sin(\pi + 2q_2 - 2q_3 - 2q_4))/2 + (\dot{q}_1^2 l_4^2 m_4 \sin(2\beta - \pi - \\
& 2q_2 + 2q_3 + 2q_4))/6 + (\dot{q}_1^2 l_3^2 m_3 \sin(\pi - 2q_2 + 2q_3))/6 - (\dot{q}_1^2 l_3^2 m_3 \sin(\pi + 2q_2 - 2q_3))/6 + (\dot{q}_1^2 l_3^2 m_4 \sin(\pi - 2q_2 + \\
& 2q_3))/2 - (\dot{q}_1^2 l_3^2 m_4 \sin(\pi + 2q_2 - 2q_3))/2 - (\dot{q}_1^2 l_4^2 m_4 \sin(2\beta - 2q_2 + 2q_3 + 2q_4))/3 - (\dot{q}_1^2 l_4^2 m_4 \sin(\beta + \pi - 2q_2 + \\
& 2q_3 + 2q_4))/2 - \dot{q}_1^2 l_4^2 m_4 \sin(2q_3 - 2q_2 + 2q_4) - (\dot{q}_1^2 l_4^2 m_4 \sin(\beta - \pi - 2q_2 + 2q_3 + 2q_4))/2 +
\end{aligned}$$

$$\begin{aligned}
& (\dot{q}_1^2 l_4^2 m_4 \sin(2\beta + \pi - 2q_2 + 2q_3 + 2q_4))/6 + (\dot{q}_1^2 l_3^2 m_3 \sin(2q_2 - 2q_3))/3 + \dot{q}_1^2 l_3^2 m_4 \sin(2q_2 - 2q_3) + \dot{q}_1^2 l_4^2 m_4 \sin(\beta - 2q_2 + 2q_3 + 2q_4) - (\dot{q}_1^2 l_2 l_3 m_3 \sin(\pi + q_3))/4 - (\dot{q}_1^2 l_2 l_3 m_4 \sin(\pi + q_3))/2 - (\dot{q}_1^2 l_2 l_4 m_4 \sin(\pi + 2q_2 - q_3 - q_4))/2 - \\
& \dot{q}_1^2 l_3 l_4 m_4 \sin(\pi + 2q_2 - 2q_3 - q_4) - 3\dot{q}_1^2 l_2 l_4 m_4 \sin(q_3 + q_4) - 4\dot{q}_2^2 l_2 l_4 m_4 \sin(q_3 + q_4) + (\dot{q}_1^2 l_2 l_4 m_4 \sin(\beta - \pi + q_3 + q_4))/4 + (\dot{q}_1^2 l_2 l_4 m_4 \sin(\beta - 2q_2 + q_3 + q_4))/2 - (\dot{q}_1^2 l_2 l_3 m_3 \sin(\pi + 2q_2 - q_3))/4 - (\dot{q}_1^2 l_2 l_3 m_4 \sin(\pi + 2q_2 - q_3))/2 - \\
& (3\dot{q}_1^2 l_2 l_3 m_3 \sin(q_3))/2 - 3\dot{q}_1^2 l_2 l_3 m_4 \sin(q_3) - 2\dot{q}_2^2 l_2 l_3 m_3 \sin(q_3) - 4\dot{q}_2^2 l_2 l_3 m_4 \sin(q_3) + 4\dot{q}_4^2 l_3 l_4 m_4 \sin(q_4) - 2\dot{q}_1^2 l_3 l_4 m_4 \sin(2q_3 - 2q_2 + q_4) + 4g l_4 m_4 \sin(\pi/2) \cos(q_3 - q_2 + q_4) + (\dot{q}_1^2 l_2 l_4 m_4 \sin(\pi - 2q_2 + q_3 + q_4))/2 - \\
& (\dot{q}_1^2 l_3 l_4 m_4 \sin(\beta - \pi - 2q_2 + 2q_3 + q_4))/2 + (3\dot{q}_1^2 l_2 l_4 m_4 \sin(\beta + q_3 + q_4))/2 + 2\dot{q}_2^2 l_2 l_4 m_4 \sin(\beta + q_3 + q_4) + (\dot{q}_1^2 l_2 l_3 m_3 \sin(\pi - q_3))/4 + (\dot{q}_1^2 l_2 l_3 m_4 \sin(\pi - q_3))/2 - (\dot{q}_1^2 l_2 l_4 m_4 \sin(\pi + q_3 + q_4))/2 + \dot{q}_1^2 l_3 l_4 m_4 \sin(\beta - 2q_2 + 2q_3 + q_4) - 2g l_4 m_4 \sin(\pi/2) \cos(\beta - q_2 + q_3 + q_4) - (\dot{q}_1^2 l_2 l_4 m_4 \sin(\beta + \pi - 2q_2 + q_3 + q_4))/4 + \\
& \dot{q}_1^2 l_3 l_4 m_4 \sin(\pi - 2q_2 + 2q_3 + q_4) + (\dot{q}_1^2 l_2 l_4 m_4 \sin(\beta + \pi + q_3 + q_4))/4 + (\dot{q}_1^2 l_2 l_3 m_3 \sin(2q_2 - q_3))/2 + \dot{q}_1^2 l_2 l_3 m_4 \sin(2q_2 - q_3) + 2g l_3 m_3 \cos(q_2 - q_3) \sin(\pi/2) + 4g l_3 m_4 \cos(q_2 - q_3) \sin(\pi/2) + (\dot{q}_1^2 l_2 l_3 m_3 \sin(\pi - 2q_2 + q_3))/4 + (\dot{q}_1^2 l_2 l_3 m_4 \sin(\pi - 2q_2 + q_3))/2 - (\dot{q}_1^2 l_2 l_4 m_4 \sin(q_3 - \pi + q_4))/2 - \dot{q}_1^2 l_2 l_4 m_4 \sin(q_3 - 2q_2 + q_4) - 2\dot{q}_4^2 l_3 l_4 m_4 \sin(\beta + q_4) - (\dot{q}_1^2 l_2 l_4 m_4 \sin(\beta - \pi - 2q_2 + q_3 + q_4))/4 - (\dot{q}_1^2 l_3 l_4 m_4 \sin(\beta + \pi - 2q_2 + 2q_3 + q_4))/2 - \\
& 2\dot{q}_1 \dot{q}_2 l_2 l_4 m_4 \sin(\beta - \pi/2 + q_3 + q_4) - 2\dot{q}_1 \dot{q}_2 l_2 l_4 m_4 \sin(\beta + \pi/2 + q_3 + q_4) - 8\dot{q}_2 \dot{q}_4 l_3 l_4 m_4 \sin(q_4) + 8\dot{q}_3 \dot{q}_4 l_3 l_4 m_4 \sin(q_4) + 2\dot{q}_1 \dot{q}_2 l_2 l_3 m_3 \sin(\pi/2 + q_3) + 4\dot{q}_1 \dot{q}_2 l_2 l_3 m_4 \sin(\pi/2 + q_3) + 4\dot{q}_1 \dot{q}_4 l_3 l_4 m_4 \sin(\pi/2 + q_4) - 2\dot{q}_1 \dot{q}_4 l_3 l_4 m_4 \sin(\beta - \pi/2 + q_4) - 2\dot{q}_1 \dot{q}_4 l_3 l_4 m_4 \sin(\beta + \pi/2 + q_4) - 2\dot{q}_1 \dot{q}_2 l_2 l_3 m_3 \sin(\pi/2 - q_3) - 4\dot{q}_1 \dot{q}_2 l_2 l_3 m_4 \sin(\pi/2 - q_3) - 4\dot{q}_1 \dot{q}_4 l_3 l_4 m_4 \sin(\pi/2 - q_3) + 4\dot{q}_1 \dot{q}_2 l_2 l_4 m_4 \sin(q_3 - \pi/2 + q_4) + 4\dot{q}_1 \dot{q}_2 l_2 l_4 m_4 \sin(\beta + q_4) - 4\dot{q}_3 \dot{q}_4 l_3 l_4 m_4 \sin(\beta + q_4)
\end{aligned}$$

$$\begin{aligned}
\ddot{q}_4 &= 4\tau_4 + (\dot{q}_1^2 l_4^2 m_4 \sin(\pi - 2q_2 + 2q_3 + 2q_4))/2 - (\dot{q}_1^2 l_4^2 m_4 \sin(\pi + 2q_2 - 2q_3 - 2q_4))/2 + (\dot{q}_1^2 l_4^2 m_4 \sin(2\beta - \pi - 2q_2 + 2q_3 + 2q_4))/6 + g l_4 m_4 \sin(\beta - \pi/2 - q_2 + q_3 + q_4) - g l_4 m_4 \sin(\beta + \pi/2 - q_2 + q_3 + q_4) - (\dot{q}_1^2 l_4^2 m_4 \sin(2\beta - 2q_2 + 2q_3 + 2q_4))/3 - (\dot{q}_1^2 l_4^2 m_4 \sin(\beta + \pi - 2q_2 + 2q_3 + 2q_4))/2 + 2g l_4 m_4 \sin(\pi/2 + q_2 - q_3 - q_4) - \\
& \dot{q}_1^2 l_4^2 m_4 \sin(2q_3 - 2q_2 + 2q_4) - (\dot{q}_1^2 l_4^2 m_4 \sin(\beta - \pi - 2q_2 + 2q_3 + 2q_4))/2 + (\dot{q}_1^2 l_4^2 m_4 \sin(2\beta + \pi - 2q_2 + 2q_3 + 2q_4))/6 + \dot{q}_1^2 l_4^2 m_4 \sin(\beta - 2q_2 + 2q_3 + 2q_4) + 2g l_4 m_4 \sin(\pi/2 - q_2 + q_3 + q_4) - (\dot{q}_1^2 l_3 l_4 m_4 \sin(\pi + q_4))/2 - \\
& (\dot{q}_1^2 l_2 l_4 m_4 \sin(\pi + 2q_2 - q_3 - q_4))/2 - (\dot{q}_1^2 l_3 l_4 m_4 \sin(\pi + 2q_2 - 2q_3 - q_4))/2 - 3\dot{q}_1^2 l_2 l_4 m_4 \sin(q_3 + q_4) - 4\dot{q}_2^2 l_2 l_4 m_4 \sin(q_3 + q_4) + (\dot{q}_1^2 l_2 l_4 m_4 \sin(\beta - \pi + q_3 + q_4))/4 + (\dot{q}_1^2 l_2 l_4 m_4 \sin(\beta - 2q_2 + q_3 + q_4))/2 - \\
& 3\dot{q}_1^2 l_3 l_4 m_4 \sin(q_4) - 4\dot{q}_2^2 l_3 l_4 m_4 \sin(q_4) - 4\dot{q}_3^2 l_3 l_4 m_4 \sin(q_4) - \dot{q}_1^2 l_3 l_4 m_4 \sin(2q_3 - 2q_2 + q_4) + (\dot{q}_1^2 l_2 l_4 m_4 \sin(\pi - 2q_2 + q_3 + q_4))/2 + (\dot{q}_1^2 l_3 l_4 m_4 \sin(\beta + \pi + q_4))/4 - (\dot{q}_1^2 l_3 l_4 m_4 \sin(\beta - \pi - 2q_2 + 2q_3 + q_4))/4 + \\
& (3\dot{q}_1^2 l_2 l_4 m_4 \sin(\beta + q_3 + q_4))/2 + 2\dot{q}_2^2 l_2 l_4 m_4 \sin(\beta + q_3 + q_4) + (\dot{q}_1^2 l_3 l_4 m_4 \sin(\pi - q_4))/2 - (\dot{q}_1^2 l_2 l_4 m_4 \sin(\pi + q_3 + q_4))/2 + (\dot{q}_1^2 l_3 l_4 m_4 \sin(\pi - 2q_2 + 2q_3 + q_4))/2 - \\
& (\dot{q}_1^2 l_3 l_4 m_4 \sin(\beta - 2q_2 + 2q_3 + q_4))/2 - (\dot{q}_1^2 l_2 l_4 m_4 \sin(\beta + \pi - 2q_2 + q_3 + q_4))/4 + (\dot{q}_1^2 l_2 l_4 m_4 \sin(q_3 - \pi + q_4))/2 - \dot{q}_1^2 l_2 l_4 m_4 \sin(q_3 - 2q_2 + q_4) + (3\dot{q}_1^2 l_3 l_4 m_4 \sin(\beta + q_4))/2 + 2\dot{q}_2^2 l_3 l_4 m_4 \sin(\beta + q_4) + 2\dot{q}_3^2 l_3 l_4 m_4 \sin(\beta + q_4) - (\dot{q}_1^2 l_2 l_4 m_4 \sin(\beta - \pi - 2q_2 + q_3 + q_4))/4 - (\dot{q}_1^2 l_3 l_4 m_4 \sin(\beta + \pi - 2q_2 + 2q_3 + q_4))/4 - 2\dot{q}_1 \dot{q}_2 l_2 l_4 m_4 \sin(\beta - \pi/2 + q_3 + q_4) - 2\dot{q}_1 \dot{q}_2 l_2 l_4 m_4 \sin(\beta + \pi/2 + q_3 + q_4) - \\
& 4\dot{q}_1 \dot{q}_3 l_3 l_4 m_4 \sin(\pi/2 + q_4) - 2\dot{q}_1 \dot{q}_2 l_3 l_4 m_4 \sin(\beta - \pi/2 + q_4) - 2\dot{q}_1 \dot{q}_2 l_3 l_4 m_4 \sin(\beta + \pi/2 + q_4) - 4\dot{q}_1 \dot{q}_2 l_3 l_4 m_4 \sin(\pi/2 - q_4) + 4\dot{q}_1 \dot{q}_3 l_3 l_4 m_4 \sin(\pi/2 - q_4) + 42\dot{q}_1 \dot{q}_2 l_2 l_4 m_4 \sin(q_3 - \pi/2 + q_4) + 4\dot{q}_1 \dot{q}_2 l_2 l_4 m_4 \sin(\pi/2 + q_3 + q_4) - 4\dot{q}_2 \dot{q}_3 l_3 l_4 m_4 \sin(\beta + q_4)
\end{aligned}$$

where  $\tau_1, \tau_2, \tau_3, \tau_4$  – torques generated by the manipulator drives and applied to the manipulator's links. From the derived equations, expressions for the angular velocity and rotation angle of each link can be obtained:

$$q_i = \int_0^t \int_0^t \ddot{q}_i dt$$

$$\omega_i = \int_0^t \dot{q}_i dt$$

where  $i$  – sequence number of the manipulator link. Thus, the dynamic model of a 4-link manipulator was obtained. The general structural diagram of the mathematical model of the manipulator used in the research is shown in Figure 4.2.

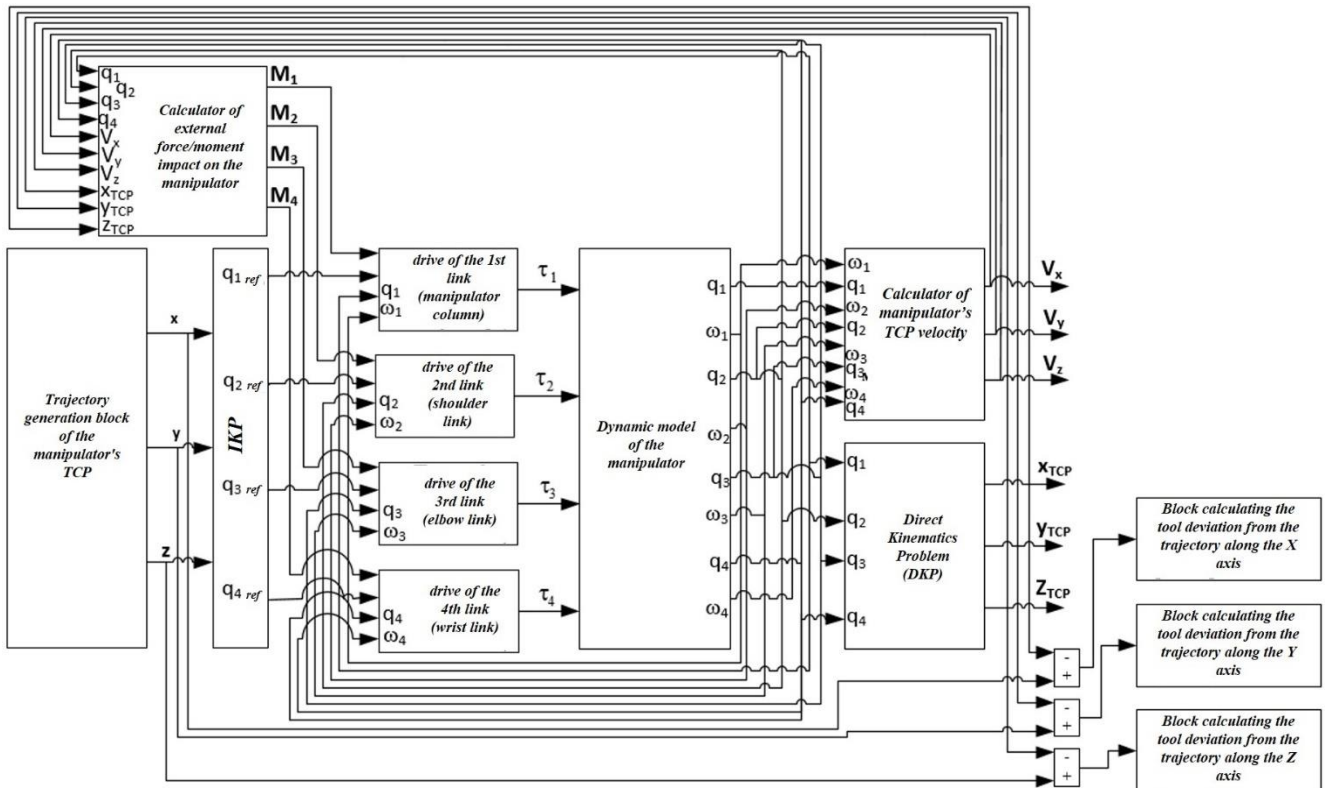


Figure 4.2. Structural diagram of the mathematical model of the robot used in the research

The computation of generalized coordinates and generalized velocities of the manipulator is implemented in the block representing its dynamic model. This block incorporates the dynamic equations of the manipulator mechanism, derived using Lagrange's equations of the second kind and the homogeneous transformation matrices  $T_1, T_2, T_3, T_4$  described earlier. The Inverse (IKP) and Direct (DKP) Kinematics Problems are solved in the respective blocks. The trajectory generation block calculates the coordinates of points along the manipulator's motion path during computer simulation.

With each integration step of this simulation model, the block outputs the coordinates of a new point, enabling contour control of the manipulator. The calculator of manipulator's TCP velocity computes components of the tool's velocity vector using expression (4.1). The calculator of external force/moment impact on the manipulator determines forces and moments acting on each link's actuators based on expression (4.2). If no external forces act on the manipulator's tool (e.g., during free motion without a technological operation), the forces and moments on each link's actuators are zero.

#### **4.2 Method for adjustment of precision dual-motor drives of technological robot**

The mathematical models of the drives are compiled using the algorithm presented in Section 2.2. In general, the requirements for selecting the motors and gearboxes of the manipulation mechanism correspond to those given in Section 1.4.1 of this paper. However, the accuracy of robot movements depends on the dynamic properties of its drives, which, in turn, depend on the choice of drive elements (motors, mechanical gears, and power converters), the structure of the controls, and the tuning of the controllers. Therefore, the usage of dual-motor servo drives for constructing a manipulation mechanism imposes additional conditions on these requirements:

1. The rated torques of the motors of the column, shoulder and elbow links of the manipulator should provide the maximum rotation frequency of these links of 2.723 rad/s, which is equal to 156 grad/s, and acceleration of 2.723 rad/s<sup>2</sup>. For the drive of the wrist link, the motors should be selected based on the requirements to ensure the maximum rotation frequency of 5.236 rad/s, which is equal to 300 grad/s, and acceleration of 5.236 rad/s<sup>2</sup>.
2. The ratio of the moment of inertia of each manipulator's link to the moment of inertia of the motor's rotor of this link, driven to the rotation shaft of this link, should be as small as possible and, preferably, close to 1, because in this case the transients in the drive become less oscillatory, and the arising oscillations are easier to damp.
3. Taking into account that the mechanical subsystems 'gearbox - manipulator link' are prone to oscillations as a result of weak internal damping, and that their dynamic properties significantly affect the manipulator properties, then, as shown in [2], to ensure stability of precision dual-motor drive, the cut-off frequency of the open-loop precision drive should be several times less than the natural frequency of the mechanical subsystem. Therefore, when selecting gearboxes, the values of their stiffness coefficients for the drive of each link must ensure the natural frequency of mechanical subsystems 'gearbox - manipulator link' not less than 40 rad/s. In this case it provides the cut-off frequency of open-loop dual-motor drives not less than 10 rad/s.

Based on these conditions, the motors and gearboxes of the manipulator built on dual-motor servo drives have been selected, which parameters are presented in Table 4.2. Here, motor models whose characteristics are similar to those of KEB 44.SM.203-34B5, 44.SM.203-34B5, 42.SM.203-34B5 and 33.SM.203-34B5 motors, respectively, are used. The shafts of these motors are fitted with resolvers with resolution of 4095 pulses/revolution. The characteristics of the gearbox models are similar to Harmonic Drive HFUC-58-2A-GR, HFUC-58-2A-GR, HFUC-45-2A-GR and HFUC-20-2A-GR wave gearboxes, respectively.

Table 4.2 - Parameter values of the dual-motor drives of the manipulation mechanism used in the research.

<b>Parameters of the dual-motor drive</b>	<b>Column and shoulder link</b>	<b>Elbow link</b>	<b>Wrist link</b>
Motors of the ISD and the loader	KEB 44.SM.203-34B5	KEB 42.SM.203-34B5	KEB 33.SM.203-34B5
Rated power, kW	2.67	1.44	0.68
<b>Motor rated torque, Nm</b>	<b>8.5</b>	<b>4.6</b>	<b>2.15</b>
Rated rotation frequency, min <sup>-1</sup>	3000	3000	3000
Gears of the ISD and the loader	Harmonic Drive HFUC-58-p2A-GR	Harmonic Drive HFUC-45-2A-GR	Harmonic Drive HFUC-20-2A-GR
<b>Gear ratio</b>	<b>120</b>	<b>120</b>	<b>80</b>
Gearbox stiffness coefficient, Nm/Rad	710000	330000	29000
<b>Backlash, arc. min.</b>	<b>1</b>	<b>1</b>	<b>1</b>
<b>PWM frequency, kHz</b>	<b>16</b>	<b>16</b>	<b>16</b>
<b>Resolver resolution (on motor), discrete/revolution</b>	<b>4095</b>	<b>4095</b>	<b>4095</b>
<b>Encoder resolution (on link), discrete/revolution</b>	<b>250000</b>	<b>250000</b>	<b>250000</b>
Loader torque (after gear), Nm	20.7	9.6	1.7

The same pairs of motors and gearboxes are used in torque loaders, which develop torques of 20.7; 20.7; 9.6 and 1.7 Nm, respectively. The manipulator also uses incremental main feedback sensors of its links position with resolution 250000 pulses/revolution.

To control the drives, controllers with inverters operating at frequency of 16 kHz are used. The controllers' gains are determined according to the algorithm presented in Section 2.4. For the drives of the column, shoulder, elbow, and wrist links, the natural oscillation frequencies of the mechanical subsystem (comprising the gear and the control object) are 41, 41, 58.7, and 67.6 rad/s, respectively. To achieve high precision of the manipulator tool's motion, the position controllers of all its actuators are tuned so that the cutoff frequencies of all servo drives in the open-loop state have the same values, as stated in [2]. The open-loop cutoff frequencies of the dual-motor drives are 11.3 rad/s.

### **4.3 Study of dynamic properties and accuracy of movements of technological robots with two-channel dual-motor drives of technological robots performing circular trajectory movements**

The most characteristic type of motion that allows detecting errors in the operation of manipulators and other technological machines is the movement of the end effector along a circular trajectory. Therefore, computer simulation was used to analyze the motion accuracy of a technological manipulator equipped with precision dual-motor servo drives when performing circular trajectories, compared to a manipulator with traditional single-motor geared servo drives.

In general, in order to choose one or another variant of drive design for industrial robots, it is important to have quantitative estimates of the potential accuracy of these variants when manipulator's end effector performs movements along typical trajectories. Therefore, a research was carried out to establish a methodology and obtain estimates of motion accuracy of technological robots built on conventional single-motor and precision dual-motor servo drives. The coordinates of the center of the desired trajectory circle were varied, as well as contour velocity (from 5 to 25 mm/s) and the radius of the circular trajectory (from 10 to 150 mm) in accordance with the requirements to technological robots designed for robotic milling, presented in Table 1.1. The conditions and results of this research are presented in Sections 4.3.1 - 4.3.3.

#### **4.3.1 Parameters of the manipulator, used in the research, constructed on conventional single-motor drives**

In this study, both variants of robot construction (with single- and dual-motor servo drives) are based on the same kinematic model of the manipulator, presented in Figure 4.1. However, the manipulator models with single- and dual-motor drives, although having the same lengths and masses of the links, differ from each other in mathematical models and values of some drive parameters.

The mathematical models of single-motor drives correspond to the mathematical models of the ISDs of dual-motor drives. PI-controllers are also used in the current and velocity control loops, and P-controllers in the position control loop. The models also include elastic gearboxes with backlashes and nonlinear correction blocks for reference signals at the inputs of the drive's position P-controllers.

When selecting motors and gearboxes for single-motor drives, the requirements listed in Section 4.2 were also taken into account. As a result, in both versions of manipulators the same models of motors and gearboxes presented in Table 4.2 are used in column, shoulder, elbow and wrist link drives. The values of the controllers' gains of the single-motor drives were selected in accordance with the

methodology presented in [65]. Since the position controllers of all manipulator drives are adjusted to ensure that the cutoff frequencies of all servo drives in the open-loop state have identical values, the open-loop cutoff frequencies of all manipulator links are equal and amount to 28.9 rad/s.

#### **4.3.2 Conditions for conducting a computational experiment to compare errors arising when manipulator with single-motor and two-channel dual-motor drives performs movements along circular trajectories**

The study of the robot's movement accuracy was performed when its end effector moved along six circular trajectories 1...6 lying in the horizontal and vertical planes, as shown in Figure 4.3. Trajectories 1, 2, 3 lie in the horizontal plane located at the same height with the axis of the manipulator's shoulder link, and trajectories 4, 5, 6 are in the vertical plane perpendicular to the  $X_0$  axis of the manipulator base coordinate system  $O_0X_0Y_0Z_0$ .

The centers of circles 2 and 5 coincide and are located in the central point. It is equidistant from the boundaries of the manipulator workspace and has the following coordinate values in the basic coordinate system:  $x_0 = 0.7975$  m,  $y_0 = 0$  m,  $z_0 = 0.68$  m. The centers of the other circular trajectories are displaced in both directions relative to the central point in their respective planes. The centers of circles 1 and 3 are displaced along  $X_0$  axis relative to the central point by  $-0.1975$  m and  $+0.1975$  m, respectively. The centers of circles 4 and 6 are offset along  $Z_0$  axis relative to the central point by  $-0.5$  m and  $+0.5$  m, respectively.

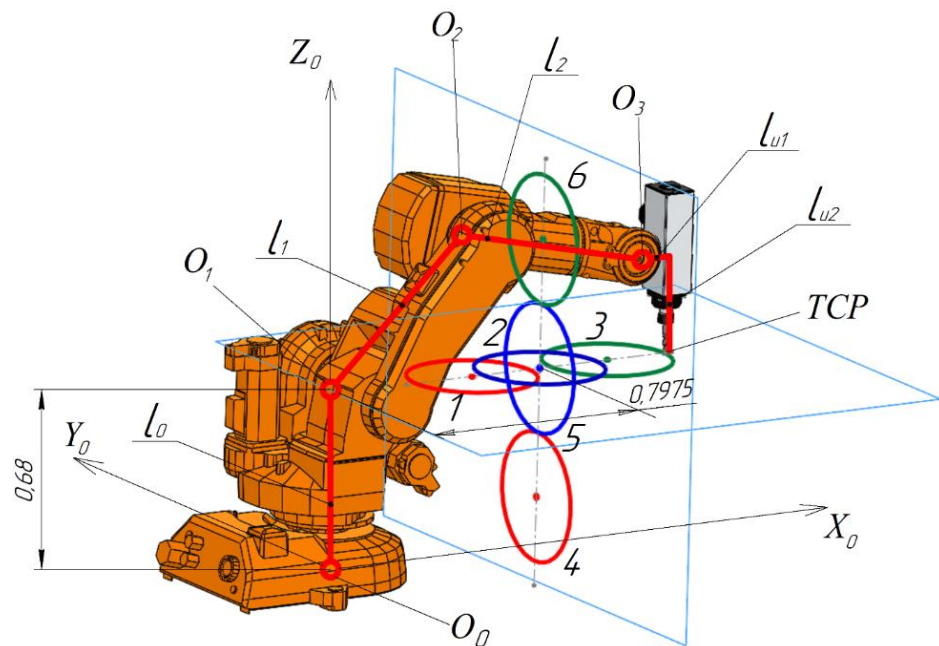


Figure 4.3. Circles performed by the manipulator's TCP in horizontal (1-3) and vertical (4-6) planes

The reference values of TCP coordinates  $x_{circ}$ ,  $y_{circ}$ ,  $z_{circ}$ , corresponding to circular trajectory lying in the horizontal plane, are determined by equations

$$\begin{aligned}x_{circ} &= x_0 + R \cos \Omega t, \\y_{circ} &= y_0 + R \sin \Omega t, \\z_{circ} &= z_0,\end{aligned}$$

where  $x_0, y_0, z_0$  – coordinates of the circle center;  $t$  – time;  $R$  – radius of the desired circle;  $\Omega$  – circular frequency, calculated by taking into account the contour velocity  $V$  by the formula

$$\Omega = VR^{-1}.$$

The desired coordinates of the end effector when moving along the circle trajectory in vertical plane are calculated according to the equations

$$\begin{aligned}y_{circ} &= y_0 + R \cos \Omega t, \\z_{circ} &= z_0 + R \sin \Omega t, \\x_{circ} &= x_0.\end{aligned}$$

It was assumed that the manipulator's tool maintains the same orientation in space at all points of the desired trajectory.

#### **4.3.3 Development of a method for assessing dynamic accuracy of movements of precision technological robots built on drives with the developed structure performing robotic milling operation**

When performing robotic milling operation, one of the most important indicators of the manipulator movement accuracy, which characterize the size and shape errors of the parts processed by the robot, is the root-mean-square radial deviation  $|R|_{avg}$  of the actual TCP trajectory of the manipulator from the desired circular trajectory in the steady-state mode of motion. It is determined by formula (4.3):

$$|R|_{avg} = \sqrt{\frac{1}{T} \int_0^T |\delta_R(t)|^2 dt}, \quad (4.3)$$

where  $t$  – time;  $T$  – duration of the manipulator tool movement along the circular trajectory;  $\delta_R(t)$  – current radial deviation. For example, when performing circular trajectories lying in the horizontal plane,  $\delta_R(t)$  is determined by the formula

$$\delta_R(t) = R_{circ} - \sqrt{(x_{rob} - x_0)^2 + (y_{rob} - y_0)^2},$$

while  $R_{circ}$  – radius of the reference circle;  $x_{rob}, y_{rob}$  – coordinates of the manipulator TCP at the current moment of time  $t$ ;  $x_0, y_0$  – coordinates of the center of the desired circle.

As a second indicator of dynamic accuracy of motions in the steady-state mode, we consider the axial RMS deviation of the manipulator TCP along the normal to the plane in which the desired motion trajectory is located. When performing movements along trajectories in the horizontal plane, the root-mean-square axial deviation is denoted as  $|Z|_{avg}$ , and in the vertical plane -  $|X|_{avg}$ . These metrics are determined by the formulas:

$$|Z|_{avg} = \sqrt{\frac{1}{T} \int_0^T |\delta_z(t)|^2 dt}, \quad (4.4)$$

$$|X|_{avg} = \sqrt{\frac{1}{T} \int_0^T |\delta_x(t)|^2 dt}, \quad (4.5)$$

$$\delta_z(t) = z_{circ} - z_{rob},$$

$$\delta_x(t) = x_{circ} - x_{rob},$$

where  $z_{circ}$  and  $z_{rob}$  – the desired and actual TCP coordinates of the manipulator at the current moment of time  $t$  along  $O_0Z_0$  axis, respectively;  $x_{circ}$  and  $x_{rob}$  – the desired and actual TCP coordinates of the manipulator at the current moment of time  $t$  along  $O_0X_0$  axis, respectively.

Thus, to evaluate dynamic accuracy of precision technological robots built on the drives of the developed structure, it is necessary to determine the accuracy metrics specified in formulas (4.3) - (4.5) through computer simulation. This should be done for robots built on dual-motor drives at various values of the desired circle's radius  $R$ , contour speed  $V$ , and different positions of the performed circular trajectories. Such a method of evaluating the dynamic accuracy of technological robots with dual-motor drives allows us to establish qualitative and quantitative relationships between the deviation of the end effector from the desired trajectory and the parameters of the robotic milling operation performed, as presented in publications [16, 78, 83, 84]. And the mathematical models developed during the study enable predicting the operational errors of the technological robot and, for each permissible deviation of the end-effector from the desired trajectory, selecting the maximum feasible contour velocity (from

accuracy standpoint) that ensures the highest performance while meeting the accuracy requirements of the technological operation.

Determination of the same accuracy indicators for a robot with drives of the traditional structure and their comparison with the indicators for a robot with the drives of the developed structure will allow us to make conclusions about the feasibility of constructing industrial robot arms on dual-motor servo drives at their analytical programming and for technological operations requiring increased accuracy, for example, robotic milling.

#### 4.3.4 Results of computer simulations

The influence of the contour speed  $V$  on the root-mean-square (RMS) radial deviation  $|R|_{avg}$  at different values of the radius  $R$  of the desired circle in the horizontal plane is shown in Figures 4.4, 4.6, 4.8. Dependences on the same factors of the root-mean-square axial deviation  $|Z|_{avg}$  are shown in Figures 4.5, 4.7, 4.9. The diagrams 1, 2, 3 and 4 in these figures correspond to radius values of 10 mm, 50 mm, 100 mm and 150 mm, respectively. The figures labelled with **a** refer to a robot with conventional single-motor servo drives, while those labelled with **b** refer to a robot with precision dual-motor drives. The values of the motion accuracy metrics are determined during computer simulation are approximated by second degree polynomials using the least squares method.

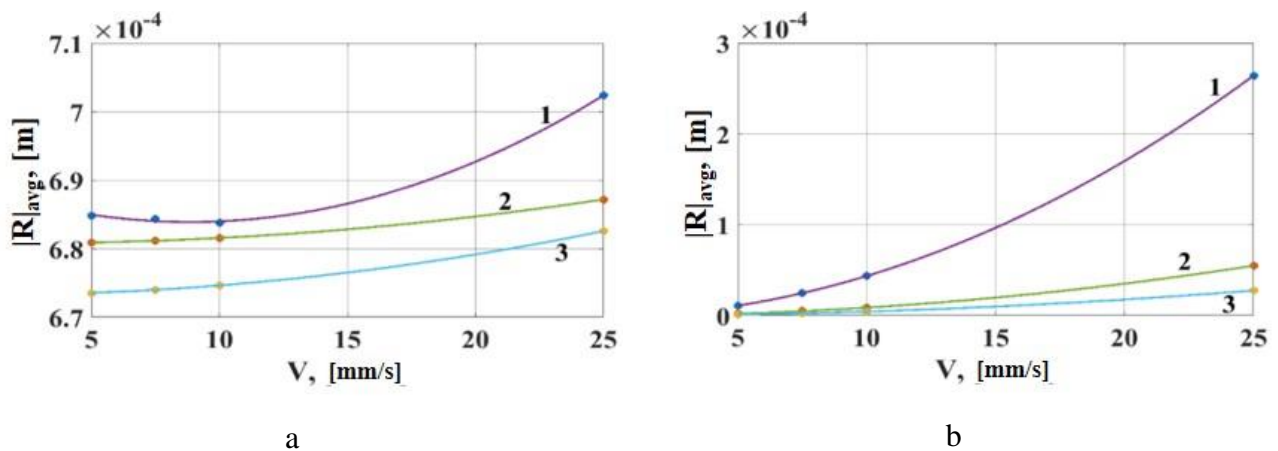


Figure 4.4. Deviations  $|R|_{avg}$  of manipulator with single-motor (a) and dual-motor (b) drives when performing movements of the end effector along circular trajectory 1 in the horizontal plane

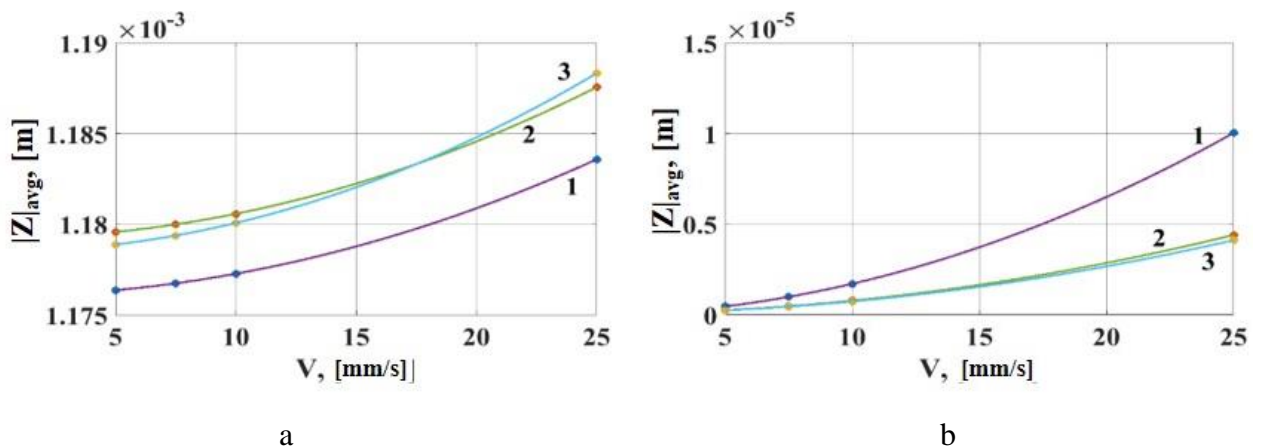


Figure 4.5. Deviations  $|Z|_{avg}$  of manipulator with single-motor (a) and dual-motor (b) drives when performing movements of the end effector along circular trajectory 1 in the horizontal plane

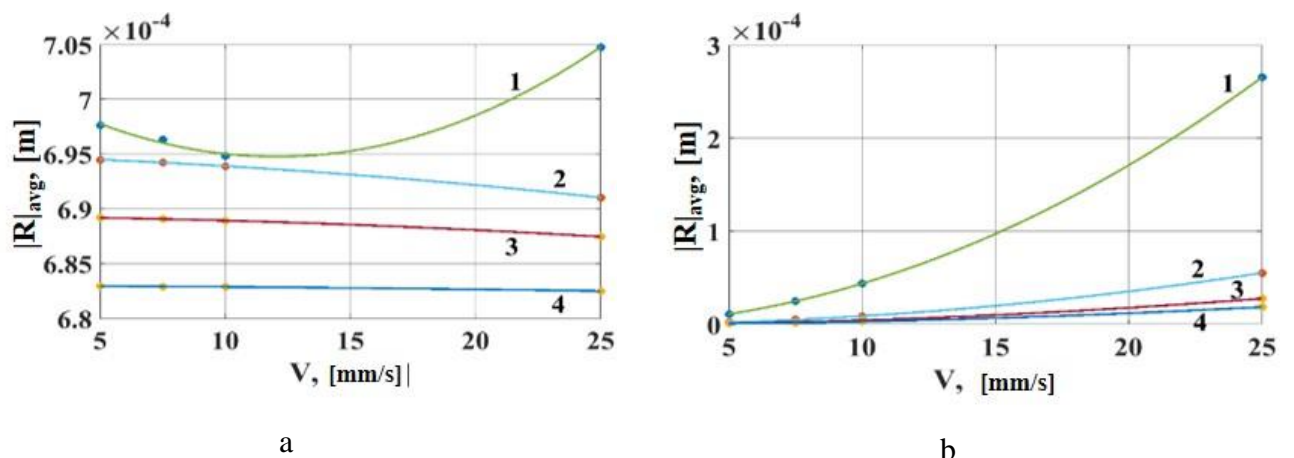


Figure 4.6. Deviations  $|R|_{avg}$  of manipulator with single-motor (a) and dual-motor (b) drives when performing movements of the end effector along circular trajectory 2 in the horizontal plane

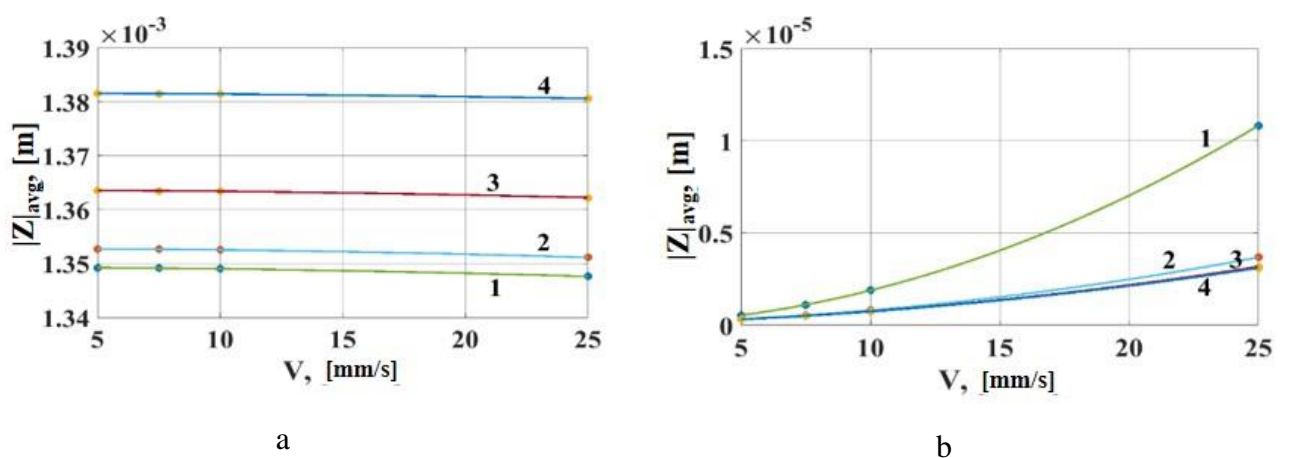


Figure 4.7. Deviations  $|Z|_{avg}$  of manipulator with single-motor (a) and dual-motor (b) drives when performing movements of the end effector along circular trajectory 2 in the horizontal plane

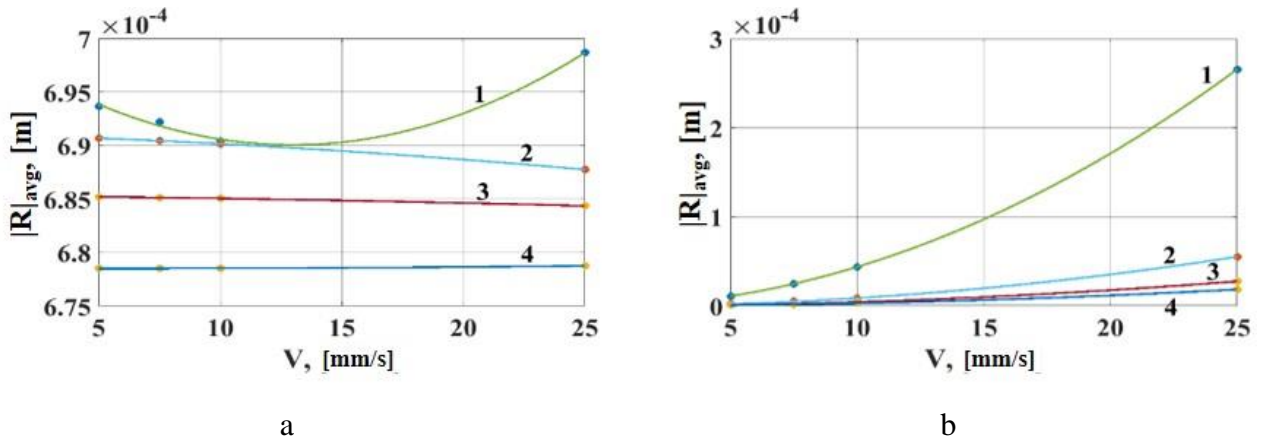


Figure 4.8. Deviations  $|R|_{avg}$  of manipulator with single-motor (a) and dual-motor (b) drives when performing movements of the end effector along circular trajectory 3 in the horizontal plane

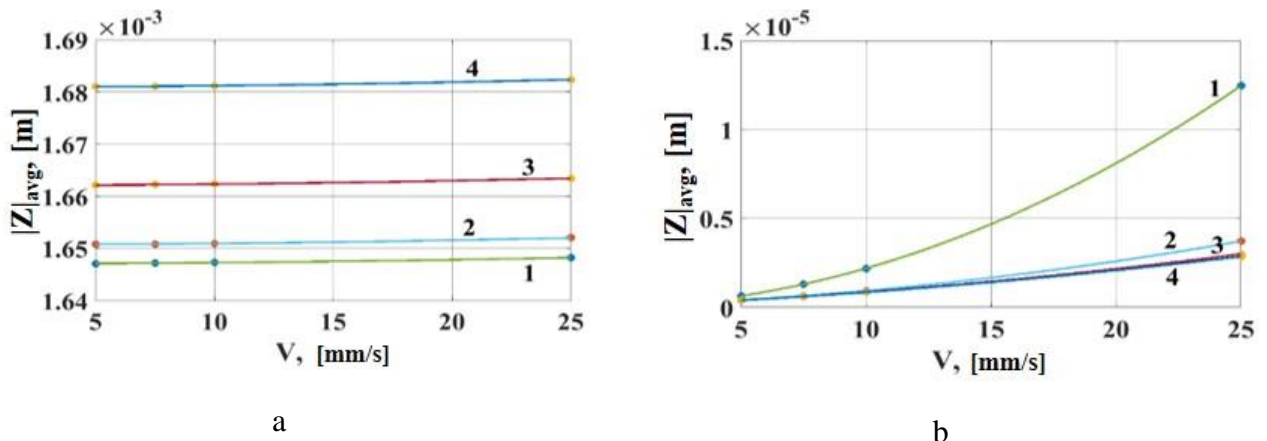


Figure 4.9. Deviations  $|Z|_{avg}$  of manipulator with single-motor (a) and dual-motor (b) drives when performing movements of the end effector along circular trajectory 3 in the horizontal plane

First of all, it should be noted that the graphs presented in Figures 4.4 - 4.9 allow us to conclude that the manipulator with precision dual-motor servo drives has significantly higher accuracy than the manipulator with single-motor drives closed by position of the motor shaft. This is also evidenced by the results of comparing accuracy of manipulators with single- and dual-motor drives when performing movements of the end effector along the circle 2 located in the horizontal plane (Table 4.3). In particular, at contour velocity of 5 mm/s and radius of 10 mm, the movement of the manipulator with dual-motor drives is accompanied by a RMS radial deviation that is 63.4 times less than the similar accuracy indicator for the manipulator with traditional single-motor drives.

Comparison of the reference (1) and actual (2) trajectories of the manipulator's TCP with single-motor (a) and dual-motor (b) drives is clearly shown in Figures 4.10, 4.11 and 4.12. The results correspond to the motion along the desired circular trajectory 2 lying in the horizontal plane.

Table 4.3 – Comparison of accuracy of manipulators with single- and dual-motor drives when performing movements of the end effector along the circle trajectory 2 in the horizontal plane

Contour velocity, mm/s	Circle radius, mm	Radial standard deviation		Accuracy improvement factor
		For manipulator with single-motor drives, $\mu\text{m}$	For manipulator with dual-motor drives, $\mu\text{m}$	
25	10	705	265	3
5	10	698	11	63
25	150	683	19	36

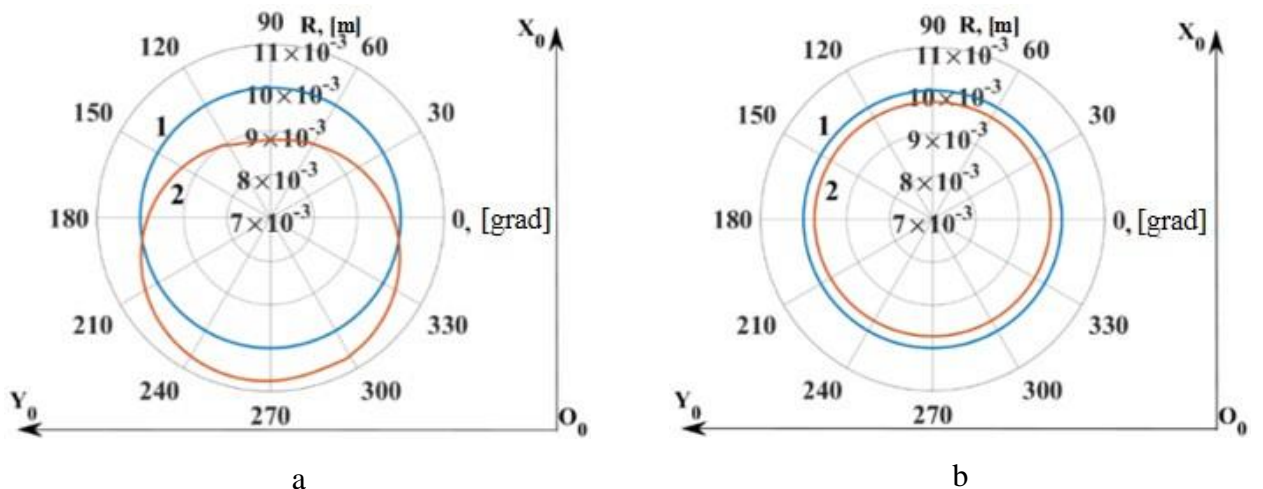


Figure 4.10. Reference (1) and actual (2) trajectories of the manipulator's TCP with single-motor (a) and dual-motor (b) drives moving along the circle trajectory 2 in the horizontal plane at contour velocity 25 mm/s and radius 10 mm

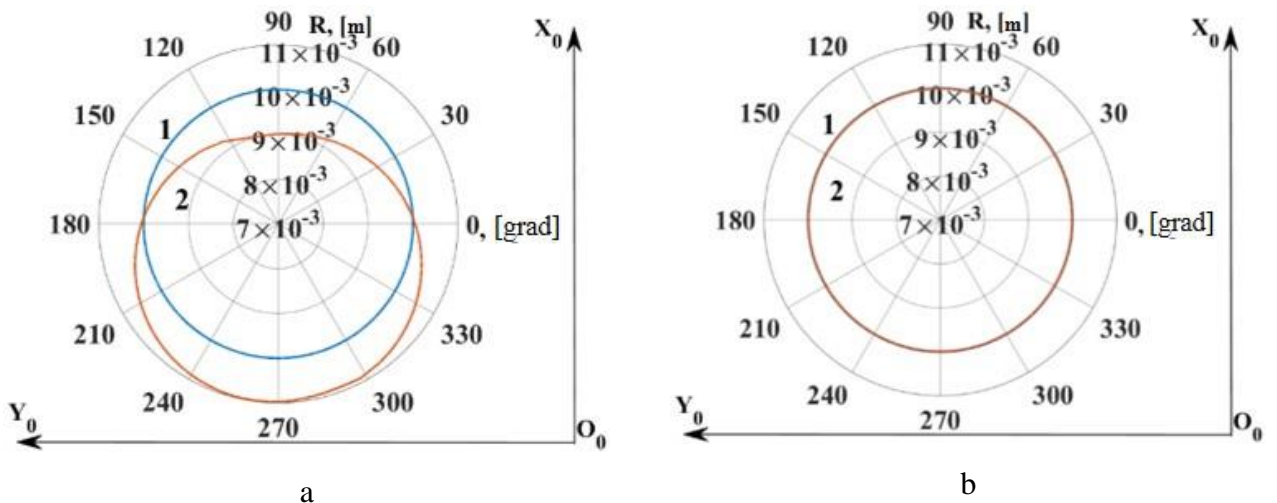


Figure 4.11. Reference (1) and actual (2) trajectories of the manipulator's TCP with single-motor (a) and dual-motor (b) drives moving along the circle trajectory 2 in the horizontal plane at contour velocity 5 mm/s and radius 10 mm

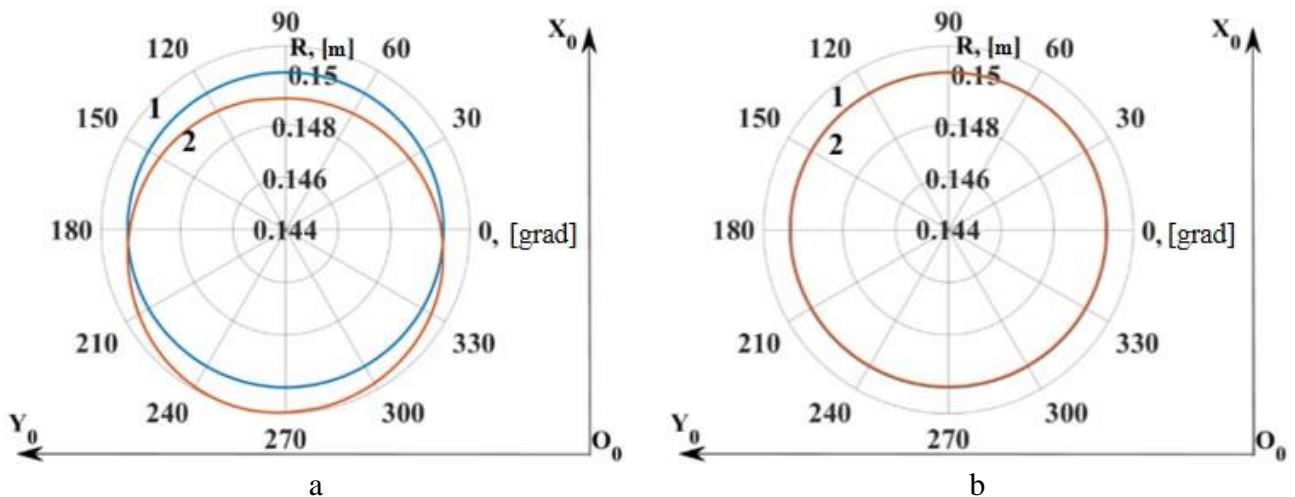


Figure 4.12. Reference (1) and actual (2) trajectories of the manipulator's TCP with single-motor (a) and dual-motor (b) drives moving along the circle trajectory 2 in the horizontal plane at contour velocity 25 mm/s and radius 150 mm

It can be seen on these figures that when the manipulator with single-motor drives performs movements along circular trajectories in these cases, there are significant deviations of the actual motion trajectory of the TCP from the desired trajectory. Meanwhile, the manipulator with dual-motor drives provides more accurate tracking of the desired trajectory.

The following explanation can be given for the obtained results indicating relatively low accuracy of the manipulator with drives closed by position of the motor shaft. In a manipulator with single-motor drives, an increase in the contour speed leads to an increase in the angular frequency  $\Omega$  at which circular motion is executed. And this leads to a decrease in the amplitude-frequency characteristics of the drives, closed by position control loops of their motor shafts. This results in a reduction of the radius along which actual motion would occur, if the mechanical transmissions of the manipulator's drives have no backlash or elastic compliance. However, in the presence of backlashes and elasticity of the gears, which are not covered by position feedbacks, under the action of centrifugal force the manipulator links will tend to take the extreme position farthest from the rotation centre. Thus, the total radial deviation of the manipulator  $R_{rad}$  will consist of 2 components:

$$R_{rad} = -R_1 + R_2.$$

The first of them,  $R_1$ , is caused by dynamics of the drive closed by position control loop of the motor shaft. The second component,  $R_2$ , is associated with the movement of the object under the influence of the centrifugal force within the range of possible displacement caused by the backlash and elasticity of the mechanical transmissions of the drives. As a result, the first component tends to deflect

the manipulator's TCP toward the center, while the second component deflects it away from the center. The sum of these two components determines the direction and magnitude of the resultant deviation of the manipulator's TCP.

As the radius of the circle increases, the component  $R_1$ , caused by the drive dynamics, becomes smaller, because the circular frequency  $\Omega$ , at which the circular motion is executed, decreases, and the amplitude-frequency characteristic of the drive increases. The component  $R_2$  remains unchanged, as it depends solely on the values of backlash and elastic compliance of the mechanical transmissions of the manipulator drives. Thus, the radial deviation of the manipulator's TCP  $R_{rad}$  increases. As the contour velocity increases, according to Figures 4.10(a) and 4.11(a), the component  $R_1$  increases, and the radial deviation of the manipulator's TCP  $R_{rad}$  decreases

When considering the axial deviations that arise during the operation of a manipulator with the drives of the traditional type, it is found that sections of the executed trajectory farther from the manipulator's base become even more distant from the base as the radius of the circular trajectory increases. As the manipulator's TCP moves farther from its base, the moments of inertia of the moving parts of the drives and the external force moments acting on them increase. This causes the TCP of a manipulator with single-motor drives to deviate along the  $O_0Z_0$  axis, resulting in its "sagging" due to the presence of backlash and elasticity in the gears. Consequently, the actual circle performed by the manipulator's TCP is shifted towards its base, which is reflected in the graphs shown in Figures 4.10(a), 4.11(a), and 4.12(a). Therefore, in Figures 4.5(a), 4.7(a), and 4.9(a), there is a general trend of increase in axial deviations as the radius of the executed circle grows. An increase in contour speed also leads to greater axial deviations for the manipulator with the drives of the traditional structure.

The peculiarity of manipulators built on dual-motor servo drives, as noted earlier, is their infinitely large static stiffness and significant dynamic stiffness. This is due to the structure of the control part of such a drive and the action of an active backlash-eliminating load device, which causes the component  $R_2$  to approach zero. Meanwhile, the component  $R_1$  causes relatively small deviations of the manipulator's TCP, as shown in Figures 4.10, 4.11, and 4.12. Also, due to the higher stiffness of these drives, the "sagging" of the manipulator is substantially less than with single-motor drives and is caused solely by the component related to the dynamics of the manipulator's drives. Therefore, axial deviation decreases with an increase in radius and increases with an increase in contour speed. It should also be noted that such dynamic behavior aligns with theoretical results of the analysis of the properties of manipulators with the drives having ideal, backlash-free mechanical transmissions.

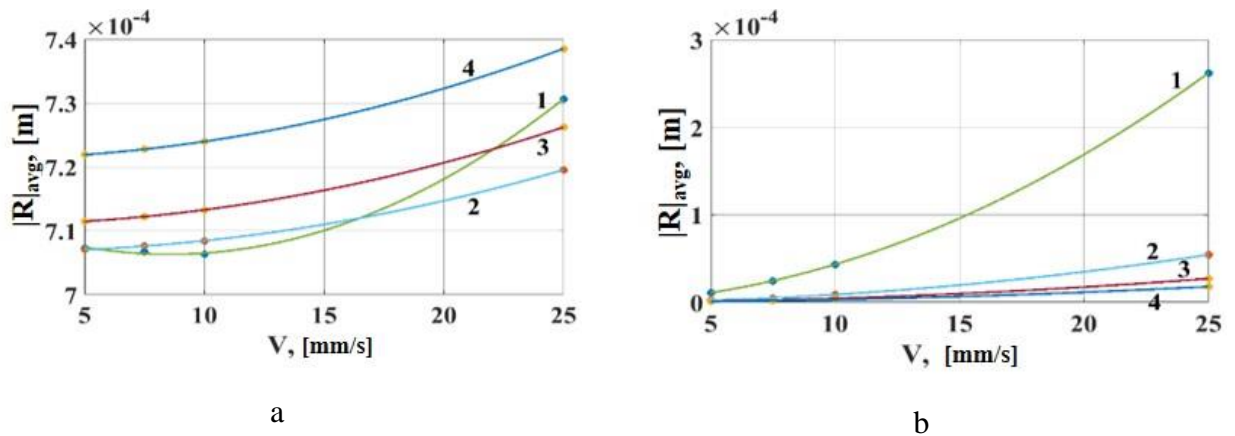


Figure 4.13. Deviations  $|R|_{avg}$  of manipulator with single-motor (a) and dual-motor (b) drives when performing movements of the end effector along circular trajectory 4 in the vertical plane

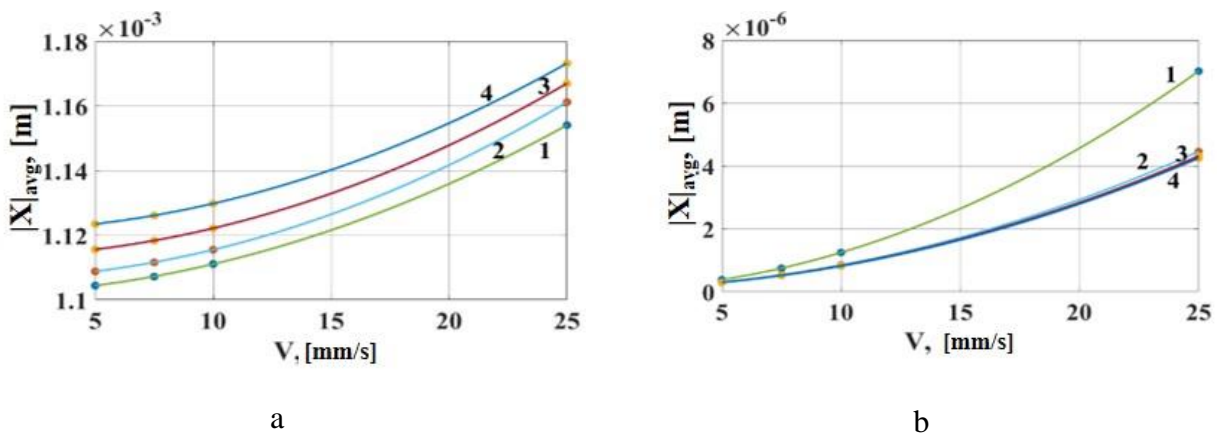


Figure 4.14. Deviations  $|X|_{avg}$  of manipulator with single-motor (a) and dual-motor (b) drives when performing movements of the end effector along circular trajectory 4 in the vertical plane

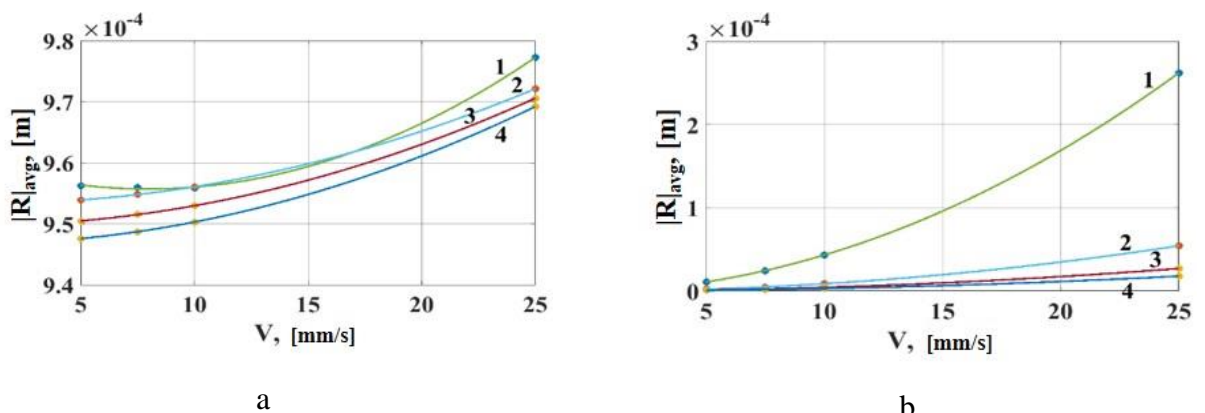


Figure 4.15. Deviations  $|R|_{avg}$  of manipulator with single-motor (a) and dual-motor (b) drives when performing movements of the end effector along circular trajectory 5 in the vertical plane

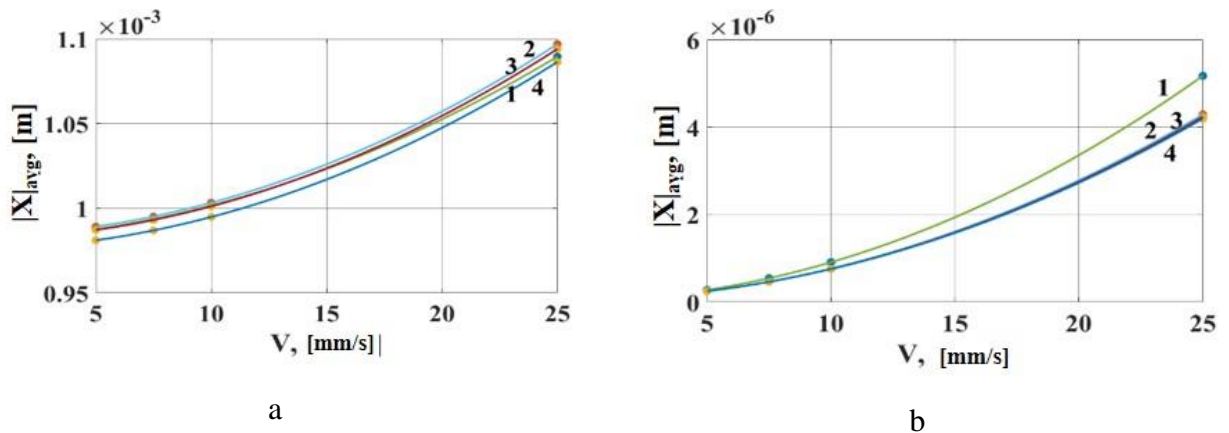


Figure 4.16. Deviations  $|X|_{avg}$  of manipulator with single-motor (a) and dual-motor (b) drives when performing movements of the end effector along circular trajectory 5 in the vertical plane

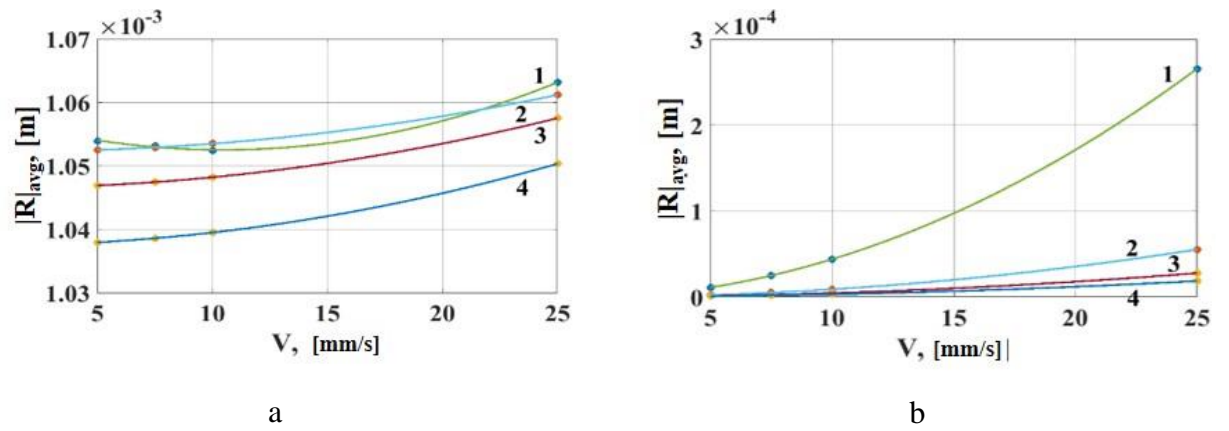


Figure 4.17. Deviations  $|R|_{avg}$  of manipulator with single-motor (a) and dual-motor (b) drives when performing movements of the end effector along circular trajectory 6 in the vertical plane

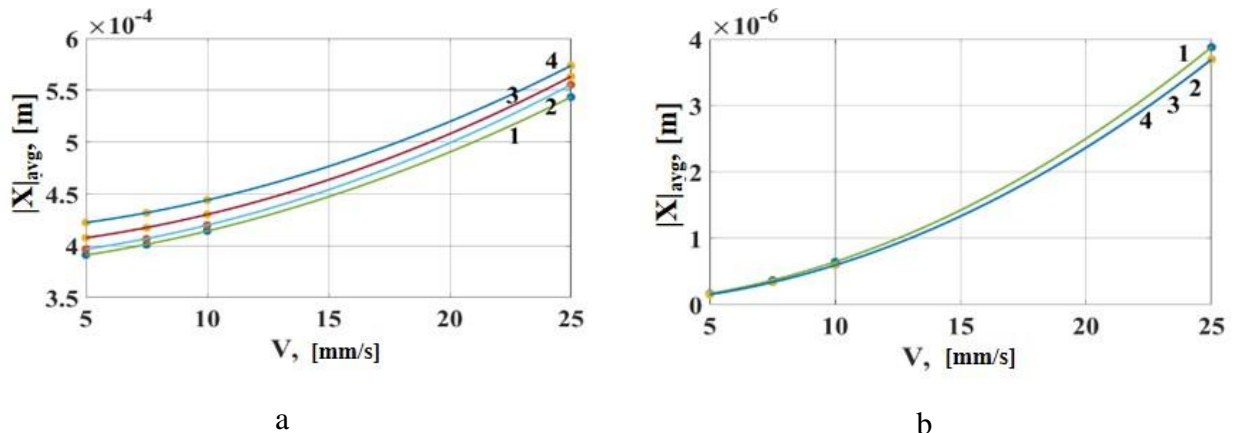


Figure 4.18. Deviations  $|X|_{avg}$  of manipulator with single-motor (a) and dual-motor (b) drives when performing movements of the end effector along circular trajectory 6 in the vertical plane

According to Figures 4.13-4.18, the character of dependences described above remains the same when the manipulator operates in the vertical plane. Radial and axial RMS deviations of the manipulator with dual-motor drives are significantly smaller than those of the manipulator with single-motor drives. For example, the results of comparing the accuracy of manipulators with single- and dual-motor drives when executing movements with contour velocity of 5 mm/s along the circle 5 located in the vertical plane and having radius of 10 mm, are presented in Table 4.4. They show that the usage of a manipulator with dual-motor drives provides an 87-fold gain in accuracy.

Table 4.4 – Comparison of accuracy of manipulators with single- and dual-motor drives when performing movements of the end effector along the circle trajectory 5 in the vertical plane

Contour velocity, mm/s	Circle radius, mm	Radial standard deviation		Accuracy improvement factor
		For manipulator with single-motor drives, $\mu\text{m}$	For manipulator with dual-motor drives, $\mu\text{m}$	
25	10	977	262	4
5	10	956	11	87
25	150	969	18	54

In addition, when simulating the process of executing circular trajectories in both planes, it was found that radial and axial deviations of the manipulator with dual-motor drives change only slightly when the position of the circle within the manipulator's workspace varies. This is supported by the data presented in Table 4.5.

Table 4.5 – Comparison of radial and axial deviations of manipulators with single- and dual-motor drives executing movements along various circle trajectories at contour speed 25 mm/s and radius 10 mm

	Radial standard deviation		Axial standard deviation	
	For manipulator with single-motor drives, $\mu\text{m}$	For manipulator with dual-motor drives, $\mu\text{m}$	For manipulator with single-motor drives, $\mu\text{m}$	For manipulator with dual-motor drives, $\mu\text{m}$
Movement of the TCP in the horizontal plane				
circle 1	702	264	1184	10
circle 2	705	265	1348	11
circle 3	699	266	1648	12
increase ratio for circles 1-3	3	2	464	2
Movement of the TCP in the vertical plane				
circle 4	731	257	1154	7
circle 5	977	262	1089	5
circle 6	1063	268	543	4
increase ratio for circles 4-6	332	11	611	3

When performing movements, especially in the vertical plane, the scatter of RMS deviation values of the manipulator with dual-motor drives is approximately 30 times less than the same indicators for the manipulator with single-motor drives. This confirms that the structure and mathematical model of the technological robot with dual-motor geared servo drives provide a significant increase in the robot's dynamic stiffness and motion accuracy.

The research presented in this chapter has been published in [78, 80, 83].

#### **4.4 Conclusions on fourth chapter**

Chapter 4 presents the results of the development of a mathematical model of a technological robot built on the two-channel dual-motor geared servo drives of the proposed structure, taking into account the factors identified in Chapter 1. The chapter includes the results of computer simulations of the movements of manipulators with the two considered types of servo drives along circular trajectories with various radius values and at different contour speeds. These results demonstrate the advantages of manipulators built on precision dual-motor drives and allow us to draw the following conclusions:

1. The mathematical models developed in the course of the research make it possible to predict the errors in the operation of a technological robot and allow selecting the maximum possible contour speed for each value of the permissible deviation of the tool from the desired trajectory based on accuracy considerations. This ensures the highest performance while meeting the accuracy requirements of the technological operation. In all the considered cases of circular trajectory execution, the root mean square radial and axial deviations of the manipulator with single-motor drives from the specified trajectory are greater than those of the manipulator with dual-motor drives. For example, at contour speed of 5 mm/s and circle radius of 10 mm, the steady-state motion of the manipulator with dual-motor drives occurs with an error approximately 87 times smaller than that of the manipulator with single-motor drives closed by position control loops of the motor shafts.

2. Changing the position of the circular trajectory in space has little effect on the deviations of the manipulator with dual-motor drives from the desired trajectory, both in terms of the radius of the executed circle and along the normal to the plane of motion. Thus, it can be stated that the stability of the parameters of a manipulator with dual-motor drives within its workspace is higher than that of a manipulator with single-motor drives.

3. The higher accuracy of manipulators with dual-motor servo drives is due to the closure of the main position feedback control loops of the of the manipulator's links, due to the presence of active backlash-eliminating devices and the structural features of the drive control units. This gives the

manipulators higher dynamic stiffness, practically eliminates the influence of backlash on motion accuracy, and allows for effective damping of oscillations.

4. The insufficient accuracy of manipulators with traditional drives, closed by position control loops of motor shafts, is caused by the negative influence of backlash and elastic compliance inherent in the mechanical transmissions (gears), which are not covered by the main feedback control loop of the position of manipulator's link.

The results of the conducted study allow us to recommend the construction of manipulators of industrial robots on dual-motor servo drives for their analytical programming and for performing technological operations requiring enhanced precision, such as robotic precision assembly of miniature products and precision laser welding.

## **CHAPTER 5. STUDY OF ACCURACY OF MOVEMENTS OF TECHNOLOGICAL ROBOTS WITH TWO-CHANNEL DUAL-MOTOR SERVO DRIVES WHEN PERFORMING ROBOTIC MILLING**

### **5.1 Features of milling by a technological robot**

Chapter 4 covered the processes of manipulators performing movements along trajectories in the absence of forces acting on the tool. Studying the properties of drives and manipulators under such conditions can indicate whether the manipulator achieves high or low accuracy during positional or contour control. However, such a study does not provide results regarding stiffness of the manipulative mechanism. Moreover, it is important to conduct research demonstrating feasibility and appropriateness of using manipulator with dual-motor drives for technological operations such as robotic milling, where forces acting on the manipulator's tool are generated by the performed operation.

Therefore, the next task was to provide such a research, and to compare the properties of technological manipulator built on such drives to the manipulator with traditional single-motor drives. Here it is important, in general, to point out the main advantages of robotic milling in comparison with traditional milling on a machine tool:

- the cost and metal consumption of the equipment is significantly lower than for milling on machine tools;
- at robotic milling the workspace is larger and the workpiece can have complex shapes of surfaces;
- expansion of the workspace is easy by introducing additional axes to the system;
- high flexibility, adaptability and programmability of the robotic system.

However, this process is accompanied by some serious problems, such as low stiffness and accuracy of the manipulation mechanism, the occurrence of oscillations during the milling process, the correlation between feed rate, workpiece quality and productivity of the operation. Thus, a reduction in feed rate increases the quality of the workpiece, but results in decrease in productivity of the operation.

At the same time, It is economically feasible to strive for the highest productivity in robotic milling while meeting the accuracy requirements to the processed part. These requirements depend on several factors, the most significant of which are the forces acting on the robot's tool during milling. These forces cause a deviation  $\delta_T$  of the tool normal to its desired trajectory, altering the dimensions and shape of the part's surface. These factors must be reflected in the mathematical model of the robot performing the robotic milling operation.

The productivity of robotic milling is higher, the higher the workpiece material removal rate, which is calculated by the formula

$$Q = BhS,$$

where  $h$  – cutting depth;  $B$  – removal width;  $S$  – tool feed rate (contour velocity).

The cutting force  $F_P$  has a significant impact on the error of tool motion during robotic milling. It should be noted that during the interaction between the milling cutter and the workpiece, the cross-sectional area of the material layer being cut by the cutter tooth does not remain constant but changes over time. As a result, the forces acting on the cutter teeth also continuously change. The resultant cutting force includes both average and variable components. This force is a vector and for convenience it is typically decomposed into three components: tangential, axial, and radial. The tangential force determines the torque of the tool spindle drive. The axial force is absorbed by the spindle bearing assembly. And the radial force acts on the spindle supports and the arbor holding the cutter.

When researching and designing milling systems, the average component of the cutting force is typically calculated using empirical formulas well-known in cutting theory and manufacturing technology, as presented in [70, 71]. The axial and radial components of the cutting force are proportional to this average component. For example, the average tangential cutting force during milling with cylindrical cutters can be estimated using an empirical formula known in manufacturing technology:

$$F_P = k_F B h^{n2} S^{n3} \quad (5.1)$$

where  $S$  – tool feed rate along the reference trajectory (contour velocity);  $h$  – cutting depth (if the manipulator tool interacts with the workpiece, then  $h \geq 0$ , but if the tool is not in contact with the workpiece, then  $h = 0$ );  $n2$  and  $n3$  – empirical measures of extent;  $k_F$  – proportional coefficient, taking into account the material properties of the workpiece and of the tool, the diameter, teeth number, rotation frequency and wear of the cutter. According to [72], it is determined by the formula

$$k_F = k_1 \frac{\left(\frac{60}{zn}\right)^{n3} z}{D^{n4} n^{n5}} \quad (5.2)$$

where  $z$  – number of cutter teeth;  $n$  – tool rotational frequency;  $D$  – mill diameter;  $n3, \dots, n5$  – empirical measures of extent;  $k_1$  – empirical coefficient. From (5.1) and (5.2) it follows, that accuracy and

productivity of the milling process are interconnected. Therefore, increase in performance is possible as long as following milling accuracy requirement is met:

$$|\delta_T| \leq \delta_{T.TOL},$$

where  $\delta_{T.TOL}$  – permissible tool deviation. It is worth noting that the deviation  $\delta_T$  decreases with a reduction in the cutting force. This can be achieved by lowering the contour speed  $S$ , but this leads to a decrease in productivity. The most promising approach to increasing both accuracy and productivity of robotic milling is based on enhancing the dynamic stiffness of the system “technological robot – milling process”.

The application of the previously described precision drives combined with corrective velocity feedback should enable achieving the highest productivity with ensuring guaranteed compliance with the accuracy requirements to executive motion. It is important to note that a positive effect can be achieved even without changing the structural elasticity of the gears of technological robot. The introduction of corrective feedback of velocities of the manipulator links is expected to beneficially modify the stiffness of the system "technological robot – milling process" and suppress resonant oscillations of the manipulator links. This should allow obtaining the maximum possible stiffness in the direction perpendicular to the desired trajectory, as well as an adjustable maximal stiffness along the trajectory and a sufficient level of damping.

To verify this, it is necessary to perform a computer simulation study of accuracy of the tool movement during robotic milling at various contour speeds of the milling cutter and nominal cutting depths, comparing the manipulator built on the proposed dual-motor drives and the manipulator built on the traditional single-motor drives. In this study it can be assumed that the links of the manipulator mechanism are absolutely rigid, and milling occurs in manipulator configurations where the angle between the shoulder and the elbow links is less than 45°.

Also, for performing robotic milling operations it is advisable to use counter milling, as with any other relatively non-rigid technological system. In this case, the cutting force component acts against the movement of the milling cutter moved by the robot, creating negative feedback and contributing to motion stabilization. In cross milling, the feedback becomes positive, and with insufficient stiffness and damping inherent in the robot's mechanical components, there is a high risk of losing stability in the feed control process, according to [2].

## 5.2 Mathematical model of the robotic milling process

In the previous chapter, the mathematical and computer simulation models of the robot built on two-channel dual-motor geared servo drives were presented. In the current chapter we present the results of the development of mathematical and computer simulation models of the robotic milling operation performed by technological robot.

Knowing the coordinates  $x_{TCP}, y_{TCP}, z_{TCP}$  of the actual manipulator's TCP position, which calculation is given in section 4.1, it is possible to determine the actual value of the radial cutting depth using the formula:

$$h = y_{edg} - \left( y_{TCP} - \frac{D}{2} \right)$$

where D – diameter of the cutter carried by the manipulator,  $y_{edg}$  – the coordinate of the edge of the machined surface of the workpiece. Since this edge has irregularities and its position coordinate is unstable and unpredictable for the robot, the cutting depth  $h$  has nominal and variable components. For simulation the position coordinate of the workpiece edge can be described by the equation

$$y_{edg} = y_{edg0} + \Delta y_{edg},$$

where  $y_{edg0}$  - nominal value of the edge coordinate,  $\Delta y_{edg}$  – deviation of the edge position from the nominal value. The following dependence of  $\Delta y_{edg}$  on the path  $L$  travelled by the milling cutter along the reference trajectory can be used:

$$\Delta y_{edg} = A_1 \sin(k_1 L) + A_2 \sin(k_2 L) + A_3 \sin(k_3 L), \quad (5.3)$$

where  $A_1 + A_2 + A_3 = 0.1 \cdot h_{nom}$ ;  $h_{nom}$  – nominal cutting depth;  $k_1, k_2, k_3$  – parameters depending on the wavelengths of irregularities  $L_{w1}, L_{w2}, L_{w3}$  and calculated by the formulas

$$k_1 = \frac{2\pi}{L_{w1}},$$

$$k_2 = \frac{2\pi}{L_{w2}},$$

$$k_3 = \frac{2\pi}{L_{w3}}.$$

For simulation it can be assumed that  $L_{w1} = 0.1 \text{ m}$ ,  $L_{w2} = 0.05 \text{ m}$ ,  $L_{w3} = 0.03 \text{ m}$ .

The speed of the manipulator's tool movement along the trajectory can be determined based on the generalized manipulator velocities using formula (4.1). Figure 5.1 shows the direction of the tangential component of the cutting force  $P_C$ , as well as its projections  $P_X$  and  $P_Y$  onto the axes of the base (world) coordinate system during counter milling. As seen in the figure, when the cutting depth  $h$  changes, the angle  $\psi$  changes accordingly, which leads to variation in the ratio of the projections  $P_X$ ,  $P_Y$  and  $P_Z$ . This angle is calculated using the formula:

$$\psi = \arccos\left(\frac{D}{2} - h \frac{2}{D}\right).$$

The projections of the force  $P_C$  on the axes of the world coordinate system during counter milling are defined as follows:

$$P_X = P_C \cos \Psi,$$

$$P_Y = -P_C \sin \Psi,$$

$$P_Z = 0,4P_C \operatorname{tg} \gamma,$$

where  $\gamma$ —inclination angle of the helical chip grooves of the milling cutter.

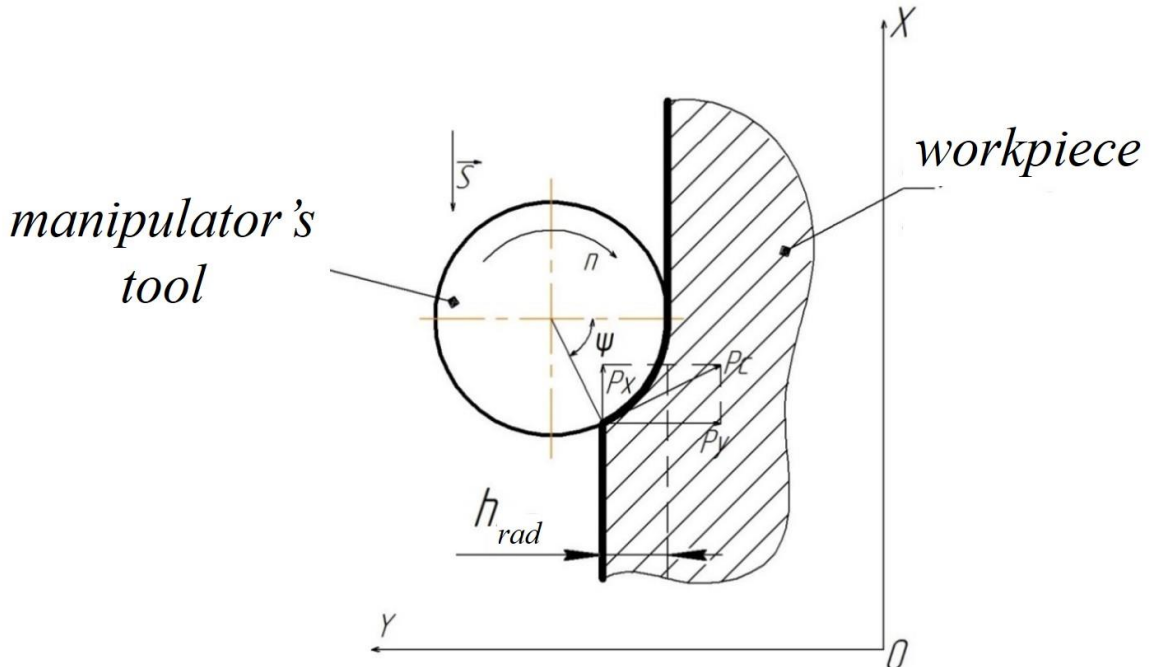


Figure 5.1. Direction of forces acting on the manipulator's tool during counter milling

We note that the component  $P_Y$  significantly affects the milling accuracy. The moments acting on the manipulator links, which represent disturbance impacts on the drives, can be calculated using formula (4.2). For simplicity, it can be assumed that at all points along the tool's trajectory, it has the same orientation in the workspace. In this case, the desired value of the generalized coordinate  $q_4$  is calculated based on the equation

$$q_4 = \text{atan} 2(l_{u2}, l_{u1}) + q_2 - q_3,$$

where  $l_{u1}, l_{u2}$  - length of the manipulator tool as shown in the figure 4.3.

As a result, a computer simulation model of the milling process can be developed, which structural diagram is shown in Figure 5.2. During the simulation, the desired trajectory of the manipulator's TCP is generated, and the coordinates of its points are calculated. The calculations of the manipulator's generalized coordinates and generalized velocities are implemented using the dynamic models of the manipulator mechanism and the drives, which are presented in Chapter 4.

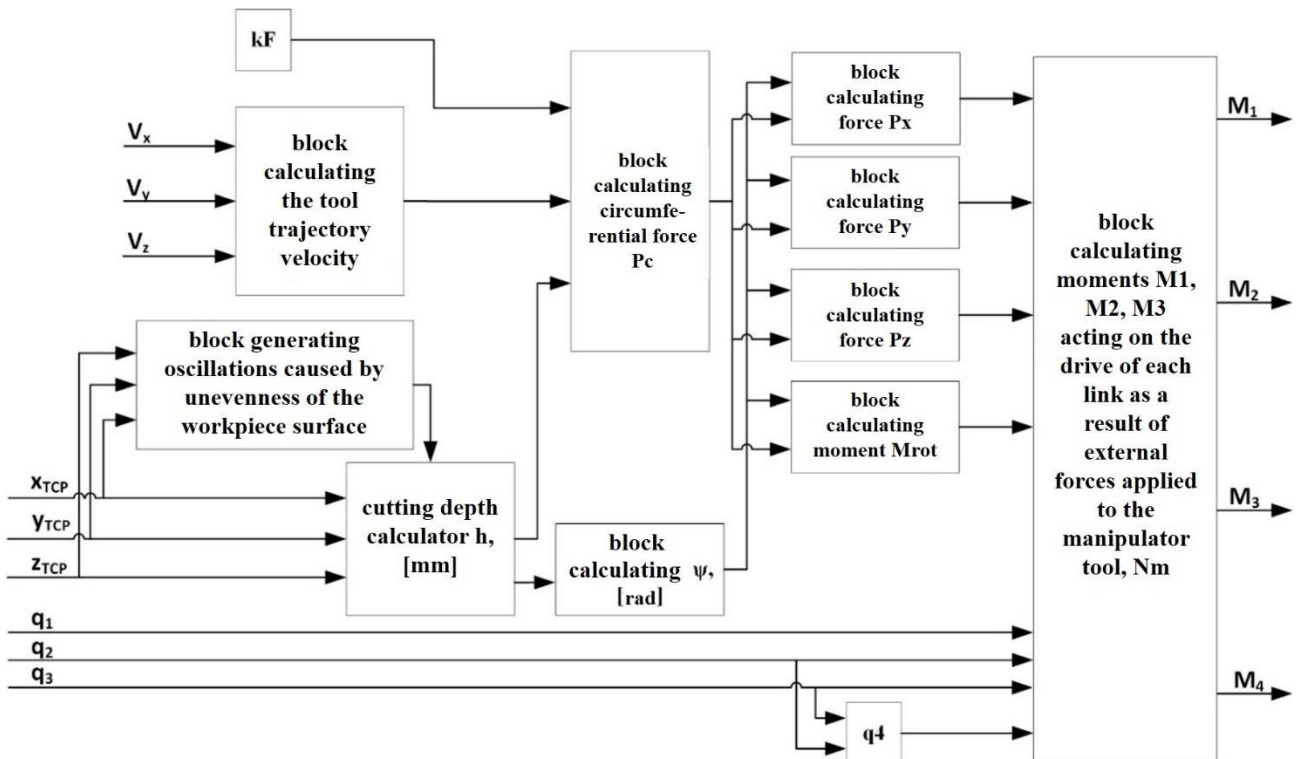


Figure 5.2. Structural diagram of the main part of the computer simulation model of the robot performing milling operations

The calculation of the circumferential cutting force  $P_c$  is carried out according to formula (5.1), taking into account the current values of the contour speed and cutting depth. The cutting width is

considered constant. It is also taken into account that, as a result of the cutting force, the values of contour speed and cutting depth change during the milling process. The calculation of the variable component of the workpiece edge coordinate  $\Delta y_k$  is implemented in the block generating oscillations caused by unevenness of the workpiece surface, according to formula (5.3). At the output of this model, the calculated values of the moments acting on the manipulator drives from the milling operation are obtained. That means, the forces acting on the tool during the milling operation are converted, according to formula (4.2), into moments acting on the drives and fed into the manipulator model as moments of external forces applied to the drives.

### **5.3 Investigation of dynamic properties and accuracy of movements of technological robots with dual-motor drives performing robotic milling along a straight trajectory**

As mentioned earlier, the computer simulation model of the robotic milling process presented in section 5.2 is used to provide a computational study of the tool movement accuracy during robotic milling at various values of the contour speed of the milling cutter and the nominal cutting depth, using manipulator built on the proposed dual-motor drives and with manipulator built on traditional single-motor drives.

#### **5.3.1 Conditions for conducting a computational experiment to compare errors arising in robotic milling operation along straight trajectory performed by manipulator with single-motor and dual-motor drives**

The research considers the scheme of cylindrical milling of the side surface of a workpiece with the form of a rectangular plate made of D16T aluminum alloy. According to this scheme the cutter is moved toward the manipulator's base along a straight trajectory parallel to  $X_0$  axis of the base coordinate system  $O_0X_0Y_0Z_0$ , which is associated with the manipulator's base (Figure 5.3). The movement starts from the point with coordinates  $X_0 = 0.6$  m,  $Y_0 = Z_0 = 0$  m. In this process, the deviation of the tool,  $\delta_T$ , normal to the desired trajectory of its movement is determined. This deviation occurs along  $Y_0$  axis and is caused by the cutting force, calculated according to formula (5.1). The directions of the components of this force,  $P_X, P_Y, P_Z$ , and the moment  $M_{rot}$  acting on the robot tool are shown in Figure 5.3.

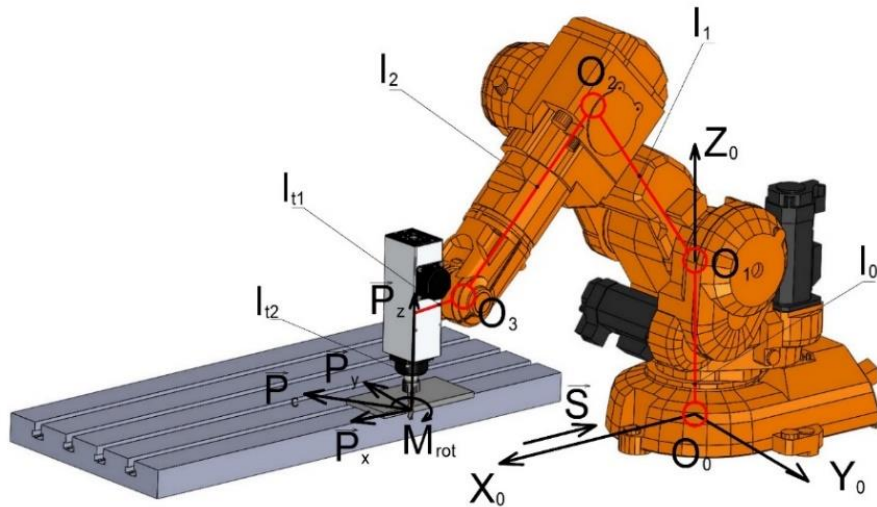


Figure 5.3. Schematic diagram of robotic milling of a workpiece edge

Table 5.1 shows the parameters of the cutter used in the simulation of the robotic milling operation.

Table 5.1 – Parameters of the cutting operation

Parameter	Value	Symbol
Workpiece material	D16T	
Number of cutter teeth	5	z
Cutter diameter, mm	6	D
Length of the cutter working part, mm	15	
Angle of inclination of screw grooves, grad	20	$\omega$
Tool rotation frequency, rpm	10000	n
Plate width, mm	12	B
Plate length, mm	200	

During the milling process the cutting depth has a significant impact on the quality of the machined workpiece. Changes in the cutting depth of the manipulator's tool cause variations in the forces acting on the tool and, consequently, in the feed rate, thereby creating a risk of system instability. Therefore, as indicators of the tool movement accuracy, the study considers the average values  $d$  of the absolute deviation of the tool from the desired trajectory along the  $Y$  axis, as well as the maximum deviation values  $\Delta d_{max}$ . These deviations of the manipulator's tool cause changes in the cutting depth and affect the milling accuracy.

The values  $d$  and  $\Delta d_{max}$  are determined by the formulas

$$d = \frac{1}{T} \int_0^T |\delta_T(t)| dt,$$

$$\Delta d_{max} = \max(|\delta_T(t)| - d).$$

where  $T$  – total movement time of the tool when milling the workpiece.

### 5.3.2 Results of Computer Simulation of robotic milling along straight line

As a result of computer simulation, the values of the accuracy indicators  $d$  and  $\Delta d_{max}$  were obtained for manipulators built on single-motor and dual-motor drives, at various values of the contour speed  $S$  and nominal milling depth  $h_0$ .

The accuracy indicator values for the manipulator with traditional single-motor drives are presented in Table 5.2. These data indicate that the accuracy indicator  $d$  depends almost linearly on the contour speed of the milling cutter and nonlinearly on the cutting depth. This conclusion is confirmed by the graph shown in Figure 5.4. The data for the manipulator with single-motor drives demonstrate significant deviations of the cutter from the desired trajectory. Specifically, the values of the accuracy indicator  $d$  in the direction perpendicular to the desired trajectory range from 78.8 to 132.4 micrometers when the speed varies from 2 to 7 mm/s and the nominal cutting depth ranges from 0.5 to 1.5 mm. With increase in contour speed and nominal cutting depth these deviations also increase.

Table 5.2 – Accuracy indicators of robotic milling when using manipulator with conventional single-motor drives

$S$ , m/s	$h_0 = 0.5$ mm		$h_0 = 1.0$ mm		$h_0 = 1.5$ mm	
	$d$ , $\mu\text{m}$	$\Delta d_{max}$	$d$ , $\mu\text{m}$	$\Delta d_{max}$	$d$ , $\mu\text{m}$	$\Delta d_{max}$
0.002	78.76	19.35	86.99	22.61	95.84	25.78
0.003	80.92	21.59	92.11	26.11	104.13	30.45
0.005	84.72	25.26	101.21	31.96	118.92	38.29
0.007	88.14	27.6	109.47	36.21	132.39	44.34

Under the same conditions, the maximum values of the indicator  $\Delta d_{max}$  range from 19 to 44 micrometers. In many practical applications such deviations are often considered unacceptable. The cause of these deviations is the component of the cutting force acting along the  $Y$  axis, which, under the same milling process parameters, ranges from 13.5 to 124.8 N, as well as the insufficient stiffness of the manipulator, which varies from 171600 to 942900 N/m depending on the contour speed and nominal cutting depth. The latter circumstance is due to the fact that the gear and the mechanical control object are outside the position control loop.

When using the manipulator with precision dual-motor drives, values of accuracy indicators acquire the values presented in Table 5.3.

Table 5.3 – Accuracy indicators of robotic milling by manipulator with precision dual-motor drives

$S$ , m/s	$h_0 = 0.5$ mm		$h_0 = 1.0$ mm		$h_0 = 1.5$ mm	
	$d$ , $\mu\text{m}$	$\Delta d_{max}$	$d$ , $\mu\text{m}$	$\Delta d_{max}$	$d$ , $\mu\text{m}$	$\Delta d_{max}$
0.002	0.0179	0.2006	0.0216	0.3306	0.0231	0.5086
0.003	0.035	0.1523	0.0421	0.2719	0.0448	0.4118
0.005	0.0851	0.1309	0.1024	0.1917	0.1086	0.2715
0.007	0.1537	0.2348	0.1846	0.3060	0.1955	0.3397

Considering the data presented in Table 5.3 and plotted on the graphs in Figure 5.5, it can be observed that the accuracy of robotic milling is significantly higher when using precision dual-motor drives. This is achieved thanks to the closure of the main feedback control loops of the positions of the manipulator links, the usage of high-precision position sensors, and the introduction of corrective feedback loops on the velocities of the manipulator links.

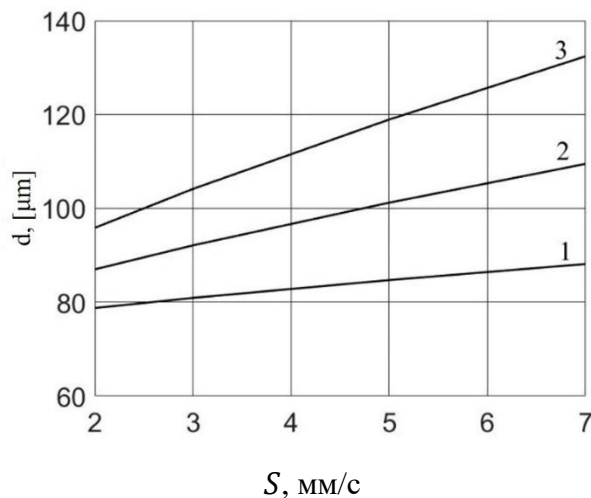


Figure 5.4. Dependency of tool deviation of the manipulator with single-motor drives on contour speed  $S$  at  $h_0 = 0.5$  mm (1), 1 mm (2), 1.5 mm (3)

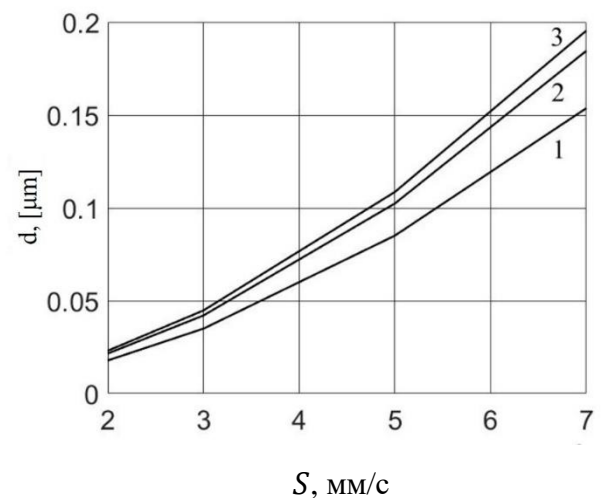


Figure 5.5. Dependency of tool deviation of the manipulator with dual-motor drives on contour speed  $S$  at  $h_0 = 0.5$  mm (1), 1 mm (2), 1.5 mm (3)

As a result of computational experiments, the stiffness coefficient values of the manipulator with dual-motor drives along the Y axis were obtained, ranging from  $1.84 \cdot 10^8$  to  $1.93 \cdot 10^9$  N/m. Thus, the usage of dual-motor geared servo drives increased the manipulator's stiffness coefficient by more than 450 times. This confirms the results of the theoretical studies presented in Chapter 2. Indeed, when the manipulator operates at the relatively low speeds typical for robotic milling, its state becomes equivalent to a static state. Consequently, the stiffness of dual-motor drives approaches infinity.

When the cutting force component acting along the  $Y$  axis ranges from 11 to 114 N, the usage of dual-motor drives provides significantly higher accuracy in robotic milling. Specifically, for contour speed  $S$  varying from 2 to 7 mm/s and nominal cutting depth  $h_0$  from 0.5 to 1.5 mm, the accuracy indicator  $d$  falls within the range of 0.018 to 0.196 micrometers. Under the same conditions, the maximum deviation indicator  $\Delta d_{max}$  ranges from 0.201 to 0.34 micrometers.

It is important to note that the accuracy indicator values were obtained under the assumptions that the links of the manipulator mechanism are absolutely rigid, and that the high-frequency oscillations arising during the milling process occur at frequencies significantly higher than both the drive cutoff frequencies and the natural frequencies of the manipulator mechanism with elastic gears.

The significant increase in accuracy of milling tool motion when using manipulators with precision drives opens broader opportunities for improving productivity of robotic milling along straight-line trajectories. For example, if we limit the allowable deviation of the tool from the desired trajectory to 100 micrometers, then with traditional solutions, the contour speed  $S$  cannot exceed 4 mm/s and the cutting depth  $h_0$  cannot exceed 1 mm. The new solution based on dual-motor drives allows us to implement milling at  $S = 7$  mm/s and  $h_0 = 1.5$  mm while maintaining a large accuracy margin.

Based on this, it can be concluded that the usage of technological robots equipped with the proposed dual-motor drives significantly contributes to increasing accuracy of tool movements during robotic milling operations along straight-line trajectories.

#### **5.4 Study of dynamic properties and accuracy of movements of technological robots with dual-motor drives performing robotic milling along circular trajectory**

For obtaining quantitative assessments of the potential accuracy of manipulators with single-motor and dual-motor drives during robotic milling operations, a study was also conducted when the manipulator was performing robotic milling operation along circular trajectories.

In this case, reference sinusoidal harmonic signals are fed to inputs of the manipulator drives. The cutoff frequencies of the manipulator drives, presented in section 4.2 for dual-motor drives and in section 4.3.1 for single-motor drives, have a significant influence on the manipulator's deviations from the desired trajectory.

During computer simulation, the root mean square deviations of the manipulator from the desired trajectory were determined both radially (deviations in the radius of the circular path) and axially (deviations perpendicular to the plane of motion).

#### 5.4.1 Conditions for conducting a computational experiment to compare errors arising in robotic milling operation along a circular trajectory performed by manipulator with single-motor and dual-motor drives

The comparative analysis of manipulators with single-motor and dual-motor servo drives is based on the same mathematical model presented in Chapter 4 of the dissertation. Chapter 4 also describes the parameters of the manipulator, its motors, and gears. The mathematical model of the robotic milling process during TCP movement along a straight trajectory is presented there. In this Chapter, the cutting model was supplemented with a subsystem for correcting cutting forces during milling, taking into account arising oscillations. When the cutter moves along a circular trajectory, at each moment the tool movement in the direction of the desired contour speed vector leads to material removal, which generates cutting forces. However, due to oscillatory processes during milling, the manipulator's tool may temporarily move in the opposite direction, where the material layer has already been removed. In this case, cutting forces are absent, and this is accounted for in the model. If the tool moves along the circular trajectory opposite to the desired contour speed vector direction, and the radius of the actual manipulator trajectory does not increase, the cutting forces are zeroed.

According to the method for determining manipulator deviations presented in section 4.3.2, the desired trajectories are chosen as circles, three of them lie in the horizontal plane (circles 1-3 in Figure 5.6) and three - in the vertical plane (circles 4-6 in Figure 5.6)

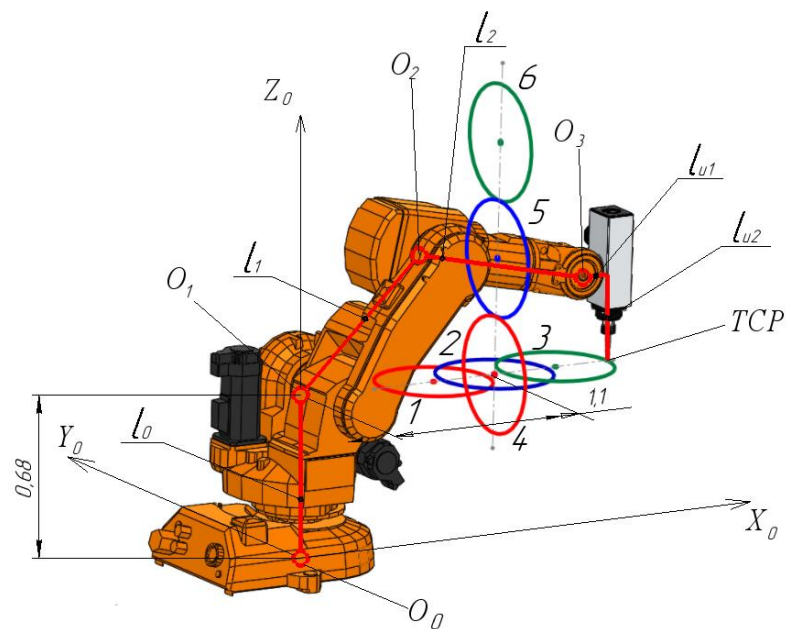


Figure 5.6. Desired trajectories of the manipulator's end-effector movement

During the study, the following parameters were varied: the coordinates  $x_0, y_0, z_0$ , which determine the position of the center of the desired circle, its radius  $R$  and contour speed  $V$  of the TCP. The center of circle 2 is located at a central point equidistant from the boundaries of the manipulator's workspace, with the following coordinates in the base coordinate system:  $x_0 = 1.1$  m,  $y_0 = 0$  m,  $z_0 = 0.68$  m. The centers of the other desired circular trajectories are shifted relative to this central point in their respective planes. The centers of circles 1 and 3 are shifted along the  $X_0$  axis relative to the central point by  $-0.2$  m and  $+0.2$  m, respectively. The centers of circles 4 and 6 are shifted along the  $Z_0$  axis relative to this point by  $+0.12$  m and  $+0.32$  m, respectively.

#### 5.4.2 Computer simulation results of milling along circular trajectory

According to the methodology presented above, to determine radial and axial RMS deviations during milling, the manipulator's tool was moved along a circular trajectory. In Figure 5.7 there are the desired and actual trajectories of TCP of the manipulator with dual-motor drives while milling of a hole along circle 1 in horizontal plane with radius 10 mm at contour speed 10 mm/s and cutting depth 0.5 mm.

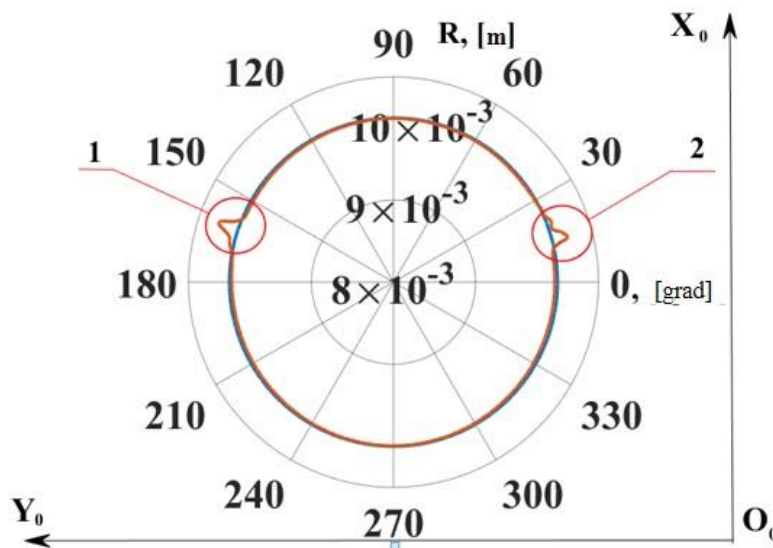


Figure 5.7. Desired and actual trajectories of TCP motion of manipulator with dual-motor drives while milling of a hole along circle 1 with radius 10 mm in horizontal plane at contour speed 10 mm/s and cutting depth 0.5 mm

As can be seen in the figure, during the operation, there are deviations, marked as 1 and 2, of the manipulator's TCP from the desired trajectory. Indeed, when the tool of the manipulator with dual-motor

drives follows a circular trajectory while performing robotic milling, oscillations may occur under the presence of forces arising during milling. These oscillations can lead to such deviations if the cumulative moment of the loader and the external moment (we will call it the load), applied to the drive from the cutting forces, is less than the required tension moment, which is determined, taking into account backlash and elasticity of the drive gears.

In dual-motor drive of the considered design, the loader generates constant torque that opposes the internal servo drive. At the same time, the external torque (load) produced by the cutting forces during the operation has a variable sign. In such cases, there are situations when the sum of the loader and the load torques passes through zero. Figure 5.8 shows the graph of the cumulative torque of the load and the loader of the drive of manipulator's column while performing robotic milling along the circular trajectory 1 in the steady-state mode. When the cumulative torque equals zero, the contact between the elastic elements of the gears in both the internal servo drive and the loader is broken and they are disconnected. These disconnections lead to the deviations observed in Figure 5.8.

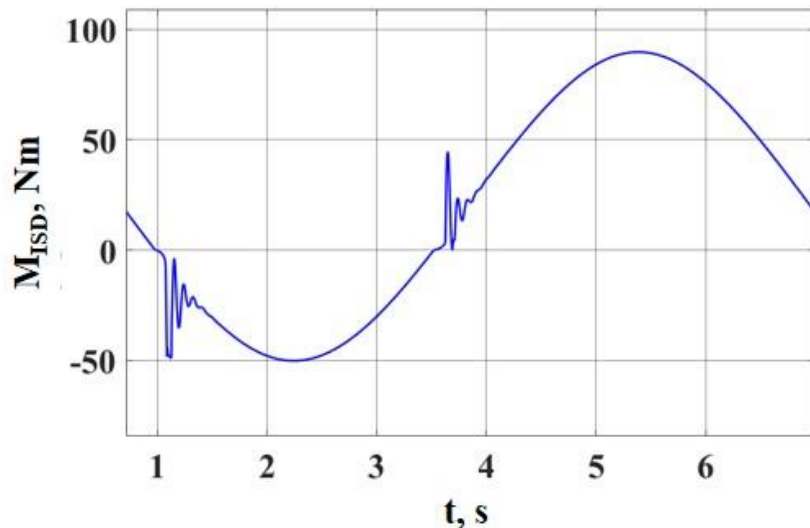


Figure 5.8. Graph of the cumulative torque of the load and torque of the loader of the drive of the manipulator column while milling along circle 1 with radius 10 mm in the horizontal plane at contour speed 10 mm/s and cutting depth 0.5 mm in the steady-state mode

When the manipulator's configuration changes, in particular when the manipulator is extended in horizontal plane, the moments of inertia of the drives of its column and the second link increase. This causes larger torques to act on the drives due to the weight of the links. Meanwhile, the loader torque of these drives remains unchanged, which leads to a reduction in the resultant tension torque between the internal servo drive and the loader. As a result, the contact between the elastic elements of the gears may also be broken, they can become disconnected and collisions between them can occur. This can also

cause divergent oscillations in the drives of the considered structure and lead to significant deviations of the TCP from the desired position.

The factors mentioned above necessitate adjustment of the torque value generated by the loader, which depends on the forces arising during the milling process and on the manipulator's configuration. Initially, the tension torque, generated by the loader, is determined by the formula given in Section 2.2:

$$M_{loader} = C_{eqv} \cdot \Delta q_{backlash}, \quad (5.4)$$

$$C_{eqv} = C_{red} q(A)_{MIN},$$

where  $C_{red}$  – stiffness coefficient of the gear of the dual-motor drive;  $q(A)_{MIN}$  – minimal value of harmonic linearization coefficient of the mechanical transmission equation of dual-motor drive;  $\Delta q_{backlash}$  – half of the gear backlash, [m];  $C_{eqv}$  – equivalent stiffness coefficient of the gear of the dual-motor drive reduced to its output shaft. Thus, at the value of half of the backlash of the gear of the drive of the manipulator column  $\Delta q_{backlash} = 0,5$  angular minutes, the gear stiffness coefficient  $C_{red} = 71000$  Nm/rad and minimal value of the harmonic linearization coefficient  $q(A)_{MIN} = 0,2$  the loader torque is  $M_{loader} = 20.7$  Nm.

When adjusting the value of the loader torque, there is no point to reduce it below the value calculated using formula (5.4), since this value guarantees the absence of self-oscillations in the dual-motor servo drive. In cases when the torque caused by the cutting forces exceeds the loader torque while acting in opposite directions, it makes sense to increase the loader torque at least up to the maximum magnitude of the acting load torque.

Taking this correction into account, during milling along circle 1 with a radius of 10 mm in the horizontal plane at contour speed 10 mm/s and cutting depth 0.5 mm, the loader torque  $M_{loader}$  became equal to 71 Nm. The actual trajectory of the manipulator's TCP with the correction of the tension torque in the drive of the column is shown in Figure 5.9.

When using a manipulator with single-motor drives for this operation under the same cutting parameters, divergent oscillations occur in the system. The desired and the actual trajectories of TCP of the manipulator with single-motor drives during this operation are shown in Figure 5.10.

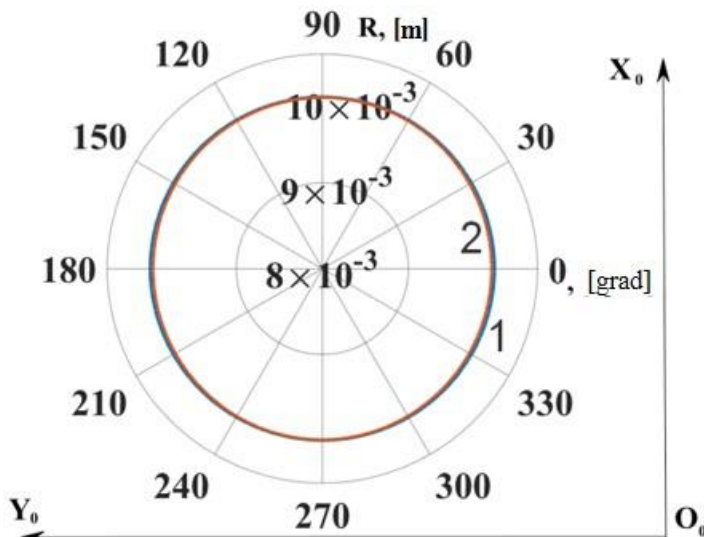


Figure 5.9. Desired (1) and actual (2) trajectories of TCP motion of manipulator with dual-motor drives while milling of a hole along circle 1 with radius 10 mm in horizontal plane at contour speed 25 mm/s and cutting depth 0.5 mm in the steady-state mode **with loader torque adaptive control**

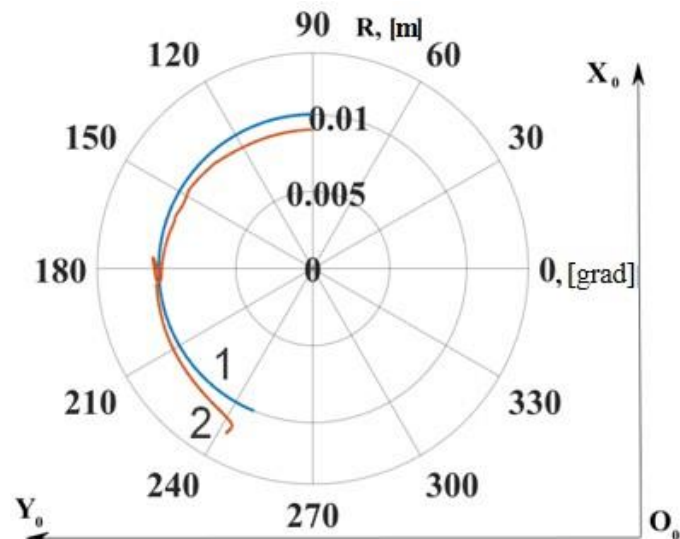


Figure 5.10. Desired (1) and actual (2) trajectories of TCP motion of manipulator with single-motor drives while milling of a hole along circle 1 with radius 10 mm in horizontal plane at contour speed 25 mm/s and cutting depth 0.5 mm in the steady-state mode

Since the manipulator performs a counter milling operation, the forces arising in the cutting process tend to pull its tool into the workpiece. When the rotational frequency of the tool's movement along the circular trajectory exceeds a certain critical value, determined by the contour speed, cutting depth, and radius of the trajectory circle, the manipulator's tool starts to be drawn more and more into the workpiece. In this case, the manipulator's drives start to develop increasingly large torques in an effort to return the tool to the desired trajectory. At a certain point, the system loses stability, and

divergent oscillations occur. The onset of this process is shown in Figure 5.10. Thus, it is concluded that a manipulator with single-motor drives is incapable of performing milling along a circular trajectory with the given cutting parameters, whereas a manipulator with dual-motor drives successfully handles this task.

In addition to the considered milling case, computational experiments were also conducted for other cutting parameter values. Table 5.4 presents the values  $M_{loader}$  of the corrected loader torque of the dual-motor drive for the manipulator's column, at which disconnections and collisions between the elastic elements of the drive gears do not occur.

Table 5.4 – The values of the loader torque of the dual-motor drive of the manipulator column while milling along circle 1 in the horizontal plane

t, [mm] at R=0.01 m	V, mm/s			
	1 mm/s	2.5 mm/s	5 mm/s	10 mm/s
	$M_{loader}$ , Nm	$M_{loader}$ , Nm	$M_{loader}$ , Nm	$M_{loader}$ , Nm
0.1	20.7	20.7	20.7	20.7
0.25	20.7	20.7	24	37
0.5	20.7	26	43	71
t, [mm] at R=0.025 m	V, mm/s			
	1 mm/s	2.5 mm/s	5 mm/s	10 mm/s
	$M_{loader}$ , Nm	$M_{loader}$ , Nm	$M_{loader}$ , Nm	$M_{loader}$ , Nm
0.1	20.7	20.7	20.7	20.7
0.25	20.7	20.7	24	40
0.5	20.7	26	44	73
t, [mm] at R=0.05 m	V, mm/s			
	1 mm/s	2.5 mm/s	5 mm/s	10 mm/s
	$M_{loader}$ , Nm	$M_{loader}$ , Nm	$M_{loader}$ , Nm	$M_{loader}$ , Nm
0.1	20.7	20.7	20.7	20.7
0.25	20.7	20.7	25	41
0.5	20.7	27	45	75

According to the methodology presented in Section 4.3.2, the radial and axial RMS deviations of TCP from the desired circular trajectory were determined for both manipulator with single-motor and dual-motor servo drives during the study. As a result, dependencies of these deviations on the contour speed, radius of the circular trajectory, and cutting depth were obtained. These dependencies for the manipulator with dual-motor drives are shown in Figure 5.11, while those for the manipulator with single-motor drives are presented in Figure 5.12. Similar to Section 4.3.3, they are approximated by second-degree polynomials using the least squares method.

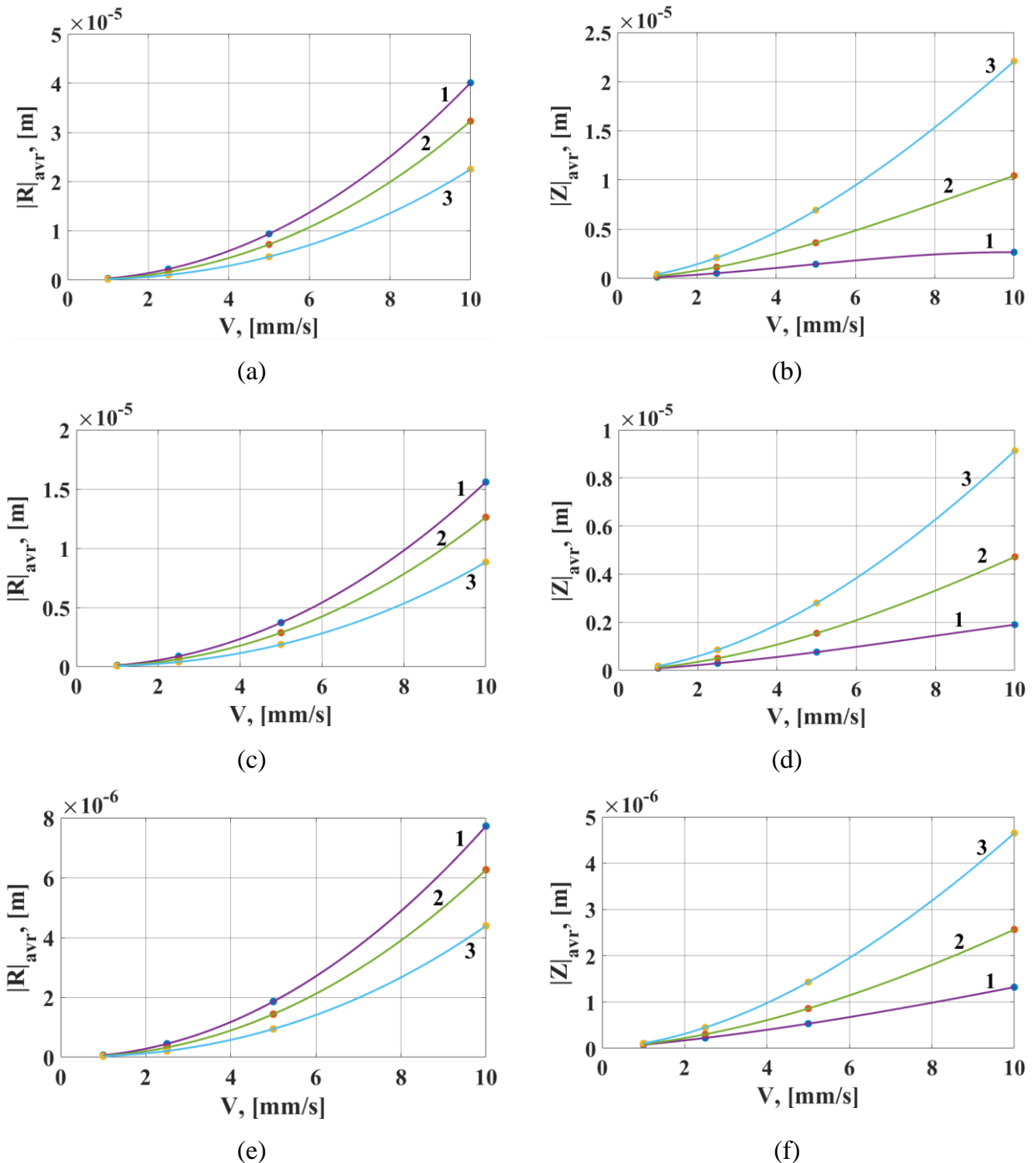


Figure 5.11. Dependencies of radial (a, c, e) and axial (b, d, f) RMS deviations of TCP of the manipulator with dual-motor drives during milling along circle 1 in the horizontal plane on the contour speed  $V$  at different values of cutting depth (1 – 0.1 mm, 2 – 0.25 mm, 3 – 0.5 mm) and different values of the radius of the circular trajectory (a & b – 10 mm, c & d – 25 mm, e & f – 50 mm)

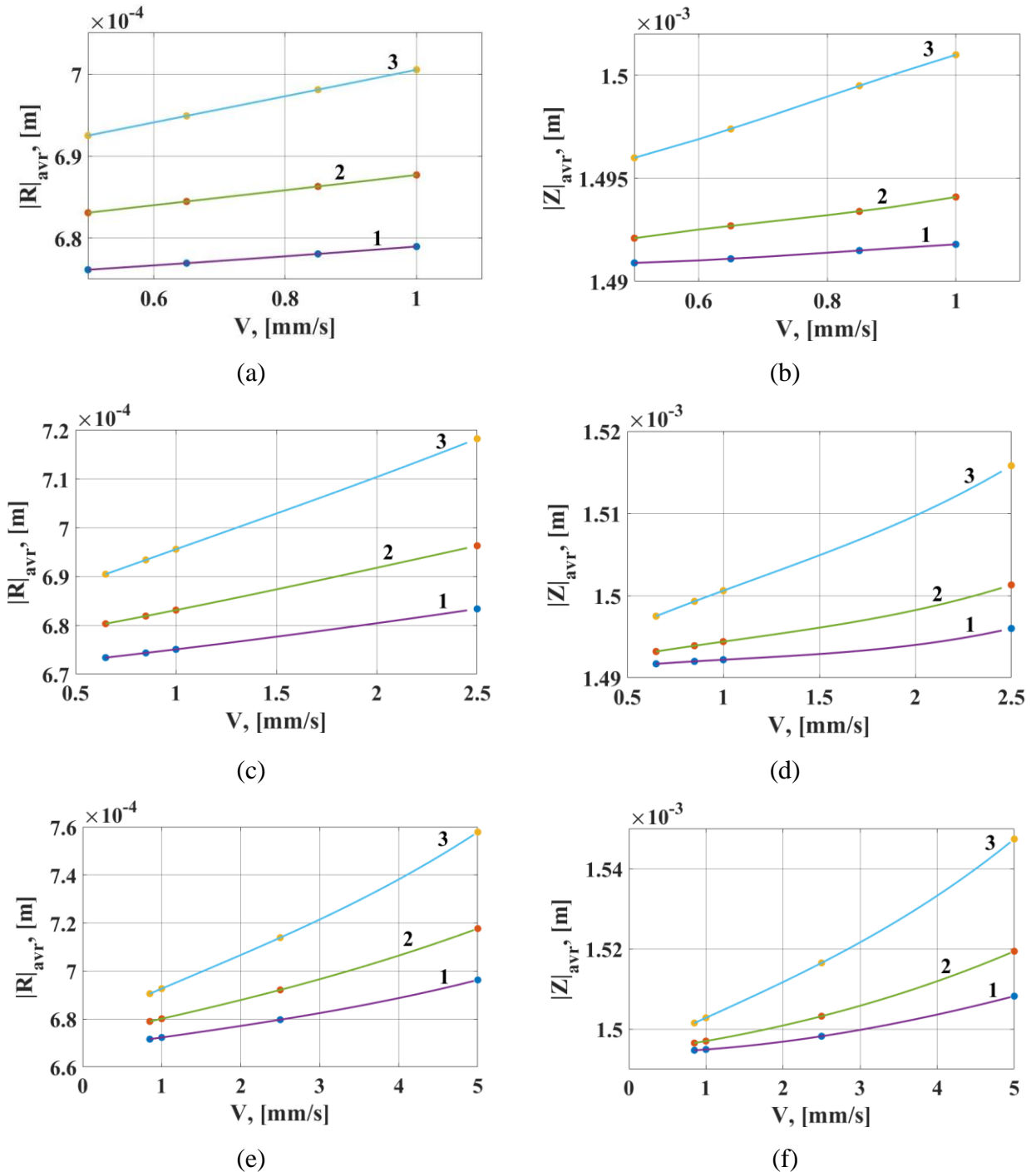


Figure 5.12. Dependencies of radial (a, c, e) and axial (b, d, f) RMS deviations of TCP of the manipulator with single-motor drives during milling along circle 1 in the horizontal plane on the contour speed  $V$  at different values of cutting depth (1 – 0.1 mm, 2 – 0.25 mm, 3 – 0.5 mm) and different values of the radius of the circular trajectory (a & b – 10 mm, c & d – 25 mm, e & f – 50 mm)

Computer simulations revealed that the manipulator with traditional single-motor servo drives commonly used in robotics is unable to perform robotic milling operations at many of the considered cutting parameter values. For example, in addition to the cases already presented in Figures 5.9 and 5.10, when milling along circle 2 with radius 50 mm in the horizontal plane, the operation can only be

performed at contour speed of no more than 5 mm/s; otherwise, divergent oscillations occur in the system. The dependencies of the RMS deviations for other cutting parameter values and the spatial position of the trajectory circle are shown in Figures 5.13–5.16. Tables 5.4, 5.5, and 5.6 present the corrected values of the loader torques for the dual-motor drive of the manipulator's column at these parameter values.

Table 5.5 – The values of the loader torque of the dual-motor drive of the manipulator column while milling along circle 2 in the horizontal plane

t, [mm] at R=0.01 m	V, mm/s			
	1 mm/s	2.5 mm/s	5 mm/s	10 mm/s
	$M_{loader}$ , Nm	$M_{loader}$ , Nm	$M_{loader}$ , Nm	$M_{loader}$ , Nm
0.1	20.7	20.7	20.7	20.7
0.25	20.7	20.7	34	45
0.5	20.7	37	62	86
t, [mm] at R=0.025 m	V, mm/s			
	1 mm/s	2.5 mm/s	5 mm/s	10 mm/s
	$M_{loader}$ , Nm	$M_{loader}$ , Nm	$M_{loader}$ , Nm	$M_{loader}$ , Nm
0.1	20.7	20.7	20.7	20.7
0.25	20.7	20.7	35	48
0.5	20.7	37	63	89
t, [mm] at R=0.05 m	V, mm/s			
	1 mm/s	2.5 mm/s	5 mm/s	10 mm/s
	$M_{loader}$ , Nm	$M_{loader}$ , Nm	$M_{loader}$ , Nm	$M_{loader}$ , Nm
0.1	20.7	20.7	20.7	22
0.25	20.7	21	35	50
0.5	20.7	38	64	91

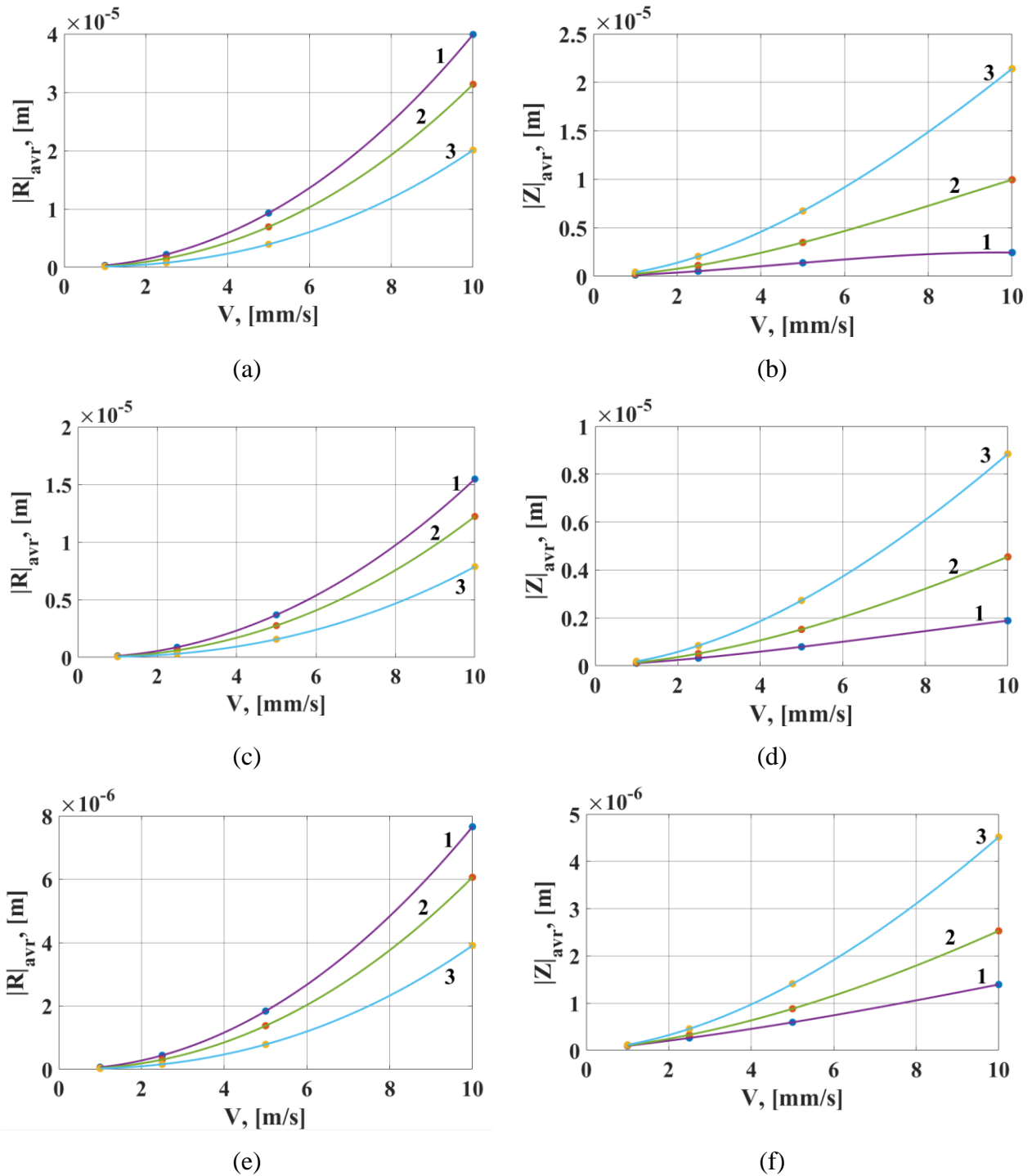


Figure 5.13. Dependencies of radial (a, c, e) and axial (b, d, f) RMS deviations of TCP of the manipulator with dual-motor drives during milling along circle 2 in the horizontal plane on the contour speed  $V$  at different values of cutting depth (1 – 0.1 mm, 2 – 0.25 mm, 3 – 0.5 mm) and different values of the radius of the circular trajectory (a & b – 10 mm, c & d – 25 mm, e & f – 50 mm)

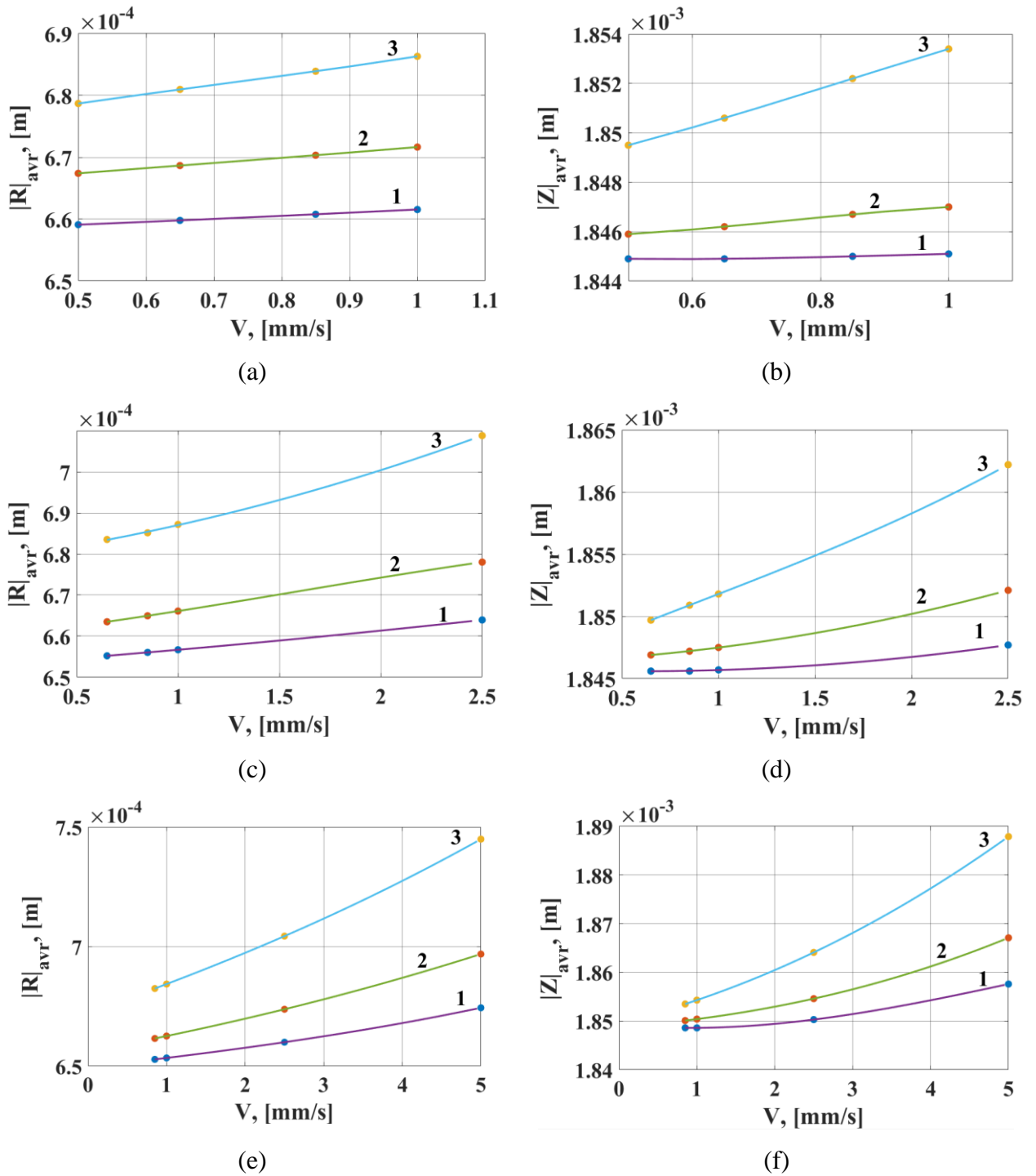


Figure 5.14. Dependencies of radial (a, c, e) and axial (b, d, f) RMS deviations of TCP of the manipulator with single-motor drives during milling along circle 2 in the horizontal plane on the contour speed  $V$  at different values of cutting depth (1 – 0.1 mm, 2 – 0.25 mm, 3 – 0.5 mm) and different values of the radius of the circular trajectory (a & b – 10 mm, c & d – 25 mm, e & f – 50 mm)

Table 5.6 – The values of the loader torque of the dual-motor drive of the manipulator column while milling along circle 3 in the horizontal plane

t, [mm] at R=0.01 m	V, mm/s			
	1 mm/s	2.5 mm/s	5 mm/s	10 mm/s
	$M_{loader}$ , Nm	$M_{loader}$ , Nm	$M_{loader}$ , Nm	$M_{loader}$ , Nm
0.1	20.7	20.7	20.7	20.7
0.25	20.7	20.7	35	52
0.5	20.7	38	63	101

t, [mm] at R=0.025 m	V, mm/s			
	1 mm/s	2.5 mm/s	5 mm/s	10 mm/s
	$M_{loader}$ , Nm	$M_{loader}$ , Nm	$M_{loader}$ , Nm	$M_{loader}$ , Nm
0.1	20.7	20.7	20.7	24
0.25	20.7	20.7	35	56
0.5	20.7	38	63	104

t, [mm] at R=0.05 m	V, mm/s			
	1 mm/s	2.5 mm/s	5 mm/s	10 mm/s
	$M_{loader}$ , Nm	$M_{loader}$ , Nm	$M_{loader}$ , Nm	$M_{loader}$ , Nm
0.1	20.7	20.7	20.7	26
0.25	20.7	21	35	59
0.5	20.7	38	64	107

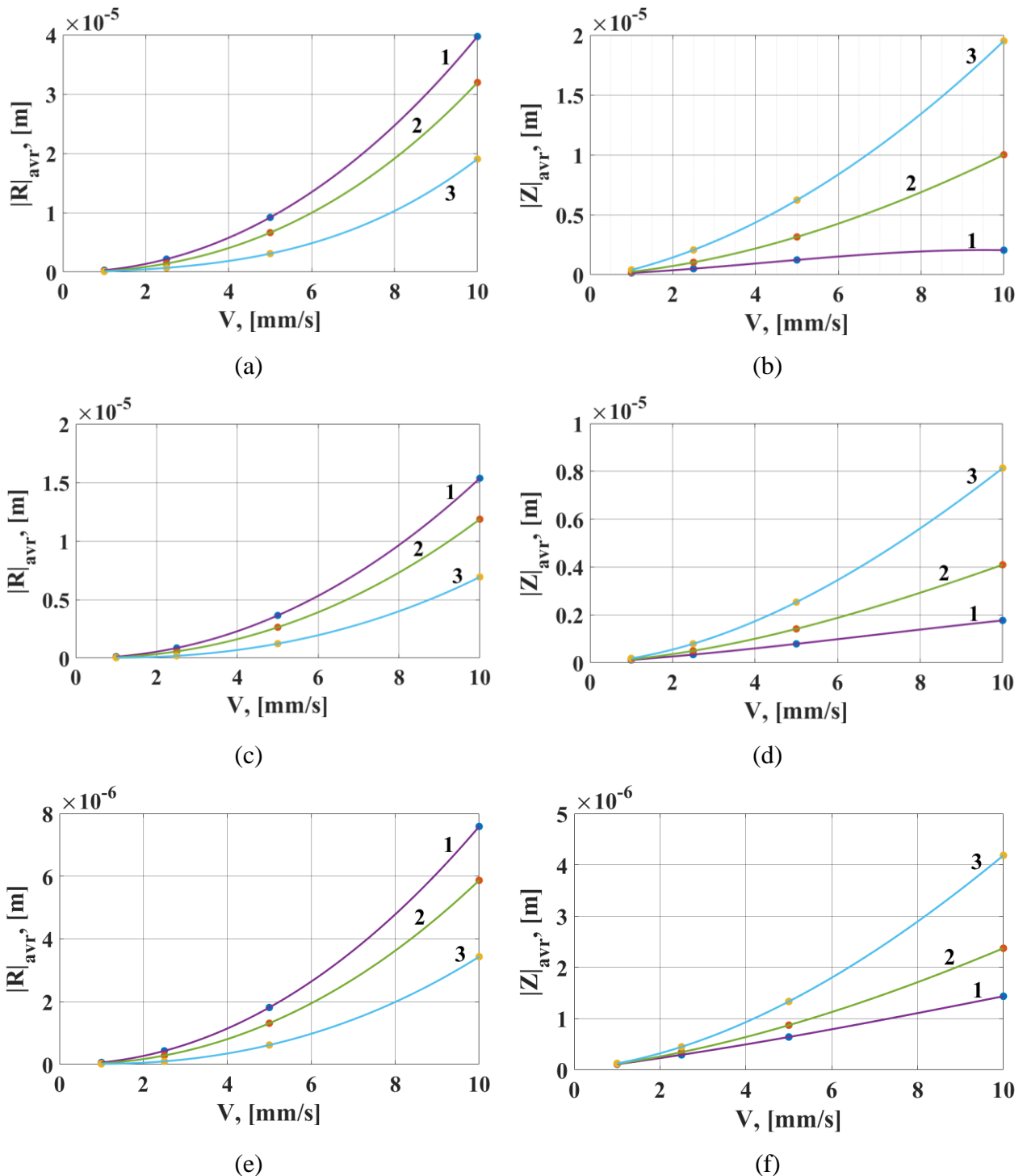


Figure 5.15. Dependencies of radial (a, c, e) and axial (b, d, f) RMS deviations of TCP of the manipulator with dual-motor drives during milling along circle 3 in the horizontal plane on the contour speed  $V$  at different values of cutting depth (1 – 0.1 mm, 2 – 0.25 mm, 3 – 0.5 mm) and different values of the radius of the circular trajectory (a & b – 10 mm, c & d – 25 mm, e & f – 50 mm)

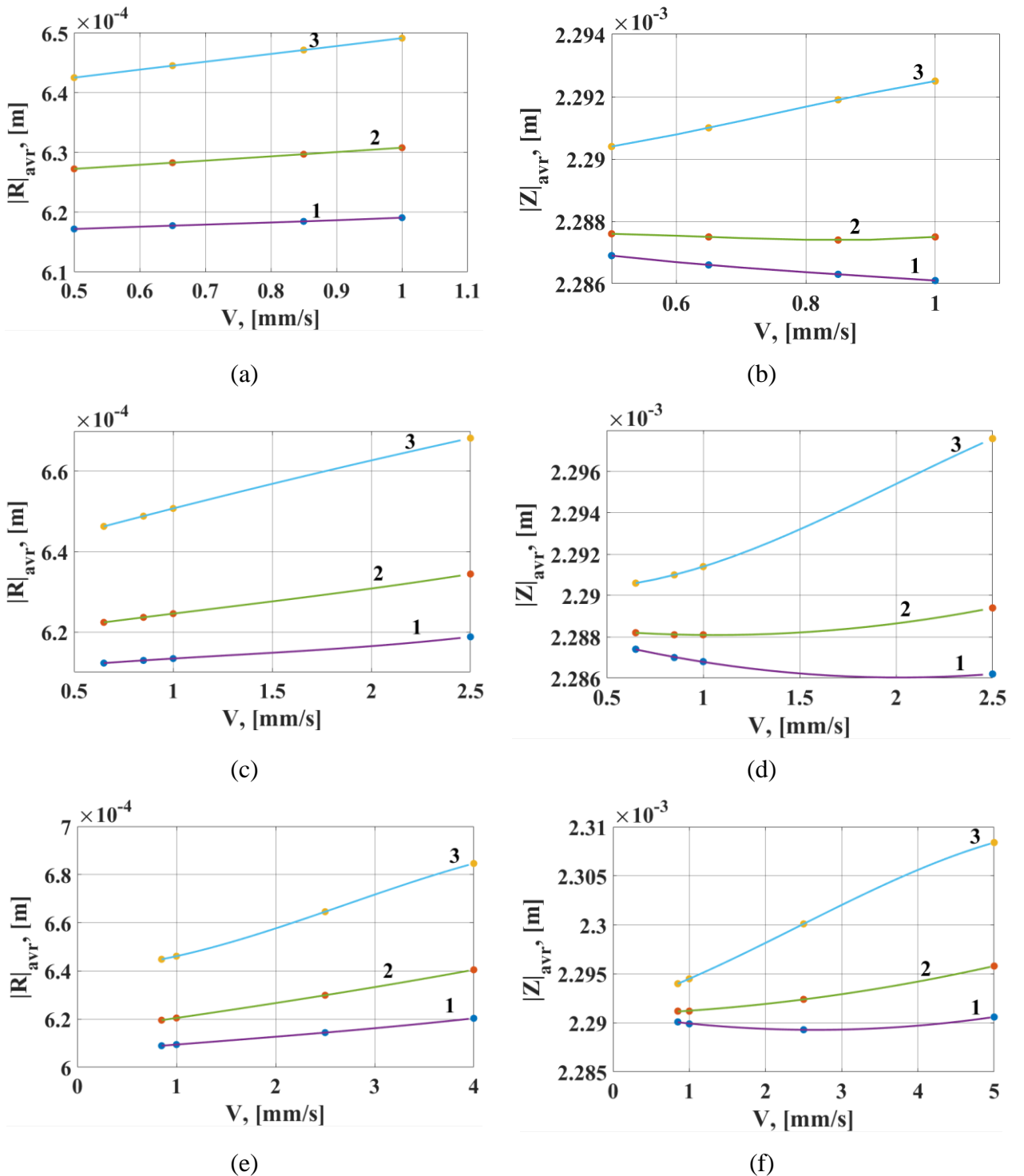


Figure 5.16. Dependencies of radial (a, c, e) and axial (b, d, f) RMS deviations of TCP of the manipulator with single-motor drives during milling along circle 3 in the horizontal plane on the contour speed  $V$  at different values of cutting depth (1 – 0.1 mm, 2 – 0.25 mm, 3 – 0.5 mm) and different values of the radius of the circular trajectory (a & b – 10 mm, c & d – 25 mm, e & f – 50 mm)

The dependencies obtained as a result of the analysis, presented in Figures 5.11–5.16, allow us to conclude that during the robotic milling operation along a circular trajectory, in all considered cases,

the manipulator with dual-motor servo drives exhibits significantly higher accuracy than the manipulator with single-motor drives.

As was previously mentioned, an earlier study presented in Chapter 4 analyzed the accuracy of manipulators with single-motor and dual-motor drives while performing movements along circle trajectories in the absence of forces acting on the manipulator's tool. In Chapter 4 there are obtained dependencies of the radial and axial RMS deviations of these manipulators on the contour speed, radius of the circular trajectory and cutting depth. The analysis of Figures 5.11–5.16 and its comparison to the results in Chapter 4 allows us to conclude that the nature of these dependencies remains consistent both in the absence of forces acting on the manipulator's tool and when such forces are present during the milling operation.

Thus, with an increase in contour speed, in most cases there is an increase in the RMS deviations, both radial and axial. The presented dependencies also show the following pattern: increasing the radius of the trajectory circle leads to a decrease in the radial RMS deviations of the manipulator with dual-motor drives, and an increase in these deviations when using the manipulator with single-motor drives. This can be explained as follows. As presented in Section 4.3.3, the total radial deviation of the manipulator with single-motor drives consists of two components. The first is caused by the dynamics of the drives closed by positions of the motor shafts, and the second component is related to the motion of the CO under the action of centrifugal force within the possible displacement range caused by backlash and elasticity of the mechanical gears of the drives. As a result, the first component tends to deflect the manipulator's TCP toward the center, while the second tends to deflect it away from the center of the circular trajectory. The sum of these two components determines the direction and magnitude of the manipulator's TCP resultant deviation.

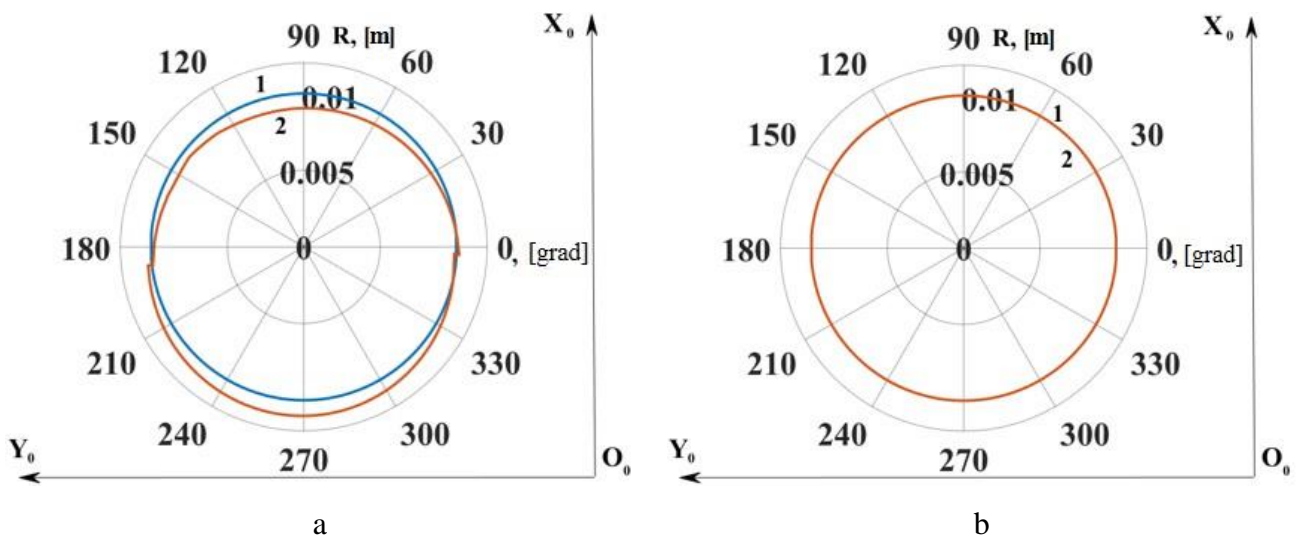
When the radius of the circle increases, the first component, caused by the drive dynamics, becomes smaller because the angular frequency at which the circular motion is executed decreases, and the frequency response (amplitude-frequency characteristic) of the drive increases. The second component, however, does not change; it is determined solely by the values of backlash and the elastic compliance of the manipulator's drive mechanical transmissions. As a result, the radial deviation of the manipulator's TCP increases. With an increase in contour speed, the first component becomes larger, and the radial deviation of the manipulator's TCP decreases for both types of the drives.

As shown earlier, a distinctive feature of manipulators with dual-motor drives is their infinitely large static stiffness and significant dynamic stiffness, which is due to the structure of the drive control system and the action of the active backlash-eliminating loader. This causes the second component of the total radial deviation of the manipulator with dual-motor drives to approach zero, while the first component causes relatively small deviations of the manipulator's TCP. Therefore, as the radius

increases, the angular frequency of the circular motion decreases, and the drive's frequency response increases, which leads to a reduction in the first component.

Also, when the manipulator performs robotic milling operation, the total radial deviations of the manipulator are influenced by a third component caused by the cutting forces. This component tends to deflect the manipulator's tool away from the center of the circle trajectory because, during counter milling, the cutting forces tend to pull the manipulator's tool into the workpiece.

As noted and demonstrated in Section 4.3.3, TCP of the manipulator with single-motor drives deviates along the  $O_0Z_0$  and  $O_0X_0$  axes, causing it to sag due to the presence of backlash and elasticity in the gears. As a result, the actual trajectory of the manipulator's TCP shifts toward its base. This effect is also observed in the present study, as shown in Figures 5.17, 5.18, and 5.19, which display the desired and actual TCP trajectories of the manipulator with single-motor (a) and dual-motor (b) drives while milling of a hole along circle 2 in the horizontal plane at various values of cutting depth, contour speed, and radius of the workpiece.



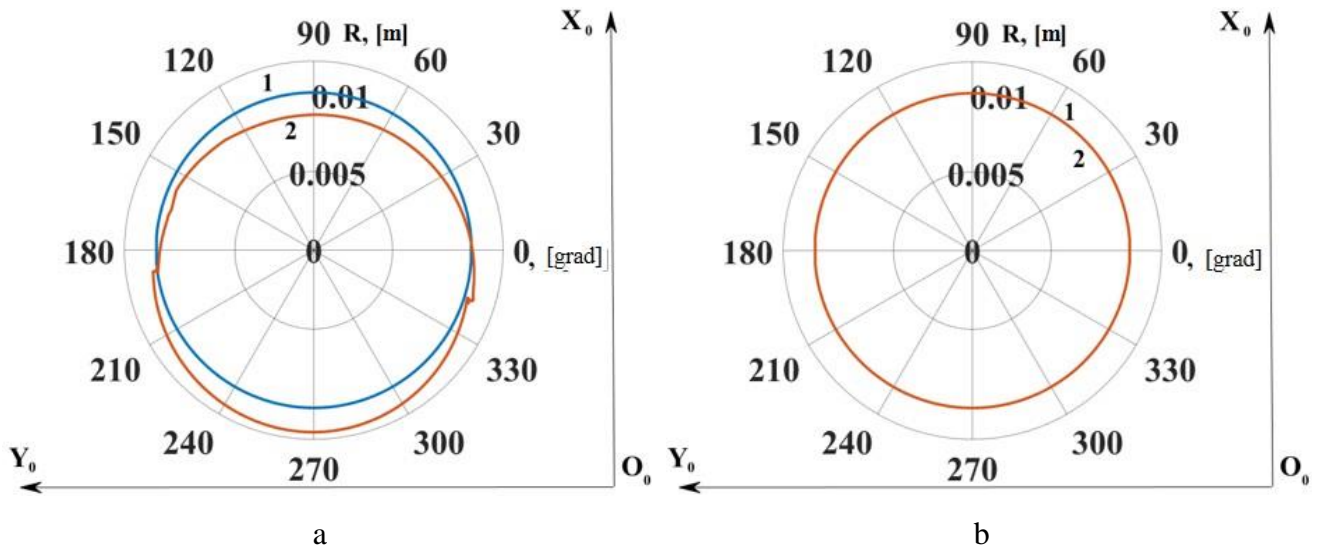


Figure 5.18. Desired (1) and actual (2) TCP's trajectories of manipulator with single-motor (a) and dual-motor (b) drives while milling of a hole along circle 2 in horizontal plane at cutting depth 0.5 mm, contour speed 0.75 mm/s and radius 10 mm

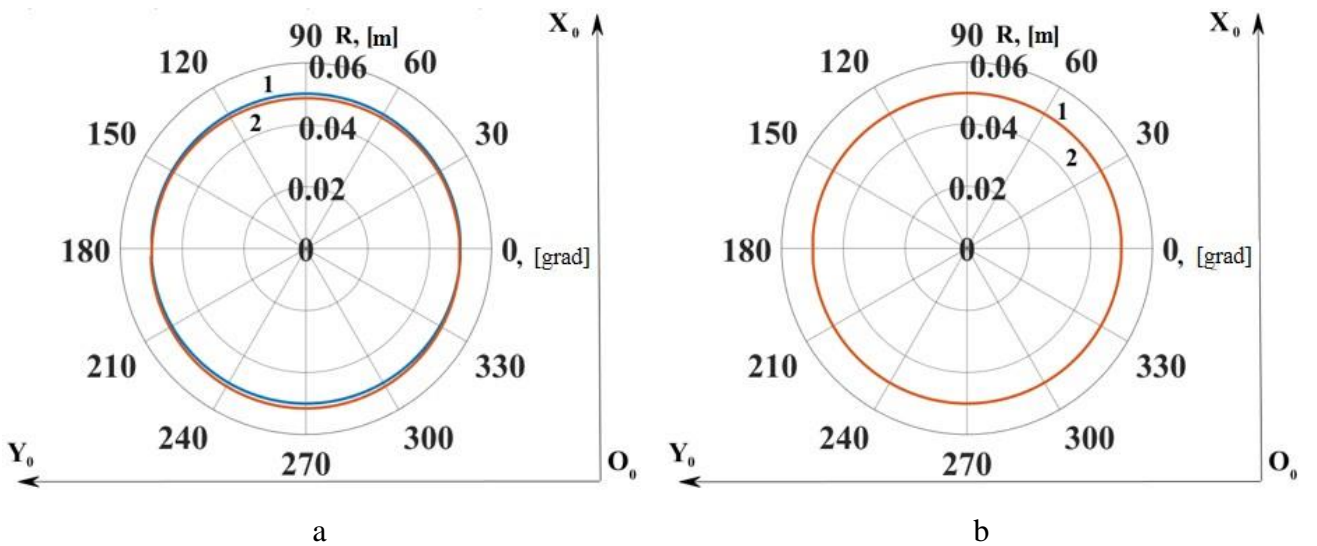


Figure 5.19. Desired (1) and actual (2) TCP's trajectories of manipulator with single-motor (a) and dual-motor (b) drives while milling of a hole along circle 2 in horizontal plane at cutting depth 0.5 mm, contour speed 1 mm/s and radius 50 mm

Since the sagging of the manipulator with dual-motor drives is caused only by the component related to the dynamics of the drives, the axial deviations of the manipulator decrease with increase in the radius, and they increase with the growth of the contour speed. This dynamic behavior is also consistent with the theoretical results of the analysis of the properties of manipulator with drives that have ideal backlash-free mechanical transmissions.

In addition, a pattern of deviation changes with varying cutting depth was identified. Specifically, an increase in cutting depth in all considered cases leads to an increase in axial RMS deviations for both manipulators with single-motor and dual-motor drives. This is explained by the increase in cutting forces, which causes larger deviations.

An increase in cutting depth also leads to an increase in the radial RMS deviations of the manipulator with single-motor drives. However, when using a manipulator with dual-motor drives, in many of the considered cases, this results in decrease in the radial RMS deviations. This can be explained by the fact that, as mentioned earlier, two components influence the total radial deviations in this case. The first, caused by the drive dynamics, tends to deflect the manipulator's tool toward the center of the circle trajectory, while the second, caused by the cutting forces, tends to deflect it away from the center. The combination of these two components determines the values of the radial RMS deviations. Thus, in many considered cases, an increase in cutting depth may lead to a decrease in the RMS deviations; however, the average deviations from these values during the process of cutting increase, as demonstrated in Figures 5.20–5.22. These figures show the graphs of the changes in the radius of the actual tool trajectory circle at different cutting depths while other cutting parameters remain constant.

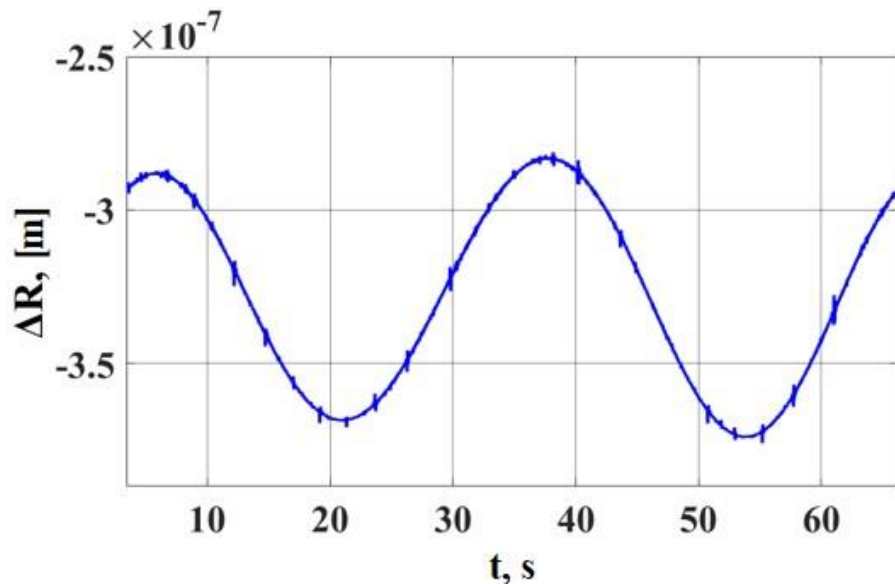


Figure 5.20. Change of radius of the actual TCP's trajectory of the manipulator with dual-motor drives while milling at contour speed 1 mm/s, cutting depth 0.1 mm and radius 10 mm

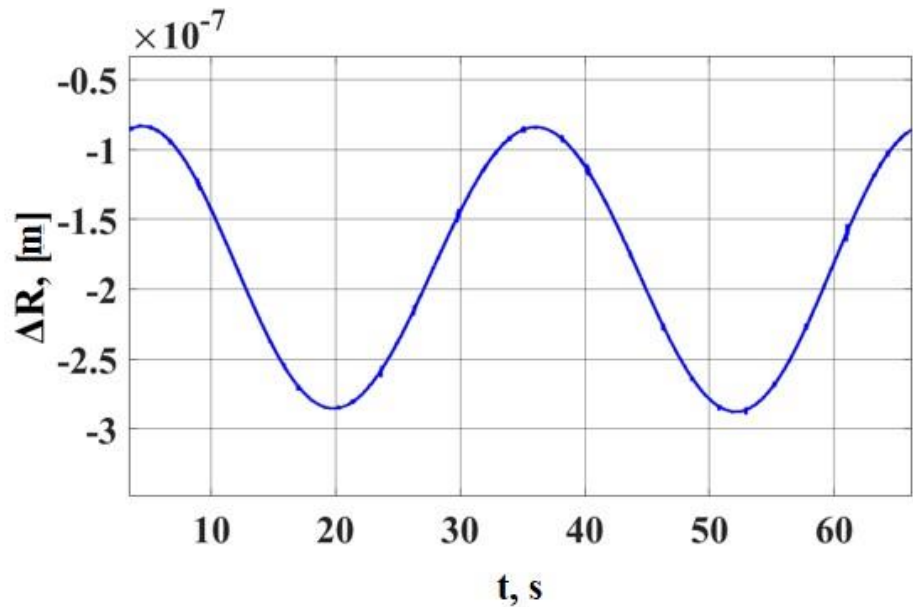


Figure 5.21. Change of radius of the actual TCP's trajectory of the manipulator with dual-motor drives while milling at contour speed 1 mm/s, cutting depth 0.25 mm and radius 10 mm

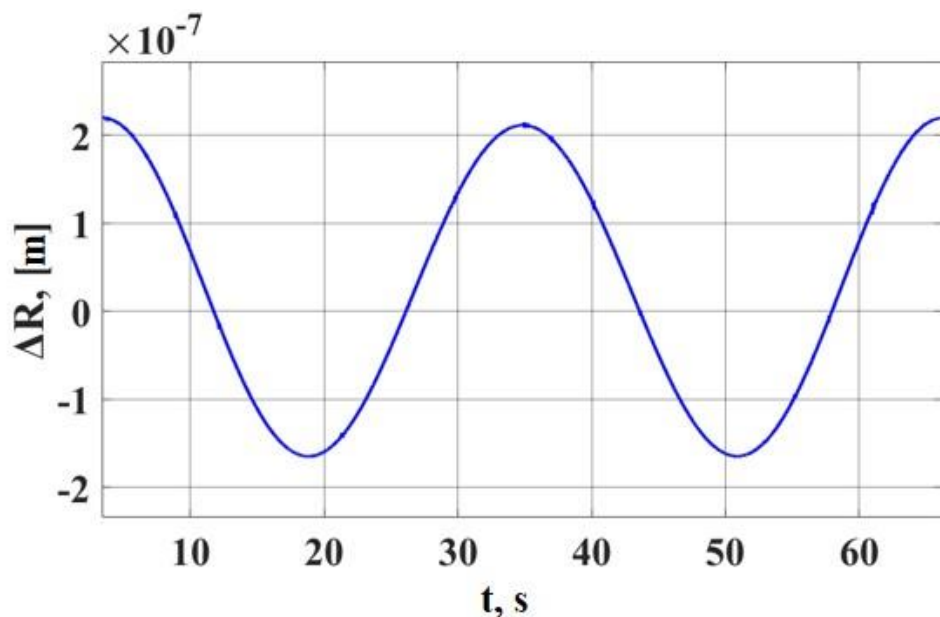


Figure 5.22. Change of radius of the actual TCP's trajectory of the manipulator with dual-motor drives while milling at contour speed 1 mm/s, cutting depth 0.5 mm and radius 10 mm

Table 5.7 presents the results of the comparison of radial RMS deviations of manipulators with single-motor and dual-motor drives at these cutting parameter values while milling of a hole along circle 2 in the horizontal plane. As a result, it was concluded that, just as in the case of the absence of forces acting on the tool, the usage of the manipulator with dual-motor drives in the robotic milling operation

significantly improved accuracy in the considered cases by many times compared to the manipulator with single-motor drives.

Table 5.7 – Comparison of accuracy of manipulators with single- and dual-motor drives when performing robotic milling along the circle trajectory 2 in the horizontal plane at cutting depth 0.5 mm

Contour velocity, mm/s	Circle radius, mm	Radial standard deviation		Accuracy improvement factor
		For manipulator with single-motor drives, m	For manipulator with dual-motor drives, m	
1	10	$6.8634 \cdot 10^{-4}$	$1.3661 \cdot 10^{-7}$	5024
0.75	10	$6.8248 \cdot 10^{-4}$	$8.8229 \cdot 10^{-8}$	7735
1	50	$6.8447 \cdot 10^{-4}$	$2.7861 \cdot 10^{-8}$	24570

When the manipulator operates in the vertical plane, as seen in Figures 5.23 and 5.24, the dependencies pattern described above is preserved. The radial and axial RMS deviations of the manipulator with dual-motor drives are significantly smaller than those of the manipulator with single-motor drives.

Table 5.8 presents the corrected values of the loader torques for the dual-motor drive of the manipulator's column during milling along circle 5, located in the vertical plane.

Table 5.8 – The values of the loader torque of the dual-motor drive of the manipulator column while milling along circle 5 in the vertical plane

t, [mm] at R=0.01 m	V, mm/s			
	1 mm/s	2.5 mm/s	5 mm/s	10 mm/s
	M <sub>loader</sub> , Nm			
0.1	20.7	20.7	20.7	20.7
0.25	20.7	20.7	29	46
0.5	20.7	31	53	89
t, [mm] at R=0.025 m	V, mm/s			
	1 mm/s	2.5 mm/s	5 mm/s	10 mm/s
	M <sub>loader</sub> , Nm			
0.1	20.7	20.7	20.7	20.7
0.25	20.7	20.7	29	48
0.5	20.7	31	52	86
t, [mm] at R=0.05 m	V, mm/s			
	1 mm/s	2.5 mm/s	5 mm/s	10 mm/s
	M <sub>loader</sub> , Nm			
0.1	20.7	20.7	20.7	21
0.25	20.7	20.7	29	48
0.5	20.7	31	52	88

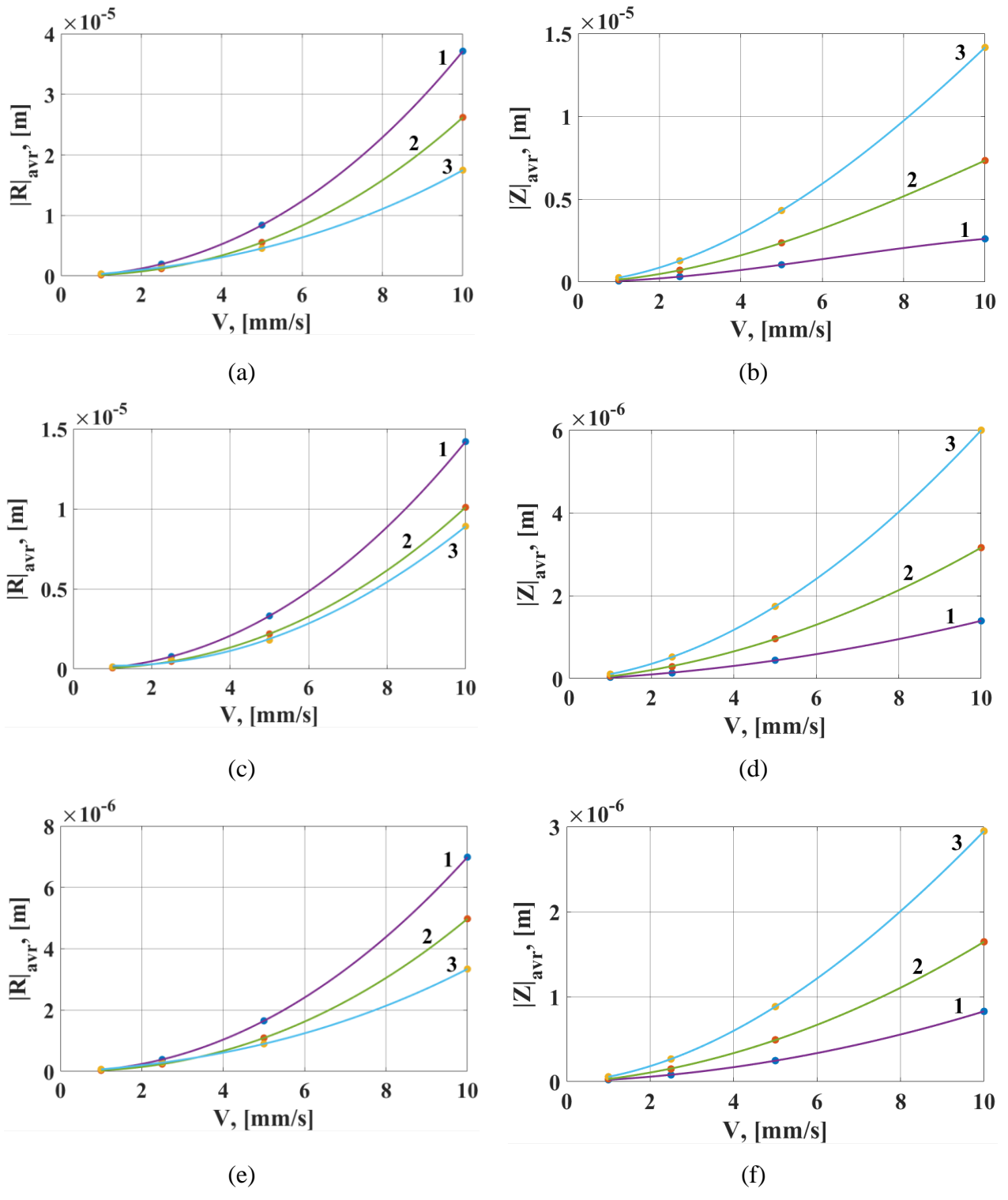


Figure 5.23. Dependencies of radial (a, c, e) and axial (b, d, f) RMS deviations of TCP of the manipulator with dual-motor drives during milling along circle 5 in the vertical plane on the contour speed  $V$  at different values of cutting depth (1 – 0.1 mm, 2 – 0.25 mm, 3 – 0.5 mm) and different values of the radius of the circular trajectory (a & b – 10 mm, c & d – 25 mm, e & f – 50 mm)

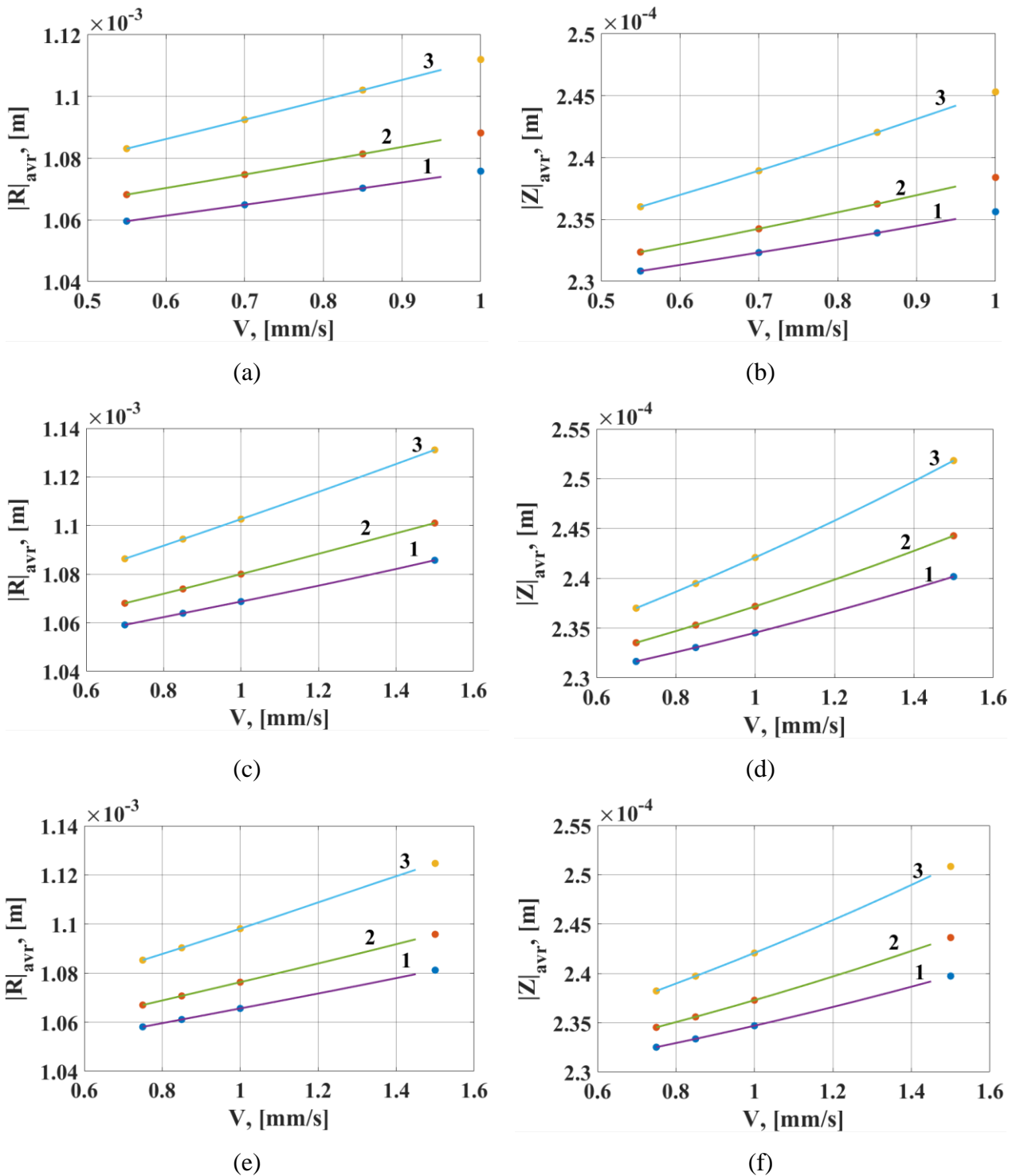


Figure 5.24. Dependencies of radial (a, c, e) and axial (b, d, f) RMS deviations of TCP of the manipulator with single-motor drives during milling along circle 5 in the vertical plane on the contour speed  $V$  at different values of cutting depth (1 – 0.1 mm, 2 – 0.25 mm, 3 – 0.5 mm) and different values of the radius of the circular trajectory (a & b – 10 mm, c & d – 25 mm, e & f – 50 mm)

As can be seen in Figures 5.23 and 5.24, the same dependencies presented in Figures 5.11–5.16 are preserved when the manipulator performs movements in the vertical plane.

Moreover, during the simulation of robotic milling along circle circular trajectory located in both planes (horizontal and vertical), in addition to the presented results, it was found that the radial and axial deviations of the manipulator with dual-motor drives change only slightly when the position of the circle within the manipulator's workspace is varied. This is confirmed by the data shown in Table 5.9.

Table 5.9 – Comparison of radial and axial deviations of manipulators with single- and dual-motor drives executing robotic milling along various circle trajectories at contour speed 1 mm/s, radius 10 mm and cutting depth 0.5 mm

	Radial standard deviation		Axial standard deviation	
	For manipulator with single-motor drives, m	For manipulator with dual-motor drives, m	For manipulator with single-motor drives, m	For manipulator with dual-motor drives, m
Movement of the TCP in the horizontal plane				
circle 1	$7.0052 \cdot 10^{-4}$	$1.7649 \cdot 10^{-7}$	$1.501 \cdot 10^{-3}$	$4.3238 \cdot 10^{-7}$
circle 2	$6.8632 \cdot 10^{-4}$	$1.3661 \cdot 10^{-7}$	$1.8534 \cdot 10^{-3}$	$4.2385 \cdot 10^{-7}$
circle 3	$6.4915 \cdot 10^{-4}$	$9.3457 \cdot 10^{-8}$	$2.2925 \cdot 10^{-3}$	$4.0017 \cdot 10^{-7}$
difference between max and min deviations	$5.137 \cdot 10^{-5}$	$8.3033 \cdot 10^{-8}$	$7.915 \cdot 10^{-4}$	$3.221 \cdot 10^{-8}$
Movement of the TCP in the vertical plane				
circle 4	$9.9927 \cdot 10^{-4}$	$2.7208 \cdot 10^{-7}$	$3.3615 \cdot 10^{-5}$	$1.9518 \cdot 10^{-7}$
circle 5	$1.0304 \cdot 10^{-3}$	$2.9421 \cdot 10^{-7}$	$9.5721 \cdot 10^{-5}$	$2.1551 \cdot 10^{-7}$
circle 6	$1.112 \cdot 10^{-3}$	$3.4236 \cdot 10^{-7}$	$2.4531 \cdot 10^{-4}$	$2.5999 \cdot 10^{-7}$
difference between max and min deviations	$1.127 \cdot 10^{-4}$	$7.028 \cdot 10^{-8}$	$2.117 \cdot 10^{-4}$	$6.481 \cdot 10^{-8}$

According to the data in the table, the range of RMS deviations for the manipulator **with dual-motor drives** is more than a **hundred times smaller** than the same indicators for the manipulator **with single-motor drives**. This indicates the feasibility and advisability of using the manipulator with dual-motor drives for performing technological operations that require high accuracy of motion, such as robotic milling, grinding, polishing, assembly, painting, laser cutting, and welding. It is also worth noting that the dependencies of the robot's end-effector motion accuracy on typical desired trajectories relative to the nominal values of parameters of the machining process, presented in Figures 5.11–5.16, 5.23, and 5.24, possess scientific novelty.

### 5.4.3 Computer simulation results of milling along circular trajectory with adaptive load torque control

In Section 5.4.2, it was already mentioned that during computer simulation of the robotic milling process, it became necessary to manually adjust the torque values generated by the loaders to eliminate self-oscillations and disconnection of the elastic elements in the gears of the dual-motor drives. In Section 2.5, computer simulation was conducted only for the dual-motor drive with adaptive control of the loader torque. This control allowed regulating the loader torque so that its value at every moment was minimal and sufficient to eliminate backlash and prevent the risk of self-oscillations. The same idea should be implemented in the drives of the technological robot performing robotic milling operation, where external forces caused by the milling process act on the robot's tool.

To implement adaptive control of the loader torque on a robot performing robotic milling, the mathematical model of the manipulator, whose structural diagram is shown in Figure 4.2, was modified as follows. It is assumed that the calculations of the force acting on the manipulator's tool, of the velocity of the manipulator's TCP, and of the position feedback are carried out in the robot controller. The force acting on the manipulator's tool is calculated based on the mathematical model shown in Figure 5.2 and according to the analytical expressions given in Section 5.2. If the forces acting on the manipulator's tool calculated in this way are considered equal to the actual forces (as a first-approach approximation), then a mathematical model can be constructed as shown in Figure 5.25, which possesses scientific novelty. This model reflects the influence of the force interaction between the tool and the workpiece and implements an adaptive algorithm for controlling the loader torque. It differs from the model shown in Figure 4.2 in that it uses simulation models of the drives, whose structural diagram is shown in Figure 2.8. The moments of external forces arising during the robotic milling operation are fed to the drives both as disturbance inputs and as values of  $M_{load}$ , used for calculating the loader torques in the adaptive control system.

In the torque controller block, the value of the loader torque is calculated according to formula (5.5). With this control, there is no need to manually determine the loader torque value that ensures the elimination of self-oscillations and backlash. If the direction of the load coincides with the direction of the loader, its torque becomes zero. If the load opposes the loader, its torque increases to maintain the tension torque between the ISD and the loader.

$$M_{loader_i} = \begin{cases} M_{tens_i} - M_{load_i}, & \text{if } 0 \leq M_{tens_i} - M_{load_i} \\ 0, & \text{if } M_{tens_i} - M_{load_i} < 0. \end{cases} \quad (5.5)$$

Here  $M_{load_i}$  – the calculated torque acting on the  $i^{\text{th}}$  drive from the load,  $M_{loader_i}$  – torque, which should be developed by the loader of the  $i^{\text{th}}$  drive,  $M_{tens_i}$  – the required tension torque between the loader and the ISD of the  $i^{\text{th}}$  drive, sufficient for elimination of backlash self-oscillations in this drive.

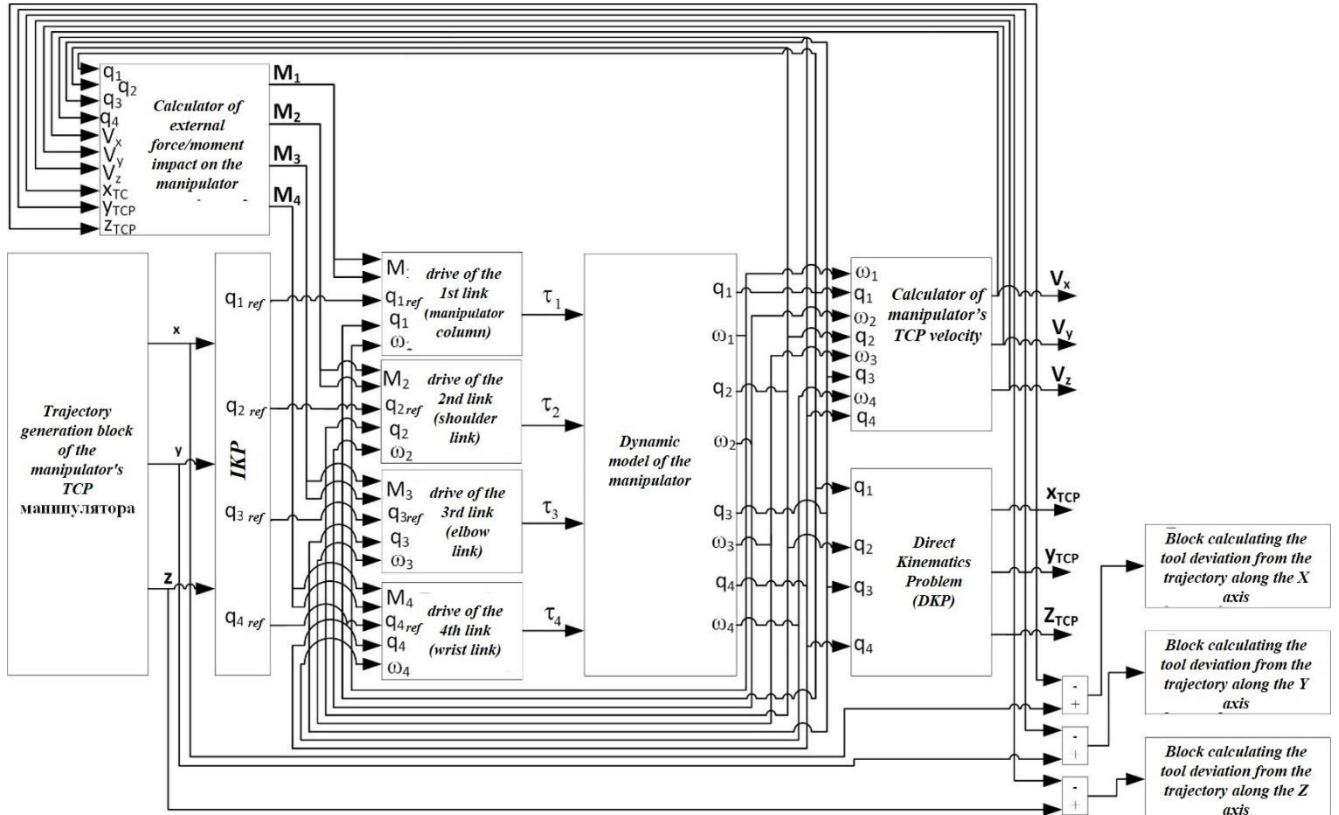


Figure 5.25. Structure diagram of the computer simulation program of the robot with adaptive control of the drives' loader torque

As shown in Figure 5.25, the signals corresponding to the calculated values of the moments of external forces acting on the manipulator's tool are fed to the input to the drive models. The moment values in the drive models are supplied both as moments of external forces and as the signal  $M_{load_i}$  in formula (5.5). At the same time, as in Section 2.5, during the execution of the technological operation by the robot, the total energy  $P_{\Sigma}$ , consumed by the robot's drives during operation, is determined by the formula (2.13).

In the study, the manipulator performed counter milling of a workpiece with parameters presented in Section 5.3.1, milling a hole along circle 3 with radius 10 mm in the horizontal plane at contour speed 25 mm/s and cutting depth 0.1 mm. As a result, without adaptive control of the loader torques, the power consumed by the first motor, acting as ISD of the manipulator's elbow link, was 175.55 W, and by the second motor, acting as the loader, was 7.12 W, totaling 182.67 W. The graphs of the current in the windings of both motors of the manipulator's elbow link are shown in Figure 5.26. In

the computer simulation program, the milling process started at time 14.57 s; before this, the manipulator's TCP first moved to the specified starting point of the circular trajectory, and then the manipulator followed the trajectory, making a full circle, without performing the milling operation, i.e., no external forces acted on its tool. After 14.57 s, the manipulator performed the milling process and completed two circles until the time of 40 s. The radial RMS deviations of the manipulator's TCP from the desired trajectory, calculated using formula (4.3), amounted to  $2.31 \cdot 10^{-6}$  m.

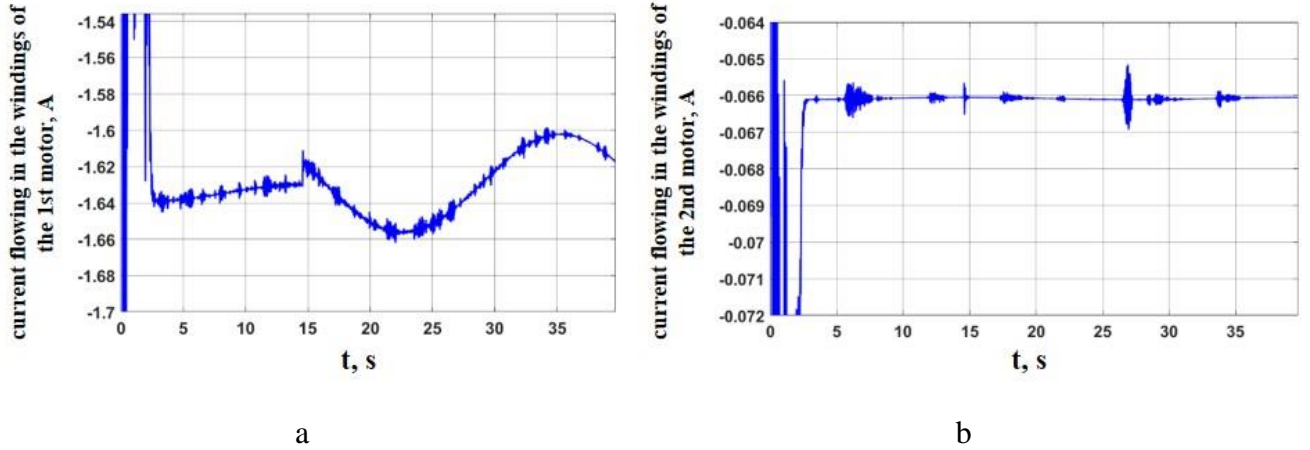


Figure 5.26. Current flowing in the windings of the 1st (a) and 2nd (b) motors of the drive of the manipulator elbow link **without adaptive loader torque control system**

After enabling adaptive control of the loader torque, the power consumed by the first motor of the manipulator's elbow link drive, acting as ISD, was 176.7 W, and by the second motor, acting as the loader, was 5.95 W, totaling 182.55 W. The obtained data are presented in Table 5.10. The graphs of the current in the windings of both motors in this case are shown in Figure 5.27.

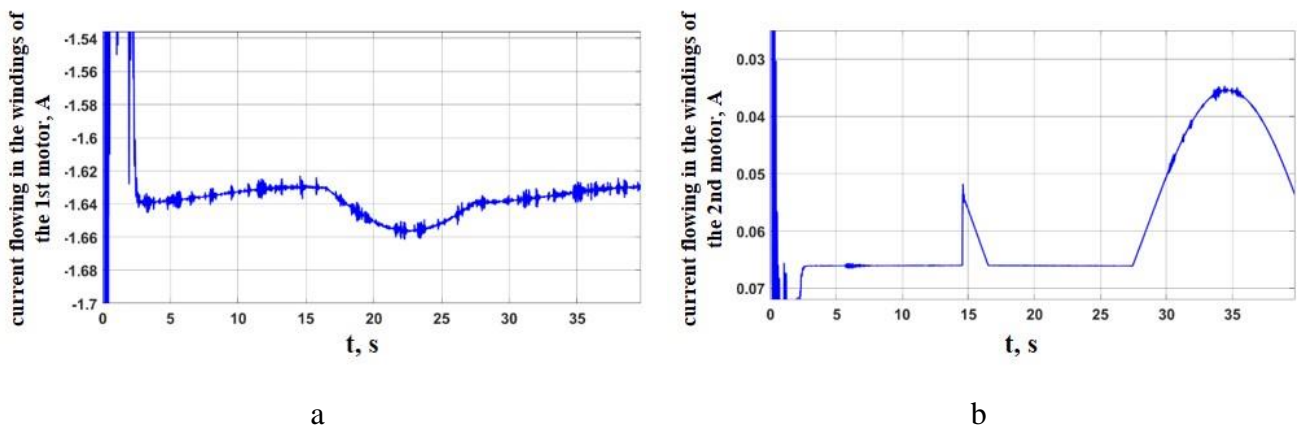


Figure 5.27. Current flowing in the windings of the 1st (a) and 2nd (b) motors of the drive of the manipulator elbow link **with adaptive loader torque control system**

As can be seen in the figure, during the milling operation, the current in the windings of the second motor, which acts as the loader, is lower at two time intervals because the load acting on the drive at those times itself ensures the elimination of self-oscillations. The graph of the radial deviation of the manipulator's TCP from the desired circular trajectory in the steady-state motion mode in this case is shown in Figure 5.28. The radial RMS deviations of the manipulator's TCP from the desired trajectory amounted to  $2.43 \cdot 10^{-6}$  m, which very slightly differs from the value without adaptive control.

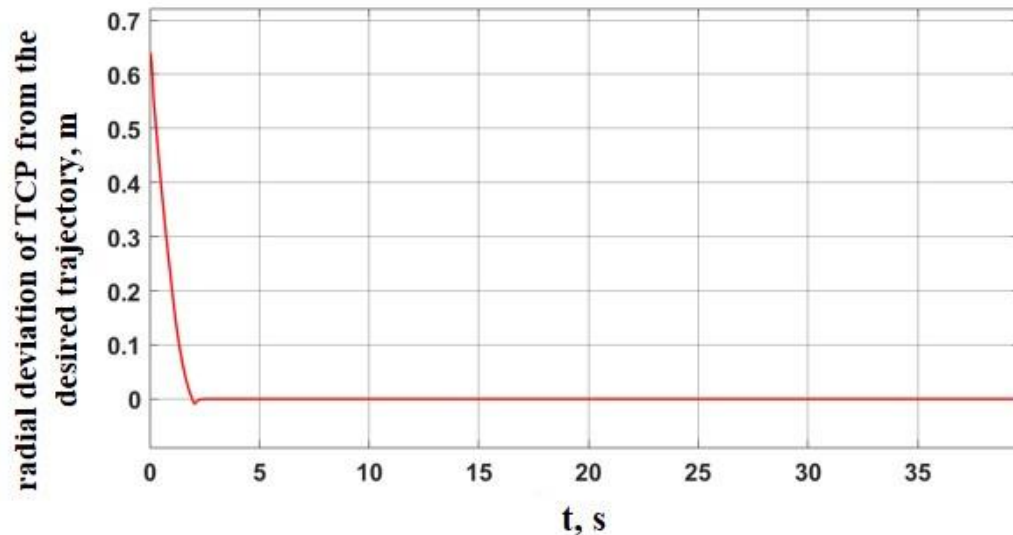


Figure 5.28. Radial deviation of the manipulator's TCP from the desired trajectory when using  
**adaptive loader torque control system**

However, as in the case considered in Section 2.5, it is possible to further reduce the energy consumption of the manipulator's drives and more efficiently utilize all the motors of the dual-motor drives of all manipulator links by switching the control system structures of the drives. Section 2.5 already presents a structural diagram of the mathematical model of the drive with structure-switching control system and adaptive control of the loader torque. To implement such control of the drives in the robot, it is sufficient to replace the drive models in the structural diagram of the robot's computer simulation program (with adaptive loader torque control) shown in Figure 5.25 with those presented in Figure 2.24. In this case, the value of the force applied to the manipulator tool and determined in the calculator of external force/moment impact on the manipulator will be fed to the input of the drive models as the torque of the load. There is also the loader torque calculation block, where the desired value of the loader torque is determined by the formula:

$$\begin{aligned}
 M_{loader_{1i}} &= \begin{cases} M_{tensi_i} - M_{load_i}, & \text{if } 0 \leq M_{tensi_i} - M_{load_i} \\ 0, & \text{if } M_{tensi_i} - M_{load_i} < 0. \end{cases} \\
 M_{loader_{2i}} &= \begin{cases} M_{load_i} - M_{tensi_i}, & \text{if } 0 \leq M_{load_i} - M_{tensi_i} \\ 0, & \text{if } M_{load_i} - M_{tensi_i} < 0. \end{cases} \\
 M_{loader} &= \begin{cases} M_{loader_{1i}}, & \text{if } \left( \left( U > \frac{U}{z} \right) \text{OR} \left( U = \frac{U}{z} \right) = \text{TRUE} \right); \\ M_{loader_{2i}}, & \text{if } \left( \left( U > \frac{U}{z} \right) \text{OR} \left( U = \frac{U}{z} \right) = \text{FALSE} \right). \end{cases} \quad (5.6)
 \end{aligned}$$

In formula (5.6), the calculation of the derivative of the input signal in the function  $\text{sign}\left(\frac{d\beta(t)}{dt}\right)$  is replaced by a comparison of the signal at the current ( $U$ ) and at the previous ( $U/z$ ) time moments in order to eliminate errors in the simulation model caused by inaccuracies in determining the derivative and to speed up the model simulation time.

After computer simulation of the robotic milling process with the same parameters as when using adaptive control of the loader torques, the power consumed by the first motor of the manipulator's elbow link drive was 90.11 W, and by the second motor was 96.23 W, totaling 186.34 W. The obtained data are presented in Table 5.10. The graphs of the current in the windings of both motors in this case are shown in Figure 5.29.

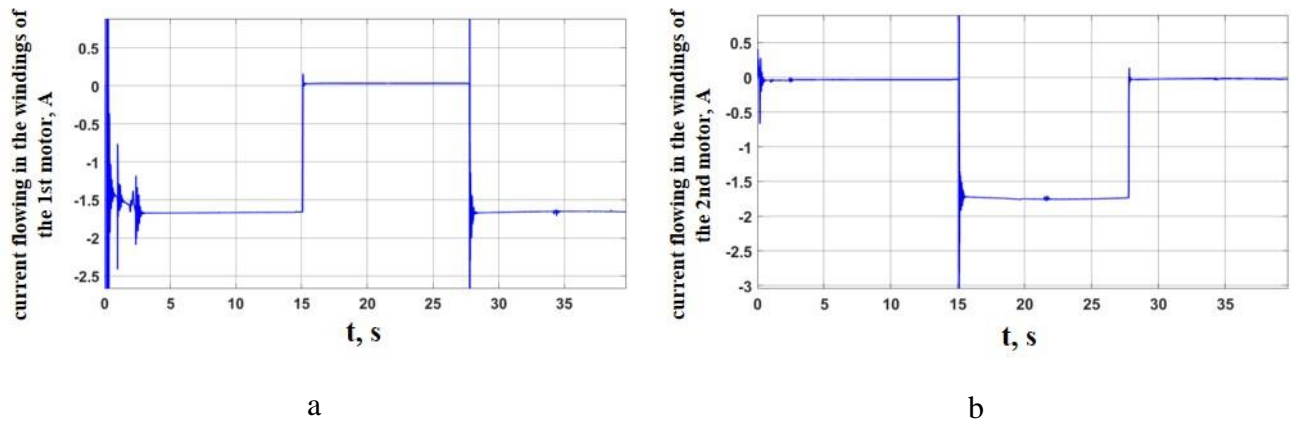


Figure 5.29. Current flowing in the windings of the 1st (a) and 2nd (b) motors of the drive of the manipulator elbow link **with adaptive loader torque control system and switching of control system structures**

The graph of the position error of the control object in this case is shown in Figure 5.30. The radial RMS deviations of the manipulator's TCP from the desired trajectory amounted to  $4.82 \cdot 10^{-5}$  m, which is significantly higher than when using only adaptive control of the loader torques.

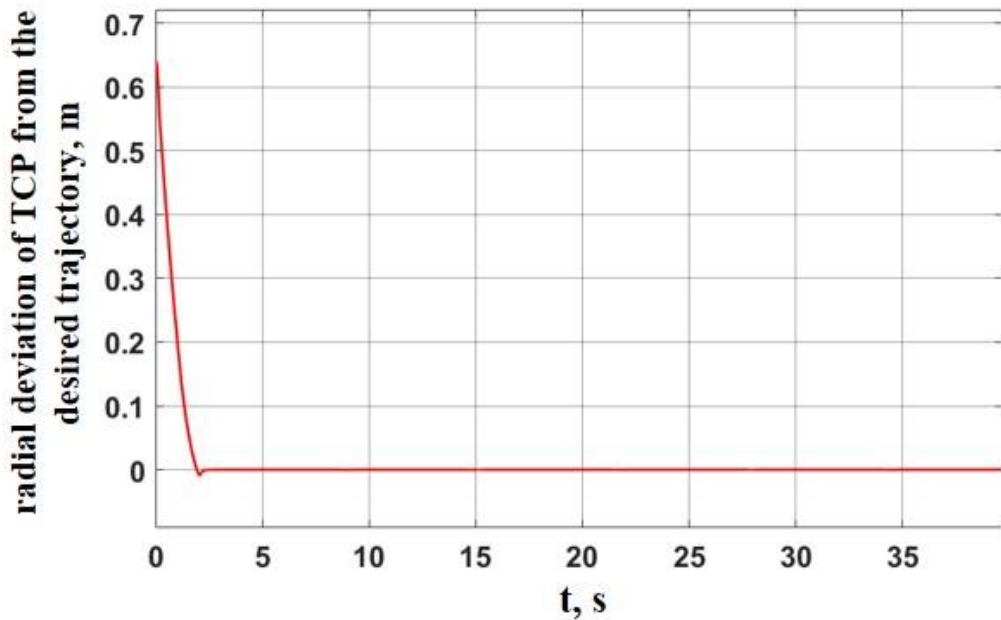


Figure 5.30. Position error of the control object in the displacement mode with changes of motion direction when **using the adaptive loader torque control system and switching of control system structures**

Table 5.10 – Comparison of power consumption P of the drives of manipulator with dual-motor drives both **without and with adaptive loader torque control system and switching of control system structures**

	P of dual-motor drive, W		P of dual-motor drive with adaptive loader torque control system, W		P of dual-motor drive with adaptive loader torque control system and switching of control system structures, W	
	ISD	loader	ISD	loader	1 <sup>st</sup> motor	2 <sup>nd</sup> motor
drive of the column	13.03	13.09	11.24	11.3	4.04	4.92
drive of the shoulder link	327.81	13.09	328.5	12.37	168.64	178.76
drive of the elbow link	175.55	7.12	176.7	5.95	90.11	96.23
drive of the wrist link	35.91	0.85	36.3	0.45	19.11	17.81
$\Sigma$	586.44		582.81		579.63	

The power consumption values of the drive of the elbow link in the last case turned out to be slightly higher than without using adaptive control. However, the total power consumed by all the robot's drives with structure-switching control system is lower when using such control together with adaptive control of the loader torques of all the manipulator drives.

The main advantage here is that in the last case, with the usage of adaptive control of the loader torques and structure-switching control system, both motors of the drives of all manipulator links were

loaded approximately equally, which may have a positive effect on the wear of the motors and the control components of the drives. However, due to the increase in the radial RMS deviations of the manipulator's TCP from the desired trajectory, such a scheme with switching of the manipulator drive control system structures requires further refinement. First and foremost, the switching of the torques and currents flowing in the motor windings of the drives should be made smoother than what is shown in Figure 5.30. The abrupt switching of torques and currents led to the occurrence of additional oscillations, which contributed to the increase in the radial RMS deviations of the TCP.

The usage of drives with structure-switching control system could also be much more effective when designing SCARA-type robots, in which all the axes are arranged vertically. In such robot designs, gear backlash is mostly pronounced because there are no static moments acting on the drives from the manipulator mechanism's links. In the case of anthropomorphic robots, such static moments themselves can act as loaders, generating torque that opposes the main motor and eliminates self-oscillations. Therefore, in SCARA robots of comparable design to anthropomorphic robots, the loader torques must be higher to eliminate self-oscillations. As a result, adaptive control of the loader torque can be even more effective in this case.

In this study, computer simulation demonstrated the feasibility of using adaptive control of the loader torques to eliminate backlash and self-oscillations in dual-motor drives of the manipulator, as well as the feasibility of using the scheme with switching control system structures in dual-motor drives to distribute the load more evenly between the 2 motors for more even wear.

The research materials presented in this chapter have been published in [16, 17, 77, 79].

## **5.5 Conclusions on the fifth chapter**

This chapter presents the mathematical model and the structure of the technological robot, equipped with a set of two-channel digital dual-motor servo drives, which possess scientific novelty. They reflect the influence of the force interaction between the tool and the workpiece and implement an adaptive algorithm for controlling the loader torque.

The results of computer simulation of the robotic milling operation indicate that, to improve accuracy and productivity of this operation, it is recommended to use technological robots built on the precision dual-motor servo drives closed by the position control loops of the manipulator links. To enhance the dynamic properties of such robots, it is advisable to implement control with corrective feedback of the velocities of the manipulator links.

Overall, the proposed solution allows for a significant increase in the static and dynamic stiffness of the robot through control means without changing the stiffness coefficients of the robot's mechanical

transmissions. This makes it possible to reduce the influence of cutting forces on the deviation of the tool from the desired trajectory and to improve the productivity of robotic milling, as confirmed by the results of the comparative analysis. Thus, when performing robotic milling operations with manipulators built on the two considered types of servo drives, moving along linear and circular desired trajectories with different radii, cutting depths, and contour speeds, the research results indicate the advantages of manipulators equipped with precision dual-motor drives. In all considered cases, the RMS radial and axial deviations of the manipulator with dual-motor drives from the specified trajectory are smaller than those of the manipulator with single-motor drives. This allows the conclusion that the results of computer and experimental studies confirmed the theoretical statement that the developed dual-motor drives provide high dynamic accuracy of motion and high robot stiffness without significant loss of performance due to improvements in the control structure and algorithms, without substantial changes in the robot's mechanical components.

Changing the position of the circular trajectory in space has little effect on the deviations of the manipulator with dual-motor drives from the desired trajectory, both along the radius of the circle trajectory and along the normal to the plane of motion. Thus, it can be said that the stability of the parameters of the manipulator with dual-motor drives within its workspace is higher than that of the manipulator with single-motor drives.

As a result of the study, dependencies of the accuracy of the robot's end-effector motion while milling along typical desired trajectories on the nominal values of the parameters of the machining process were obtained, possessing scientific novelty. The results also allow the conclusion that the usage of technological robots with the proposed dual-motor drives contributes to a significant increase in the accuracy of tool movements and enables the realization of precision and high-performance robotic milling. Robots equipped with such drives are recommended for use in enterprises implementing technologies that require enhanced positioning and movement accuracy of end-effectors along specified trajectories. In addition to robotic milling, this also applies to technological operations such as grinding, polishing, assembly, painting, laser cutting, and welding.

## CONCLUSION

1. The dissertation presents a novel, scientifically validated solution to the urgent problem of increasing accuracy of technological robot motion through a new control structure and control algorithms for two-channel digital servo drives with position feedback of the control objects (manipulator links). This approach is particularly crucial for analytically programmed industrial robots.
2. The results of the conducted research demonstrated the feasibility of using precision two-channel dual-motor geared servo drives in industrial robots with open kinematic chains. The second control channel in such drives is necessary for continuous control of the torque developed by the loader in order to maintain the tension torque between the two motors at a minimum level, sufficient to eliminate self-oscillations. The results of the research show that such a drive possesses both high stiffness and sufficient damping.
3. The results of computer simulation and experimental studies have confirmed the theoretical proposition that the developed dual-motor drives ensure high dynamic accuracy and stiffness of the robot without significant loss of performance as a result of improvement of the control structure and control algorithms without significant modifications to the robot's mechanical components.
4. The results of theoretical study and computer simulation showed that the positioning accuracy depends mainly on the error and resolution of the sensor directly measuring the position of the control object. The results of the experimental study showed that when using an encoder installed on the control object's shaft generating 250000 pulses per revolution, and when responding only on step reference input values, the dual-motor servo drive achieves 40 times higher accuracy than a single-motor servo drive, closed only by position feedback of its motor shaft.
5. A problem related to the occurrence of self-oscillations has been identified, which is caused by insufficient resolution of the position sensor on the motor shaft of the primary (first) control channel. To eliminate these self-oscillations, it is recommended to use the position sensor installed on the motor shaft with increased resolution. In particular, it is shown that by using an encoder generating 2048 pulses per revolution, a trade-off between encoder cost and drive accuracy is achieved in the absence of self-oscillations.
6. The experimental results confirm the results of the theoretical research and allow us to recommend dual-motor drives for the construction of technological robots that have manipulation mechanisms with open kinematic chain, particularly for analytically programmed robots intended for high-precision operations such as robotic milling. For example, the

considered dual-motor servo drive is 40 times more accurate than a single-motor servo drive of the traditional structure, closed by position control loop of its motor shaft, when responding on a step reference input 0.1 rad. The dual-motor servo drive responds on harmonic reference input with amplitude 0.1 rad and circular frequency 0.5 rad/s with a maximum error of  $8.4 \times 10^{-4}$  rad, which is 5.5 times more accurate than a single-motor servo drive.

7. The mathematical models developed during the research make it possible to predict the errors in technological robot operation and allow the selection of the maximum allowable contour speed for any given tolerance of the toolpath deviation, ensuring optimal performance while meeting precision requirements. In all the considered variants of performing circular motion trajectories, the root-mean-square radial and axial deviations of manipulators with single-motor drives from the specified trajectory exceeded those of manipulators with dual-motor drives. For instance, at a contour speed of 5 mm/s and a circle radius of 10 mm, the steady-state error of the manipulator with dual-motor drives was approximately 87 times smaller than that of manipulator with single-motor drives, closed by position feedback of the motor shaft.
8. Computer simulation results demonstrated that the energy efficiency of the developed drive improves through structure-switching and adaptive control of the loader torque. When the roles of the motors of the dual-motor servo (the motor of the internal servo drive and the motor of the torque loader) can be dynamically reassigned, the power consumed by the drive is significantly reduced without degrading transient performance, even while responding on the reference input with sharp changes in motion direction. And introduction of adaptive control of the loader torque allows to develop the smallest value of the torque, sufficient for elimination of backlash and self-oscillations. This enables higher allowable contour speeds and performance of manipulators built on such drives, expanding their functional capabilities.
9. Robots equipped with dual-motor servo drives with controlled loaders are recommended for enterprises implementing technologies that demand enhanced positioning accuracy and precise trajectory control of end-effectors. Their applications include robotic milling, grinding, polishing, assembly, painting of miniature components, laser cutting, and welding.

## REFERENCES

1. Executive Summary World Robotics 2020 Industrial Robots [Электронный ресурс]: International Federation of Robotics – Режим доступа: [https://ifr.org/downloads/press/Executive\\_Summary\\_WR\\_2020\\_Industrial\\_Robots.pdf](https://ifr.org/downloads/press/Executive_Summary_WR_2020_Industrial_Robots.pdf) – 22.01.21.
2. Ilyukhin, Yu. V. Creation of highly effective control systems of executive movements of robots and mechatronic devices on the basis of the technologically determined method of synthesis: Doctor of Technical Sciences : 05.02.05 / Ilyukhin Yuri Vladimirovich - M., 2001. - 378 p.
3. Makarov, I. M. Automation of designing and programming of robots and GPS: collection of scientific papers / edited by I. M. Makarov and E. P. Popov // Nauka, 1988. - 240 p.
4. Zenkevich, S. L. Robot Control. Fundamentals of manipulation robots control: a textbook for universities / S. L. Zenkevich, A. S. Yushchenko. - Moscow: Bauman Moscow State Technical University, 2000. - 400 p.
5. Medvedev, B. C. Control systems for manipulation robots / B. C. C. Medvedev, A. G. Leskov, A. C. Yushchenko. Yushchenko. - Moscow: Nauka, 1978. - 416 p.
6. Poduraev, Yu.V. Contour force control of technological robots on the basis of tensor-geometric method: Dr. Sci. (in Russian) : 05.02.05 / Yuri V. Poduraev. - M., 1993. - 38 p.
7. Yogesh D. P. Optimization of Quality Characteristics of Laser Cutting / D. P. Yogesh, Dr. K. H. Inamdar // International Journal of Emerging Technologies and Innovative Research, № 2 (6), 2015. pp. 1959-1963. ISSN:2349-5162
8. Whitcher, J. Laser Welding: Metal Fastening with Microscopic Precision / J. Whitcher // Medical Device & Diagnostic Industry, June 2007
9. Kang Hee-Shin. Robot based Laser Welding Technology / Hee-Shin Kang, Jeong Suh, Taik-Dong Cho // Materials Science Forum, Volume 580 (2008), pp. 565—568
10. Lange, F. Adaptive minimization of the maximal path deviations of industrial robots / F.Lange, G.Hirzinger // Proceedings of the European Control Conference, Karlsruhe, 1999.
11. Luo, Zh. Predictive seam tracking with iteratively learned feedforward compensation for high-precision robotic laser welding / Zhenjun Luo, Jian S. Dai, Chenyuan Wang, Fengli Wang, Yongli Tian, Mingyang Zhao // Journal of Manufacturing Systems. Volume 31, Issue 1 (2012), pp. 2-7. ISSN 0278-6125
12. Kang, H.S. Welding on the fly by using laser scanner and robot / H.S. Kang, J. Suh and S.J. Kwak // 2011 11th International Conference on Control, Automation and Systems, 2011, pp. 1688-1691.

13. Klimchik, A. Comparison Study of Industrial Robots for High-Speed Machining / A. Klimchik, A. Ambiehl, S. Garnier, B. Furet, A. Pashkevich // Mechatronics and Robotics Engineering for Advanced and Intelligent Manufacturing, 2017, pp.135-150
14. Beck, J. Design of a flexure-based active fixture system for precision robotic deburring / J. Beck, B. Sencer, R. Balasubramanian, J. Meader. // Automated Robotic Deburring, 2018
15. Schneider, U. Experimental Investigation of Sources of Error in Robot Machining / U. Schneider, M. Ansaloni, M. Drust et al. // Robotics in smart manufacturing / под ред. P. Neto, A. P. Moreira. – Berlin, Heidelberg: Springer Berlin. Heidelberg, 2013, pp.14–26.
16. V. A. Grechishnikov, Yu. V. Ilyukhin, A.V. Isaev, P. M. Pivkin, A. A. Vorotnikov, R. V. Kolesnichenko. Robotic milling. MSUT «STANKIN», 2016.– 80 p. ISBN 978-5-7028-0574-0
17. V. A. Grechishnikov, S. N. Grigoriev, Yu. V. Ilyukhin, A.V. Isaev, A. R. Maslov, Yu. E. Petukhov, P. M. Pivkin, V. B. Romanov, A. A. Vorotnikov, R. V. Kolesnichenko, P. V. Domnin, V. A. Kosarev. Instrumental systems of integrated machine-building industries and robotic complexes: Monograph. KURS, 2017 – 400 p. ISBN 978-5-906923-70-7
18. Petko, M. Trajectory tracking controller of the hybrid robot for milling / M. Petko, G. Karpel, K. Gac, G. Góra, K. Kobus, J. Ochonski // Mechatronics, 2016, Vol. 37, pp. 100–111.
19. Brunete, E. Hard material small-batch industrial machining robot / E. Brunete, J. Gambao, T. Koskinen, K. Heikkilä, B. Kaldestad, I. Tyapin, G. Hovland, D. Surdilovic, M. Hernando, A. Bottero, S. Anton // Robotics and Computer-Integrated Manufacturing. Volume 54, 2018, Pp. 185-199.
20. Zhu, Z. High precision and efficiency robotic milling of complex parts: Challenges, approaches and trends / Z. Zhu, X. Tang, C. Chen, F. Peng, R. Yan, L. Zhou, Z. Li, J. Wu // Chinese Journal of Aeronautics, 2021.
21. Sörnmo, O. Increasing Time-Efficiency and Accuracy of Robotic Machining Processes Using Model-Based Adaptive Force Control / O. Sörnmo, B. Olofsson, A. Robertsson, R. Johansson // 10th IFAC Symposium on Robot Control, SYROCO 2012, September 5–7, 2012, Croatia.
22. Chen, C. Stiffness performance index-based posture and feed orientation optimization in robotic milling process / C. Chen, F. Peng, R. Yan, Y. Li, D. Wei, Z. Fan, X. Tang, Z. Zhu // Robotics and Computer-Integrated Manufacturing. Volume 55, Part A, 2019, Pp. 29-40.
23. GOST R 60.3.3.1.1-2016/ISO 9283:1998. Industrial manipulation robots. OPERATION CHARACTERISTICS AND RELATED TESTING METHODS (2018) // System of Standards for Information, Library and Publishing Business. Moscow: Standartinform.
24. Reinl, C. Model-based Off-line Compensation of Path Deviation for Industrial Robots in Milling Applications / C. Reinl, M. Friedmann, J. Bauer, M. Pischan, E. Abele, O. von Stry // 2011

IEEE/ASME International Conference on Advanced Intelligent Mechatronics (AIM2011). Budapest, Hungary, 2011. 367 – 372.

25. Mithran, N. Design and Development of Cartesian Robot for Machining with Error Compensation and Chatter Reduction / N. Mithran and R. Gangadevi // International Journal of Engineering Research and Technology. ISSN 0974-3154 Vol. 6, No. 4 (2013), pp. 449—454.
26. Slamani, M. Characterization and experimental evaluation of gear transmission errors in an industrial robot / M. Slamani, I.A. Bonev // Industrial Robot: An International Journal. – 2013. – Vol.40, №5. – Pp.441–449.
27. Švaco, M. Calibration of an Industrial Robot using a Stereo Vision System / M. Švaco, B. Šekoranja, F. Šuligoj, B. Jerbic // 24th DAAAM International Symposium on Intelligent Manufacturing and Automation, DAAAM 2013. Procedia Engineering 69 (2014), Volume 100, pp. 459 – 463.
28. Nubiola, A. Geometric approach to solving the inverse displacement problem of calibrated decoupled 6R serial robots / Albert Nubiola, Ilian A. Bonev // Transactions of the Canadian Society for Mechanical Engineering, 2014, Vol. 38, №1, pp. 31-44.
29. Servo drives: In 3 vol. 2nd ed., supplement and revision / Edited by B.K. Chemodanov. Theory and Design of Servo Drives / E.S. Blaze, A.V. Zimin, E.S. Ivanov et al. // Bauman MSTU Publishing House, 1999. – 904 p.
30. Ilyukhin Yu. V. Electrical drives of robots and mechatronic devices: textbook / Yu.V. Ilyukhin, A.A. Zelensky // FGBOU VO MSUT «STANKIN», 2020.- 440 p.: ill. ISBN 978-5-6044658-7-5
31. Bortsov, Yu.A. Automated electric drive with elastic links / Yu.A. Bortsov, G.G. Sokolovskiy // Energoatomizdat, 1992. - 288 p.
32. Kuzovkin, V. A. Nonlinear models of dynamic processes in impulse control systems of brushless DC motors / V. A. Kuzovkin, V. V. Filatov, M. V. Chumaeva // Journal of computer and systems sciences international, volume 53, issue 3, May 2014, pp. 420-429.
33. Andreev, A. G. Formation of stator currents in the simulation of switched electric drives in robots / A. G. Andreev, M. M. Stebulyanin // Russian Engineering Research, volume 30, issue 10, October 2010, pp. 1046-1052.
34. Wescott, T. Applied Control Theory for Embedded Systems / T.Wescott // Elsevier, 2006, pp.320.
35. Bortsov, Yu.A. Electromechanical systems with adaptive and modal control / Yu.A. Bortsov, N.D. Polyakhov, V.V. Putov - L.: Energoatomizdat, 1984. Putov - L.: Energoatomizdat, 1984. – 216 p.

36. Sokolovskiy, G.G. Control of the elastic mechanism electric drive using the extended information about the object / G.G. Sokolovskiy, Yu.V. Postnikov // Automated electric drive / Edited by N.F. Ilyinsky and M.G. Yunkov. - Moscow: Energoatomizdat, 1990. - p. 65-76.
37. Shen, X. Experimental study on backlash compensation of CNC machine tool / X. Shen, J. HU, M. Zhang, L. Zhang // Advanced Materials Research, volume 580, Trans tech Publications, Switzerland, 2012, pp. 419-422.
38. Feng, B. Backlash compensation on CNC machine tool based on semi-closed loop control / B. Feng, X.S. Mei, L. Guo, D.S. Zhang, Y.L. Cheng // Advanced Materials Research, volume 346, September 2011, pp. 644-649.
39. Lukinov, A.P. Tabular regulation of mechatronic drives based on asynchronous motors with vector control / A.P. Lukinov, D.P. Soloviev // Bulletin of MSUT «STANKIN», No. 4(31), 2014.
40. Martinov, G.M. Formation of the basic computational platform of CNC for building specialised control systems / G.M. Martinov, L.I. Martinova // Bulletin of MSUT «STANKIN», No. 1(28), 2014. - P. 92 - 97.
41. Bushuev, V. V. Designing of gear hobbers of new generation on the basis of mechatronic modules / V. V. Bushuev, A. G. Ostretsov // MSUT «STANKIN», volume №3 (26), MSUT «STANKIN», Moscow, 2013.
42. Ilyukhin, Yu.V. Designing of the robots' executive systems. Linearised systems / Yu.V. Ilyukhin, Yu.V. Poduraev // MPI, 1989. - 75 p.
43. Vukobratovich, M. Control of manipulation robots: Theory and Applications. Transl. from English / Vukobratovich M., Stokic D. // Nauka, 1985. - 384 p.
44. Vukobratovic, M. Non-adaptive and adaptive control of manipulation robots: Per. from Engl. / M. Vukobratovic, D. Stokic, N. Kirchanski // Mir, 1989.
45. Timofeev, A.B.. Robot control / A.B. Timofeev // Leningrad University, 1986. - 240 p.
46. Sabinin, Yu.A. Operation of the robot electric drive at a variable moment of inertia / edited by N.F. Ilyinsky and M.G. Yunkov // Automated electric drive - M.: Energoatomizdat, 1990. - p. 237-243.
47. Egorov, I.N. Position-force control of manipulation robots / I.N. Egorov // Proc. of V All-Union Council on Robotics Systems, Part 1 - M.: Institute of Mechanics Problems, USSR Academy of Sciences, VINITI, 1990. - p. 50-51.
48. Egorov, I.N. Position-force control of the technological robots under the action of external links / I.N. Egorov, B.C. Kuleshov // Proceedings of the VIII scientific and technical conference 'Extreme robotics'. 'Extreme Robotics. - S-Pb: Izd-vo SPbSTU, 1997.-p. 269-274.

49. Application of remote-automatic control systems for technological robots to increase the efficiency and safety of labour in mechanical engineering / Yu.V. Ilyukhin // Proceedings of the international conference "Production. Technology. Technology. Ecology. PROTEK-98." Moscow: MSUT «STANKIN», 1998. p. p. 146-148.
50. Ilyukhin, Yu.V. Microcomputer control of robot drives with asynchronous motors on the basis of fuzzy logic / Yu.V. Ilyukhin, G.K. Chibisov // Proceedings of the 10th Scientific and Technical Conference "Extreme Robotics" - St. Petersburg: Central Research Institute of RTK, SPbSTU Publishing House, 1999, - p. 462-469. 462-469.
51. Lokhin, V.M. Organisation of the intellectual control of the complex dynamic objects / V.M. Lokhin, I.M. Makarov, S.V. Manko, M.P. Romanov // Proceedings of the 10th Scientific and Technical Conference "Extreme Robotics" - St. Petersburg: Central Research Institute of Robotics, SPbSTU Publishing House, 1999. - p. 17-25.
52. Lokhin, V.M. Intellectual control systems: concepts, definitions, principles of construction / V.M. Lokhin, V.N. Zakharov // Mechatronics, No. 2, 2001, p. 27-35.
53. Makarov, I.M. New generation of the intellectual regulators (in Russian) / I.M. Makarov, V.M. Lokhin, D.M. Eremin et al. // Control Devices and Systems, No. 3, 1997, p. 2-6.
54. Makarov, I.M. Development of the expert systems technology for controlling the intellectual robots / I.M. Makarov, G.N. Lebedev, V.M. Lokhin et al. // Izvestia RAS. Theory and control systems. 1994. №6. P. 161-176.
55. Ilyukhin, Yu.V. Increasing the accuracy of mechatronic drives of technological robots / Yu.V. Ilyukhin, Yu.V. Poduraev // STIN - 2015. - № 9 - P.30 - 37.
56. Robertz, S.G. Precise robot motions using dual motor control / S.G. Robertz, L. Halt, S. Kelkar, K. Nilsson, A. Robertsson, D. Schar, J. Schiffer // IEEE International Conference on Robotics and Automation, Anchorage, 2010, pp. 5613 - 5620.
57. SINUMERIK 840D sl, Special functions, Function Manual, Nurnberg, Siemens, 2012, pp. 507 – 536.
58. Schiffer, J. Dual motor control for backlash reduction / J. Schiffer // Lund University Department of Automatic Control, Lund, Sweden 2009.
59. Ilyukhin, Y. Impedance Control of High-Precision Geared Servo Drives with Two Motors for Technological Robots / Y. Ilyukhin, R. Kolesnichenko // Proceedings of the 26th International DAAAM Symposium 2016 / B. Katalinic: DAAAM International Vienna, 2016. – Pp.599–607.
60. Polskiy V. A. Polskiy, V. A.; Vanin, A. V.; Thanh, L. V. // Mechatronics, Automation, Control, 2007. №10. P. 34 - 40.

61. Mosadeghzad, M. Impedance control of a class of series elastic actuators: performance limitations arising from link dynamics, disturbance attenuation and impedance emulation / M. Mosadeghzad, G.A. Medrano-Cerda, J.A. Saglia, N.G. Tsagarakis, and D.G. Caldwell // IEEE Int. Conf. on Robotics and Biomimetics (ROBIO), Dec 2014
62. Zhao, Y. Sensitivity comparison to loop latencies between damping versus stiffness feedback control action in distributed controllers / Y. Zhao, N. Paine, and L. Sentis // ASME 2014 Dynamic Systems and Control Conference, DSCC2014, October 2014
63. Chen, C. A velocity-based impedance control system for a low impact docking mechanism (LIDM) / C. Chen, H. Nie, J. Chen, and X. Wang // Sensors 14(12), December 2014
64. Ilyukhin, Yu. V. Task for the development and research of the electromechanical tracking robot drive / Yu. V. Ilyukhin // MSUT «STANKIN», 2013.
65. Ilyukhin, Yu.V. Computer control of mechatronic systems / Yu.V. Ilyukhin // FGBOU VPO MSUT «STANKIN». - 2014. - 320 p.: ill.
66. Barntrup. KEB Servo Motors. KEB instruction manual / Barntrup, June 2004.
67. Ilyukhin, Yu.V. Nonlinear Adaptive Correction of Continuous Path Speed of the Tool for High Efficiency Robotic Machining / Yu.V. Ilyukhin, Yu.V. Poduraev, A.V. Tatarintseva // 25th DAAAM International Symposium on Intelligent Manufacturing and Automation, DAAAM 2014. Procedia Engineering (2015), Volume 100, pp. 994-1002.
68. Fu, K. Robotics / K. Fu, R. Gonzalez, K. Li // Mir. 1989.
69. Denavit, J. A kinematic notation for lower-pair mechanisms based on matrices / J. Denavit, R. Hartenberg // Transactions of ASME — Journal of Applied Mechanics, 22(2), pp. 215-221, June 1955.
70. Rosenberg, A.M. Dynamics of milling / A.M. Rosenberg // Soviet Science, 1945. – 360 p.
71. Reference book of the technologist-machine engineer. In 2 Vol. 2 / Edited by A.G. Kosilova and R.K. Mescheryakov. - Moscow: Mashinostroenie, 1986. - 420 p.
72. Grigoriev, S.N. Modern tool materials / S.N. Grigoriev, V.A. Grechishnikov, A.R. Maslov, A.G. Skhirtladze // MSUT «STANKIN». - 2011. - 103 p.
73. Andreescu, G. D. Torque-speed adaptive observer and inertia identification without current transducers for control of electric drives / G.D. Andreescu, R. Rabinovici // International conference on electrical machines, Espoo, FINLANDE (28/08/2000). 2000. – pp. 1428-1432.
74. Servo drives. In 2 books. Edited by B.K. Chemodanov. Book one. - M.: Energia, 1976. - 480 p.
75. R. V. Kolesnichenko. Feasibility analysis of constructing precision technological robots on dual-motor geared servo drives. VESTNIK MSUT «STANKIN», Moscow, No2 (49) 2019. Pp. 111-118.

76. R. V. Kolesnichenko. Experimental study of dynamic properties of high-precision dual-motor geared servo drives for technological robots. VESTNIK MSUT «STANKIN», Moscow, No4 (55) 2020. Pp. 68-77.
77. V. A. Grechishnikov, Yu. V. Ilyukhin, A.V. Isaev, R. V. Kolesnichenko, P. M. Pivkin, A. A. Vorotnikov, J. Bianchi, N. Pedrocchi. Improving accuracy and productivity of robotic milling operation based on trajectory-impedance control. VESTNIK MSUT «STANKIN», Moscow, No4 (39) 2016. Pp. 8-16.
78. Yu. V. Ilyukhin, R. V. Kolesnichenko. Accuracy analysis of manipulator built on single-motor and precision dual-motor drives while implementing movements along circular trajectories. // Fundamental and applied problems of engineering and technology, No 6, 2017. Pp. 114-127.
79. Ilyukhin, Yu. V. High-Precision Servo Drives Technological Robots. Problems and Solutions / Yu. V. Ilyukhin, R. V. Kolesnichenko // 2nd School on Dynamics of Complex Networks and their Application in Intellectual Robotics (DCNAIR), Institute of Electrical and Electronics Engineers Inc, 2018.
80. Ilyukhin, Yu. V. Accuracy of Milling by Robots with Two-Motor Servo Drives / Yu. V. Ilyukhin, R. V. Kolesnichenko // Russian Engineering Research, 2019, Vol. 39, No. 12, pp. 1069 – 1072.
81. Ilyukhin, Yu.V. Investigation of the possibility of application of geared dual-motor tracking drives for technological robots / Yu.V. Ilyukhin, R.V. Kolesnichenko // Automation and control in mechanical engineering M.: MSUT «STANKIN», № 1 (23) 2016. P. 32-38.
82. Ilyukhin, Yu. V. Increasing the accuracy of technological robots on the basis of improving the accuracy and speed of their digital tracking drives / Yu.V. Ilyukhin, R.V. Kolesnichenko // In Proceedings of the Regional Scientific and Technical Conference of Young Scientists "Mechatronics and Robotics" MiR-2017, Oryol, 2017.
83. Ilyukhin, Yu.V. An Increase in Accuracy of Robotic Milling / Yu.V. Ilyukhin, R. V. Kolesnichenko // Applied Mechanics and Materials. – 2017. – V. 865. P. 450–456.
84. Ilyukhin, Yu.V. Analysis of motion accuracy during milling by robots with precision dual-motor drives / Yu.V. Ilyukhin, R.V. Kolesnichenko // STIN. 2019. - № 7. - P.18-21. ISSN 0869-7566
85. Ilyukhin, Yu.V. High-precision tracking systems of technological robots. Problems and solutions / Yu.V. Ilyukhin, R.V. Kolesnichenko // Proceedings of the International Conference DCNAIR - 2018 - P. 114 – 116
86. Sokolovskiy, G.G. AC electric drives with frequency regulation: textbook for students of higher educational institutions / G.G. Sokolovskiy. - Moscow: Publishing center “Academy”, 2006. - 272 p.

87. Chilikin, M.G. Theory of the automated electric drive / M.G. Chilikin, V.I. Klyuchev, A.S. Sandler // Energia, 1979. - 616 p.
88. Afonin, V.L. Control of the technological robots and flexible modules / V.L. Afonin, V.E. Kovalev, S.V. Kolodezov, N.G. Rasskazchikov, P.I. Chinaev // Nauka, 1992. - 143 p.
89. Şirinterlikçi, A. Repeatability and Accuracy of an Industrial Robot: Laboratory Experience for a Design of Experiments Course / A. Şirinterlikçi, M. Tirayakioğlu, A. Bird, A. Harris, K. Kweder // Technology Interface Journal/Spring 2009, Vol. 9, No. 2
90. Greenway, B. Robot accuracy / B. Greenway // Industrial Robot: An International Journal, 2000, Vol. 27, No. 4, Pp. 257–265
91. Hoffmann, Ch. Accuracy-Tests for Industrial Robots / Ch. Hoffmann // IFAC Proceedings Volumes, 1988, Vol. 21, Is. 16, Pp. 103-108
92. Ilyukhin, Yu.V. Precision drives for measuring robots / Yu.V. Ilyukhin, Yu.V. Poduraev, M.G. Kovalsky // Legislative and Applied Metrology. 2015. - № 2(135). - P.13-21.

## LIST OF PAPERS PUBLISHED BY THE AUTHOR ON THE SUBJECT OF THE THESIS

In journals from the VAK (Russian Attestation Commission) list

1. R. V. Kolesnichenko. Feasibility analysis of constructing precision technological robots on dual-motor geared servo drives. *VESTNIK MSUT «STANKIN»*, Moscow, No2 (49) 2019. Pp. 111-118.
2. R. V. Kolesnichenko. Experimental study of dynamic properties of high-precision dual-motor geared servo drives for technological robots. *VESTNIK MSUT «STANKIN»*, Moscow, No4 (55) 2020. Pp. 68-77.
3. V. A. Grechishnikov, Yu. V. Ilyukhin, A.V. Isaev, R. V. Kolesnichenko, P. M. Pivkin, A. A. Vorotnikov, J. Bianchi, N. Pedrocchi. Improving accuracy and productivity of robotic milling operation based on trajectory-impedance control. *VESTNIK MSUT «STANKIN»*, Moscow, No4 (39) 2016. Pp. 8-16.
4. Yu. V. Ilyukhin, R. V. Kolesnichenko. Accuracy analysis of manipulator built on single-motor and precision dual-motor drives while implementing movements along circular trajectories. *Fundamental and applied problems of engineering and technology*, No 6, 2017. Pp. 114-127.

In Scopus peer-reviewed publications

1. Ilyukhin, Y. Impedance Control of High-Precision Geared Servo Drives with Two Motors for Technological Robots / Y. Ilyukhin, R. Kolesnichenko // Proceedings of the 26th International DAAAM Symposium 2016 / B. Katalinic: DAAAM International Vienna, 2016. – Pp.599–607.
2. Ilyukhin, Yu. V. Accuracy of Milling by Robots with Two-Motor Servo Drives / Yu. V. Ilyukhin, R. V. Kolesnichenko // Russian Engineering Research, 2019, Vol. 39, No. 12, pp. 1069 – 1072. ISSN 1068-798X, DOI: 10.3103/S1068798X19120086
3. Ilyukhin, Yu. V. High-Precision Servo Drives Technological Robots. Problems and Solutions / Yu. V. Ilyukhin, R. V. Kolesnichenko // 2nd School on Dynamics of Complex Networks and their Application in Intellectual Robotics (DCNAIR), Institute of Electrical and Electronics Engineers Inc, 2018.

### In other publications

1. Yu. V. Ilyukhin, R. V. Kolesnichenko. Investigation of the possibility of using geared dual-motor geared servo drives for technological robots. Automation and control in mechanical engineering. MSUT «STANKIN», No1 (23), 2016. Pp. 32-38.
2. V. A. Grechishnikov, Yu. V. Ilyukhin, A.V. Isaev, P. M. Pivkin, A. A. Vorotnikov, R. V. Kolesnichenko. Robotic milling. MSUT «STANKIN», 2016.– 80 p. ISBN 978-5-7028-0574-0
3. V. A. Grechishnikov, S. N. Grigoriev, Yu. V. Ilyukhin, A.V. Isaev, A. R. Maslov, Yu. E. Petukhov, P. M. Pivkin, V. B. Romanov, A. A. Vorotnikov, R. V. Kolesnichenko, P. V. Domnin, V. A. Kosarev. Instrumental systems of integrated machine-building industries and robotic complexes: Monograph. KURS, 2017 – 400 p. ISBN 978-5-906923-70-7
4. Yu. V. Ilyukhin, R. V. Kolesnichenko. Improving accuracy of technological robots based on improving accuracy and speed of their digital servo drives. Collection of materials of the regional Scientific and Technical Conference of young Scientists "Mechatronics and Robotics" MiR-2017, Orel, 2017.Ilyukhin, Yu.V. An Increase in Accuracy of Robotic Milling / Yu.V. Ilyukhin, R. V. Kolesnichenko // Applied Mechanics and Materials. – 2017. – T. 865. C. 450–456.
5. Yu.V. Ilyukhin, R. V. Kolesnichenko. Accuracy analysis of movements realized by robots with precision dual-motor drives at milling operation. STIN. 2019. No 7. Pp.18-21. ISSN 0869-7566
6. Yu.V. Ilyukhin, R. V. Kolesnichenko. High-precision servo systems for technological robots. Problems and solutions. Collection of materials of the international conference DCNAIR. 2018. Pp. 114 – 116

**APPENDIX A. Stand control program code.**

```

#include <stdio.h>
#include <conio.h>
#include <math.h>
#include <stdlib.h>
#include <dos.h>
#include <alloc.h>
#include "833drive.h"

//=====
// Description of variables and parameters
//=====

unsigned BIOSTimerSpeed=1;
unsigned TimerFreq=(unsigned)(1193181L/65536L);
static cnt=0;
unsigned char maskpuls,aush,ausl,maskupr,diskrupr,diskruph;
unsigned int base=0x0200; // base address of PCL-833
unsigned int baseacl=0x2C0; // base address of ACL-6126
unsigned int iflag=0; // interrupt flag
long q1,q2,E1,E2; // sensor position, error
float q1p,q2p,q2pd,q2p0; // desired position
float far buff_q1[16000], far buff_q2[16000], far buff_q1p[16000], far buff_q2p[16000]; // position
buffers
long buff_i; // buffer index
//float kusp1=1, kusp2=1;
// variables that are used to determine the position from the sensors
short int U1,U2;
long UP1,UP2;
int u,r,b,znak;
unsigned char uu,rr,bb,mask;
long intr1, intu, intb, p1, p2;
long res;
//=====

float Ed2ip=0; // previous integral

```

```

float Ed2i; // current integral
float Ed2t; // current error value
float Ed2p=0; // previous error value
float qs2=0; // drive velocity feedback
float kusp1=80;
float Ki=110; //30//115;//46;// coefficient of the I- controller of the CO position
float Kos2=0.13; //0.12//0.086;//0.14;// velocity feedback gain coefficient of CO
float kusp2=90; //60//250;//50;// position gain coefficient
float q1pr=0; // previous value of q1
=====

float Period;
int flag_start=0; // interrupt handler enable flag (at 1)
int t_smb=0; // pressed key code, 27 = esc
float proc_time; // opeation time
float betta, bettaref; // to calculate the input
char buf[14]; // data file name

#ifndef __cplusplus
#define __CPPARGS ...
#else
#define __CPPARGS
#endif

void interrupt NewInt08(__CPPARGS);
void interrupt (*SvInt08)(__CPPARGS)=NULL;

void STOP_intr();
int SetTimer(unsigned cnt); // timer setting
void SetTimerFreq(unsigned freq); // frequency setting
void DeactivateTimer(void); // timer switch off
void Set8254Counter(unsigned cnt);
void zadergka(int aa); // cycle delay
void outzap(int U,int basezap); // control output

```

```

int main(void) // main function
{
    flag_start=0;
//=====
clrscr();

// Initialization of PCL-833

outportb(base+0, 0x00); // Channel 1 count ban
zadergka(200);
outportb(base+1, 0x00); // Channel 2 count ban
zadergka(200);
outportb(base+2, 0x00); // Channel 3 count ban
zadergka(200);
outportb(base+3, 0x00); // Software latching for 1 channel. Do not reset the counter during reading.
zadergka(200);
outportb(base+4, 0x00); // Software latching for 2 channel. Do not reset the counter during reading.
zadergka(200);
outportb(base+5, 0x00); // Software latching for 3 channel. Do not reset the counter during reading.
zadergka(200);
outportb(base+6, 0x07); // Continue counting after overflow
zadergka(200);
outportb(base+8, 0x00); // 8 MHz, 24 bit
zadergka(200);
outportb(base+7, 0x07); // Resetting all counters
zadergka(200);
outportb(base+0, 0x03); // Stop x4 mode for channel 1. Set 0 when resetting the counters.
zadergka(200);
outportb(base+1, 0x03); // Stop x4 mode for channel 2. Set 0 when resetting the counters.
zadergka(200);
outportb(base+2, 0x03); // Stop x4 mode for channel 3. Set 0 when resetting the counters.
zadergka(200);
outportb(base+10,0x00); // divider = 0
zadergka(200);

```

```

// Initial values of variables

q1p=0; q2p=0;
U1=0; U2=0;

//=====
mask=0x80; // mask for highlighting the sign of the sensor signal

SetTimer(4096); // At 4096, the frequency approx. = 291 Hz
Period=0.0034364261; // At 4096 period 0.0034364261 s
//=====

enable();

outportb(base+7, 0x07); // Resetting all counters
zadergka(200);

q1=0; q2=0;
q1p=0; q2p=0;
//=====

gotoxy(1,1); printf("the programme is ready for use");
//

//getch();

===== end of initialisation =====

gotoxy(1,2); printf("recording'... ");

int k=0, i=0;
buff_i = 0;
betta = 0;
bettaref=0;
proc_time = 0;
flag_start=1; // The timer interrupt is now handled
while (k==0)
{
    // exit the loop by pressing esc or reaching 16000 clock cycles
}

```

```

if(kbhit()) { t_smb=getch(); if(t_smb==27) {k=1;} };
if (buff_i > 15999){k=1;}

if (iflag==1)
{

iflag = 0; // resetting the interrupt flag
//      if (buff_i > 5000)
//      {
//          getch();
//      }

// Ed2ip=Ed2i; // previous integral
// Ed2p=Ed2t; // previous error
// q1pr=q1; // previous rotation angle of the CO
proc_time = proc_time+Period;
// Formation of the following position
q1p=1000;
q2p=250000*4/2/3.14159265359*0.1*sin(proc_time*0.5); // control input signal of the
position of the CO
// q2pd=250000*4/2/3.14159265359*0.1*cos(proc_time*0.5)*0.5/27; // combined
control signal
// q2p=4096/2/3.14159265359*1*(betta); // control input signal for the position of the
ISD (during setting)

bettaref=0.1;
/* // setting a linearly increasing input signal
betta=bettaref;
if (1.05*(proc_time-1) >= bettaref) betta=bettaref;
//else betta=0;
else if (1.05*(proc_time-1) <= 0) betta=0;
else betta = 1.05*(proc_time-1);
q2p=250000*4/2/3.14159265359*1*(betta);
*/
gotoxy(1,3); printf("indeks: %d /16000 ", buff_i); // Output the index of a data array

```

```

}

}

flag_start=0; // Now timer interrupts are not handled
gotoxy(1,4); printf("recording is complete, enter the file name (*.csv): "); gets(buf); // requesting a file
name for writing data
// writing data in .csv format
FILE *lout;
lout = fopen(buf, "wt");
fprintf(lout,"takt;q1;q2;q2p\n");
for(i=0; i<buff_i; i++) fprintf(lout,"%d;%f;%f;%f\n", i, buff_q1[i], buff_q2[i], buff_q2p[i]); // // buff_q1p[i]
fclose(lout);

gotoxy(1,5); printf("operation completed ");

//=====

disable();
flag_start=0;
delay(1000); // Delay = 1 s to complete transients
// setting 0 actuator velocity, control prohibition
outzap(0,baseacl);
outzap(0,baseacl+2);
outzap(0,baseacl+4);
STOP_intr();
getch();
return 0;
} // End of main

//=====

void zadergka(int aa)
// aa=200 daet 3,3 μs
// aa=60,6 daet 1 μs

```

```

{ while(aa>0) aa=aa-1; }

//=====

void outzap(int U,int basezap)
{
    int UZ,hbyte,lbyte;
    if(U>2047) U=2047;
    if(U<-2047) U=-2047;
    UZ=U+2048;
    hbyte=UZ/256;
    outportb(basezap,hbyte);
    zadergka(200);
    lbyte=UZ-hbyte*256;
    outportb(basezap+1,lbyte);
    zadergka(200);
}

```

```

//=====

void STOP_intr()
{
    disable();
    asm {
        push ds
        push si
        push di
        cli
        mov al,0x20
        out 0x20,al
    }
    SetTimer(0);
    _dos_setvect(8,SvInt08);
    asm {
        sti
        pop di
        pop si
    }
}
```

```

pop ds
}

enable();
}

//=====

int SetTimer(unsigned count)
{ /* if 0 is passed, disable the processing procedure */
  if(!count)
    { Set8254Counter(0);
      /* disconnect from the interrupt */
      if(SvInt08) _dos_setvect(8,SvInt08);
      return 0;
    }
  TimerFreq=1193181L/count;
  Set8254Counter(count);
  SvInt08=_dos_getvect(8); _dos_setvect(8,NewInt08);
  atexit(DeactivateTimer);
  return 1;
}

// =====

void SetTimerFreq(unsigned freq)
{ SetTimer((unsigned)(1193181L/freq)); }

void DeactivateTimer(void)
{ SetTimer(0); }

void Set8254Counter(unsigned cnt)
{ long l=cnt;
  if(!cnt) l=65536L; /* if 0, it's actually 65536 */
  BIOSTimerSpeed=(unsigned)(65536L/l);
  outportb(0x43,6);
  outportb(0x40,(char)cnt);
}

```

```

    outportb(0x40,(char)(cnt>>8));
}

//*****************************************************************************
/*          Interrupt handling subroutine      */
//*************************************************************************/
void interrupt NewInt08(__CPPARGS)
{
    cnt++; /* increment the clock count */

    /* if it's time to call the BIOS handler */
    if(cnt>=BIOSTimerSpeed) { cnt=0; SvInt08(); }

    /* otherwise enable the following interrupts */
    iflag =1;

    // At flag_start==0 the drives do not respond to timer interrupts in any way
    if(flag_start==0) goto finish;

    //Drive-1 sensor data acquisition
        b = importb(base+2);
        zadergka(200);
        u = importb(base+1);
        zadergka(100);
        r = importb(base+0);
        znak=b&mask;
        if(znak==0) { intr1=(long)r; intu=(long)u; intb=(long)b;

    res=intb*65536+intu*256+intr1; }

        else { rr=~r; uu=~u; bb=~b;
        intr1=(long)rr; intu=(long)uu; intb=(long)bb;
        intr1=intr1+1;
        if(intr1==256) { p1=1; intr1=0; } else { p1=0; }
        intu=intu+p1;
        if(intu==256) { p2=1; intu=0; } else { p2=0; }
}

```

```

intb=intb+p2;
res=intb*65536+intu*256+intr1;
res=-res;
}

q1=res;

//===== !!!!!!! =====
// calculation of the error and the setting effect
E1=q1p-q1; UP1=kusp1*E1/100;
if(UP1>2000) UP1=2000; if(UP1<-2000) UP1=-2000;
U1=(short int)UP1;
outzap(U1,baseacl+0); // Setpoint output

//Drive-2

b = importb(base+6);
zadergka(200);
u = importb(base+5);
zadergka(100);
r = importb(base+4);
znak=b&mask;
if(znak==0) { intr1=(long)r; intu=(long)u; intb=(long)b;

res=intb*65536+intu*256+intr1; }

else { rr=~r; uu=~u; bb=~b;
intr1=(long)rr; intu=(long)uu; intb=(long)bb;
intr1=intr1+1;
if(intr1==256) { p1=1; intr1=0; } else { p1=0; }
intu=intu+p1;
if(intu==256) { p2=1; intu=0; } else { p2=0; }
intb=intb+p2;
res=intb*65536+intu*256+intr1;
res=-res;
}

q2=res;

//===== !!!!!!! =====
// I- controller of drive position with velocity feedback of the CO

```

```

Ed2t=q2p+q1; // current error
Ed2ip=Ed2ip+Ed2t*Period; // current integral
Ed2i=Ki/100*Ed2ip;
qs2=Kos2*(-q1+q1pr); // Drive velocity feedback
E2=Ed2i-q2-qs2; // for the entire precision dual-motor drive
//Ed2ip=Ed2i; // previous integral
//Ed2p=Ed2t; // previous error
q1pr=q1; // previous rotation angle of the CO
//E2=q2p-q2; // only ISD
//E2=q2p-q2+q2pd; // only ISD with combined control
UP2=kusp2*E2/100;
if(UP2>2047) UP2=2047; if(UP2<-2047) UP2=-2047; // overflow
saturation
U2=(short int)UP2;
outzap(U2,baseacl+2); // writing the value to the DAC

if(flag_start==1) // buffering
    if(buff_i<16000) { buff_q1(buff_i)=q1; buff_q2(buff_i)=q2;
buff_q1p(buff_i)=q1p; buff_q2p(buff_i)=q2p; buff_i++; };

finish:
outportb(0x20,0x20);
}

// end of the interrupt handling subroutine
//===== programme end =====

```

## APPENDIX B. Program code for obtaining symbolic model of a 4-link manipulator in MATLAB and SIMULINK.

```
% clearing the workspace and command window in Matlab
clear all
clc
% description of symbolic variables of generalised coordinates, link lengths, angle B
% (formed by the vertical axis and the wrist link), transition matrices
syms q1
A01 = [cos(q1), -sin(q1), sym(0), sym(0); sin(q1), cos(q1), sym(0), sym(0); sym(0),
sym(0), sym(1), sym(0); sym(0), sym(0), sym(0), sym(1)] % rotation around the axis 00Z0 by
angle q1
syms l1
A02 = [sym(1), sym(0), sym(0), sym(0); sym(0), sym(1), sym(0), sym(0); sym(0),
sym(1), l1; sym(0), sym(0), sym(1)] % displacement along the axis 00Z0 by l1
A03 = [sym(1), sym(0), sym(0), sym(0); sym(0), cos(-(sym('pi')/2)), -sin(-(sym('pi')/2)),
sym(0); sym(0), sin(-(sym('pi')/2)), cos(-(sym('pi')/2)), sym(0); sym(0), sym(0), sym(0),
sym(1)] % rotation around the 01X1 axis
syms q2
A04 = [cos(-q2), -sin(-q2), sym(0), sym(0); sin(-q2), cos(-q2), sym(0), sym(0); sym(0),
sym(0), sym(1), sym(0); sym(0), sym(0), sym(0), sym(1)] % rotation around the axis 01Z1 by
angle q2
syms l2
A05 = [sym(1), sym(0), sym(0), l2; sym(0), sym(1), sym(0), sym(0); sym(0), sym(0), sym(1),
sym(0); sym(0), sym(0), sym(0), sym(1)] % displacement along the axis 01Z1 на l2
syms q3
A06 = [cos(q3), -sin(q3), sym(0), sym(0); sin(q3), cos(q3), sym(0), sym(0); sym(0),
sym(0), sym(1), sym(0); sym(0), sym(0), sym(0), sym(1)] % rotation around the axis 02Z2 by
angle q3
syms l3
A07 = [sym(1), sym(0), sym(0), l3; sym(0), sym(1), sym(0), sym(0); sym(0), sym(0), sym(1),
sym(0); sym(0), sym(0), sym(0), sym(1)] % displacement along the axis 02Z2 на l3
syms q4
A08 = [cos(q4), -sin(q4), sym(0), sym(0); sin(q4), cos(q4), sym(0), sym(0); sym(0),
sym(0), sym(1), sym(0); sym(0), sym(0), sym(0), sym(1)] % rotation around the axis 03Z3 by
angle q4
syms l4
A09 = [sym(1), sym(0), sym(0), l4; sym(0), sym(1), sym(0), sym(0); sym(0), sym(0), sym(1),
sym(0); sym(0), sym(0), sym(0), sym(1)] % displacement along the axis 03Z3 на l4
syms B
A10 = [cos(B), -sin(B), sym(0), sym(0); sin(B), cos(B), sym(0), sym(0); sym(0),
sym(0), sym(1), sym(0); sym(0), sym(0), sym(0), sym(1)] % rotation around the axis 03Z3 by angle B
% obtaining homogeneous transformation matrices
T1 = simplify(A01 * A02 * A03)
T2 = simplify(T1 * A04 * A05)
T3 = simplify(T2 * A06 * A07)
T4 = simplify(T3 * A08 * A09 * A10)
simplify(A01 * A02 * A03 * A04 * A05 * A06 * A07 * A08 * A09 * A10)
simplify(T4 + simplify(A01 * A02 * A03 * A04 * A05 * A06 * A07 * A08 * A09 * A10) * -1)
A1 = A01 * A02 * A03
O1 = A1(sym(1):sym(3), sym(1):sym(3))
r1 = A1(sym(1):sym(3), sym(4):sym(4))
R1 = T1(sym(1):sym(3), sym(1):sym(3))
P1 = T1(sym(1):sym(3), sym(4):sym(4))
A2 = A04 * A05
O2 = A2(sym(1):sym(3), sym(1):sym(3))
r2 = A2(sym(1):sym(3), sym(4):sym(4))
```

```

R2 = T2(sym(1):sym(3), sym(1):sym(3))
P2 = T2(sym(1):sym(3), sym(4):sym(4))
A3 = A06 * A07
O3 = A3(sym(1):sym(3), sym(1):sym(3))
r3 = A3(sym(1):sym(3), sym(4):sym(4))
R3 = T3(sym(1):sym(3), sym(1):sym(3))
P3 = T3(sym(1):sym(3), sym(4):sym(4))
A4 = A08 * A09 * A10
O4 = A4(sym(1):sym(3), sym(1):sym(3))
r4 = A4(sym(1):sym(3), sym(4):sym(4))
R4 = T4(sym(1):sym(3), sym(1):sym(3))
P4 = T4(sym(1):sym(3), sym(4):sym(4))
fi = q1
% obtaining the solution to the direct kinematics problem (TCP (tool center point)
% coordinates by axes)
x = simplify(P4(sym(1):sym(1), sym(1):sym(1))) % TCP coordinate in the OX axis
y = simplify(P4(sym(2):sym(2), sym(1):sym(1))) % TCP coordinate in the OY axis
z = simplify(P4(sym(3):sym(3), sym(1):sym(1))) % TCP coordinate in the OZ axis
% получение матрицы Якоби
J = [diff(x, q1), diff(x, q2), diff(x, q3), diff(x, q4); diff(y, q1), diff(y, q2), diff(y, q3), diff(y, q4); diff(z, q1), diff(z, q2), diff(z, q3), diff(z, q4); diff(fi, q1), diff(fi, q2), diff(fi, q3), diff(fi, q4)]
% obtaining the solution to the direct dynamics problem (projection of TCP velocity on
% coordinate axes)
syms dq1 dq2 dq3 dq4
Vvector = J(sym(1):sym(3), sym(1):sym(4)) * reshape([dq1; dq2; dq3; dq4], sym(4), sym(1))
Vx = simplify(Vvector(sym(1):sym(1), sym(1):sym(1))) % TCP speed projection on the OX axis
Vy = simplify(Vvector(sym(2):sym(2), sym(1):sym(1))) % TCP speed projection on the OY axis
Vz = simplify(Vvector(sym(3):sym(3), sym(1):sym(1))) % TCP speed projection on the OZ axis
% obtaining the transpose Jacobi matrix
Jtransp = transpose(J)
% description of symbolic variables characterizing the forces acting on the manipulator
% tool and torque around the vertical axis
syms Fx Fy Fz Mfi
% obtaining the torques acting on the actuators of the manipulator links as a result of
% these forces and torques
Momentvector = simplify(Jtransp * reshape([Fx; Fy; Fz; Mfi], sym(4), sym(1)))
Mtorq1 = Momentvector(1) % torque acting on the drive of the first link of the manipulator
Mtorq2 = Momentvector(2) % torque acting on the drive of the second link of the
% manipulator
Mtorq3 = Momentvector(3) % torque acting on the drive of the third link of the manipulator
Mtorq4 = Momentvector(4) % torque acting on the drive of the fourth link of the
% manipulator
% description of additional symbolic variables necessary for calculation and obtaining the
% auxiliary matrix U necessary for determining the matrix of inertial characteristics of the
% manipulator
syms q i j T Tc qc k m
T = {sym([T1]); sym([T2]); sym([T3]); sym([T4])};
q = {sym([q1]); sym([q2]); sym([q3]); sym([q4])};
for i = 1 : 4
    for j = 1 : 4
        U{i,j} = simplify(sym([diff(sym(T(i)), sym(q(j)))]));
    end;
end;
% description of symbolic variables of link masses and derivation of link inertia matrices
syms m1 m2 m3 m4
H1 = [sym(0), sym(0), sym(0), sym(0); sym(0), m1*l1^2/3, sym(0), m1*l1/2; sym(0), sym(0),
sym(0), sym(0); sym(0), m1*l1/2, sym(0), m1];
H2 = [m2*l2^2/3, sym(0), sym(0), -m2*l2/2; sym(0), sym(0), sym(0), sym(0); sym(0), sym(0),
sym(0), sym(0); -m2*l2/2, sym(0), sym(0), m2];

```

```

H3 = [m3*13^2/3, sym(0), sym(0), -m3*13/2; sym(0), sym(0), sym(0), sym(0); sym(0), sym(0),
      sym(0), sym(0); -m3*13/2, sym(0), sym(0), m3];
H4 = [m4*14^2/3, sym(0), sym(0), -m4*14/2; sym(0), sym(0), sym(0), sym(0); sym(0), sym(0),
      sym(0), sym(0); -m4*14/2, sym(0), sym(0), m4];
H = {sym([H1]);sym([H2]);sym([H3]);sym([H4])};
% determination of components of the matrix of inertial characteristics of the manipulator
i = 0;
j = 0;
k = 0;
A = {sym(0), sym(0), sym(0), sym(0); sym(0), sym(0), sym(0), sym(0); sym(0), sym(0),
      sym(0), sym(0); sym(0), sym(0), sym(0), sym(0)};
for i = 1 : 4
    for j = 1 : 4
        for k = 1 : 4
            acur = simplify(sym([trace(U{k,i}*H{k}*transpose(U{k,j}))]));
            A{i,j} = sym(A{i,j})+acur;
            A{i,j} = simplify(A{i,j});
        end;
    end;
end;
% obtaining the auxiliary matrix Utd, necessary for determining the matrix characterizing
the Coriolis and centrifugal forces acting on the mechanism links
i = 0;
j = 0;
k = 0;
for i = 1 : 4
    for j = 1 : 4
        for k = 1 : 4
            Utd{i,j,k} = simplify(sym([diff(sym(U{i,j}),sym(q(k)))]));
        end;
    end;
end;
% obtaining the auxiliary matrix Bf, necessary for determining the vector characterizing
Coriolis and centrifugal forces acting on the mechanism links
i = 0;
j = 0;
k = 0;
p = 0;
Ba = {sym(0), sym(0), sym(0), sym(0); sym(0), sym(0), sym(0), sym(0); sym(0), sym(0),
      sym(0), sym(0); sym(0), sym(0), sym(0), sym(0)};
Bf = cat(3, Ba, Ba, Ba, Ba);
for i = 1 : 4
    for j = 1 : 4
        for k = 1 : 4
            for p = 1 : 4
                bcur = simplify(sym([trace(Utd{p,j,k}*H{p}*transpose(U{p,i}))]));
                Bf{i,j,k} = sym(Bf{i,j,k}) + bcur;
                Bf{i,j,k} = simplify(Bf{i,j,k});
            end;
        end;
    end;
end;
% determination of vector components characterizing Coriolis and centrifugal forces acting
on the mechanism links
syms dq
dq = {dq1;dq2;dq3;dq4};
i = 0;
k = 0;
m = 0;
Bm = {sym(0); sym(0); sym(0); sym(0)};
for i = 1 : 4

```

```

for k = 1 : 4
    for m = 1 : 4
        bmcur = simplify(sym([Bf{i,k,m}*dq{k}*dq{m}]));
        Bm{i} = sym(Bm{i})+bmcur;
        Bm{i} = simplify(Bm{i});
    end;
end;
% Determination of the components of the vector that takes into account external forces
% and moments acting on the mechanism
syms g
g = [sym(0) sym(0) -g sym(0)];
M = [m1 m2 m3 m4];
pro = {[sym(0); 11/2; sym(0); 1]; [-12/2; sym(0); sym(0); 1]; [-13/2; sym(0); sym(0); 1];
[-14/2; sym(0); sym(0); 1]};
i = 0;
j = 0;
D = {sym(0); sym(0); sym(0); sym(0)};
for i = 1 : 4
    for j = 1 : 4
        dcur = simplify(sym([-M(j)*g*U{j,i}*pro{j}]));
        D{i} = sym(D{i})+dcur;
        D{i} = simplify(D{i});
    end;
end;
% inverting the matrix of inertial characteristics
Amatrix = cell2sym(A);
Am1matrix = inv(Amatrix);
% definition of symbolic variables characterizing the torques, created by link drives and
% applied to the links of the manipulation mechanism
syms mu1 mu2 mu3 mu4
% obtaining the general equation of motion of the manipulator
Eq = simplify(j*([mu1; mu2; mu3; mu4] - cell2sym(Bm) - cell2sym(D)));
Eq;
% obtaining the equations of motion of the manipulator separately for each link
d2q1 = Eq(1);
d2q2 = Eq(2);
d2q3 = Eq(3);
d2q4 = Eq(4);
% generation of blocks in Simulink, in which the obtained equations are implemented, to
% create a model of the manipulator dynamics
new_system('Manipulator_4DOF_dynamics')
matlabFunctionBlock('Manipulator_4DOF_dynamics/d2q1',d2q1)
matlabFunctionBlock('Manipulator_4DOF_dynamics/d2q2',d2q2)
matlabFunctionBlock('Manipulator_4DOF_dynamics/d2q3',d2q3)
matlabFunctionBlock('Manipulator_4DOF_dynamics/d2q4',d2q4)
matlabFunctionBlock('Manipulator_4DOF_dynamics/Vx',Vx)
matlabFunctionBlock('Manipulator_4DOF_dynamics/Vy',Vy)
matlabFunctionBlock('Manipulator_4DOF_dynamics/Vz',Vz)
matlabFunctionBlock('Manipulator_4DOF_dynamics/Mtorq1',Mtorq1)
matlabFunctionBlock('Manipulator_4DOF_dynamics/Mtorq2',Mtorq2)
matlabFunctionBlock('Manipulator_4DOF_dynamics/Mtorq3',Mtorq3)
matlabFunctionBlock('Manipulator_4DOF_dynamics/Mtorq4',Mtorq4)
matlabFunctionBlock('Manipulator_4DOF_dynamics/x',x)
matlabFunctionBlock('Manipulator_4DOF_dynamics/y',y)
matlabFunctionBlock('Manipulator_4DOF_dynamics/z',z)
save_system('Manipulator_4DOF_dynamics')

```